PL-TR-95-2060(I)
Special Reports, No. 274

PROCEEDINGS OF THE 17TH ANNUAL CONFERENCE ON ATMOSPHERIC TRANSMISSION MODELS, 8-9 JUNE 1994

Editors:

Gail P. Anderson
Richard H. Picard
James H. Chetwynd

DTIC
ELECTE
JUN 2 7 1995
F

24 May 1995

PHILLIPS LABORATORY
Directorate of Geophysics
AIR FORCE MATERIEL COMMAND
HANSCOM AFB, MA 01731-3010

DTIC QUALITY INSPECTED 3

19950626 009

"This technical report has been reviewed and is approved for publication"

William A.M. Blumberg

WILLIAM A.M. BLUMBERG, Chief
Simulation Branch
Optical Environment Division

Roger A. Van Tassel

ROGER A. VAN TASSEL, Director
Optical Environment Division

REPORT DOCUMENTATION PAGE

1. AGENCY USE ONLY (Leave blank)	2. REPORT DATE 24 May 1995	3. REPORT TYPE AND DATES COVERED Scientific

4. TITLE AND SUBTITLE
PROCEEDINGS OF THE 17th ANNUAL CONFERENCE ON ATMOSPHERIC TRANSMISSION MODELS, 8-9 JUNE 1994.

5. FUNDING NUMBERS
PE: 62101F
PR: 3054
TA: GD
WU: 01

6. AUTHOR(S)
Editors: GAIL P. ANDERSON
RICHARD H. PICARD
JAMES H. CHETWYND

7. PERFORMING ORGANIZATION NAME(S) AND ADDRESS(ES)
Phillips Laboratory/GPOS
29 Randolph Road
Hanscom AFB, MA 01731-3010

8. PERFORMING ORGANIZATION REPORT NUMBER
PL-TR-95-2060(I)
SR, No. 274

9. SPONSORING/MONITORING AGENCY NAME(S) AND ADDRESS(ES)

10. SPONSORING/MONITORING AGENCY REPORT NUMBER

11. SUPPLEMENTARY NOTES
Volume I consists of pages 1 through 467
Volume II consists of pages 468 through 822, Including A1 through A46

12a. DISTRIBUTION/AVAILABILITY STATEMENT
Approved for public release; distribution unlimited

12b. DISTRIBUTION CODE

13. ABSTRACT (Maximum 200 words)

CONTAINS THE VIEWGRAPHS AND OTHER MATERIALS FOR THE 45 PAPERS PRESENTED AT THE 17th ANNUAL REVIEW CONFERENCE ON ATMOSPHERIC TRANSMISSION MODELS HELD AT THE GEOPHYSICS DIRECTORATE, PHILLIPS LABORATORY (AFMC), HANSCOM AFB, MA ON: 8-9 JUNE 1994.

DTIC QUALITY INSPECTED 3

14. SUBJECT TERMS
Atmospheric transmittance   Clouds
Aerosols   Radiative transfer
Atmospheric propagation   Optical turbulence

15. NUMBER OF PAGES
441

16. PRICE CODE

17. SECURITY CLASSIFICATION OF REPORT	18. SECURITY CLASSIFICATION OF THIS PAGE	19. SECURITY CLASSIFICATION OF ABSTRACT	20. LIMITATION OF ABSTRACT
Unclassified	Unclassified	Unclassified	SAR

TABLE OF CONTENTS

ATMOSPHERIC RADIATION CODES

AEROSOLS, CLOUDS AND SCATTERING

ENVIRONMENTAL APPLICATIONS

PREFACE

The Seventeenth DoD Tri-Service Review Conference on Atmospheric Transmission Models was held at the Geophysics Directorate of the USAF Phillips Laboratory at Hanscom AFB, Massachusetts on 7-8 June 1994.

More than 190 authors and participants presented 45 papers in the field of the coupling and interaction of optical and atmospheric phenomena. Sessions were held on Atmospheric Radiation Codes; Aerosols,Clouds and Scattering; Structure and Turbulence; High-Altitude Models and Measurements; Environmental Applications: a Poster Session featuring other topics was also held.

These volumes include the abstracts and hard-copy and any other material provided by the authors for their presentations. An Author Index and a partly overlapping attendee's list are also provided.

The abstracts are grouped at the back of the second volume on pages A1-A45 for ease of reference and perusal. The author list includes both abstract (A#) and paper references. Because of the delay between the submission of the abstract and the hard-copy there is not always an exact correspondence between the two.

Gail P. Anderson
Simulation Branch
Optical Environment
 Division

ix

17th ANNUAL TMOSPHERIC TRANSMISSION MODELING
ANNUAL REVIEW CONFERENCE

7 JUNE 1994
GEOPHYSICS DIRECTORATE/PHILLIPS LABORATORY

FASCODE: Validation and Applications

G.P. Anderson, J.H. Chetwynd, J. Wang*
Geophysics Directorate/PL
*NRC Fellow (on leave from Univ. of Michigan)

J.-M. Theriault
DREV/Defence Research Establishment Valcartier

L.W. Abreu
ONTAR, Inc.

S.A. Clough, J.-L. Moncet
Atmospheric and Environmental Research, Inc.

FASCOD3: Its Future

Who are we?
>Gail Anderson, Jim Chetwynd, Steve Miller, Jinxue Wang
>PL/GPOS

What are we doing? (FY94/95)
>VALIDATION
>GEOMETRY
>LASER/LIDAR Specificity
>Inversion Algorithm Development
>Collaboration with DOE's LBLRTM

How are we doing it?
>LBLRTM = Line-by-Line Radiative Transfer Model
>>Predicated on FASCODE; Funded for last 4 yrs by DOE
>>Responsible AER Authors: Clough, Worsham, Moncet
>FASE: FAScode for the Environment; Moncet, Gallery (AER)
>>and Wang (GPOS/NRC)
>Combination of best in both LBL Codes:
>>non-LTE, geometry, & lidar applications
>>>from FASCODE
>>vectorization, radiance algortithm, optimization
>>>from LBLRTM
>Inversion: Miller (GPOS) and Moncet (AER);
>>also Theriault (DREV) and Wisc.
>>Nadir: Univ. of Wisc. HIS Bomem ER-2 Spectrometer
>>Up-Looking: Wisc. AERI & HIS; Miller
>>Limb: Nadile (CIRRIS-1A); O'Neil (MSX)
>Validation:
>>IR: WMO ICRCCM (Ellingson) IR by Wang (GPOS)
>>mm: WMO ICRCCM (Westwater) mm by Chetwynd, Hoke
>>>(GPOS) & Clough (AER)

FASCODE: Fast Atmospheric Signature Code

Version 3 - β

AFGL:

F.X. Kneizys

S.A. Clough[1]

— Primary

G.P.Anderson   - UV, Constituent Profiles

J.H. Chetwynd   - Programming, Validation

L.W. Abreu   - LOWTRAN7 Compatibility

W.O. Gallery[1]   - Geometry

L.S. Rothman   - Line Atlas

M.L. Hoke   - Line Coupling

E.P. Shettle[2]   - Aerosols/Hydrometeors

R.D. Worsham[3]   - X-sections, etc.

[1] currently at Atmospheric and Environmental Research, Inc.
[2] currently at Naval Research Laboratory
[3] at Atmospheric and Environmental Research, Inc.

FASCODE: Fast Atmospheric Signature Code

Version 2 and Version 3-β

Visidyne:	H.J.P. Smith D.J. Dube M.E. Gardner	- contributions to FASCOD1C (1978)
	T.C. Degges	- NLTE theory (1977, 1985)
Sonicraft:	W.L. Ridgway R.A. Moose A.C. Cogley	- contributions to FASCOD2 (1985)
AER, Inc.:	R.G. Isaacs R.D. Worsham	- multiple scattering (1987) - programming contributions to FASCOD3 & MS (1988-91)
	S.A. Clough	- radiance algorithm, etc. (1990-1991)

HISTORY

DoD Plan for Atmospheric
Transmission Research and Development

AIR FORCE
- o Maintain DoD Standard Atmospheric Optical/IR models:
  (LOWTRAN), MODTRAN, FASCODE, HITRAN Database
- o Publish and Brief Model Updates
- o Conduct Annual Tri-Service Review
- o Measure and Model Propagation Effects of the
  Free Atmsophere

ARMY
- o Study Battlefield Conditions
- o Develop Models of Dust, Smoke, Chemicals, Propagation,
  and Diffusion Effects

NAVY
- o Develop Models for Marine Environment
- o Measure/Model Atmospheric Propagation

The Problem: *RADIATIVE TRANSFER*

1. The Atmosphere as a contaminant for E/O Systems
2. The Atmosphere as a signature source for natural variability

Solutions: *DEFINITIONS*

1. State variables (T, p, μ_i, Cld, Aer) along line-of-sight
2. Spectral Characteristics of the Path Variables
3. Viewing Geometry
4. E/O System Characteristics (Spectral Range & Resolution, Platform, Objective)

Solutions: *OPTIMIZATION*

1. Efficient Mathematical Algorithms (Line-by-Line)
2. Accurate Band Model Options
3. User Friendly
4. Validation/Documentation

Solutions: *DATA ANALYSIS*

1. Information Theory
2. Inversion Algorithm Development
3. Ground Truth
4. Validation and Error Estimation

DEFINITIONS

κ_i = absorption cross section, related to molecular properties, pressure (p), temperature (θ)

η_i = column amount of absorbing (i'th) species = $\int n_o ds$

ds = path increment; n_o = volumn density

τ_i = optical depth = $\kappa_i \acute{\eta}_i$

T_i = transmittance = exp $(-\tau_i)$

T_{mol} = total molecular transmittance = $\P T_i = T_1 \cdot T_2 \cdot T_3 \cdot T_4 \cdots$

T_T = total transmittance = $T_{mol} \cdot T_{continua} \cdot T_{scat} \cdot T_{aerosol}$

$B(\theta)$ = Planck Function for temperature θ

$\pi \mathscr{F}$ = Solar (Lunar) Source Function

$\mathscr{E}$ = Non-LTE Source Term

W = Weighting Function = (dT_T/ds)

OPERATIVE EQUATION:

$\mathfrak{R}$ = Thermal Radiance = $\int B(\theta) \, dT_T = \int B(\theta) \, (dT_T/ds) \, ds$

AND FOR A SINGLE LAYER:

$\mathfrak{R} = \int B(\theta) \, dT_T = B(\theta) \, [1-T_T]$

and, finally, combining thermal, solar, and non-LTE sources
with multiple scattering,

one can replace the Planck source function with a more general
source function:

$$B(\theta) \Rightarrow J(\tau, \zeta)$$

$J(\tau, \zeta)$ = general source function dependent on optical depth (τ) and
viewing geometry (ζ = zenith & azimuth cosines)

$$= (\omega_o / 4\pi) \, \pi \mathscr{F} \, T(\zeta) \, \wp \qquad \text{[SOLAR]}$$

$$+ [1-\omega_o] \, B(\theta) \qquad \text{[THERMAL]}$$

$$+ \mathscr{E} \qquad \text{[N-LTE]}$$

$$+ J_{MS} \qquad \text{[MUL.SCAT.]}$$

where:
ω_o = single scattering albedo = $\tau_s / (\tau_s + \tau_a)$
$T(\zeta)$ = transmittance from top of atmosphere to layer
$\wp$ = scattering phase function
J_{MS} = m.s. for both solar and thermal terms (complicated)

and other terms are as previously defined!!

* VALIDATION for Signatures

    1. targets/pollutants against backgrounds-
        estimate of variability
        estimate of go/nogo
        estimate of true/false; reduce false ID
        incorporate "target signatures"

    2. atmospheric specification
        local and/or global "weather"
        atmospheric contaminants become signatures

    3. higher resolution spectroscopy with high spectral
        accuracy may minimize confusion, increasing
        signal/noise for both contaminants and state
        specification.

* REAL-TIME ANALYSIS with speed

    1. Line-by-line (LBL) codes and their derivatives work -
        "exact" physics must remain state-of-the-art;
    Because physicists drive technology to higher resolution:
        lidar/laser applications
        interferometers at $<.01cm-1$ resolution
        remote sensing issues: line coupling, mm-wave
        new/old/unsettled issues:
            CFC x-sections, $H2O$ continua, $CO2$ χ factor
            NLTE issues
    However:
    "LBL" is slow, slow, slow!!!

    2. Band Models (pragmatic,expedient parameterizations) trail
    "LBL" in "state-of-the-art",
        but they are the codes of the NOW and FUTURE for
        issues and analyses with compatible spectral resolution!

FASCODE

WAVENUMBER CM-1

10

SPECTRE EXPERIMENT: case1

Solid: FASCOD3 calculation
Dot: LBLRTM calculation

Residual: FASCOD3 minus LBLRTM

Figure 1

11

SPECTRE EXPERIMENT: case2

Solid: FASCOD3 calculation
Dot: LBLRTM calculation

Residual: FASCOD3 minus LBLRTM

RADIANCE (mw/m²-str-cm⁻¹)

WAVENUMBER(cm⁻¹)

Figure 2

12

SPECTRE EXPERIMENT: case3

Solid: FASCOD3 calculation
Dot: LBLRTM calculation

Residual: FASCOD3 minus LBLRTM

Figure 3

13

SPECTRE EXPERIMENT: case4

Solid: FASCOD3 calculation
Dot: LBLRTM calculation

Residual: FASCOD3 minus LBLRTM

Figure 4

14

Fig. 4. Down-welling (zenith up-looking) radiance in the microwave region from 0 to 8 cm^{-1} calculated with FASCOD3 under 1976 U. S. Standard Atmosphere conditions. Location of the ITRA/mw channels are indicated.

ITRA: microwave
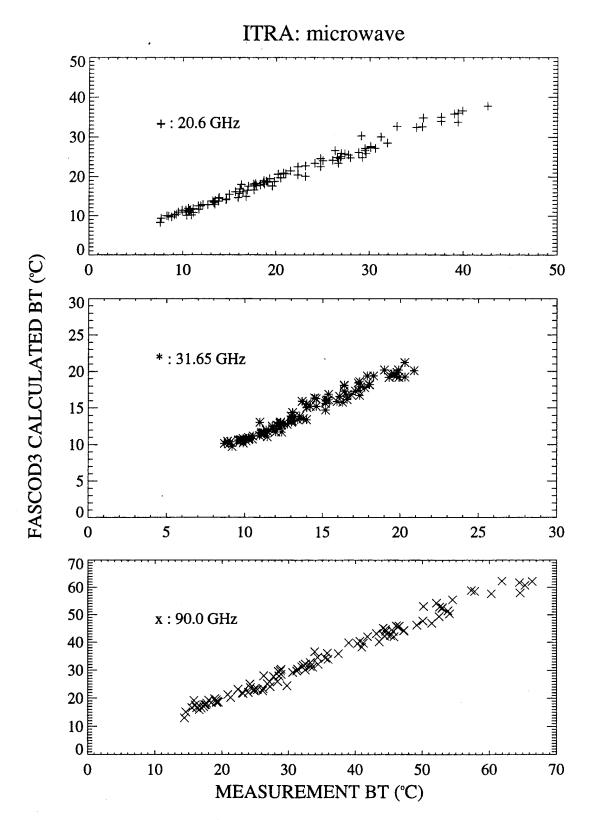
Fig. 5. Correlation plots of FASCOD3 calculated brightness temperatures and measured brightness temperatures supplied by E. Westwater.

16

FASCODE - FASCOD3P (1Q-1992)
Fast Atmospheric Signature CODE
Version 3 - Prelimary

POINTS OF CONTACT:

Gail P. Anderson/James H. Chetwynd
Simulation Branch
Optical Environment Division
Geophysics Directorate/PL
  29 Randolph Road
Hanscom AFB, MA 01731-3010
617-377-2335/2613; FAX xxx-8900.

FASCODE

OBJECTIVE: To provide:

o "exact" spectroscopic calculations of:

       molecular radiative transfer properties
       Voigt line shape
       LTE and non-local thermodynamic equilibrium (non-LTE)
       line-by-line (LBL) code
       heavy molecule x-sections (i.e. chloro-fluorocarbons, etc.)
       laboratory and atmospheric simulations
       provisions for:
         Non-molecular (clouds, aerosols, geometry, etc.)
            from LOWTRAN/MODTRAN
       altitude range: open
       lines-of-sight: open
       spectroscopic constants from HITRAN92 and/or other sources
       x-sections from HITRAN92 and/or other sources
       non-LTE populations from SHARC

FASCODE

TECHNICAL DESCRIPTION:

FASCODE calculates atmospheric radiance ($\mathfrak{R}$) and transmittance (T)
for the following conditions:

full Voigt spectral resolution from 0 to 50000 cm-1
"exact" line-by-line radiative transfer in UV/Vis/IR
optimized line shape and layering
scattering: Rayleigh, Mie, single, multiple
6 climatological descriptions: tropical, mid-lat sum/win,
       subarctic sum/win, and US Std. for
6 atmospheric gases: H_2O, CO_2, O_3, N_2O, CO, CH_4, plus
a "default" profile for each HITRAN gas (up to 35 species)
10 "greenhouse" (CFC) gas cross-sections and profiles
aerosol profiles:
       tropospheric: rural, urban, desert, Navy, fogs,
       stratospheric: background, volcanic (background,
              aged, high, fresh, and extreme)
clouds/rain: cumulus, altostratus, stratus, strato cumulus,
       nimbostratus, cirrus (standard, subvisual and NOAA)
geometric lines-of-sight: H1 (observer location) to H2
       (end of path) with H1 or H2 = surface, space, or
       anyplace within.
radiance sources: LTE, non-LTE, thermal and surface radiation
primitive target specification
laser applications
ground emittance and reflectance
user profile specifications
instrument specifications: plot, scan, filter options
weighting functions, primitive flux calculations
external data sources: HITRAN and SHARC

FASCODE

BACKGROUND:

o Requirement:

an exact spectral simulation code, containing the true
physical equations of radiative transfer.

DoD standard for judging the accuracy of
more pragmatic and/or efficient algorithms

** need cannot be overstated **
provides a window upon the actual workings
of the atmosphere (and lab)

o Penalty:

FASCODE is ponderous and time-consuming
no solar capability
large storage requirements for some paths

o Code development/maintenance is mandated by:

DoD 1978/83 Atmospheric Transmission Plan
no single "sponsor" for the code.

FASCODE

ASSUMPTIONS/CAVEATS:

o Accuracy:
   FASCODE is spectroscopicly a 1-3% code, with caveats

   line shape description is generally within 1%

   end-to-end accuracy:
          spectroscopic line parameters (1-3%)
          scattering algorithms (10%)
          LTE field descriptors, p, T, N(i),(all at 5-10%)
          non-LTE field descriptors, excited state populations
               from SHARC (approximately 10%)
          governing physical equations, molecular (1-5%),
               particulate (5-20%)

NOTE: Discrepancies with measurements can often be used to infer
the state of the atmosphere through inversion or to define the need
for improved spectroscopic identifications.

In summary:		
	altitude limits	0-+120km (LTE, non-LTE)
	spectral limits	0-50000cm-1 (Δ 500cm-1)
	accuracy	1-3% for spectroscopy
	field descriptors	
	LTE & NLTE	5-15%
	applications	thermal radiance
		transmittance
		contrast studies
		surveillance
		plumes
		laser/lidar
		high spectral resolution
		microwave

FASCODE

CURRENT STATUS:

o FASCOD3P access:

- available in FORTRAN for mainframe or workstation
- implemented on Cyber, Cray, Apollo, VAX, and SUN
- NOS, VMS, and UNIX/ULTRIX operating systems
- transfer medium: 9-track magnetic tape

successful in-house PC version is under development

REMINDERS:

o negatives:
- not particularly user-friendly
- computer time and storage intensive
- no solar capabilty

o balance between "first principles" scientific algorithms
versus more expedient and rapid codes (such as MODTRAN, LOWTRAN,
SHARC, and their derivatives)

o singular capabilities:
- 15 micron CO2 line coupling
- O2 mm line coupling
- chloro-fluorocarbon (CFC) cross-sections
- high altitude weighting functions
- high spectral resolution (> 1cm-1) calculations at
low altitude
- laser/lidar transmittances, etc.

FASCODE

PLANNED UPGRADES:

o   maintain state-of-the-art physics and
       state-of-the-art computational speed

o   new physics algorithms include:
       improved line coupling (CO2 and O2)
       line shape (CO2 and H2O),
           important for remote sensing applications

o   new radiance algorithm with:
       compatible multiple scattering,
       solar insolation, and flux capability ;

o   more realistic/pratical weighting function formulations

o   AND with cooperation from DOE, a major effort to:
       implement vectorized coding and efficient/accurate
       flux divergence coding, ultimately intended for
       parallel processors

FASCODE

USER COMMUNITY: There are over 100 new users of FASCOD3P, plus over 200 users of FASCOD2. Users and uses include:

SSGM (Strategic Scene Generation Model)	SDIO
TDA (Tactical Decision Aids)	AF
EOSAEL (Army Atmos. Models)	Army
SPIRITS (Target Surveillance Code)	AF
CIRRIS data analysis	AF
Climate studies	DOE
Validation (SHARC, MODTRAN, MOSART)	AF
etc.	+200

o Suitable for:

- all non-solar LOWTRAN/MODTRAN studies
- recalculating entire systems designs and algorithms
- simulations relative to surveillance implications
- implement the CFC cross-sections for 8-10um window region
- evaluate/validate all systems codes

[any application that involves exact or any broader spectral resolution under both equilibrium and non-LTE conditions may be suitable for FASCODE simulation]

FASCODE

AVAILABILITY:

FASCODE is available for:
mainframe computers, work stations, and, potentially PC's.

The word size and FORTRAN 77 coding are appropriately formulated with double precision declarations.

FASCODE is, in general, not being incorporated into assorted larger codes, e.g. SSGM, EOSAEL, SPIRITS, TDA, etc., because of its required storage and running times.

However, it is usually maintained "off line" for validation of more pragmatic codes.

MODTRAN3, MODTRAN4 AND BEYOND

by

A. Berk, P.K. Acharya, L.S. Bernstein, D.C. Robertson
Spectral Sciences, Inc., Burlington, MA

G.P. Anderson, J.H. Chetwynd, F.X. Kneizys,
L.M. Kimball, J.J. Vail
Geophysics Directorate, Phillips Laboratory, Hanscom AFB, MA

E.P. Shettle, Naval Research Laboratory, MD

L.W. Abreu, ONTAR Corp., North Andover, MA

J. Conant, Aerodyne Research, Inc., Billerica, MA

Presented At

17th Annual Review Conference
on Atmospheric Radiation Models
7 JUNE 1994

OUTLINE

- MODTRAN2 OVERVIEW
- MODTRAN3 UPGRADES
  - NEW FEATURES
  - SAMPLE RESULTS
- MODTRAN4 AND BEYOND
- SUMMARY

MODTRAN2 / FASCOD3P COMMON ELEMENTS

- PREDICT SPECTRAL TRANSMITTANCES, RADIANCES, SOLAR IRRADIANCES AND WEIGHTING FUNCTIONS FOR ARBITRARY LINES-OF-SIGHT IN THE ATMOSPHERE.

- UV TO MICROWAVE (.2 to $\infty \mu m$, 0 to 50,000cm^{-1})

- DEFAULT DATABASES

  MOLECULAR PROFILES & CONTINUA CROSS-SECTIONS
  AEROSOL, CLOUD, RAIN & FOG MODELS
  SOLAR/LUNAR SOURCE SPECTRA
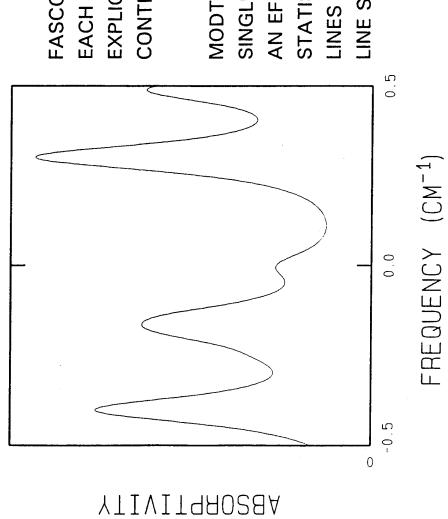
- SPHERICAL REFRACTIVE GEOMETRY

- SINGLE & MULTIPLE SCATTERING

- INSTRUMENT CONVOLUTION FUNCTIONS

- HITRAN92 COMPATIBILITY

28

MODTRAN2 FEATURES

- 2 cm^{-1} RESOLUTION FROM 1 cm^{-1} BAND MODEL

- EMBEDS LOWTRAN

- TWELVE MOLECULAR RADIATORS

  H_2O CO_2 O_3 N_2O CO CH_4 O_2 NO SO_2 NO_2 NH_3 HNO_3

- LOCAL THERMODYNAMIC EQUILIBRIUM ONLY

  UPPER ALTITUDE LIMIT OF $\approx$ 60 km

- SOLAR MULTIPLE SCATTERING

- 10 TO 1000 TIMES FASTER THAN FASCODE

- MANY APPLICATIONS

  BACKGROUNDS, POLLUTANTS, TARGETS, PLUMES, CLIMATOLOGY, INVERSION ALGORITHMS, E/O DESIGN, DATA ANALYSIS, ETC.
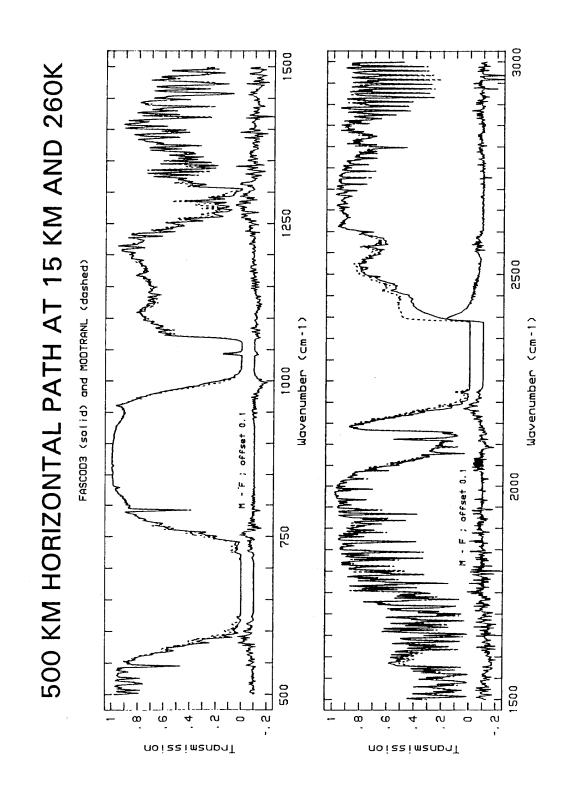
BAND MODEL APPROACH

FASCODE INTEGRATES OVER
EACH SPECTRAL BIN BY
EXPLICITLY SAMPLING ALL
CONTRIBUTING LINE SHAPES.

MODTRAN INTEGRATES IN A
SINGLE STEP BY DEFINING
AN EFFECTIVE NUMBER OF
STATISTICALLY DISTRIBUTED
LINES AND AN AVERAGE
LINE STRENGTH.

ABSORPTIVITY

FREQUENCY (CM^{-1})

-0.5   0.0   0.5

MODTRAN2 / FASCOD3 COMPARISON

500 KM HORIZONTAL PATH AT 15 KM AND 260K

FASCOD3 (solid) and MODTRANL (dashed)
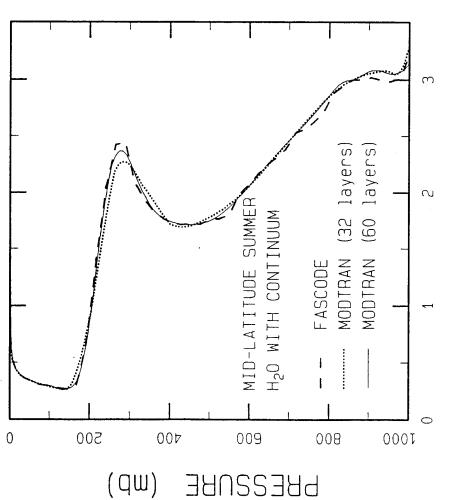
MODTRAN3 UPGRADES

- INCREASED LAYER RESOLUTION

- SPECTRALLY VARYING SURFACE ALBEDOS

- CFC CROSS-SECTIONS AND PROFILES

- UV NO_2, SO_2 & NEW O_3 CHAPPUIS-WULF CROSS-SECTIONS

- IMPROVED SINGLE SCATTER SOLAR RADIANCE ALGORITHM

- NEW MULTIPLE SCATTERING ROUTINE

- RE-INTRODUCED CO_2 CONTINUUM

- UPGRADED SOLAR SOURCE SPECTRUM

- HITRAN94 BASED BAND MODEL DATA (175 TO 325K)

- ADJUSTED TREATMENT OF WATER VAPOR CONTINUA

- REFINEMENT OF LOW SUN CALCULATIONS

INCREASED LAYER RESOLUTION

- THE MAXIMUM NUMBER OF LAYERS IS NOW DEFINED IN A PARAMETER STATEMENT.
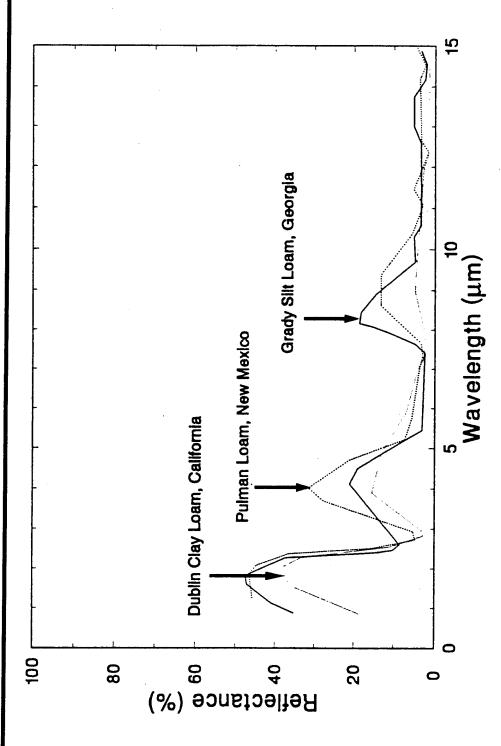
- ADDITIONAL LAYERS FACILITATE CONVERGENCE IN COOLING RATE CALCULATIONS.

MID-LATITUDE SUMMER
H_2O WITH CONTINUUM

- - - FASCODE
.... MODTRAN (32 layers)
——— MODTRAN (60 layers)

PRESSURE (mb)

COOLING RATE (K/DAY)
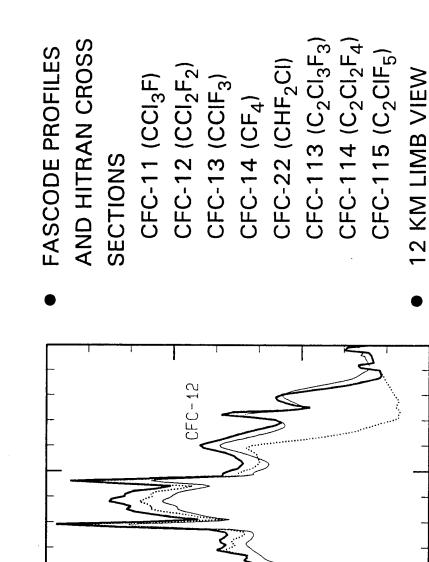
SPECTRALLY VARYING SURFACE ALBEDOES

THE IR/EO SYSTEMS HANDBOOK, Vol 1, SOURCES OF RADIATION, G.J. ZISSIS, Ed.

CHLOROFLUOROCARBONS

- **FASCODE PROFILES AND HITRAN CROSS SECTIONS**
  - CFC-11 (CCl_3F)
  - CFC-12 (CCl_2F_2)
  - CFC-13 ($CClF_3$)
  - CFC-14 (CF_4)
  - CFC-22 (CHF_2Cl)
  - CFC-113 ($C_2Cl_3F_3$)
  - CFC-114 ($C_2Cl_2F_4$)
  - CFC-115 (C_2ClF_5)

- **12 KM LIMB VIEW**

EXTENSION INTO THE ULTRAVIOLET
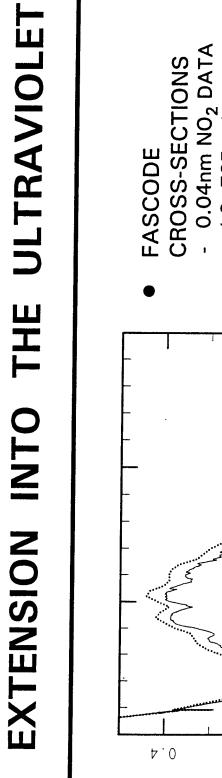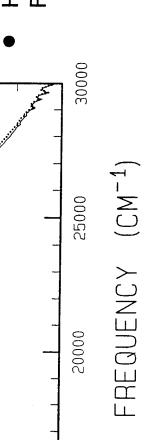
- FASCODE
  CROSS-SECTIONS
  - 0.04nm NO_2 DATA
    (.2-.725μm)
  - 0.1nm SO_2 DATA
    (.19-.403μm)
  - TEMPERATURE
    DEPENDENT O_3
    CHAPPUIS-WULF
    DATA (1. TO .25nm
    RESOLUTION FROM
    .407 TO 1.089μm)

- HALF-LIMB VIEW
  FROM 15 KM

MODTRAN2
MODTRAN3

FREQUENCY (CM^{-1})
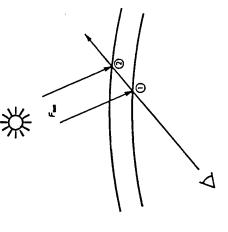
TRANSMITTANCE

SINGLE SCATTER SOLAR RADIANCE

- **EXACT EXPRESSION**

$$\Delta I_{ss} = F_{sun} \, P(\theta) \int_{\tau_{sct}(2)}^{\tau_{sct}(1)} \tau_{abs}^{L} \, \tau_{sct}^{sun} \, d\tau$$

- **MODTRAN2**
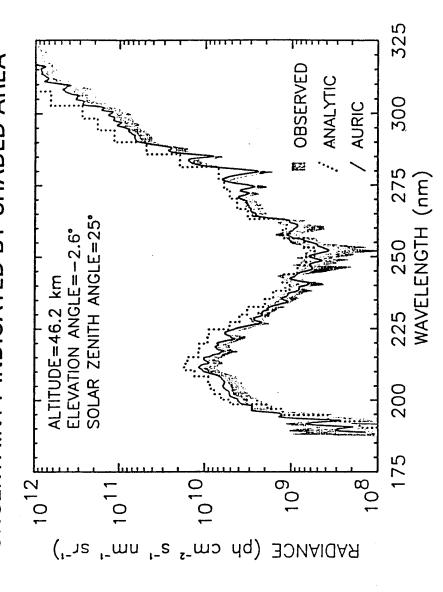
$$\Delta I_{ss} \approx F_{sun} \, P(\theta) \, [\tau_{sct}(1) - \tau_{sct}(2)] \; \frac{\tau_{abs}^{L}(1) \, \tau_{sct}^{sun}(1) + \tau_{abs}^{L}(2) \, \tau_{sct}^{sun}(2)}{2}$$

- **MODTRAN3**
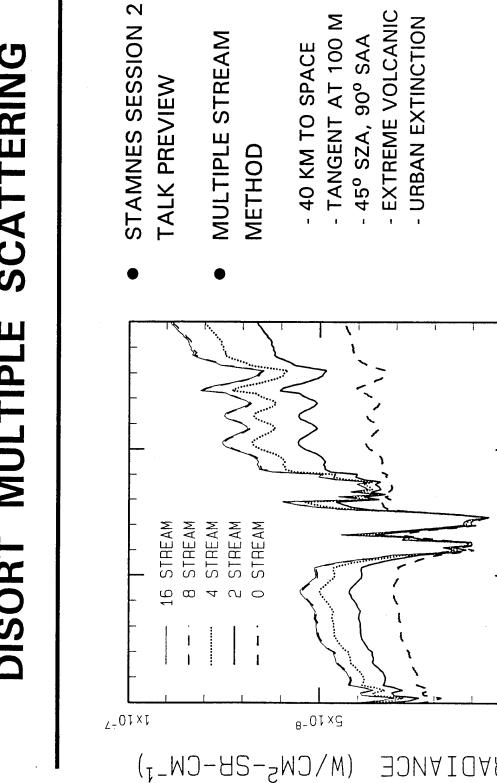
$$\Delta I_{ss} \approx F_{sun} \, P(\theta) \, \ln\left(\frac{\tau_{sct}(1)}{\tau_{sct}(2)}\right) \; \frac{\tau_{ext}^{L}(1) - \tau_{ext}^{L}(2)}{\ln[\tau_{ext}^{L}(1) \, / \, \tau_{ext}^{L}(2)]}$$

SINGLE SCATTER VALIDATION

- BALLOON-BORNE UV SPECTROMETER DATA
  - OVER PALESTINE, TEXAS (16APR83)
  - UNCERTAINTY INDICATED BY SHADED AREA
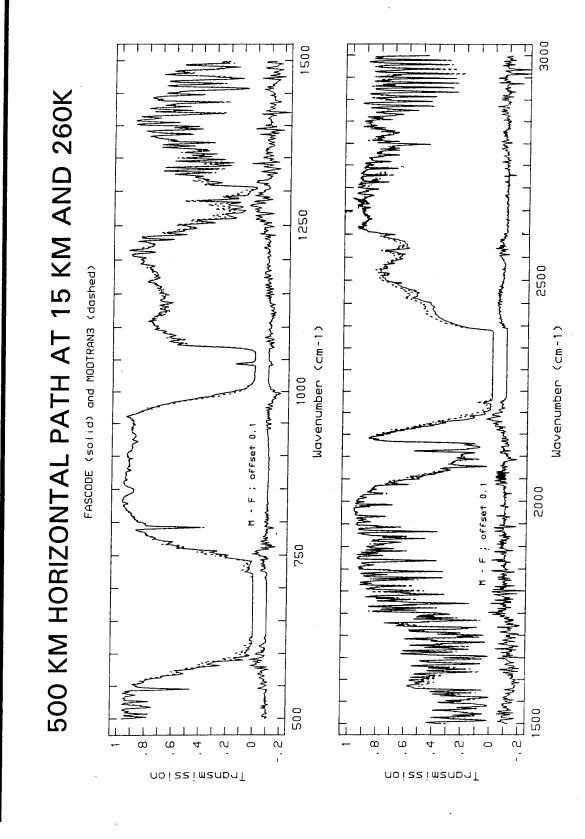
DISORT MULTIPLE SCATTERING

- STAMNES SESSION 2 TALK PREVIEW

- MULTIPLE STREAM METHOD
  - 40 KM TO SPACE
  - TANGENT AT 100 M
  - 45° SZA, 90° SAA
  - EXTREME VOLCANIC
  - URBAN EXTINCTION

Legend:
- 16 STREAM
- 8 STREAM
- 4 STREAM
- 2 STREAM
- 0 STREAM

Y-axis: RADIANCE (W/CM^2-SR-CM^{-1})
- 1×10^{-7}
- 5×10^{-8}
- 0

X-axis: FREQUENCY (CM^{-1})
- 3000
- 3500
- 4000
- 4500

MODTRAN3 / FASCOD3 COMPARISON

500 KM HORIZONTAL PATH AT 15 KM AND 260K

FASCODE (solid) and MODTRAN3 (dashed)

MODTRAN4 AND BEYOND

- AUTOMATED COOLING RATE/FLUX CALCULATIONS

- INCORPORATION OF NRL CLIMATOLOGIES VIA SAG

- UPGRADED AEROSOL DATA (AFTER PINATUBO)

- $0.2CM^{-1}$ BAND MODEL

- VECTOR OPTIMIZATION

  - PARALLEL PROCESS SPECTRAL CALCULATIONS

COOLING RATES / VERTICAL FLUXES

CAN BAND MODELS PREDICT ACCURATE COOLING RATES (<.2 K/DAY) AND FLUXES (<2%)?   YES!!!
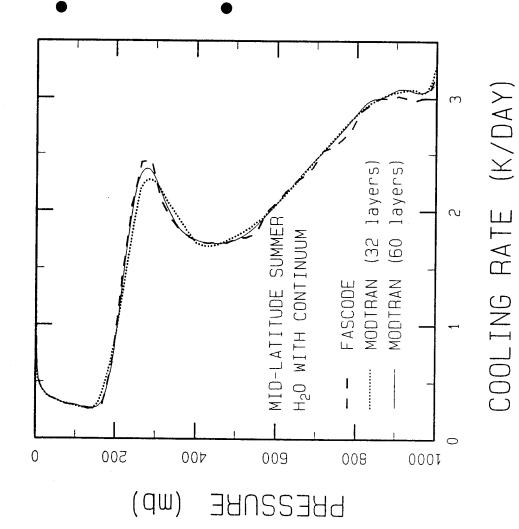
BUT, MODTRAN REFINEMENTS ARE REQUIRED.

- UPGRADE THERMAL EMISSION CALCULATION
    - REPLACE LINEAR-IN-TAU WITH BAND MODEL EQUIVALENT

- UNIFY GEOMETRY ROUTINES
    - ASSUME DENSITIES VARY EXPONENTIALLY WITH ALTITUDE
    - ASSUME TEMPERATURES VARY LINEARLY WITH ALTITUDE

- IMPLEMENT O_3 3-PARAMETER CURTIS-GODSON METHOD

- IMPROVE LINE OVERLAP MODEL
    - COMBINE COINCIDENT & NEARLY COINCIDENT LINES

- REVISE SCATTERED RADIANCE CALCULATIONS

42

SAMPLE COOLING RATE CALCULATION
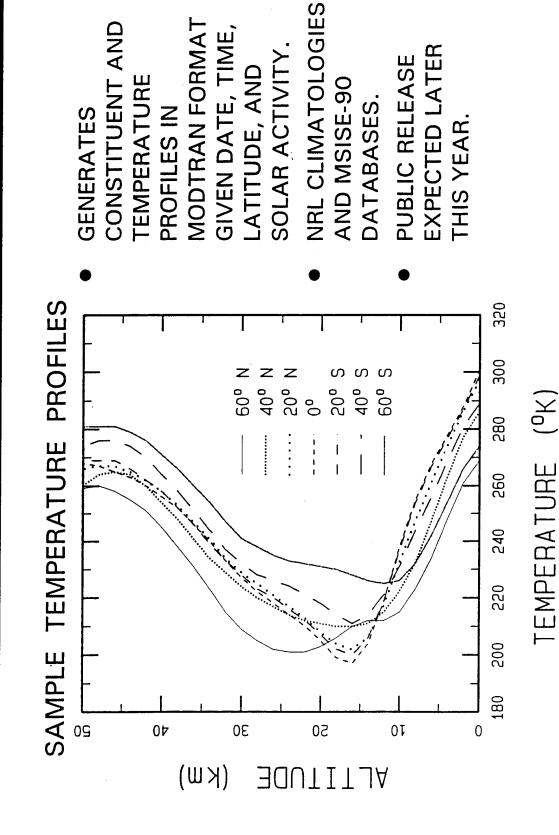
- DIFFERENCES OF LESS THAN 0.1 K/DAY AT ALMOST ALL ALTITUDES.

- DISCREPANCIES NEAR THE SURFACE ARE THOUGHT TO ARISE FROM DIFFERENCES IN THE H_2O CONTINUUM CALCULATIONS.

MID-LATITUDE SUMMER
H_2O WITH CONTINUUM

- - - FASCODE
..... MODTRAN (32 layers)
――― MODTRAN (60 layers)

PRESSURE (mb)

COOLING RATE (K/DAY)

43

THE ATMOSPHERE GENERATOR - SAG

- GENERATES
  CONSTITUENT AND
  TEMPERATURE
  PROFILES IN
  MODTRAN FORMAT
  GIVEN DATE, TIME,
  LATITUDE, AND
  SOLAR ACTIVITY.

- NRL CLIMATOLOGIES
  AND MSISE-90
  DATABASES.

- PUBLIC RELEASE
  EXPECTED LATER
  THIS YEAR.

SAMPLE TEMPERATURE PROFILES

60° N
40° N
20° N
0°
20° S
40° S
60° S

ALTITUDE (KM)

TEMPERATURE (°K)

SUMMARY / STATUS

- MODTRAN IS CONTINUOUSLY BEING UPDATED TO MEET THE NEED OF ALL ITS USERS.

- PUBLIC RELEASE OF MODTRAN3 IS EXPECTED LATER THIS YEAR.

- MODTRAN4 RELEASE IS PLANNED FOR FY95.

- MODTRAN CAN BE OBTAINED FROM THE NATIONAL CLIMATIC DATA CENTER - NOAA (704) 259-0682

- QUESTIONS/PROBLEMS WITH MODTRAN SHOULD BE SENT TO GAIL ANDERSON OR JIM CHETWYND: FAX (617) 377-8900

MOSART

An Update on the Moderate Spectral Atmospheric Radiance and Transmittance Code

by

William M. Cornette
Photon Research Associates

Prabhat K. Acharya and David C. Robertson
Spectral Sciences, Inc.

Gail P. Anderson and James H. Chetwynd
Geophysics Directorate, Phillips Laboratory (PL/GPOS)
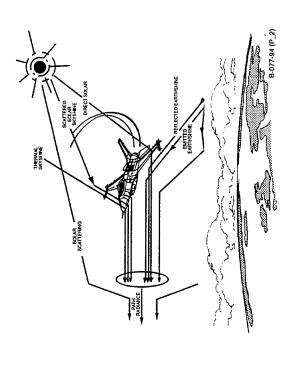
Presented at the
1994 Annual Review Conference on Atmospheric Models
Hanscom AFB, Massachusetts
7-8 June 1994

MOSART RADIATIVE ENVIRONMENT CODE

- Merging of MODTRAN and APART Capabilities

- Observables-Driven Architecture

- Molecular Absorption
  - 2 cm^{-1} Resolution
  - 0.2 - 50 μm + Millimeter Wave
  - Five Parameter Voight Model

- Three-Flux Multiple Scattering

- Turbulence/Sky Noise

- Forward In-Scatter

- Backgrounds
  - Contrast
  - Structured
  - Global Data Base
  - Bidirectional Materials

- Global Atmosphere Data Base

- Hydrometeors
  - Clouds (Water/Ice)
  - Fog
  - Rain
  - Snow

B-077-94(6-1).2

MOSART APPLICATIONS

- **LOS Attenuation and Radiance**
  - Atmospheric Sensitivity
  - Atmospheric Profiling

- **Horizon and Limb Scenes**

- **Terrain Scenes**
  - Deterministic Scene Modelling
  - Atmospheric Correction
  - Structured Statistical Scene Modelling

- **Cloud Scenes**

- **Target Signatures**
  - Hardbody
  - Exhaust Plumes
  - Pollution Studies

- **Turbulence**
  - Scintillation
  - Image Blur
  - Path Radiance Variability

- **LTE/NLTE Coupled Code (Pending)**

CURRENT STATUS OF MOSART

- **MOSART 1:**
  - Initial Version Complete (FY 93)
  - Draft User's Manual Completed
  - Beta Evaluation in Progress
  - Earth/Skyshine Added
  - Molecular Data Base Upgrade
  - Global Aerosol/Visibility Model
  - Tangent Point Specified by Latitude/Longitude
  - Minor Upgrades/Modifications

- **MOSART 2:**
  - Upgrading Global Surface Data Bases
    - -- Increasing Resolution
    - -- New Thermal and Optical Properties
    - -- Improved Clutter Model
  - Interface with SHARC/SAMM Atmospheric Generator
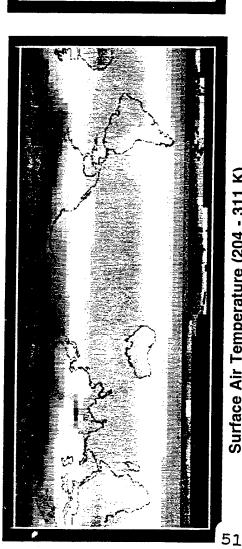
ATMOSPHERIC CHARACTERIZATION
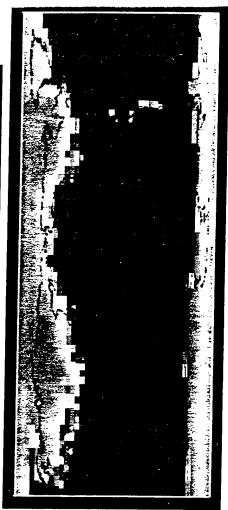
- **Expanded Basic MODTRAN Profiles**

- **Atmospheres:**
  - 23 Model Atmospheres
  - Global Atmosphere
  - User-Defined Atmospheres

- **Aerosol Types and Haze Profiles:**
  - MODTRAN Aerosols Plus Temperature-Dependent Background Stratospheric
  - MODTRAN Plus Atmosphere Dependent Haze Profiles

- **Hydrometeors:**
  - Four Fog Models
  - Eleven Non-Precipitating Clouds
  - Five Precipitating Clouds
  - Five Rain Models
  - Six Snow Models
  - User Defined Profile

- **Cirrus Clouds:**
  - Standard (64 μm + Extinction)
  - Subvisual (4 μm + Extinction)
  - Heymsfield (Temperature Dependent)

B-077-94(6-1).6
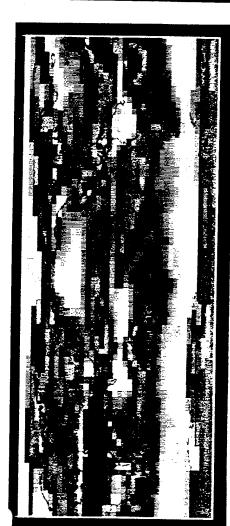
GLOBAL CLIMATOLOGY DATA BASES
APRIL

Snow Cover (0 - 100%)

Cirrus Cloud Cover (0 - 34%)
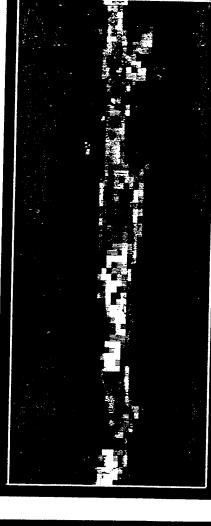
Surface Air Temperature (204 - 311 K)

Total Cloud Cover (0 - 100%)
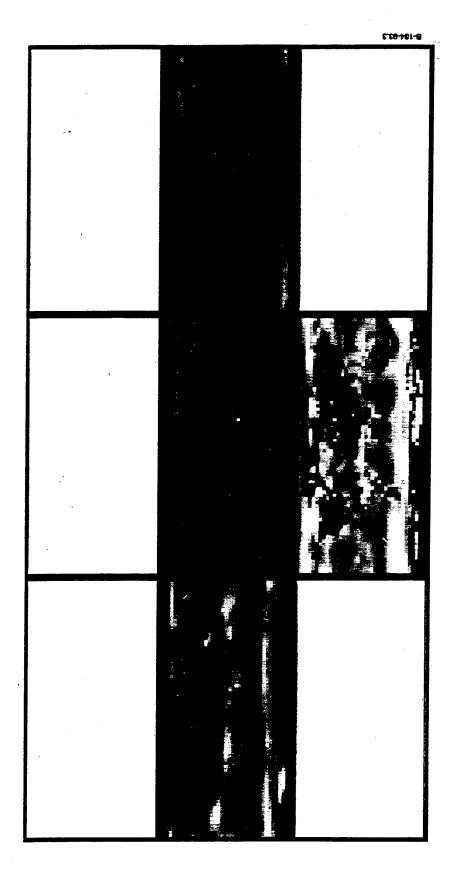
- Five Year (1985 - 89) Average From NOAA Nimbus-7

B-077-94(6-1),6

51

NCAR PROFILE DATA

- 5° x 5°, Monthly Averages
- Pressure, Temperature, Dew Point Temperature
  (Surface, 850 mb, 700 mb, 500 mb, Tropopause)

B-077-94(6-1).7

BACKGROUND REPRESENTATION

- **Composite Terrain Scenes:**
  - Global Coverage (10 Minute Resolution)
  - 35 Reference Scenes
  - Monthly Snow Cover (4.5° Resolution)
  - Water (10 Minute Resolution)
  - Urban Areas (in Development)

- **Terrain Altitude (10 Minute Resolution)**

- **Terrain Materials:**
  - 28 Types
  - Optical Properties
  - Thermal Properties

- **Broad Band Heat Transfer:**
  - Solar Loading
  - Thermal Loading
  - Diurnal Temperature Cycle

- **Space:**
  - Zodiacal Light
  - Mean Star Radiance
  - Galactic and Extra-Galactic Radiances

B-077-94(6-1).9

GLOBAL TERRAIN ALTITUDES

- Obtained from National Geophysical Data Center

- Resolution: 10 Minute ≈ 18.5 km
- Altitudes: -121 to 7833 Meters at 1 Meter Resolution
  - Dead Sea: -400 m
  - Mount Everest: 8848 m
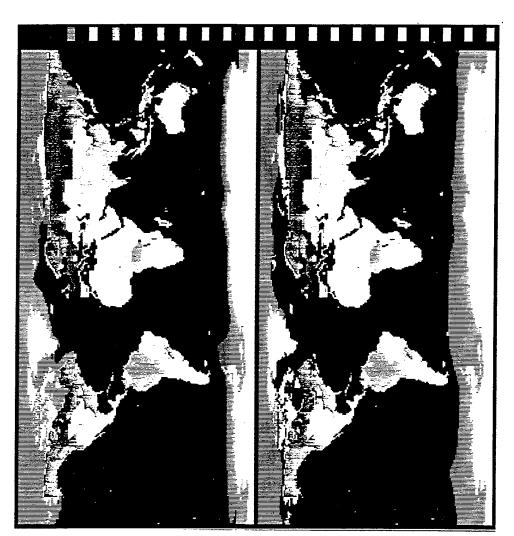
SURFACE CLASSIFICATION MAP

Photon Research Associates, Inc.

B-077-94(6-1).10

Scene Types

Open Ocean/Lake
Multi-Year Sea Ice
Continental Ice
Forested Low Relief
Flat Agricultural
Forested Mountains/Cultural
Pine Forest
Mixed Forest/Farmland
Tropical Forest
Tropical Land/Sea Interface
Desert Pavement with Dunes
Desert Land/Sea Interface
Southern California Land/Sea Interface
Scrub Desert
Tropical Savannah
Grassland/Savannah
Scrub/Chaparral
Subarctic Rocky Land/Sea Interface
Arctic Tundra Land/Sea Interface
Arctic Mountains with Scrub
Tundra

APR - SEPT

OCT - MAR

- 1° Spatial Resolution

ECOSYSTEM CLASSIFICATIONS

- **10 Minute Resolution**

PRELIMINARY TERRAIN MATERIAL MAP
(10 MINUTE RESOLUTION)

Photon Research Associates, Inc.

B-077-94(6-10).3

B-077-94(6-1).12

57
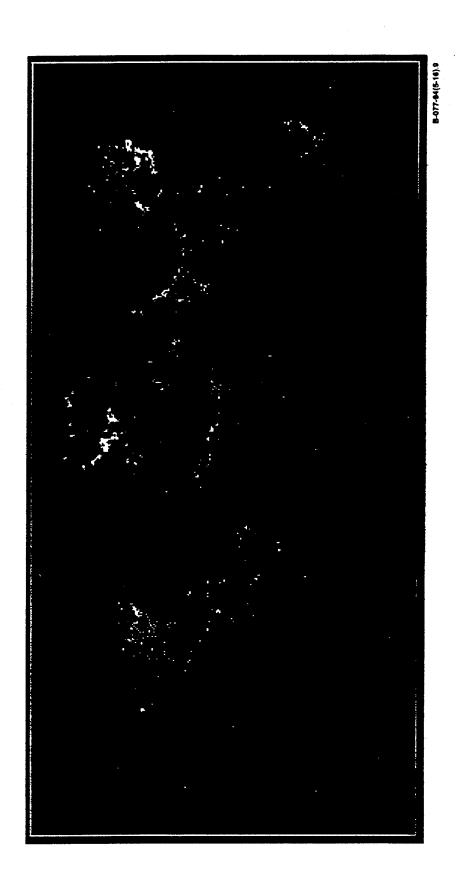
FRACTION WATER COVERAGE
(10 MINUTE RESOLUTION)

WORLD AT NIGHT
(~20 MINUTE RESOLUTION)

B-077-94(5-16),9

B-077-94(6-1),14
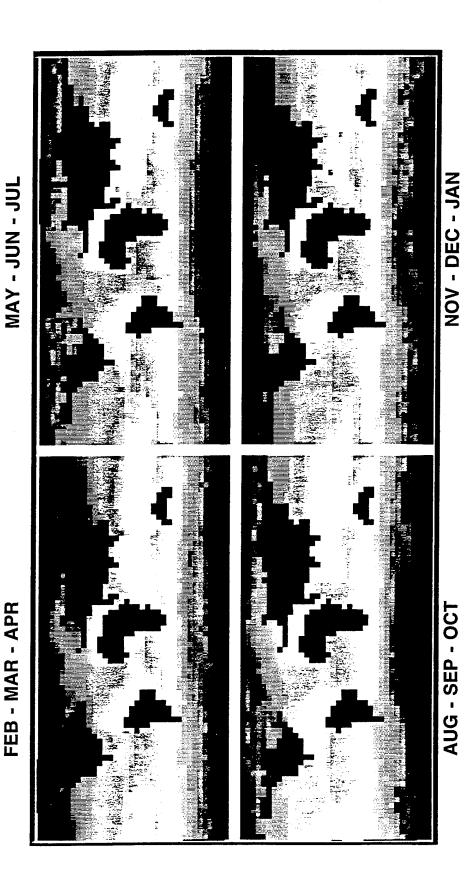
PRELIMINARY BOUNDARY LAYER AEROSOL MAP
(10 MINUTE RESOLUTION)

B-077-94(5-18),8

B-077-94(6-1),15

Photon Research Associates, Inc.

60

OCEAN SURFACE TEMPERATURE

FEB - MAR - APR

MAY - JUN - JUL

AUG - SEP - OCT

NOV - DEC - JAN

Ref.: S. Levitus, Climatological Atlas of the World Ocean
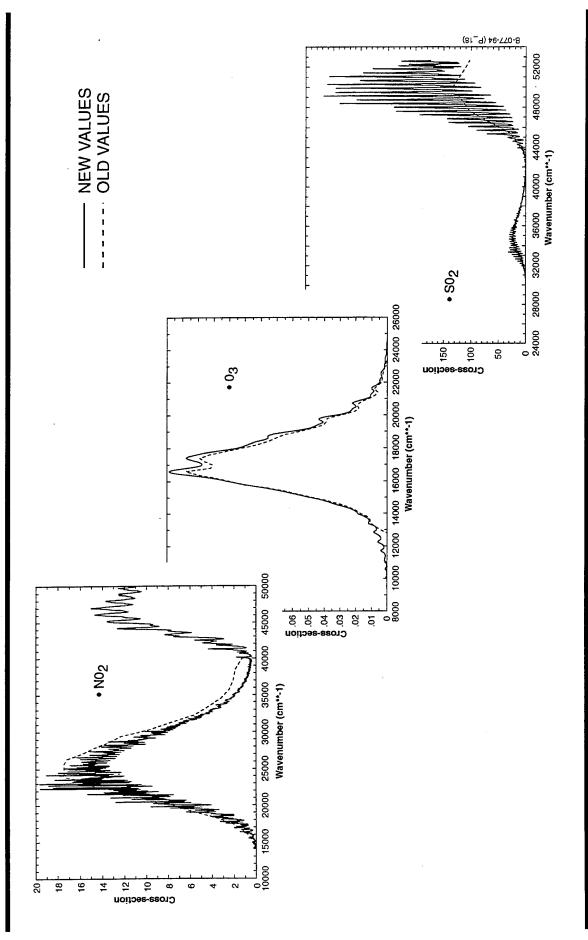
RADIATIVE TRANSFER

- Molecular Parameters (13):
  - LOWTRAN 7: 20 cm^{-1}
  - MODTRAN 2: 1 cm^{-1}

- Multiple Scattering:
  - LOWTRAN: 3 Terms
  - MODTRAN: 2 - 15 Terms (Malkmus Curve-of-Growth)
  - Cornette-Shanks Phase Function
  - N-Stream Model

- Correlation Along "Bent" Lines-of-Sight

- Continuous Atmosphere Solution to Equation of Transfer

- In-Scattered Transmittance Calculated

- Turbulence Calculations:
  - Scintillation
  - Emitted and Scattered Path Radiance Variations

- Resolution:
  - Triangular Slit Function
  - Square Slit Function
  - User-Designed Slit Function

- Broad-Band Thermal and Solar Loading

B-077-94(6-1).17

NEW MOLECULAR CROSS-SECTIONS

MISCELLANEOUS FEATURES

- **Automatic Atmosphere Profiling:**
  - In-Band and Spectral
  - Atmospheric Analyses
  - Terrain Altitude Effects

- **Spectral Calculations:**
  - Variable Spectral Sampling
  - Wavelength vs. Wavenumber
    Resolution and Sampling

- **Ray Tracing:**
  - Refractivity
  - Anomalous Propagation

- **Ephemeris:**
  - Solar and Lunar
  - Year-to-Year Variations

- **Relative Humidity (Goff-Gratch)**

- **Additional Molecules in Ultraviolet:**
  - O_2
  - O_3 (*)
  - H_2O
  - SO_2 (*)
  - N_2O
  - NO_2 (*)
  - N_2O_2

  - **Chloro-Fluorocarbons**
    - CFC-11 - CFC-22
    - CFC-12 - CFC-113
    - CFC-13 - CFC-114
    - CFC-14 - CFC-115

  (*) New Cross-Section

Photon Research Associates, Inc.
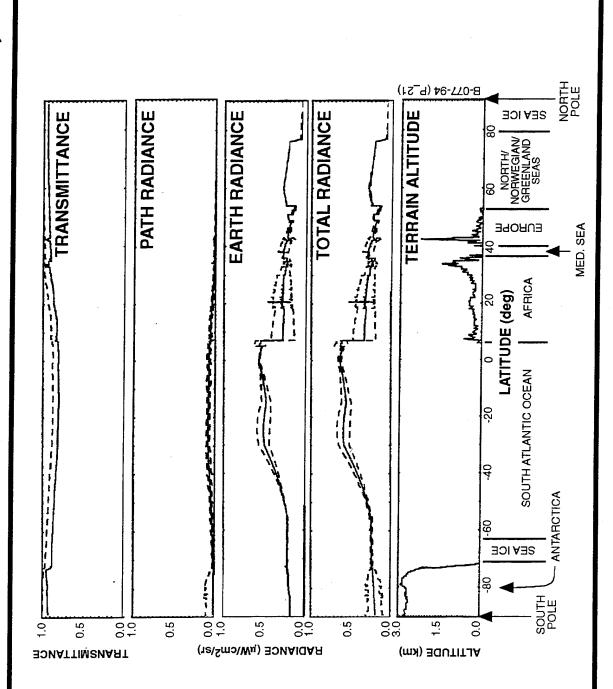
CODE DOCUMENTATION

- Internal Documentation:
  - Routine Prologues
  - Comments

- External Documentation:
  - Installation Reference Manual
  - User Reference Manual
  - Technical Reference Manual
  - Software Reference Manual

GLOBAL CLIMATOLOGY PROFILE: 4 μm; NADIR VIEW; 0° LONGITUDE; 21 DECEMBER 1993, 12:00

Photon Research Associates, Inc.

Scenes
Sea Ice
Ocean/Lake
Forest/Lake
Forest/Mountains
Chaparral
Southern
California
Savannah
Scrub Desert
Tropical Land/Sea
Continental Ice

TRANSMITTANCE
PATH RADIANCE
EARTH RADIANCE
TOTAL RADIANCE
TERRAIN ALTITUDE

B-077-94 (P_21)

B-077-94(6-1).21
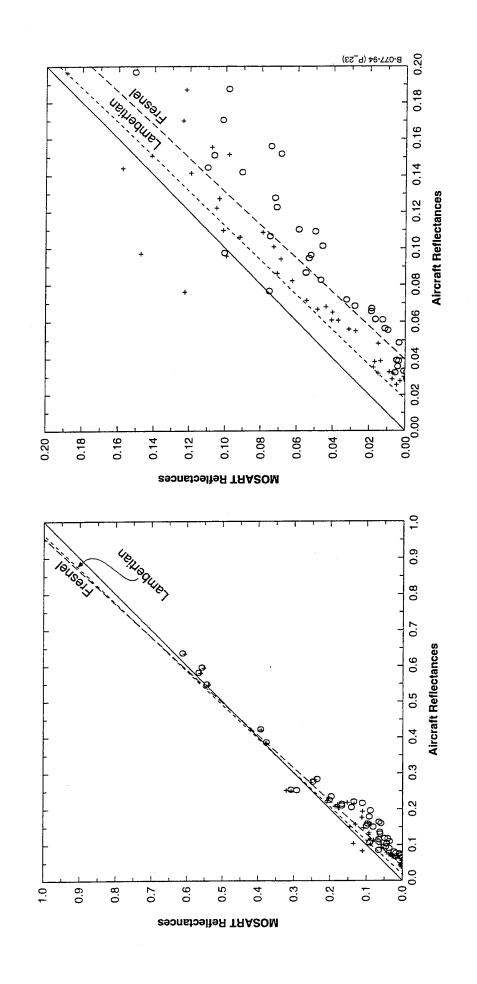
MARICOPA, AZ, LANDSAT SCENES
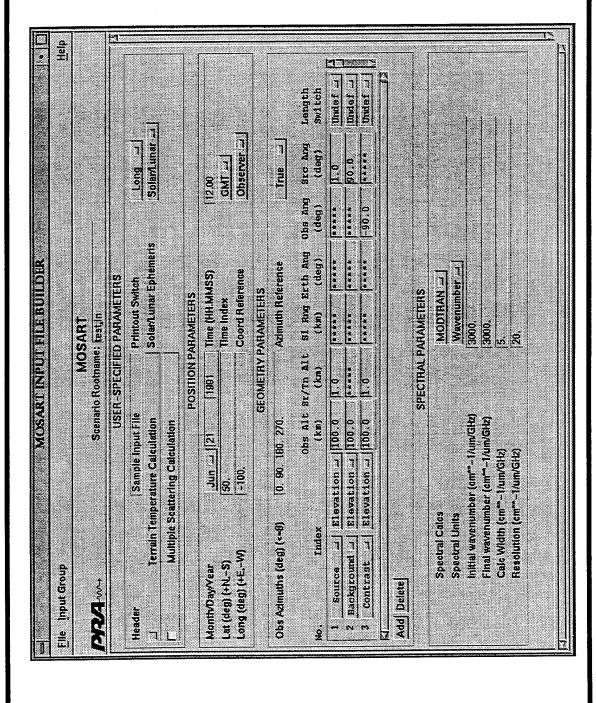
- Seven (7) Dates 1985-86

- Time ~17:33 GMT

- Latitude 33.075°N

- Longitude 111:983°W

- Terrain Altitude 358 m

- Satellite Altitude 705 km

- Satellite Azimuth 99°

- Spectral Bandpass Shapes

- 20% Relative Humidity

CALIBRATED AIRCRAFT REFLECTANCES VS. PREDICTED LANDSAT REFLECTANCES (CLARK, 1986)

B-077-94 (P_23)

B-077-94(6-1).23

MOSART GUI: MAIN PANEL

FUTURE PLANS FOR MOSART

- **MOSART 1**
  - Obtain Public Release
  - Minor Upgrades
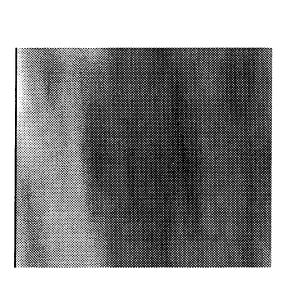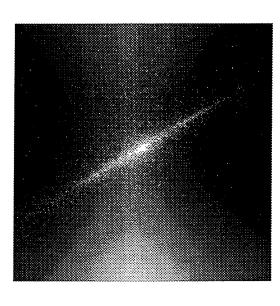
- **MOSART 2**
  - Upgrade Terrain Data Bases
  - 3-D Global Model
  - Multiple Scattering Algorithm
  - Interface with SAMM-2
  - Upgrade Cloud Models
    - -- Broken Cloud Fields
      - -- Deterministic Shadow/Sun
  - Interface with AURIC
  - Respond to User Requirements
  - Upgrade Turbulence/Scintillation/Sky Noise
  - Polarization

PLEXUS

PHILLIPS LABORATORY

Geophysics Directorate Backgrounds Codes

Geophysics Directorate, Phillips Laboratory, Hanscom Air Force Base, MA
Department of the Air Force
fax:617-377-8780, internet fclark@plh.af.mil

PLEXUS
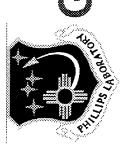
Geophysics Directorate

- ## Existing Codes
    - Expert System Packaging
    - Easy to use
    - Interactive stand-alone mode
    - Non-interactive hardware independent mode

- ## Proposed upgrades

Geophysics Directorate Codes

PLEXUS Expert System Environment

- **MODTRAN (successor of LOWTRAN)**
  - Equilibrium lower atmosphere
- **SHARC**
  - Non-equilibrium upper atmosphere
- **FASCODE**
  - high resolution (lasers, radar)
- **SAMM (SHARC & MODTRAN MERGED)**
  - first principles combination
- **RADTRAN**
  - fast RF propagation

(We have you covered!)

Dr. Frank O. Clark PL-GPOB, HAFB

PHILLIPS LABORATORY

Geophysics Directorate Codes
Standard Atmospheric Generator
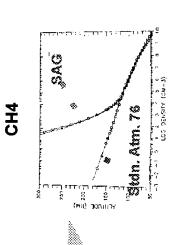
- **Based on Modern Data**
  - Geographical variability
  - Seasonal variability
  - Time variability
- **NASA MSIS 90E**
  - satellite data base
- **NRL climatology**
  - data base (AWS)
- **Contiguous ground-300 km**
- **Greatly improves code results**
- **Drives all codes in PLEXUS**
  - default
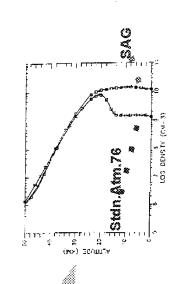
CH4

HNO3

Geophysics Directorate Codes

Celestial Background Scene Descriptor

Rosette Nebula
H II Region
at 25 microns
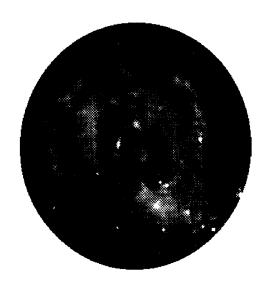
- **Astronomical Background**
  - Visible to 30 microns
  - Accurate Positions (2")
    » Naval Observatory positions
  - Accurate brightness
    » Model fitted to data
  - Unique infrared calibrators & positions

Dr. Frank O. Clark PL-GPOB, HAFB

PHILLIPS LABORATORY

PLEXUS

Interactive Mode

Ground to Space

Background & Transmission

SAG Variability, Weather

MODTRAN & SHARC Atmosphere
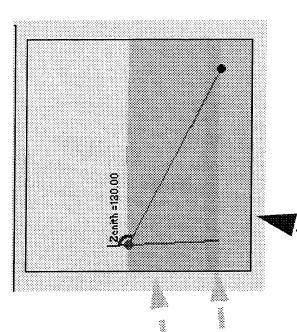
single answer

CBSD Celestial Background

Expert System Based
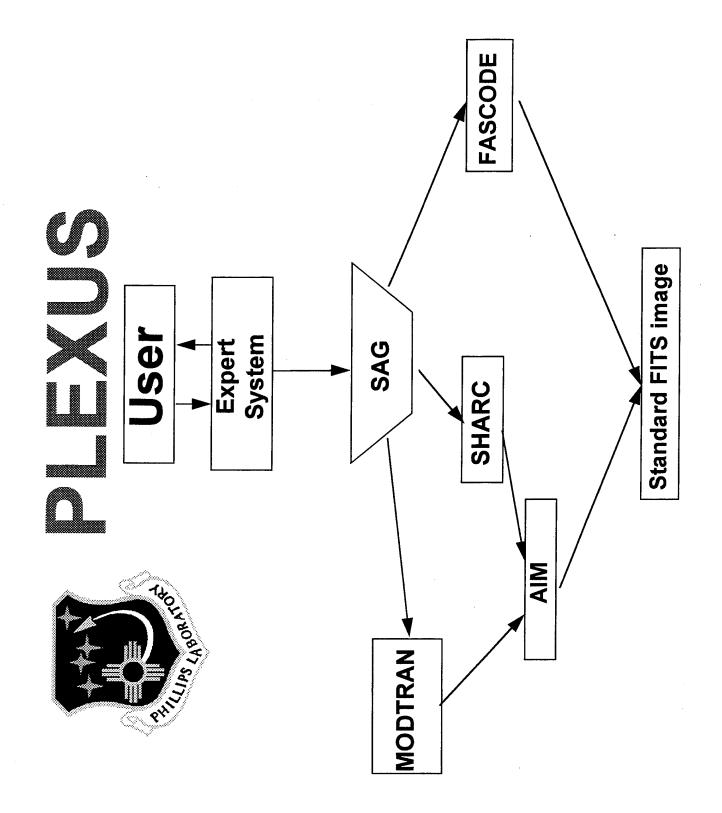
Easy Rapid Setup

Visual Feedback

Zenth =120.00

On-line Geometry

Dr. Frank O. Clark PL-GPOB, HAFB

PHILLIPS LABORATORY

PLEXUS

Common user oriented interface

Expert system suggests most proper code

Improvements

- **FASCODE**
  - laser & radar
  - beta version out now
- **UNIX Port (alpha test now)**
- **Non-interactive plug in mode**
- **Batch Mode**
- **Upgrade internal structure for extensibility**
- **Scalable Task Manager**

PHILLIPS LABORATORY

PLEXUS

Planned Upgrades

- **SAMM**
  - first principles ground - space
  - nlte populations to FASCODE
- **WEATHERMAN (in progress)**
  - time sequence weather player
- **MOSART**
  - versatile global data bases
  - surface air temperature
  - cloud cover & aerosols
- **GEM - Geophysics Earth Model (proposed)**
  - lat, lon, alt, terrain type
- **Cloud Scene Simluation Model**

PHILLIPS LABORATORY

Celestial Background Scene Descriptor
CBSD

CBSD Scene

- Suite of Models
  - visible to 30 microns
- Solar System:
  - Zodiacal Emission
  - Asteroids, Sun, Moon, Planets
- Galaxy:
  - Statistical stellar model
  - IRAS PSC
  - H II regions (extended)
- Infrared Calibration Stars
  - Primary IR calibration stars
  - Secondary calibration stars
  - Infrared Astrometric Catalog (positions)
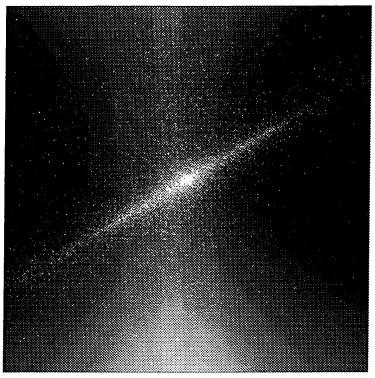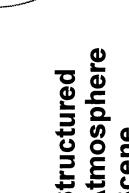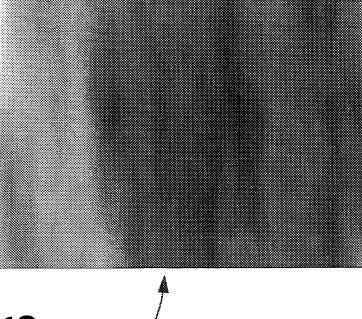
PHILLIPS LABORATORY

SASS

**Structured
Atmosphere
Scene
Simulator**

Work in Progress

- **Altitude dependent structure**
- **Array of structure values**
  - statistics of altitude dependent PSD
- **Structure added upon radiance from any model**
- **FITS output (universal image format)**
- **FORTRAN**
- **Designed as a testbed**
  - determine effective structure techniques

PHILLIPS LABORATORY

Dr. Frank O. Clark
Geophysics Directorate
Phillips Laboratory
Hanscom Air Force Base, Massachusetts

Geophysics Directorate Codes

Summary

Environment including multispectral weather effects

- **Multi-spectral environment**
  - user oriented
  - ground to space
  - multi-spectral: UV to microwave
  - validated, widely used
  - organized as an entity
  - expert system based
  - weather object under construction
  - unix port & non-interactive mode

ARMY RESEARCH LABORATORY

EOSAEL92 Update

Alan Wetmore awetmore@arl.army.mil and Jim Williams jimw@arl.army.mil

Atmospheric Simulation Division
Battlefield Environment Directorate
Army Research Laboratory
White Sands Missile Range, New Mexico 88002 USA
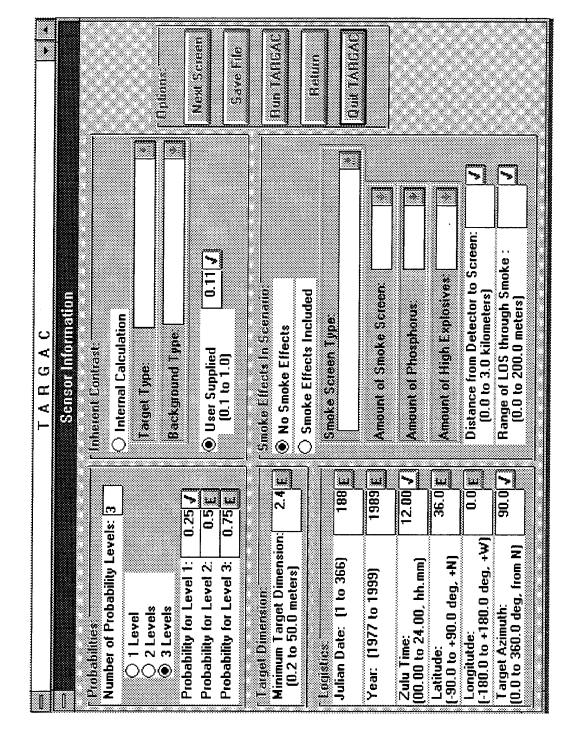
EOSAEL Capabilities
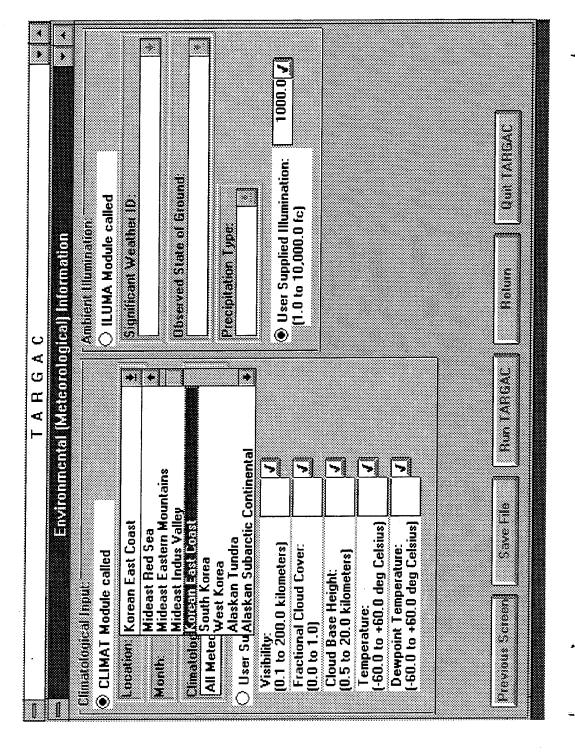
- Atmospheric Gases — LOWTRN, LZTRAN, NMMW, UVTRAN

- Natural Aerosols — XSCALE, CLTRAN

- Battlefield Aerosols — COMBIC, FITTE

- Radiative Transfer — OVRCST, ILUMA, FASCAT, GSCAT, LASS, NBSCAT

- Laser Propagation — LZTRAN, NOVAE

- Target Acquisition — TARGAC, RADAR, REFRAC

- Support Modules — PFNDAT, AGAUS, BITS, CLIMAT

- Tactical Decision Aids — KWIK, GRNADE, MPLUME, COPTER

- Acoustic Propagation — SCAFFIP

TARGAC Scenario Specifications

TARGAC

Sensor Information

Options:

Next Screen

Save File

Run TARGAC

Return

Quit TARGAC

Inherent Contrast:

○ Internal Calculation

Target Type

Background Type

● User Supplied
[0.1 to 1.0]   0.11 ✓

Smoke Effects In Scenario:

● No Smoke Effects

○ Smoke Effects Included

Smoke Screen Type:

Amount of Smoke Screen:

Amount of Phosphorus:

Amount of High Explosives:

Distance from Detector to Screen:
[0.0 to 3.0 kilometers]

Range of LOS through Smoke :
[0.0 to 200.0 meters]

Probabilities:

Number of Probability Levels: 3

○ 1 Level
○ 2 Levels
● 3 Levels

Probability for Level 1:   0.25 ✓

Probability for Level 2:   0.5 E

Probability for Level 3:   0.75 E

Target Dimension:

Minimum Target Dimension: 2.4 E
[0.2 to 50.0 meters]

Logistics:

Julian Date: [1 to 366]   188 E

Year: [1977 to 1999]   1989 E

Zulu Time: 12.00 ✓
[00.00 to 24.00, hh.mm]

Latitude: 36.0 E
[-90.0 to +90.0 deg., +N]

Longitutde: 0.0 E
[-180.0 to +180.0 deg., +W]

Target Azimuth: 90.0 ✓
[0.0 to 360.0 deg. from N]

TARGAC Selecting Climatology Region

TARGAC

Environmental (Meteorological) Information

Climatological Input:

◉ CLIMAT Module called

Location: Korean East Coast

Mideast Red Sea
Mideast Eastern Mountains
Mideast Indus Valley
Korean East Coast
South Korea
West Korea
Alaskan Tundra
Alaskan Subarctic Continental

Month:

Climatolog

All Meteo

◯ User Su

Visibility:
[0.1 to 200.0 kilometers]

Fractional Cloud Cover:
[0.0 to 1.0]

Cloud Base Height:
[0.5 to 20.0 kilometers]

Temperature:
[-60.0 to +60.0 deg Celsius]

Dewpoint Temperature:
[-60.0 to +60.0 deg Celsius]

Ambient Illumination:

◯ ILUMA Module called

Significant Weather ID:

Observed State of Ground

Precipitation Type:

◉ User Supplied Illumination: 1000.0
[1.0 to 10,000.0 fc]

Previous Screen   Save File   Run TARGAC   Return   Quit TARGAC

UVTRAN for MS-WINDOWS

UVTRAN

Version 3.0
Program calculates transmission of Lidar

Constants

- Setup Aerosol Profiles
- Edit/Set Default Ozone Levels
- Edit/Set Default Trace Gas Levels

Calculation Type

Run it!

Calculation Type

Calculation type
- ● Transmission
- ○ LIDAR

10 Ranges

Calculation Range/Interval
0.10 Shortest   0.10 Interval

Edit Parameters   Accept Values

UVTRAN for MS-WINDOWS

Aerosol Profiles:

Visual Range [km]   10.0

Altitude of receiver [km]   1.00

of visibility measurement [1.00

Accept Values

Aerosol Attenuation
- ○ Constant with heig
- ● Increases with hei
- ○ Decreases with he

Path Direction
- ○ Horizont
- ○ Vertical.
- ● Slant...

% Change in:

0.97   100.0

Attenuation   **Ver Distance**

Zenith Angle

45.00

Enter new Angle

UVTRAN for MS-WINDOWS

Ozone Levels

Present values for trace constituents are based on 1976 standard atmosphere values. Ozone data are given for each km for altitudes between 0 and 20 km.

Level	Value	Level	Value	Level	Value
Level 1	26.60	Level 8	50.00	Level 15	496.00
Level 2	29.30	Level 9	59.50	Level 16	655.00
Level 3	32.50	Level 10	87.00	Level 17	853.00
Level 4	33.20	Level 11	131.00	Level 18	1170.00
Level 5	34.00	Level 12	200.00	Level 19	1600.00
Level 6	37.50	Level 13	311.00	Level 20	2050.00
Level 7	41.50	Level 14	390.00	Level 21	2610.00

Accept Values   Reset Default Values

UVTRAN for MS-WINDOWS

Results

Print Output | Write to File | Close Window

visibility = 10 km at an altitude of 1 km
particle extinction changes by -.9606814 per 100 meter altitude increase
low resolution data
initial altitude = 1 km   zenith angle = 45 degrees

Range (km)	Final Alt. (km)	Wavelength (nm)	Transmission
0.10	1.07	200.00	6.398e-02
		222.22	6.252e-01
		244.44	8.081e-01
		266.67	8.354e-01
		288.89	8.922e-01
		311.11	9.142e-01
		333.33	9.234e-01
		355.56	9.304e-01
		377.78	9.362e-01
		400.00	9.411e-01
0.20	1.14	200.00	4.172e-03
		222.22	3.921e-01
		244.44	6.537e-01
		266.67	6.984e-01

90

NMMW Gaseous Absorption Update

The Millimeter-wave Propagation Model (MPM85) was reported in H. Liebe, *An updated model for millimeter-wave propagation in moist air*, Radio Science, vol. 20, no. 5, pp. 1069–1089, 1985. Molecular absorption by O_2, H_2O, and N_2 is considered, as well as dielectric loss for haze and fog/cloud conditions (Rayleigh absorption approximation), and dielectric plus scatter losses (aR^b — approximation to Mie's theory) under rain conditions. The complex atmospheric refractivity N (or path-specific rates of attenuation A and delay B) were upgraded.

NMMW Gaseous Absorption Update

- Humidity profiles through 30 km

- Rural, Urban, and Maritime hygroscopic aerosols

- Improved model for the dielectric properties of liquid water to calculate Rayleigh absorption and delay by suspended water droplets for haze, fog, and cloud conditions.
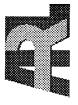
- New temperature-dependent linewidth data ($b_3, \ldots, b_6$) for the water vapor lines below 1-THz, and a 5 percent increase in the strength b_1 of the 22-GHz and 183-GHz lines.

- New set of line mixing coefficients ($a_5, \ldots, a_6$) for dry air, and their improved fit to the extensive 60-GHz lab data.

- Approximation for Zeeman, O_2, and Doppler, H_2O, line-broadening to cover heights up to 100 km.

- New pseudo-line water vapor continuum formulation.

- Detailed treatment of the anisotropic, mesospheric Zeeman effect of O_2 microwave lines.

- H. Liebe, G. Hufford, and M. Cotton, *Propagation modeling of moist air and suspended water/ice particles at frequencies below 1000 GHz*, Proc. AGARD Conf. Paper 3/1-10, Palma De Mallorca, Spain, May 1993.

Verification of LZTRAN

- Verification determines whether the model accurately reflects its conceptual description as given in requirements and design specifications.

- Logical Verification.
  - Review data sources and documentation.
    * Verify laser line database and all polynomial coefficients.
    * Verify all polynomial coefficients (plots).
  - Comparison of requirements and design to code.

- Code Verification – most important part of verification.
  - Code walk-through.
  - Stand-alone algorithm checks.
    * Calculation of water vapor saturation.
    * Vertical profiles of temp and pressure for all six model atmospheres.
    * H_2O and N_2 continuum absorption calculations.
    * Adjustments to negative extinction coefficients.
  - Sensitivity analyses.
    * Investigate temp, pressure, water vapor boundary conditions.

Validation of LZTRAN

- Validation determines the extent to which the model produces results expected in the real world.

- Structural Validation.

  - Examination of model assumptions:

    * One regression polynomial for all laser lines as a function of temperature, pressure, and water vapor for all laser lines.

    * FASCODE 2 (using HITRAN92) effectively models laser systems.

  - Review algorithms in context of intended use:

    * Examine sensitivity to different data sets.

    * Ensure that algorithms are modeled completely.

- Output Validation.

  - Compare model results against both FASCODE 2 and real world data.

  - Examine sensitivity and reasonableness of model output as input varies.

  - Subject matter expert will review input and output.

ACOUSTICS— SCAFFIP

Prediction of acoustic propagation based on:

- Geometric Spreading
- Molecular Absorption
- Refraction
- Acoustically Complex Ground Impedance
- Diffraction Over Benign Terrain

ACOUSTICS

$$c(T) = \sqrt{\frac{\gamma R T}{M}} \tag{1}$$

$$h = \frac{100(RH)P_{\text{sat}}}{P} \tag{2}$$

$$\gamma = \frac{7+h}{5+h} \tag{3}$$

$$M = 29 - 11h \tag{4}$$

$$c_{\text{eff}} = c(T) + u\cos(\theta_w - \pi - \theta_R) \tag{5}$$

96

Wave Solution

$$\nabla^2 p - \frac{1}{c_2}\frac{\partial^2 p}{\partial t^2} = -4\pi\delta(x, y, z) \tag{6}$$

$$\nabla^2 p + kp^2 = -4\pi\delta(x, y, z) \tag{7}$$

$$\frac{\partial^2 p}{\partial r^2} + \frac{1}{r}\frac{\partial p}{\partial r} + \rho\frac{\partial}{\partial z}\left(\frac{1}{\rho}\frac{\partial p}{\partial z}\right) + k^2 p = \frac{-2}{r}\delta(r)\delta(z - z_s) \tag{8}$$

97

Acoustic Attenuation

$$\alpha_{\text{cl}} = 5.578 \times 10^{-9} \frac{T/T_0}{T + 110.4 P/P_0} f^2 \tag{9}$$

$$\frac{\alpha_{\text{rot}}}{\alpha_{\text{cl}}} = 4.16 e^{-16.8 T^{1/3}} \tag{10}$$

$$\alpha_{\text{cr}} = \alpha_{\text{cl}} + \alpha_{\text{rot}} \tag{11}$$

$$\alpha_{\text{vib},j} = \frac{4p X_j}{35c} \left(\frac{q_j}{T}\right)^2 \frac{e^{-q_j/(T f^2)}}{f_{r,j} + f^2/f_{r,j}} \tag{12}$$

$$f_{r,\text{O}} = \frac{P}{P_0}\left(24 + 4.04 \times 10^4 h \frac{0.02 + h}{0.391 + h}\right) \tag{13}$$

$$f_{r,\text{N}} = \frac{P}{P_0}\sqrt{\frac{T_0}{T}}\left(9 + 280 h e^{-4.170(T_0/T)^{1/3}-1}\right) \tag{14}$$

Complex Ground Impedance

$$Z_c = \frac{\frac{4q^2}{3\Omega} + i\frac{S_f^2 \sigma}{\omega \rho_0}}{k_b} \tag{15}$$

$$k_b \cong \sqrt{\gamma \Omega} \left[\left(\frac{4}{3} - \frac{\gamma - 1}{\gamma} N_{pr} \right) \frac{q^2}{\Omega} + i\frac{S_f^2 \sigma}{\omega \rho_0} \right]^{1/2} \tag{16}$$

$$Z(d) = \left[\frac{Z_2 - iZ_1 \tan(k_b d)}{Z_1 - iZ_2 \tan(k_b d)} \right] Z_1 \tag{17}$$

99

EOSAEL on TECNET

- Test and Evaluation Community NETwork

- DoD TRI-Service Sponsored

- Hosted at, NAWC, Patuxent River, MD

- Dial-up and Internet Access

- AGAUS AUXLRY CLIMAT COMBIC LZTRAN NMMW XSCALE

- EOSAEL Source Code and DOS Executable Files

The Navy Oceanic Vertical Aerosol Model in a FORTRAN subroutine Format

S.Gathman   NRaD

THE NAVY OCEANIC VERTICAL AEROSOL MODEL
IN A FORTRAN SUBROUTINE FORMAT

Stuart G. Gathman

NCCOSC RDTE DIV 543
53170 Woodward Road
San Diego, CA 92152

A FORTRAN version of the Navy Oceanic Vertical Aerosol Model, NOVAM, has been completed and is ready to be interfaced with other types of transmission models. The model is available in the form of a NCCOSC RDT&E DIV technical report #1634 which contains: (a) a written description of the model, (2) the printed code of the subroutine, (3) the printed code of the associated subroutines and functions, and (4) a sample driver which can be used for batch processing of data. The model requires meteorological data in the form of both surface and atmospheric sounding data files. NOVAM predicts the vertical distribution of aerosol in the first 6 km above the ocean. Outputs of the model include optical properties in the wavelength band from 0.2 to 40 micrometers at any altitude. These properties include the volume extinction and absorption coefficient, the relative humidity, as well as parameters describing the aerosol size distribution in terms of dN/dr at that altitude. This paper will describe the model and some sample applications.

Technique

- Represent aerosol size distribution as a set of lognormal functions.

- Function parameters are empirically related to meteorological observations.

NOVAM

- Uses the NAM concept as a kernel.

- Output of optical parameters

  - at any wavelength

  - at any altitude.

- Vertical structure - 1 dimension only.

- Only available meteorology data to be used.

Construction of NOVAM concepts

- History of development

  - NRL, NOSC and NPS

  - Testing and redesign

  - Field tests

Earlier versions of NOVAM

- Structure of MBL needed
  - manual
    - operator hand analysis needed
  - semi automatic
    - operator – computer interaction
  - fully automatic method needed but not available.
- Characterization of the air mass parameter
  - earlier methods not really satisfactory for LOWTRAN/MODTRAN
  - use of visibility to determine a.m.p.

Assimilation of atmospheric structure into model

- **manual approach**
  - input hand calculated parameters from the profile into an input data file.

- **semi automatic approach**
  - stand alone aerosol program for the PC
  - computer makes a best guess, and then the user interactively adjusts curve to fit the data as needed

- **fully automatic approach -- needed for a non interactive programs**
  - a FORTRAN subroutine developed for LOWTRAN/MODTRAN

107

Structure of NOVAM subroutine
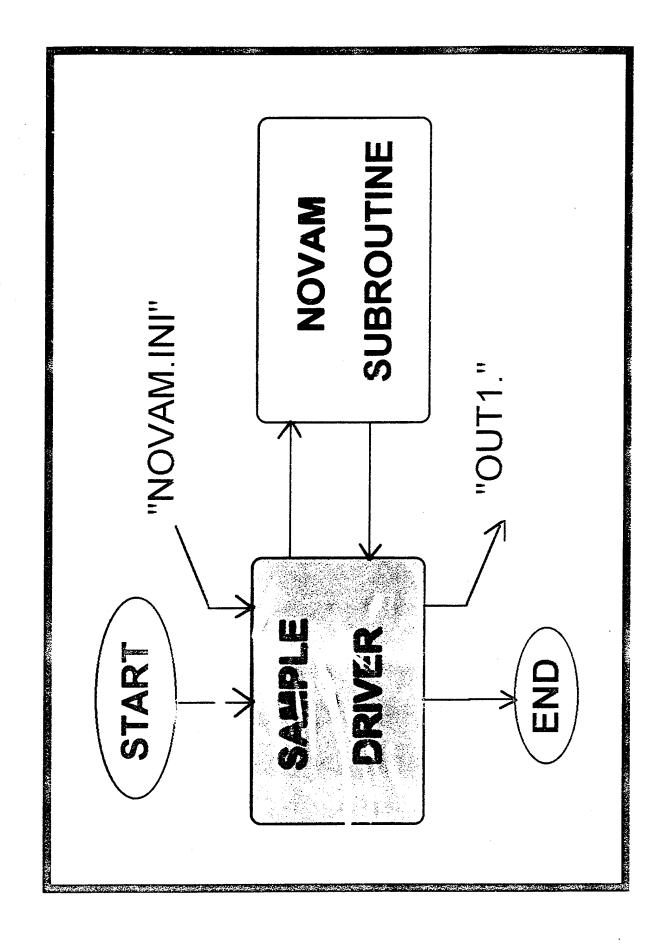
- FORTRAN batch version
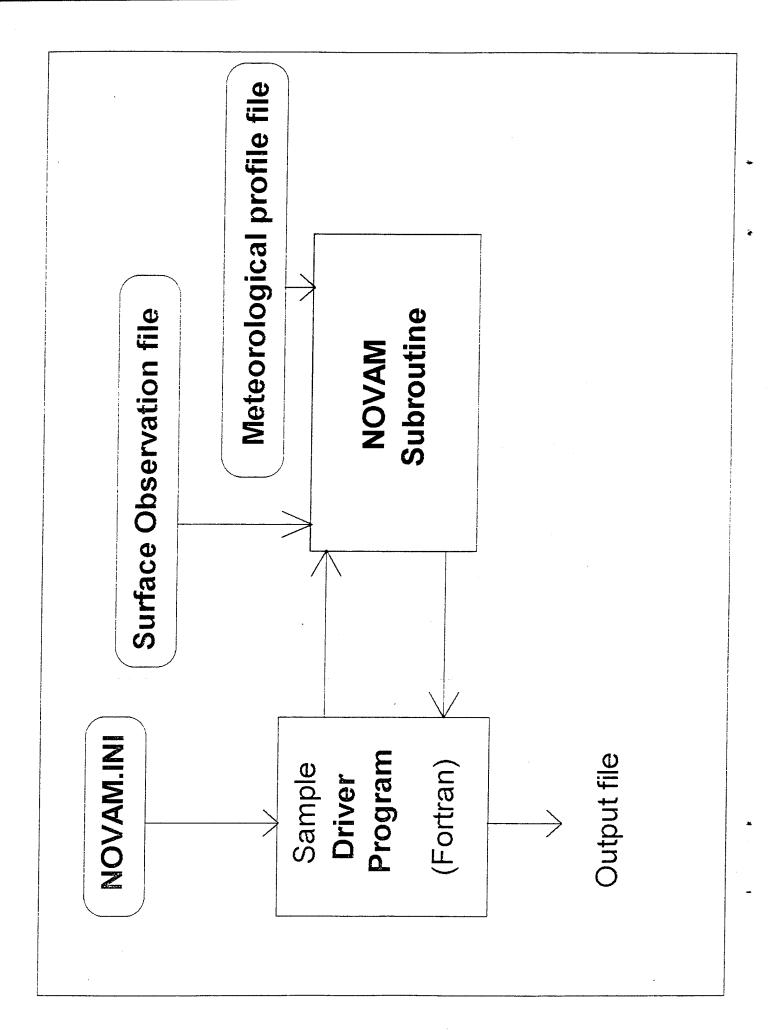
  - Some features left out to allow for fully automatic mode operation

- automatic MBL structure interpreter
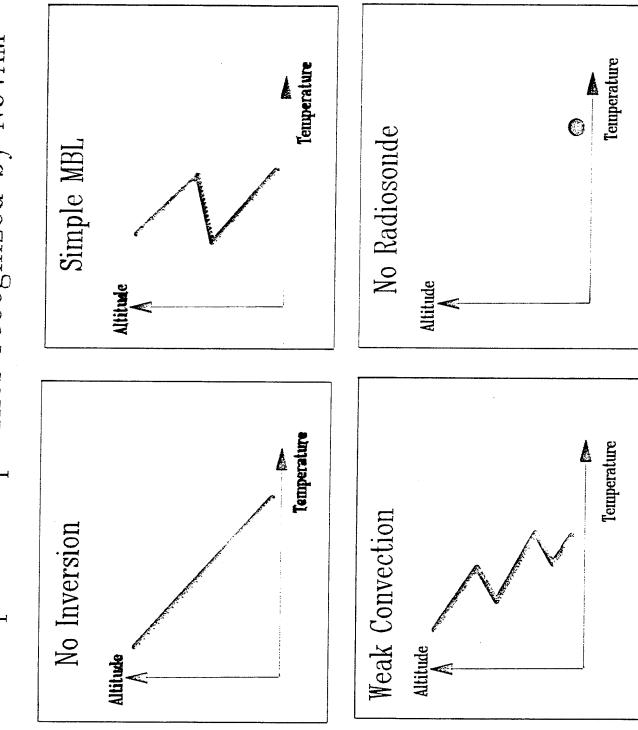
- a.m.p. calculated from the visibility data
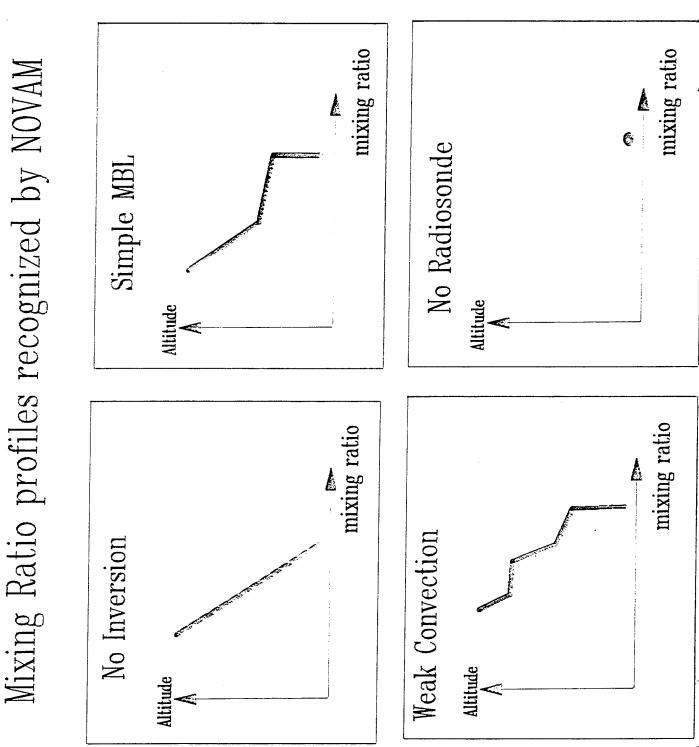
- makes output at significant values only

NOVAM.INI

Surface Observation file

Meteorological profile file

NOVAM
Subroutine

Sample
Driver
Program
(Fortran)

Output file
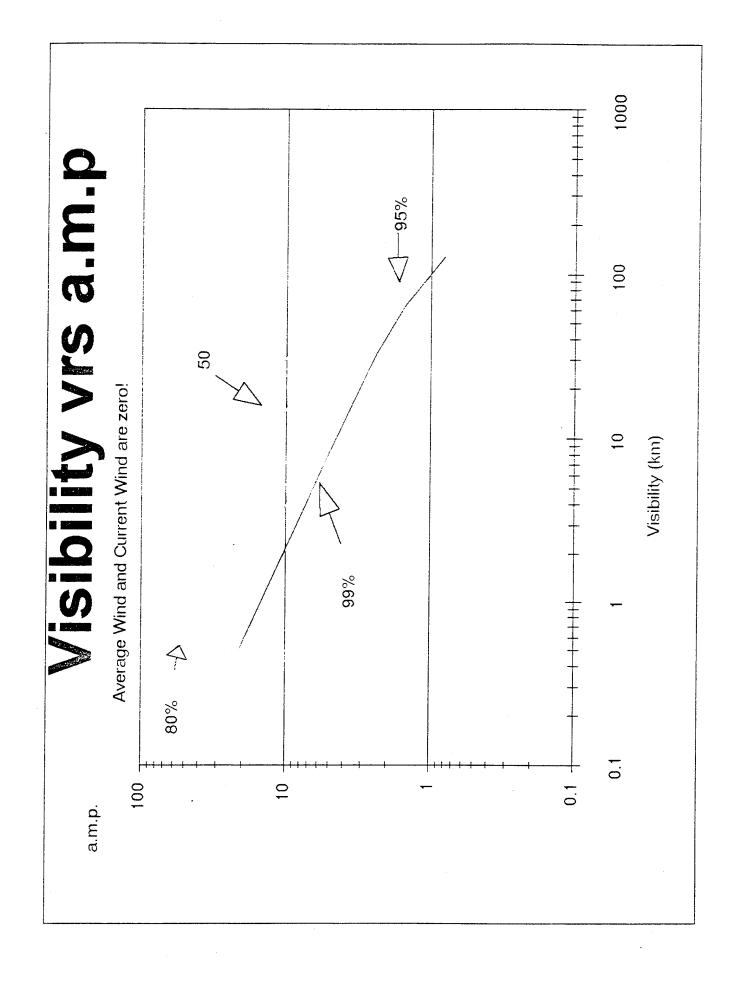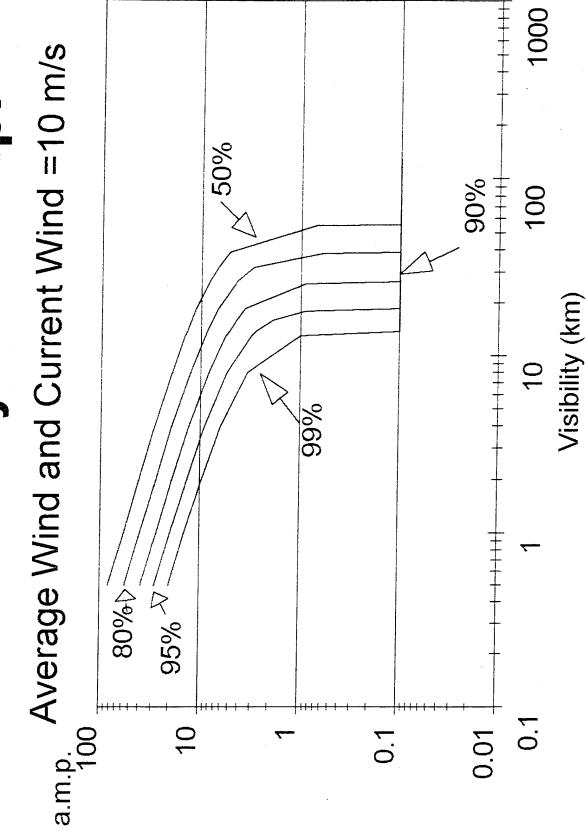
Temperature profiles recognized by NOVAM

No Inversion

Altitude

Temperature

Simple MBL

Altitude

Temperature

Weak Convection

Altitude

Temperature

No Radiosonde

Altitude

Temperature

Mixing Ratio profiles recognized by NOVAM

Simple MBL

No Inversion

No Radiosonde

Weak Convection

Visibility vrs a.m.p

Average Wind and Current Wind are zero!

Visibility vrs a.m.p.

Average Wind and Current Wind =10 m/s

114

Technical Report 1634
December 1993

The Navy Oceanic Vertical Aerosol Model

S. G. Gathman
K. L. Davidson, NPGS

EXECUTIVE SUMMARY

OBJECTIVE

The object was the development of the FORTRAN version of the Navy oceanic vertical model (NOVAM). The model predicts the vertical distribution of aerosol in the first 6000 meters above the ocean.

RESULTS

The NOVAM was developed from extensive marine aerosol studies from different laboratories. The climax was a multimenu-driven interactive program that allows mouse selection of menu items needed for the calculation. It includes graphics and editing capabilities useful to the researcher. When used with an appropriate method to determine the profile parameters, it could be used in a fully automatic mode in which the program could access sets of data and produce an analysis of the data sets in an unattended background mode. The final NOVAM code is intended, however, to be used in conjunction with a LOWTRAN/MODTRAN program and to supply the electro-optical (EO) propagation characteristics to the calling program that are produced by the unique aerosol found in the marine atmosphere. It is written in FORTRAN so it can be integrated into LOWTRAN/MODTRAN codes to improve model performance in marine environment.

RECOMMENDATIONS

The model has several shortcomings that will be addressed in future modifications. The region of applicability leaves two areas not covered well by the model. First, higher altitudes, various models developed by the U. S. Air Force and included in the LOWTRAN/MODTRAN code will be more accurate. Second, propagation paths that graze the sea surface or pass through the region within a meter or so of the sea surface are not adequately covered by NOVAM. This problem is being remedied by a large-scale experiment off the Dutch coast sponsored by NATO. Another shortcoming is the limited types of weather situations in which it is applicable. Advances in these areas await development of models from the basic research community in the future. Another area of concern is the use of the model in close-in coastal areas. Compensation was introduced, but experience has shown this is one of the weakest parts of the model. It is the author's opinion that a special coastal aerosol model needs to be developed that will adequately take into account local sources of aerosol.

CONCLUSIONS

We have presented a model for describing the EO properties of the unique marine aerosol found in the regions from shipboard height to above several kilometers in altitude. The model has been written as a self-contained FORTRAN subroutine so it could be incorporated into larger scale models such as the LOWTRAN and MODTRAN codes. The model needs information on the meteorological sounding at the site where the calculation is made as well as information on certain meteorological parameters near the surface of the sea. The model has certain shortcomings that need to be addressed in future modifications. First of all, the region of the applicability is from shipboard level (about 5 to 10 meters) to regions above the lower troposphere where other aerosol models will be more appropriate. This leaves two areas that are not covered well by the model. At the higher altitudes, various models developed by the U. S. Air Force and included in the LOWTRAN/MODTRAN codes will be more accurate. On the other extreme, an important propagation path that grazes the sea surface or passes through the region within a meter or so of the sea surface is not adequately covered by NOVAM. This is because NOVAM is in part an empirical model and based on measurements in the real world. Current interest from shipboard level on down currently lacks observation data because of the difficulty in obtaining them. This region will be especially important to IR propagation during rough weather and high seas where many marine-generated drops and droplets are suspended in these lower levels of the atmosphere. This problem is currently being remedied by a large-scale experiment called the Marine Aerosol Properties and Imager Performance (MAPTIP) trial off the Dutch coast sponsored by NATO. The results of this experiment will contribute to the development of an advanced Navy aerosol model (ANAM) currently under development. These results can be added into the modular format of NOVAM to increase its regions of application.

Another shortcoming in NOVAM is its somewhat limited types of weather situations in which it is applicable. An earlier version of NOVAM included the region just below stratus clouds, but because this model had a limited band of wavelength validity and required inputs that are really incompatible with a self-contained model, this submodel was dropped from the current model. Advances in these areas await the development of models from the basic research community sometime in the future.

An area of concern in the application of models such as NAM and NOVAM is the use of the models in the close-in coastal areas. As these models were developed for the open ocean region far away from the land influences, error would be expected when unusual sources of aerosol are sent into the atmosphere by man-made sources. The amp concept was introduced into NAM and NOVAM to compensate for these problems, but experience has shown that this is one of the weakest parts of the models. It is the author's opinion that a special coastal aerosol model needs to be developed that will adequately take into account local sources of aerosol.
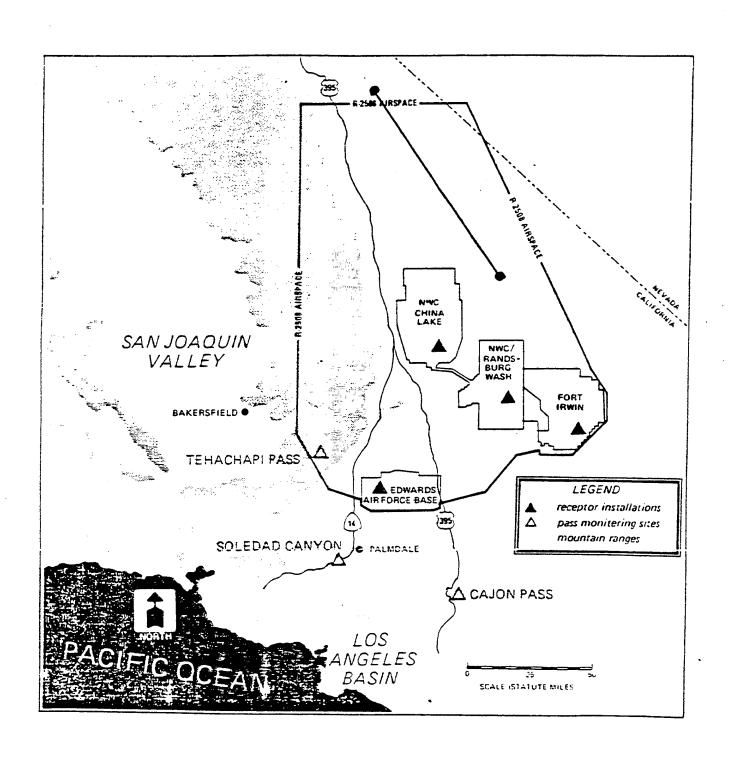
THE NATURE OF DESERT AEROSOLS: SUMMARY OF CHINA LAKE STUDIES TO DATE

P.L. Walker
Physics Department, Code PH
Naval Postgraduate School
Monterey, CA 93943-5117
walker@physics.nps.navy.mil

L.A. Mathews, ret.
Research Department
Naval Air Warfare Center - Weapons Division
China Lake, CA 93555

ABSTRACT

The Naval Air Warfare Center has been conducting desert aerosol characterization measurements at China Lake at ground level in 1987; at 15,000 feet in connection with Long Jump in 1988; at ground level in the western Mojave including Edwards AFB and China Lake in 1990; and will be conducting further measurements in the western Mojave in the summer of 1994. This presentation will present an over view of the analysis of data to date. The properties of desert aerosol that are appearing are some what different than those proposed by Longtin and Shettle in that the accumulation mode is dominated by the presence of large numbers of organic carbon particles while dust is characterized by the presence of clay particles in the dust size distribution mode with few quartz particles being present and no quartz dominated blowing sand mode. . We will compare particle size and composition at 15,000 feet and ground level, further micrographic studies of the composition of high altitude aerosols and the effect of wind speed on aerosol characteristics at ground level.

LEGEND

▲ receptor installations
△ pass monitering sites
mountain ranges

R-2508 Airspace

OUR ROLE IN LONG JUMP

OUR MISSION WAS TO DETERMINE THE OPTICAL PROPERTIES OF THE ATMOSPHERE ALONG THE FLIGHT PATH AND IN THE VICINITY OF WHITE MOUNTAIN AND TO MAKE THE METEOROLOGICAL MEASUREMENTS AT BARCROFT

FROM AN INSTRUMENTED PIPER NAVAJO WE MADE MEASUREMENTS OF AEROSOLS, CO_2 CONTENT, TEMPERATURE AND DEW POINT TEMPERATURE BETWEEN TEST FLIGHTS FROM WHICH THE INFRARED TRANSMISSION CHARACTERISTICS FOR THE FLIGHT PATH COULD BE DEDUCED

WE MADE 16 FLIGHTS BETWEEN AUGUST 16 AND 25, 1988

EACH DAY OF OPERATIONS WE MADE ONE FLIGHT IN THE LATE MORNING, ONE IN THE EARLY AFTERNOON AND ON ONE OCCASSION A FLIGHT AT 1700

AT 15,500 FT OUR AIRCRAFT FLEW JUST BELOW THE TOP OF THE MIXING LAYER AND IN FACT THE TOP OF THE LAYER DROPPED BELOW THE AIRCRAFT ON THE RETURN LEG OF THE FLIGHT AT 1700

MEASUREMENTS

AIR TEMPERATURE AND DEW POINT

CARBON DIOXIDE CONTENT

AEROSOL SAMPLES FOR ELEMENTAL ANALYSIS WERE OBTAINED USING A 9 STAGE CASCADE IMPACTOR

AEROSOL SIZE DISTRIBUTION DATA WAS OBTAINED USING A TSI AERODYNAMIC PARTICLE SIZER MODEL APS33 AND A TSI MODEL 390039 ELECTRICAL AEROSOL ANALYZER FOR THE SIZE RANGES 0.5 TO 15 MICRONS AND 0.024 TO 0.75 MICRONS, RESPECTIVELY

AEROSOL SAMPLES AND DEW POINT TEMPERATURES WERE TAKEN FROM THE COLLECTION CHAMBER PICTURED

AIR WAS DRAWN INTO THE CHAMBER THROUGH A PITOT TUBE LOCATED LOCATED ON THE ROOF OF THE AIRCRAFT AND EXITED THROUGH A VENTURI TUBE LOCATED IN THE BELLY

Particle Collection

- Particulate samples collected on four stages of a QCM microbalance cascade impactor

- Impactor flown at elevation of 15,500 ft ($\approx$ 5 km), MSL

  - Over 103 nautical mile course in east-central California

  - 16 round trip flights over a 2 week interval in August 1988

  - Air collected through an isokinetic probe located 18 in (45 cm) into undisturbed airstream.

- Only 4 stages of the ten-stage impactor was used and covered the following particle diameter ranges:

  - Stage 3: 6 μm and greater

  - Stage 5: 1 to 6 μm

  - Stage 7: 0.4 to 1 μm

  - Stage 9: 0.1 to 0.4 μm

A Comparison of Ground Aerosol Sizes and Concentrations with Those Near 15,500 ft.

Dust Mode

@15,500 ft.	No = 0.6 particles/cc	number density
	Dn = 0.285 microns	mode diameter
	$Log(\sigma) = 0.7$	mode width
@Ground	No = 5 particles/cc	
	Dn = 0.35 microns	
	$Log(\sigma) = 0.9$	

Accumulation Mode

@15,500 ft.	No ~ 5×10^2 /cc
	Dn ≈ .07 μ
	$Log(\sigma) \approx 0.28$
@Ground	No ~ 2×10^3 /cc
	Dn = ≥ 0.1μ
	$Log(\sigma) \cong 0.47$
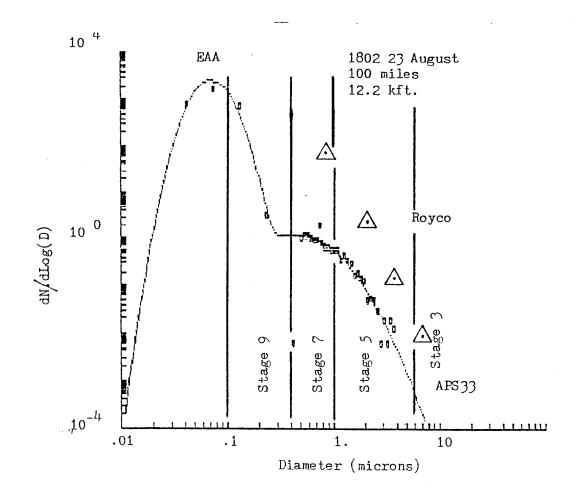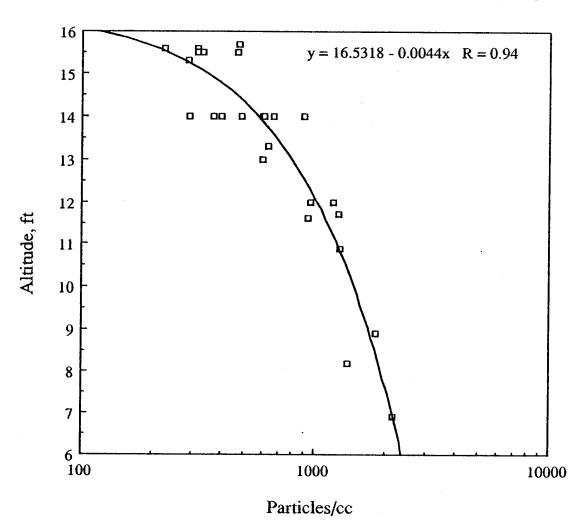
Accumulation Mode Particle Concentration vs Altitude for Flight 15.

$y = 16.5318 - 0.0044x$ $R = 0.94$

Altitude, ft

Particles/cc

Particle Composition at 15,000 ft

- Calcium and phosphorus particles having featureless surface characteristics were found in all size ranges. One particle was associated with chlorine, sulfur and possibly clay in the 0.1 to 0.4μ size range during stagnant atmospheric conditions.

- Clay was found in all size ranges and always in association with sulfur for stagnant conditions, but only for the 0.4 to 1.0μ range during storm conditions.

- Sulfur is not restricted to the accumulation mode. Sulfur composes an increasing proportion of the alumino-silicate/sulfur mass for decreasing particle size. This phenomena is consistent with the concept of sulfuric acid absorption into alumino-silicate surface layers.

- Chlorine was also associated with alumino-silicates in all size ranges for stagnant conditions but was not sought for storm conditions. This association is consistent with accumulation of chlorine from sea salt under stagnant atmospheric conditions.

- Chlorine and sulfur occurred in a fixed ratio except for one instance.

- Gypsum was found in size ranges greater than one micron for stagnant conditions.

- Sodium sulfate was found in the 0.4 to 1.0μ range during storm conditions.

Summary of Composition of Particles at 15,000 Feet Captured on Cascade Impactor in August 1988

$6\mu <$ Dia	$1\mu <$ Dia $< 6\mu$	$0.4\mu <$ Dia $< 1\mu$	$0.1\mu <$ Dia $< 0.4\mu$
	Week 1 - Stagnant Weather Conditions		
Montmorillonite+(S+Cl)	Illite + $CaSO_4$	$CaPO_4$ Clay + S + Cl Clay + (S+Cl)	$CaPO_4$ + (S + Cl) Clay + (S + Cl) $CaPO_4$ + (S + Cl)
	Week 2 - Stormy Weather Conditions		
$CaPO_4$ Quartz	$CaPO_4$	$NaSO_4$ $CaPO_4$ Clay + S $(NH_3)_2SO_4$	$(NH_3)_2SO_4$

Smog and Dust in the Mojave Desert

Ground level atmospheric extinction from 0.5 to 12 microns was determined as a function of date and time of day by a combination of direct visibility measurements and Mie calculations.

Simultaneous Measurements were made using

>   Nephelometer
>   Telephotometer
>   Aerosol

instruments in the Indian Wells Valley from April through July 1987.

Spectral Extinction was calculated using measured aerosol size distributions and composition estimated from the RESOLVE Report.
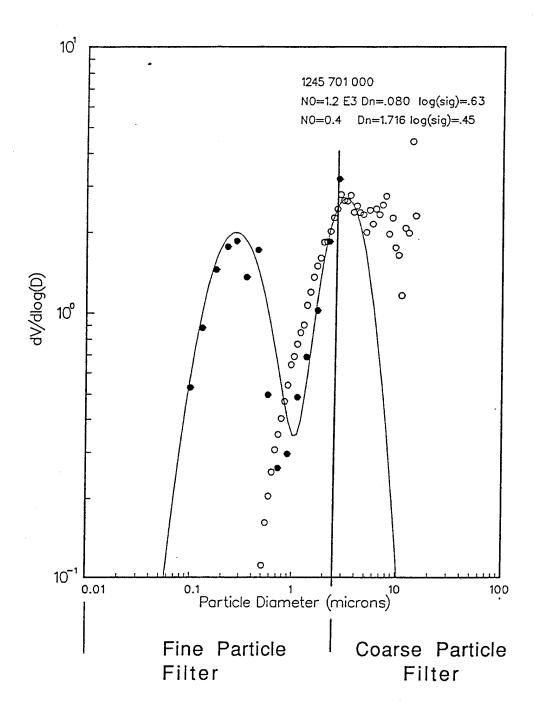
Results

Unexpectedly high extinction in the 8 - 12 micron range agrees with anecdotal information: In side by side operation at the Naval Weapons Center detectors operating in the 8 - 12 do not perform as well as those operating in the 3 - 5 micron range.

The situation may be worse than what we have calculated:

Mid-day (when most of our data were taken) accumulation mode aerosol concentrations were only 60% of the twenty-four hour average and sometimes only a quarter of the midnight concentrations.

Measured organic aerosol concentration may be too high by a factor of two due to 2X4 filter contamination. That would imply that $(NH_4)_2SO_4$ induced extinction could be twice what we have calculated.

1245 701 000
NO=1.2 E3 Dn=.080 log(sig)=.63
NO=0.4   Dn=1.716 log(sig)=.45

Fine Particle
Filter

Coarse Particle
Filter

Soot   Organic   Dust
Ammonium Sulfate   Carbon
Ammonium Nitrate

Overlap of RESOLVE 2x4 Filters with Aerosol
Size Distribution Modes
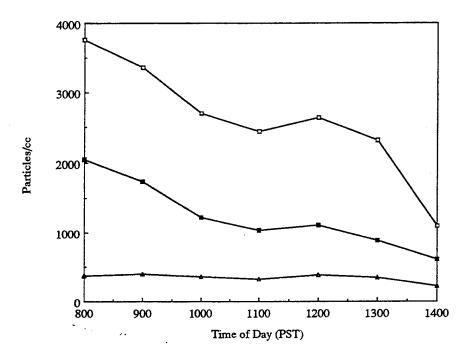
FIGURE 20. Daytime Accumulation Mode Particle Concentrations. The middle points were averaged over four months starting in April. The other points are the extreme concentrations observed for that time of day in the four months of data taking.
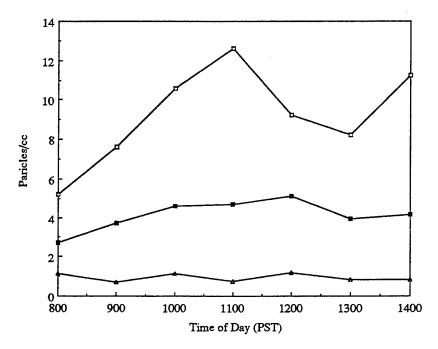
FIGURE 21. Daytime Dust Mode Concentrations. The middle points were averaged over three months starting in May 1987.

Accumulation Mode

	No	ΔNo%	Dn	ΔDn%	Log(sigma)	ΔLog(sigma)%	Mass
April	883	75	0.122	6	0.452	11	2.1
May	526	26	0.136	6	0.49	5	2.1
June	1109	62	0.12	9	0.458	12	2.6
July	2260	23	0.097	16	0.513	16	3.5

Dust Mode

	No	ΔNo%	Dn	ΔDn%	Log(sigma)	ΔLog(sigma)%	Mass
May	6.54	28	.544 (.337*)	20	0.903	5	13.71*
June	3.28	47	.615 (.381*)	42	0.911	9	10.6*
July	6.67	40	.323 (.200*)	37	0.969	9	5.1*

* Computed assuming dust particle specific gravity of 2.6.

Table 8 . Monthly Average Log-Normal Fit Parameters.

Month	Soot	Sulfate	Nitrate	Organic Carbon	Dust	Fine Mass (mcrg/m^3)
April	6.1	24.2	12.2	24.2	33.3	8.2
May	10	20	5	35	30	10
June	7.4	19.4	18.5	27.8	26.9	10.8
July	6.4	29.4	2.7	45	16.5	10.9
August:						
24 Hour	6	31	1	40	22	10.3
Daytime	4.8	25.8	9.7	40.3	19.4	8.9

TABLE 13. Fine Particle Mass Composition from RESOLVE. Values are in percent mass.

Material	% of Dust	Density
Montmorillonite Clay	3.57	2.5
Kaolinite Clay	5.32	2.64
Illite Clay	25.3	2.75
Quartz	22.38	2.65
Sodium Nitrate	23.45	2.26
Calcite	2.41	2.71
Potassium Nitrate	2.06	2.11
Dolomite	5.79	2.86
Hematite	5.71	5.24
Halite	4.01	2.17

Average dust density = 2.61 gm/cc

Table 17. China Lake Dust Using Pye Model.

Material	% of Dust
Montmorillonite Clay	20.3
Kaolinite Clay	10.1
Illite Clay	10.6
Quartz	15.5
Sodium Nitrate	21.1
Calcite	3.6
Potassium Nitrate	5.6
Dolomite	4.2
Hematite	5.4
Halite	3.8

Average dust density = 2.55 gm/cc

Table 18. China Lake Dust Using Hoidale Model.
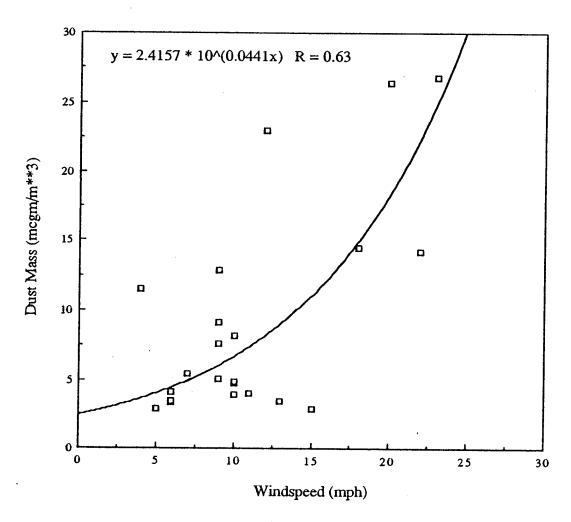
Figure   . Dust Mass versus Windspeed.

$$y = 0.2689 + 0.0145x \quad R = 0.33$$
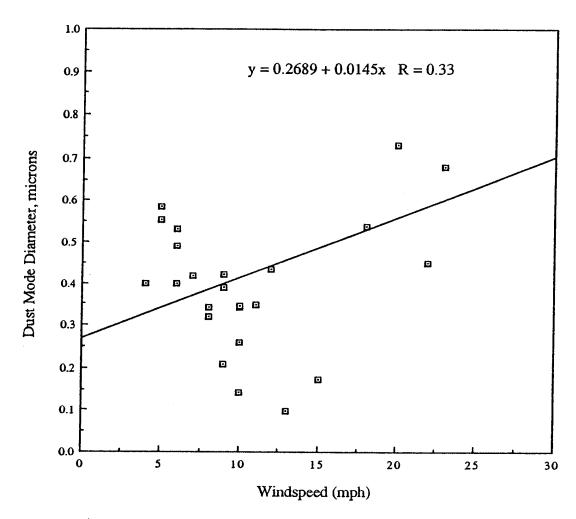
Figure . Dust Mode Diameter versus Windspeed.

$$y = 0.8923 + 0.0037x \quad R = 0.19$$
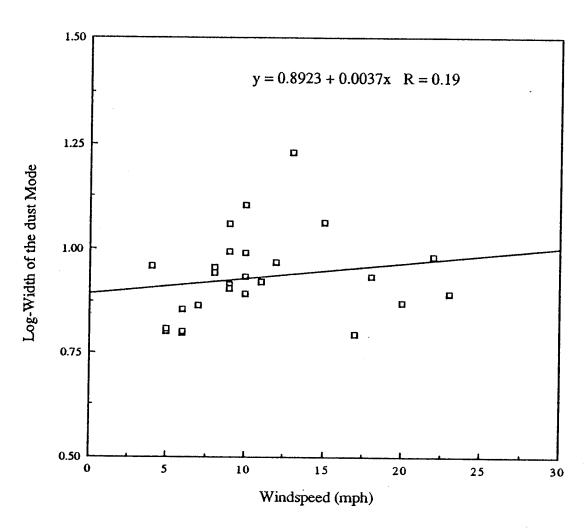
Figure . Width of the Dust Mode versus Windspeed.

SAMPLING EQUIPMENT AT EDWARDS AFB

Edwards AFB (elevation = 2,421 ft MSL)

TSI Differential Mobility Particle Sizer (DMPS) (0.01 to 0.5 microns)

TSI Aerodynamic Particle Sizer (APS 33B)

MRI 1560/1590 Integrating Nephelometer

Wedding 2X4 Sampler (PM2.5, PM10 & chemistry - 24hr)

NEA Sequential Filter Sampler (PM2.5, PM10 & chemistry - am & pm)

Tracer Technologies Sampling System (Perfluorocarbons - sampled during 4 tracer release periods)
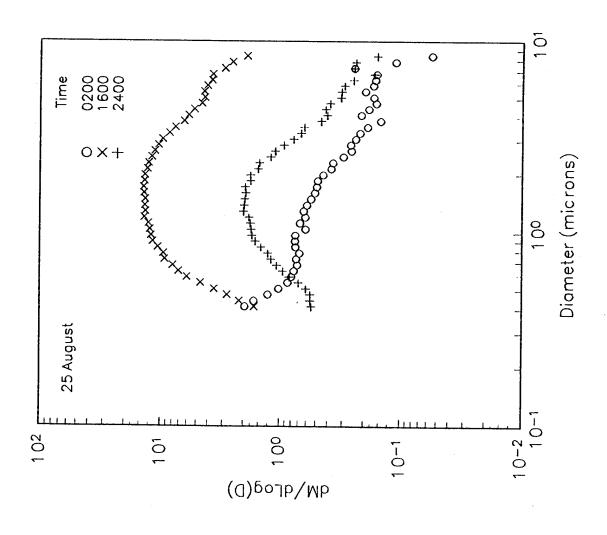
Climatronics System (Meteorology - wind, temperature, & relative humidity)

DASIBI 1003 AH Ozone Analyzer

CSI 1600 Chemiluminescent NOx Analyzer
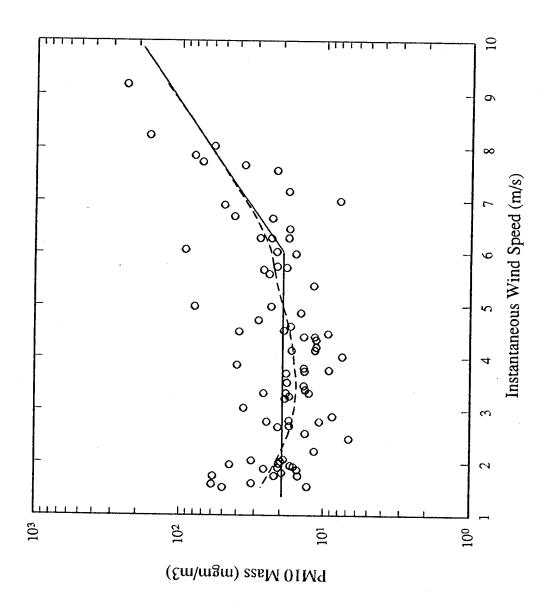
Table 1. Composition of Aerosol Captured on PM2.5 and PM10 Filters. Comparison of the PM10 aerosol with clay compositions indicates that Edwards dust is composed of illite clay and gypsum. The accumulation mode aerosols, however, are predominantly organic.

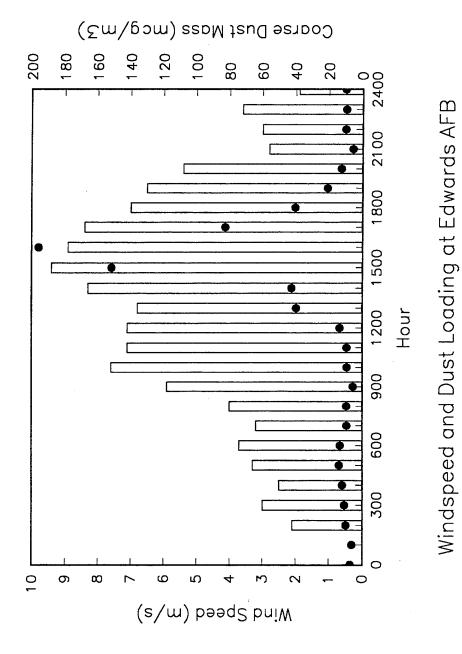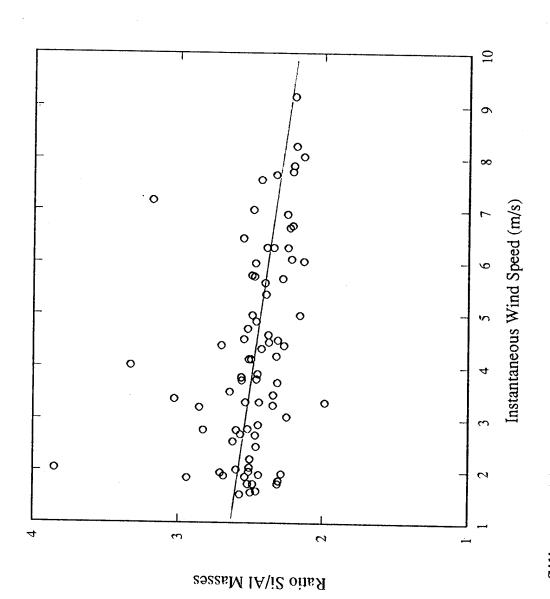| Ions	% Mass		% Mass of Clay Elements									
	PM2.5	PM10	Illite	Glauconite	Montmorillinite	Chlorite	Illite Montmorillinite	Chlorite Montmorillinite	Palygorskite	Sepiolite	Kaolinite	Allophanes
Chloride	0.4											
Nitrate	5.0											
Sulfate	16.4											
Ammonium												
Organic Carbon	42											
Elemental Carbon	7.4											
Elements												
Al	4.0	20.4	24	9.15	21.93	33.52	28.5	12.1	6.82	0.6	35.18	44.95
Si	10.4	47.9	51.7	49.22	59.49	39.85	51.5	41.2	61.6	52.5	48.8	26.68
P		0.04										10.57
S	6.9	5.6										0.22
Cl		0.07										
K	2.3	7.1	5.59	6.88	0.34	1.61	9.07	0.22			0.4	
Ca	1.9	6.3	0.97	0.64	1.18	0.15	0.05	1.4	0.67	0.47	0.22	2.37
Ti	0.3	0.9	0.68		0.25	1.03	0.77	0.04			0.61	
Mn	0.1	0.2										
Fe	3.5	11	4.57	21.38	3.97	4.56	1.52	2.13	0.87	3.6	1.24	0.12

137

Mass Distribution from beginning to end of Storm

Windspeed and Dust Loading at Edwards AFB

SFS Filter Mass vs Five Hour Averaged Wind Speed

Silicon to Aluminum Mass Ratio *vs* Wind Speed. The authors do not know why the silicon to aluminum content decreases with wind speed.

Future Work

- Investigate organic aerosol problem by comparing mass captured on filters to mass calculated from size distribution. Use a denuder (pre-filter) to remove organic vapors.

- Use LIDAR to get vertical aerosol profiles to 15,000 to 20,000 ft.

- Make greater effort to get all the instruments working all the time in order to obtain comparison and rare event data.

- Use impactor and x-ray elemental mapping more extensively than here-to-fore in order to deduce particle composition statistics.

- Relate aerosol and meteorological data to meteorological codes that will run on a work station. Codes that do not appear to be suitable are NOGAPS, COAMPS and NORAPS since they take hours to run on a Cray C-90.

Application of the MODTRAN2 code to the modeling of silicate dust clouds.

S. Mazuk
D. K. Lynch

The Aerospace Corporation
P.O. Box 92957
Los Angeles, CA 90009

Application of the MODTRAN2 code to the modeling of silicate dust clouds.

Abstract

The MODTRAN2 code has been used to model the thermal infrared radiance from a dust cloud formed during an explosives test. High signal-to-noise ratio infrared spectra (3 - 14 microns, $\lambda/\Delta\lambda \approx 0.1$ microns) of the dust cloud were measured and they showed the presence of silicate particles. In an attempt to model the thermal emission of the dust cloud and reproduce the silicate feature, a silicate dust cloud was generated, and MODTRAN2 was used to calculate radiance spectra between 6 and 16 microns. A description of the analysis, comparison with experimental data, and the problems encountered will be presented.

1. Observations

An explosives test in U.S. southwest desert lofted a large amount of dust into the atmosphere to altitudes of several thousand meters above ground level (AGL). High signal to noise spectra of the resulting dust cloud were measured in the 3-14 micron range using a nonscanning array spectrograph (Hackwell et al. 1990). Data were taken during the initiation, growth and dispersion of the dust cloud (Lynch et al. 1994). In addition, spectra of the clear sky and that of a cumuloform water cloud were also collected. The spectra of the dust cloud showed clear evidence of the silicate Si_xO_y vibrational emission band near 10 microns (Figures 1, 2). Laboratory analysis of soil samples collected from ground zero before and after the test confirmed the identification.

Owing to the limited slant angles, column densities, composition and other atmospheric variables, we decided to model the dust cloud radiance using a general purpose atmospheric radiance code. The initial objective was to calculate the infrared spectra expected from a model silicate cloud and compare this to the observed data. The MODTRAN2 model was chosen based on available expertise in running the code, adequate spectral resolution to match the instrument used for the observations, and an existing dust model built into the code.

144

The very existence of the silicate emission feature gives some indication of the particle size. Optically thick particles would not show a silicate feature. For typical silicates for which the imaginary parts of the indices of refraction around 10 microns are near unity (highly absorbing), the maximum particle size that would show silicate emission is of order 10 microns in radius. With this in mind, we used the indices of refraction for various silicate minerals (including MODTRAN2's volcanic aerosols), computed the absorption and extinction efficiencies Q_{abs} and Q_{ext} using Mie theory, then defined a dust cloud at a height and size consistent with the cloud produced in the test. This cloud was approximately 500 meters thick, approximately 3 km AGL and observed from the ground with a zenith angle of about 60 degrees. The extinction coefficients were computed and used as inputs to MODTRAN2.

3. Aerosols and MODTRAN2

In operation, the MODTRAN2 model will define a model atmosphere layering based on predefined altitudes for four different aerosol regions. A first attempt at defining a model atmosphere was made by allowing MODTRAN2 to generate its own layering. For this observing geometry, and given our plans to change the defined aerosol layer contents, the default layering was inadequate. While MODTRAN2 performs some scaling of the aerosol profiles based on the actual starting altitude for the observation (through the GNDALT input), the boundaries of the four built-in aerosol layers are fixed at 0 to 2 km, 2 to 10 km, 10 to 30 km, and 30 to 100 km. For this viewing site, the altitude for our test was close to the first aerosol layer boundary at two kilometers. Because of this, the MODTRAN2 atmosphere allowed only three layers for the boundary layer aerosol before the second predefined aerosol layer boundary was reached.

Using the MODTRAN2 generated layering as a guide, a model atmosphere was created using 100 meter laying through 4 kilometers, with the remaining layers spread upwards to 100 kilometers. This was the only way to redefine the aerosol layer boundaries in the MODTRAN2 inputs. One of the difficulties in this process occurred because MODTRAN2 limits the model atmosphere to only 34 layers. In this case the layer limitations required that the stratospheric ozone layering be made coarser to allow for better modelling of the boundry layer aerosols.

The extinction and scattering coefficients of the dust were calculated using the Mie theory code developed by Bohren and Huffman (1983). This calculation assumes that the particles are spherical in shape. While the assumption of sphericity is valid for liquid aerosol particles, the variety of shapes in dust particles can give rise to errors. Although this assumption may yield answers that are not entirely correct, the uncertainties in the optical constants and size distributions are certainly more significant. The values of Qext and Qscat were calculated for each of the 47 wavelength values required by the MODTRAN2 code. The optical constants for the silicate material were obtained from Palik (1982), which compiles the data from numerous sources.

In addition to using these calculated values, the extinction and absorption coefficients for the volcanic aerosols available in MODTRAN2 were used to define the dust cloud. The structure in the 'aged volcanic' absorption suggests that this aerosol contains some silicates (Volz 1973, Shettle and Volz, 1976).

The scattering coefficients were then included into the second of the four aerosol regions in the model atmosphere described above. Only the aerosol species of interest was changed when the dust cloud was loaded into the model atmosphere; the other aerosol species and the atmospheric layering remained unchanged.

4. Comparison with Observations.

Figure 3 shows a comparison between the observed spectrum and that calculated by the default layering generated by MODTRAN. The tropical atmosphere profile was required to match the observed radiance, indicating a large amount of water vapor was present in the atmosphere even though the observing site was in a desert. The deficit between the calculated and observed radiances is probably due to a hygroscopic aerosol haze in the atmosphere, and could be modelled by using a rural aerosol model. Further investigation of this will be done using the sonde data in a follow-on study.

Figure 4 shows a comparison between the observed radiance and a MODTRAN2 calculated spectra using the 'aged volcanic' aerosol absorption and extinction coefficients that are built into the MODTRAN2 code. The observed spectrum used for this comparison was taken thirty minutes after the initial cloud was formed, so the

dust particles should be in thermal equilibrium with the surrounding atmosphere. The agreement between the two is reasonable, showing the expected silicate emission in the 8.5 to 9.5 micron band. Unfortunately, since the actual composition and particle sizes of the 'aged volcanic' material were not known to us at the time of this study, a further comparison could not be made.

In Figure 5 the radiance from a cloud composed only of amorphous SiO_2 particles of 5 micron radius is compared with the observed cloud data. The differences in these spectra between 8.5 and 9.5 microns clearly indicate that the structure of the amorphous silicate emission is not adequate to model this cloud. This comparison, combined with laboratory analysis of dust from the site, suggested the use of a crystalline silicate material to better model the spectral structure.

5. The 47 wavelength problem.

When we began to include a crystalline silicate material, quartz, into a dust cloud model, a significant problem was encountered. Figures 6 and 7 show the scattering coefficients calculated for input into MODTRAN2 for a 5 micron radius cloud composed of quartz, using the optical constants from Palik (1985). The full resolution values are drawn in the solid lines, while the values which MODTRAN2 uses are shown as the dashed line. Note that significant spectral structure is lost, particularly near the 9.5 micron absorption, as well as near the 12.5 micron absorption bands.

Apart from selecting which optical constants to use for the dust cloud model, the fixing of the wavelengths at which the optical constants can be input to the MODTRAN2 code poses a serious limitation to accurately modelling the emission from the dust cloud. While the model does allow for an input wavelength from card 2D2, these values are discarded since they must conform to the required 47 input wavelengths. While the choice of these 47 wavelengths does perhaps make some sense in the context of an overall atmosphere (e.g. interference from the ozone band near 9.5 microns), this imposes a limitation on the types of materials that can be modelled. This limitation does not render the model useless, since these wavelengths do work well for some materials. For example figures 8 and 9 show a comparison of the amorphous SiO_2 optical constants that can be input to MODTRAN2 with the actual values. For

this material, the fixed wavelengths are a reasonable approximation to the real values.

6. Discussion

In attempting to define our own aerosol cloud, a number of difficulties were encountered in using MODTRAN2 code. While the LOWTRAN manuals provided some guidance for constructing a model atmosphere, the process of introducing a user defined aerosol brought out several questions. Among these, there is a question as to why there are four regions allowed for the user defined aerosols, yet there are five total aerosol regions which are defined in the code. The use of this fifth aerosol region, and therefore its effect on the data, is still unclear.

A second issue is the composition and particle size distributions of the built-in dust aerosols. Volz (1972) and Shettle and Volz (1976) discuss the absorption and transmission of field gathered dust particles without a discussion of the composition of dust itself.

As discussed above, the restriction of wavelengths at which the scattering parameters can be input limits the aerosol materials that can be modelled. To explore this further, we have modified the MODTRAN2 code to remove this wavelength restriction. However the restriction to 47 wavelength values has not yet been removed, and makes the selection of the appropriate wavelengths for each aerosol material very important. The results of this investigation will be discussed in a future study. It is interesting to note that other investigators have also encountered this difficulty, Hammer has made similar modifications to the LOWTRAN code in connection with his work on cirrus clouds (Hammer et al. 1994).

7. Conclusions and directions for further work

The MODTRAN2 model works reasonably well for modelling the infrared spectra from a silicate cloud in a model atmosphere.

The user defined aerosol layer capability of the MODTRAN2 model works well for materials whose spectral structure is smooth so

that the scattering parameters are well sampled by the available input values.

We recommend the following modifications of MODTRAN2 be made. The existing restriction of 47 fixed wavelengths at which the scattering parameters can be input should be removed. This restriction limits the aerosol materials that can be modelled using the MODTRAN2 code.

8. Acknowledgements

We would like to thank Paul Adams and Ann Mazuk for assistance on this project.

Bohren, C. and D. Huffman, <u>Absorption and Scattering of Light by Small Particles</u>, John Wiley & Sons, New York (1983)

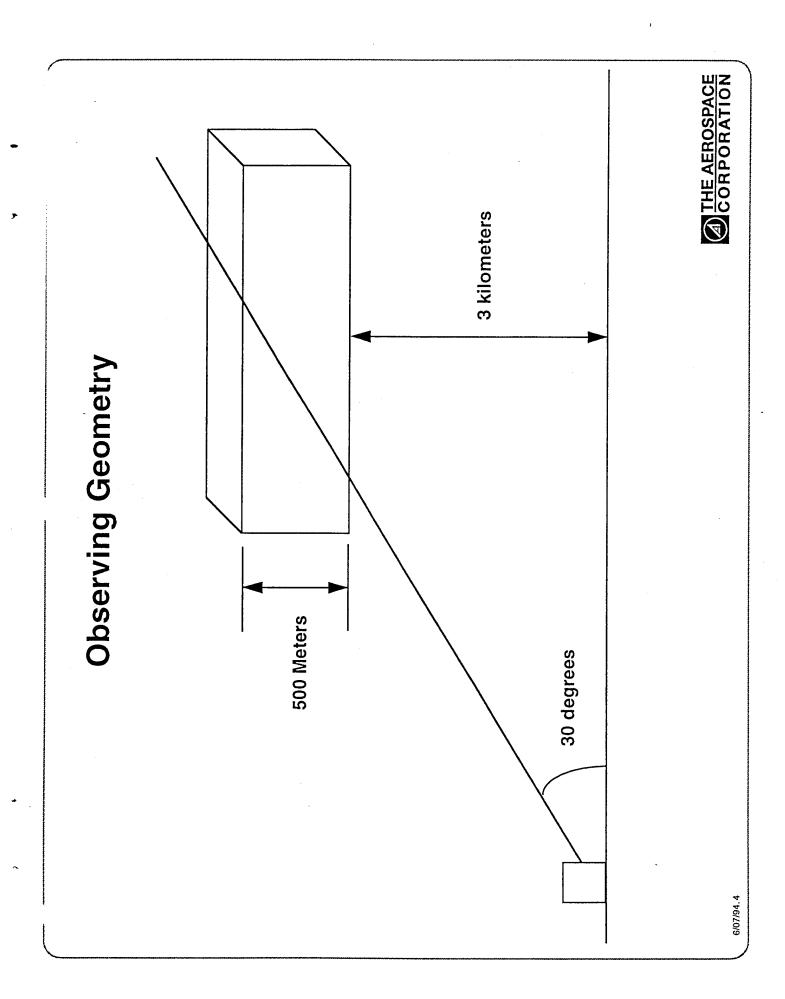Palik, Edward D., <u>Handbook of Optical Constants of Solids</u>, Academic Press, Orlando (1985)

Hackwell, J. A., D. W. Warren, M. Chatelain, Y. Dotan, P. Li, D. K. Lynch, D. Mabry, R. W. Russell, and R. Young, "A Low Resolution Array Spectrograph for the 2.9 - 13.5 μm Spectral Region", Proc. SPIE Conference 1235 on <u>Instrumentation in Astronomy VII</u> (1235), 171-180 (1990)
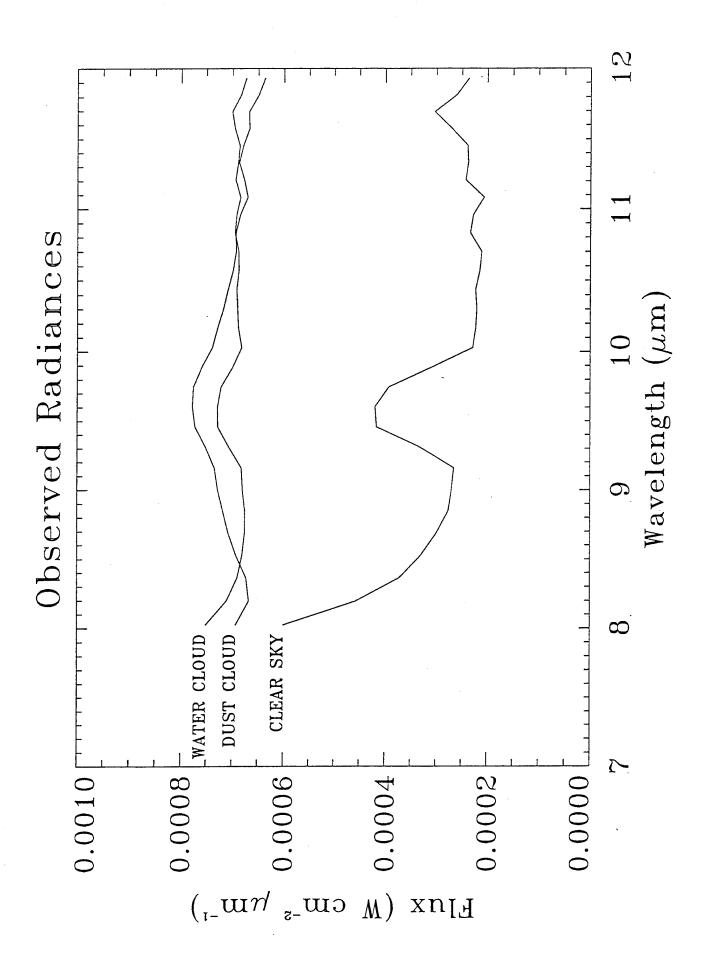
Hammer, P.D., F.P.J. Valero, and W.H. Smith, "Spectral Imaging of Clouds using a Digital Array Scanned interferometer", <u>Atmospheric Research</u>, in press (1984)
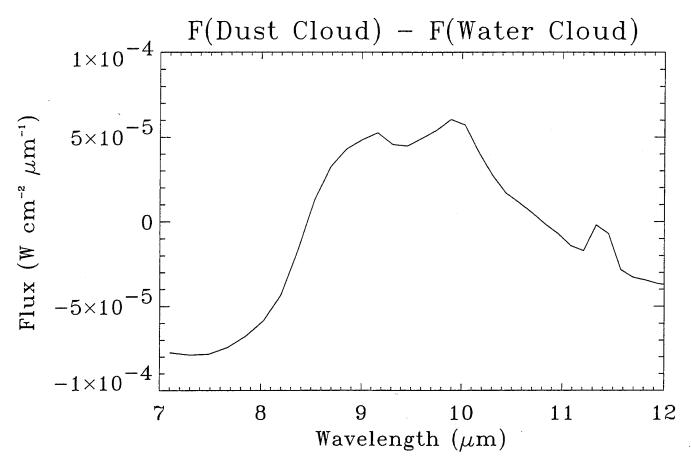
Lynch, David K., Mark A. Chatelain, Theo K. Tessensohn, Paul M. Adams, " 3 - 14 μm Nonscanning Spectra of the Minor Uncle Dust Cloud", Proc. Minor Uncle Symposium, FCDNA, Albuquerque Feb 3-4, 1994 (in press)
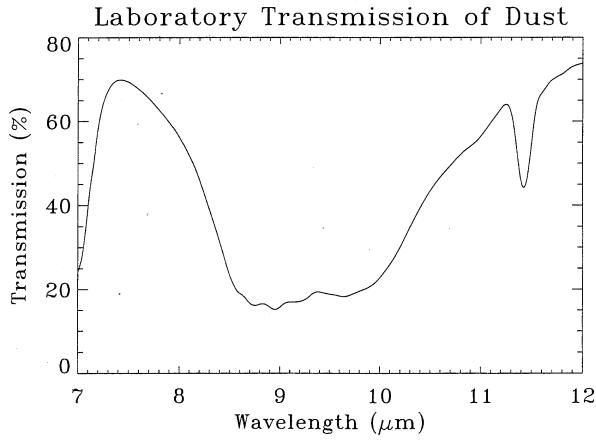
Shettle, E.P. and F.E. Volz, "Optical Constants for a Meteoric Dust Aerosol Model", <u>Atmospheric Aerosols: Their Optical Properties and Effects </u>, A Topical Meeting on Atmospheric Aerosols sponsored by the Optical Society of America and NASA Langley Research Center, Williamsburg, Virginia, 13-15 December 1976, NASA CP-2004
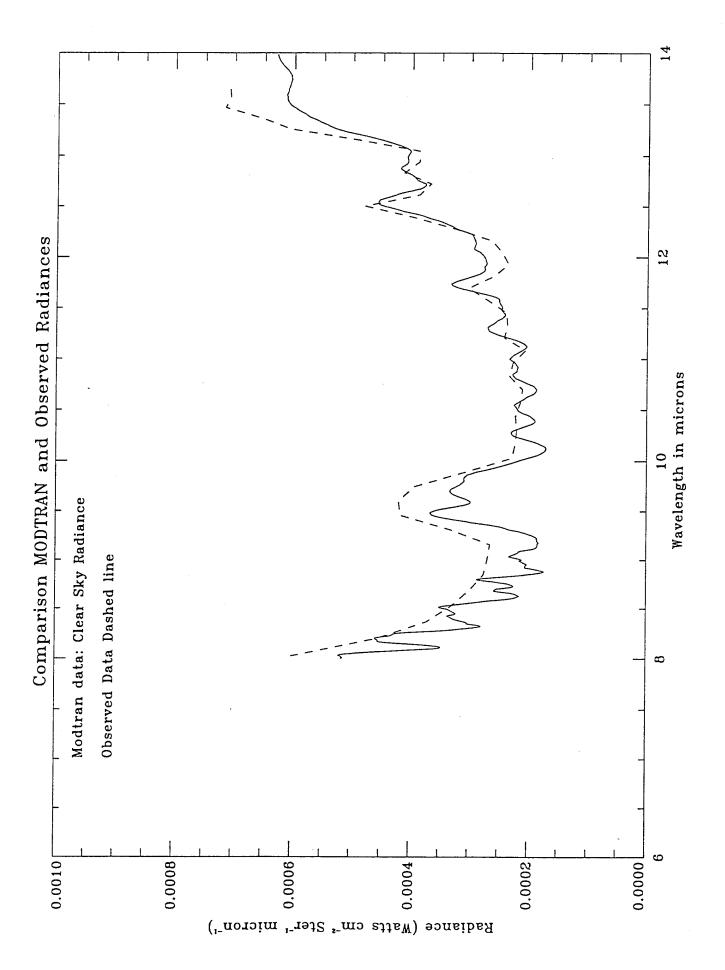
Volz, F. E., "Infrared Optical Constants of Ammonium Sulfate, Sahara Dust, Volcanic Pumice, and Flyash", <u>Applied Optics</u>, Vol. 12, 564-568, (1973)

Observing Geometry

500 Meters

3 kilometers

30 degrees

6/07/94. 4

151

Observed Radiances

WATER CLOUD

DUST CLOUD

CLEAR SKY

Flux (W cm^{-2} μm^{-1})

Wavelength (μm)

F(Dust Cloud) – F(Water Cloud)

Laboratory Transmission of Dust

Comparison MODTRAN and Observed Radiances

Modtran data: Clear Sky Radiance

Observed Data Dashed line

Comparison MODTRAN and Observed Radiances

Modtran data: Aged Volcanic

Observed Data Dashed line

Wavelength in microns

Radiance (Watts cm⁻² Ster⁻¹ micron⁻¹)

Comparison MODTRAN and Observed Radiances

Modtran data: Silicate Glass

Observed Data Dashed line

Wavelength in microns

Radiance (Watts cm⁻² Ster⁻¹ micron⁻¹)

Comparison of Original Optical Data To Modtran

Comparison of Original Optical Data To Modtran

Comparison of Original Optical Data To Modtran

Qextinction

Wavelength in Microns

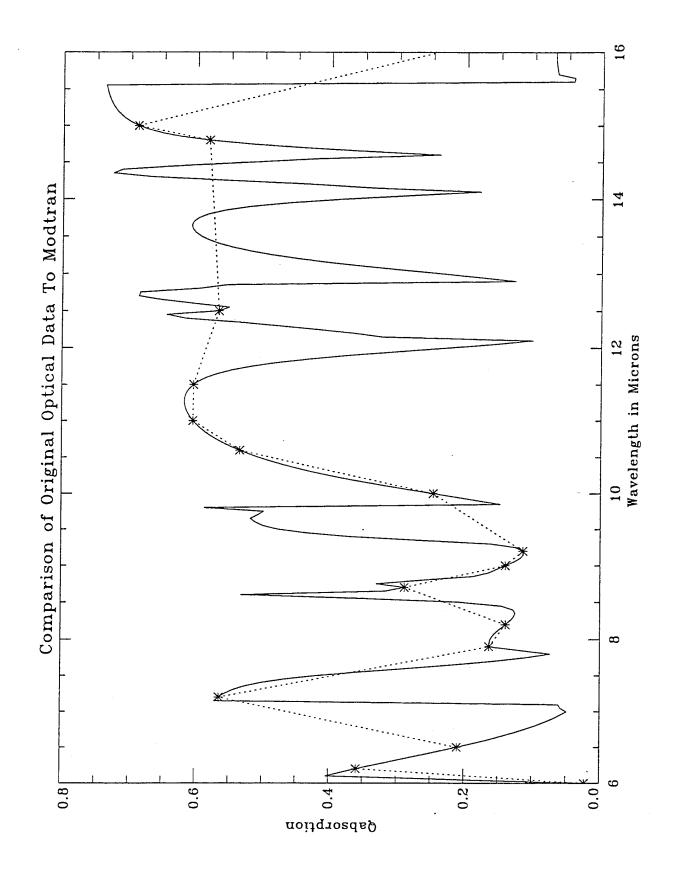Comparison of Original Optical Data To Modtran
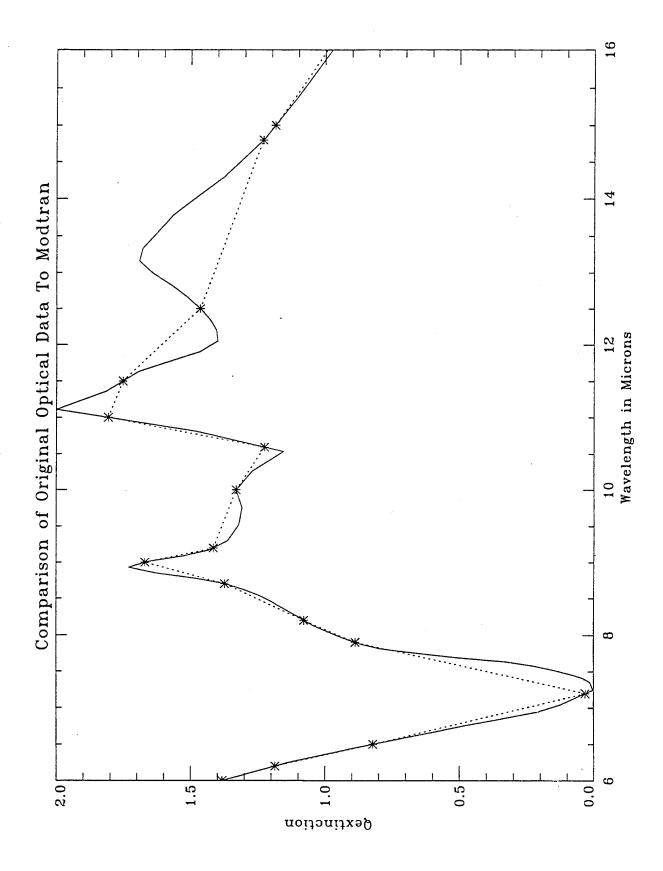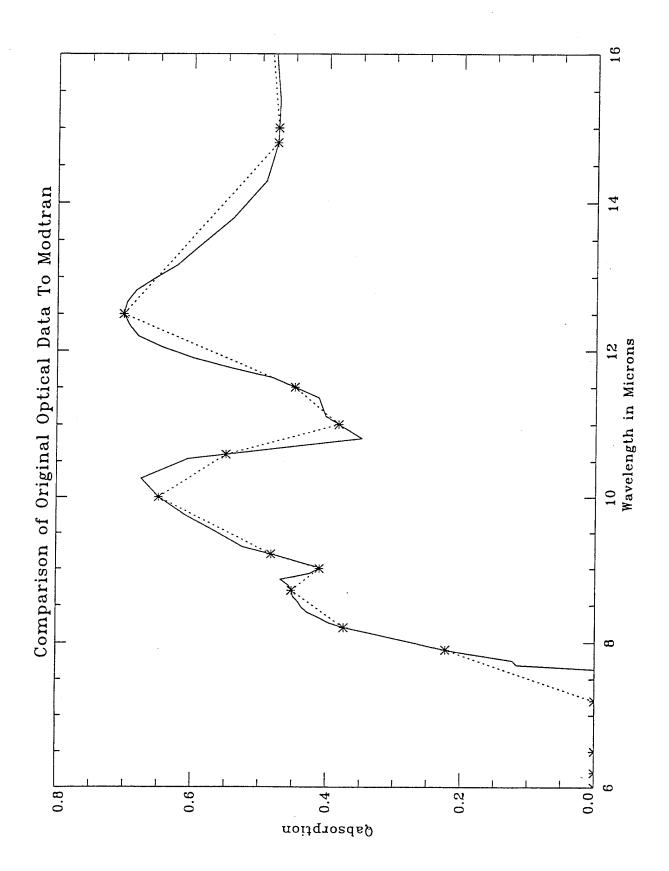
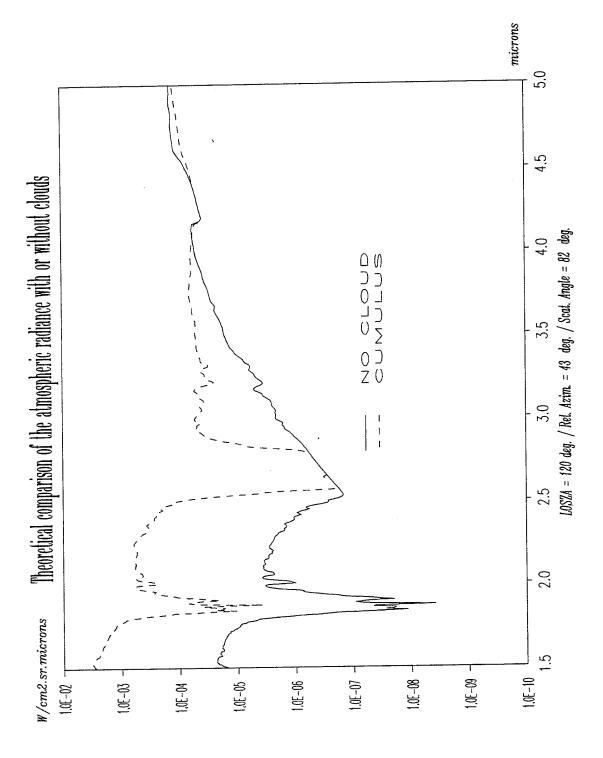Qabsorption

Wavelength in Microns

Conclusions

Modtran Works Reasonably Well for Modeling the Thermal Infrared Radiance From a Silicate Dust Cloud.

The User Defined Aerosol Input To Modtran Works Well for Materials Whose Spectral Shape is Smooth.

We Recommend that the Wavelength Restriction for the User Defined Aerosol Inputs be Removed.

6/07/94.6

Airborne measurements of cloud radiation
and
comparison with theory

C.Malherbe, P.Simoneau, P.Michon
A.Boischot, G.Durand, J.Deschamp, G.Gregoire

1/ Introduction

2/ Airborne measurements

3/ Comparisons with LOWTRAN7

4/ Improvement of the model $\longrightarrow$ NUALUM

5/ Results

6/ Conclusion

Theoretical comparison of the atmospheric radiance with or without clouds

W /cm2.sr.microns

LOSZA = 120 deg. / Rel. Azim. = 43 deg. / Scat. Angle = 82 deg.

NO CLOUD
CUMULUS

microns

INTRODUCTION

Requirements at ONERA

Modelisation of the infrared atmospheric and terrestrial backgrounds in presence of clouds:
- fluctuations of the atmospheric background
- fluctuations of satellites terrestrial pictures

Tools

- airborne measurements
- computer models

CLOUD CAMPAIGN ONERA

objective:
- measure of the cloud radiance fluctuations
- validation of NUALUM

2 july 1992 fly:
azimut = 0° to 360°
- losza = 30°
- losza = 15°
- losza = 0°

3000m

losza

2500m

cumulus
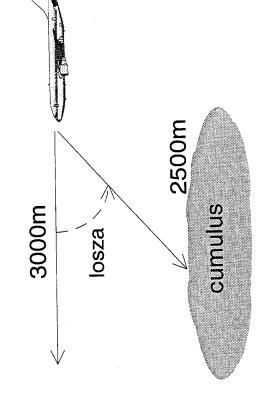
SICAP Spectra (Spectromètre Infrarouge Cryogénique AéroPorté)

165

Airborne measurements

Spectromètre Infrarouge Cryogénique AéroPorté (SICAP)

(airborne cryogenic IR spectrometer)

→ IR Spectrometer: - circular variable filter
          - band: 1.5 - 5.5 μm
          - resolution: $\Delta\lambda/\lambda = 2\%$

→ Cryogenic $\Longrightarrow$ low thermal noise

→ Airborne $\Longrightarrow$ C.E.V.'s caravelle 116

Spectromètre Infrarouge Cryogénique AéroPorté

(SICAP)

Fuselage

ZnS Window

Tracking mirror

Spectrometer

I.R.

Visible

T.V

Tracker

Computer

167

Line of Sight

Longitude - deg

Latitude - deg

GEOMETRY

Cloud campaign: 2 july 1992 / SZA = 48 deg.

W/cm2.sr.microns

LOWTRAN7
MEASUREMENTS

LOSZA = 119 deg. / Rel. Azim. = 138 deg. / Scat. Angle = 144 deg.

microns

Cloud campaign: 2 july 1992 / SZA = 48 deg.

W/cm2.sr.microns

2.00E-04

1.75E-04

1.50E-04

1.25E-04

1.00E-04

7.50E-05

5.00E-05

2.50E-05

0.00E+00

2.6   3.0   3.4   3.8   4.2   4.6   5.0   *microns*

LOWTRAN7
MEASUREMENTS

LOSZA = 119 deg. / Rel. Azim. = 138 deg. / Scat. Angle = 144 deg.

Cloud campaign: 2 july 1992 / SZA = 48 deg.

LOSZA = 107 deg. / Rel. Azim. = 132 deg. / Scat. Angle = 132 deg.

LOWTRAN7
MEASUREMENTS

W/cm2.sr.microns

microns

Cloud campaign: 2 july 1992 / SZA = 48 deg.

W/cm.2.sr.microns

LOWTRAN7
MEASUREMENTS

LOSZA = 106 deg. / Rel. Azim. = 42 deg. / Scat. Angle = 70 deg.

microns

Cloud campaign: 2 july 1992 / SZA = 48 deg.

W/cm2.sr.microns

—— LOWTRAN7
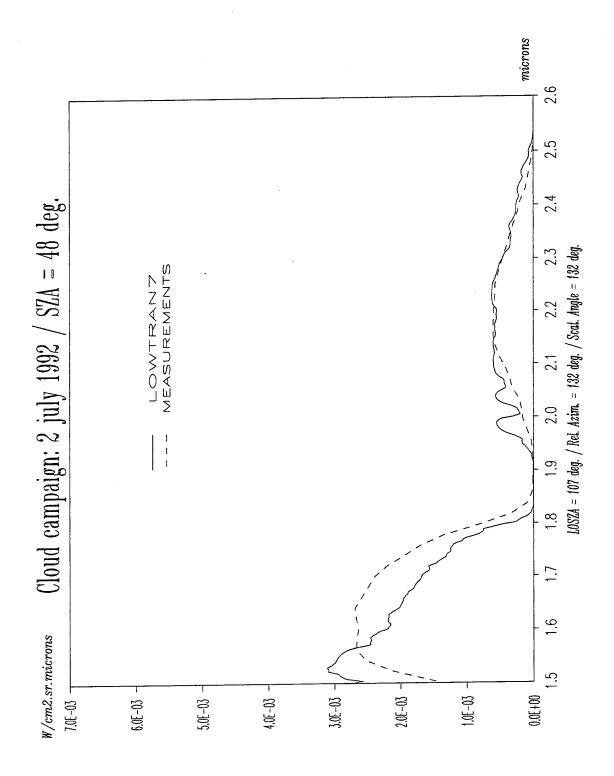- - - MEASUREMENTS

LOSZA = 95 deg. / Rel. Azim. = 11 deg. / Scat. Angle = 49 deg.

microns
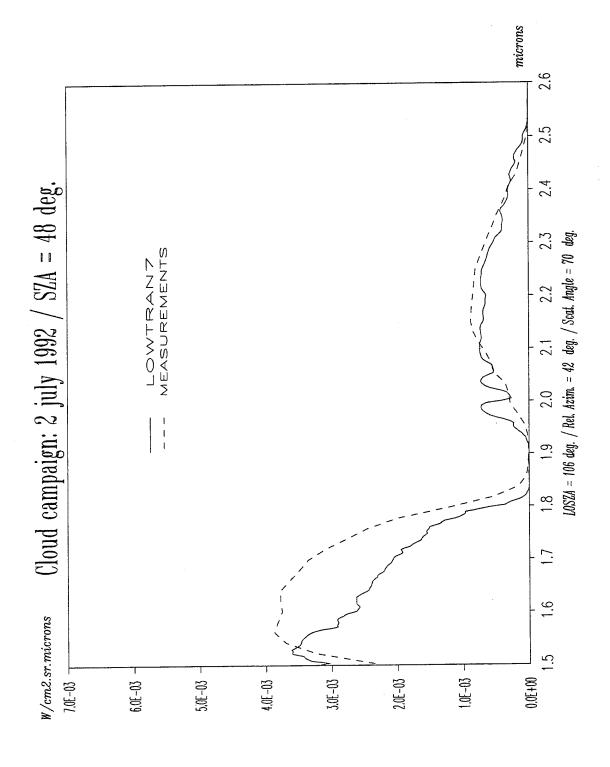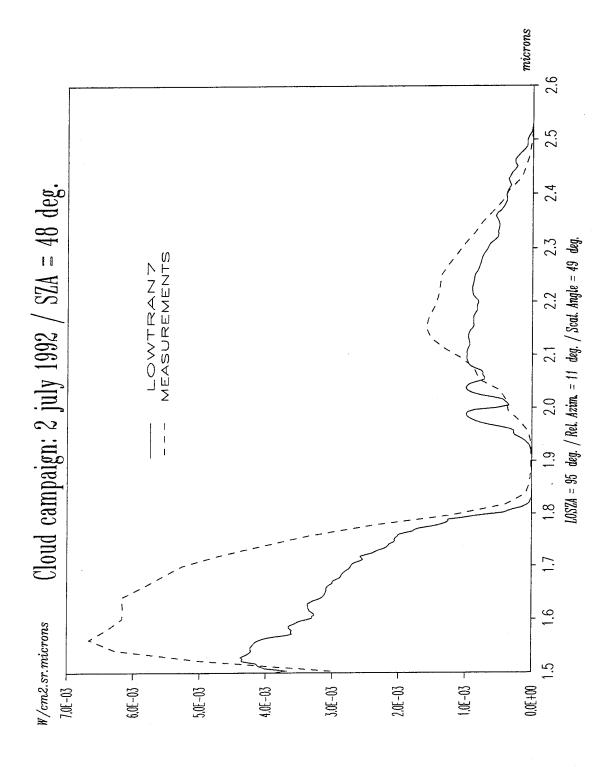
Discussion

Comparisons measurements with LOWTRAN7

➤ approximative method for the computation
of the multiple scattering (two stream method)

Improvements

➤ more accurate method (Discrete Ordinate Method)
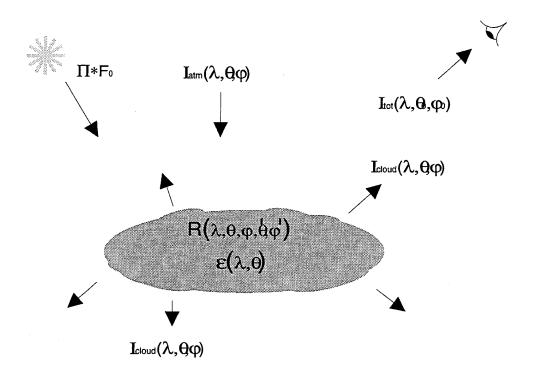
➤ microphysical parameters

⇨ **NUALUM**

Cloud radiation pattern

$\Pi * F_0$ $I_{atm}(\lambda,\theta,\varphi)$

$I_{tot}(\lambda,\theta,\varphi_0)$

$I_{cloud}(\lambda,\theta,\varphi)$

$R(\lambda,\theta,\varphi,\theta'\varphi')$
$\varepsilon(\lambda,\theta)$

$I_{cloud}(\lambda,\theta,\varphi)$

$$I_{tot}(\lambda,\theta,\varphi_0) = \mu_0\,\Pi\,F_0\;R(\lambda,\theta,\varphi_0,\theta_s,\varphi_s)\,T_{co}(\lambda) + I_{cloud}(\lambda,\theta,\varphi_0)\,T_{co}(\lambda) + I_{atm}(\lambda,\theta,\varphi_0)$$

$$+\;T_{co}(\lambda)\int_{\theta,\varphi} R(\lambda,\theta_0,\varphi_0,\theta,\varphi)\,I_{atm}(\lambda,\theta,\varphi)\,d\theta\,d\varphi$$

$$\mu_0 = \cos\theta_0$$

$$I_{cloud}(\lambda,\theta,\varphi_0) = \varepsilon(\lambda,\theta_0) * B(\lambda,T)$$

$R(\lambda,\theta,\varphi,\theta'\varphi')$, $\varepsilon(\lambda,\theta)$, Π^*F_0, $B(\lambda,T)$, $I_{atm}(\lambda,\theta,\varphi)$, $T_{co}(\lambda)$ **?**

Organigram (1)

1/ Mie scattering code (J.V.Dave)

$$k_{ext}(i,\lambda) = \int dn(i,r)/dr \ \sigma_{ext}(\lambda) \ dr$$

$$k_{abs}(i,\lambda) = \int dn(i,r)/dr \ \sigma_{abs}(\lambda) \ dr$$

$$g(i,\lambda) = 1/2 \int_{-1}^{1} P(i,\cos\theta)\cos\theta d\cos\theta$$

$$\tau(i,\lambda) = k_{ext}(i,\lambda) \ \Delta z$$

for each layer " i " in the cloud (inhomogeneous cloud)
and n(r) given by Diem's distribution with: - r = 5 μm
- eqlwc = 0.6 g/cm^3

2/ DISORT (K.Stamnes and Collaborators)
(discrete ordinate radiative transfert)

$$k_{ext}(i,\lambda)$$
$$k_{abs}(i,\lambda)$$
$$g(i,\lambda)$$
$$\tau(i,\lambda)$$

→ **DISORT** 32 stream

↘ $R(\lambda,\theta,\varphi,\theta,\varphi')$
↗ $\varepsilon(\lambda,\theta)$

Organigram (2)

3/ LOWTRAN7 (PL/GL)

Atmospheric data
(radiosoundings)

$P(z)$, $T(z)$, $[H_2O]$
Z_{top}, Z_{bottom}

$\longrightarrow$ LOWTRAN7

ΠF_0

$T_{co}(\lambda)$

$I_{atm}(\lambda,\theta,\varphi)$
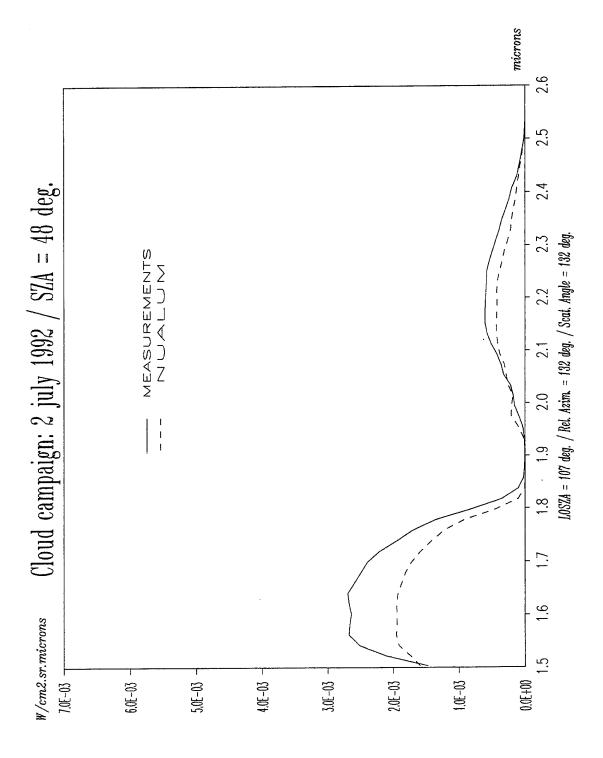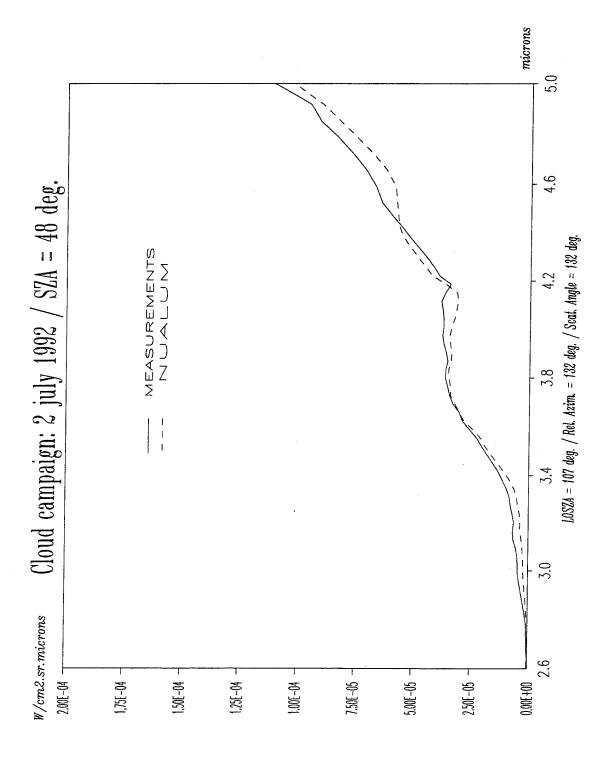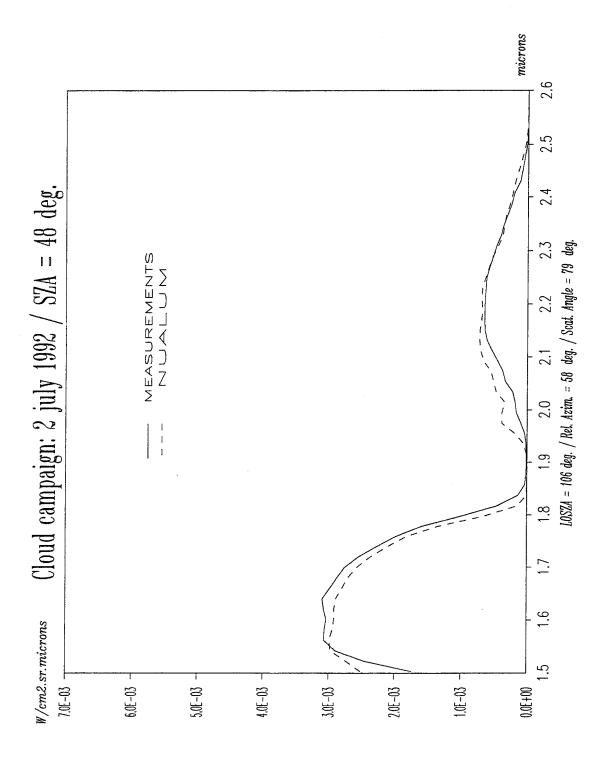
4/ NUALUM (ONERA)
(nuage luminance)

$T_{co}(\lambda)$
ΠF_0
$I_{atm}(\lambda,\theta,\varphi)$ $\longrightarrow$ NUALUM $\longrightarrow$ $I_{tot}(\lambda,\theta,\varphi)$
$R(\lambda,\theta,\varphi,\theta',\varphi')$
$\varepsilon(\lambda,\theta)$

with $\displaystyle\int R(\lambda,\theta,\varphi,\theta',\varphi')\, I_{atm}(\lambda,\theta,\varphi')\, d\theta' d\varphi' \ll \Pi F_0 * R(\lambda,\theta,\varphi,\theta'\varphi')$

Cloud campaign: 2 july 1992 / SZA = 48 deg.

MEASUREMENTS

NUALUM

$W/cm2.sr.microns$

LOSZA = 107 deg. / Rel. Azim. = 132 deg. / Scat. Angle = 132 deg.

microns

Cloud campaign: 2 july 1992 / SZA = 48 deg.

W/cm2.sr.microns

MEASUREMENTS
NUALUM

LOSZA = 107 deg. / Rel. Azim. = 132 deg. / Scat. Angle = 132 deg.

microns

Cloud campaign: 2 july 1992 / SZA = 48 deg.

MEASUREMENTS
NUALUM

W/cm2.sr.microns

LOSZA = 106 deg. / Rel. Azim. = 58 deg. / Scat. Angle = 79 deg.

microns

Cloud campaign: 2 july 1992 / SZA = 48 deg.

W/cm2.sr.microns

MEASUREMENTS
NUALUM

LOSZA = 106 deg. / Rel. Azim. = 42 deg. / Scat. Angle = 70 deg.

microns

Cloud campaign: 2 july 1992 / SZA = 48 deg.

MEASUREMENTS
NUALUM

W/cm2.sr.microns

LOSZA = 95 deg. / Rel. Azim. = 11 deg. / Scat. Angle = 49 deg.

microns

Cloud campaign: 2 july 1992 / SZA = 48 deg.

MEASUREMENTS
Itot( )
Iatm( )
$\int_{e_{\ell}} Iatm(\ )*R(\ )*T(\ )\,d\omega d\ell$
$I_{cloud}(\ )*T(\ )$
PI*FO*R( )*T( )

$W/cm.2.sr.microns$

LOSZA = 106 deg. / Rel. Azim. = 42 deg. / Scat. Angle = 70 deg.

microns

24

Cloud campaign: 2 july 1992 / SZA = 48 deg.

$W/cm.2.sr.microns$

MEASUREMENTS
Itot( )
Iatm( )
$\int_{\partial\rho}$Iatm( )*R( )*T( )$\partial\sigma\sigma\rho$
Icloud( )*T( )
PI*FO*R( )*T( )
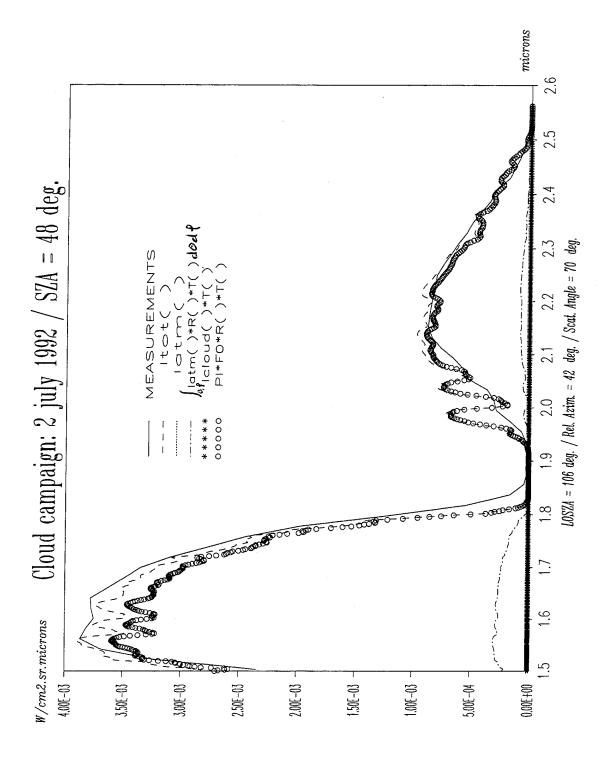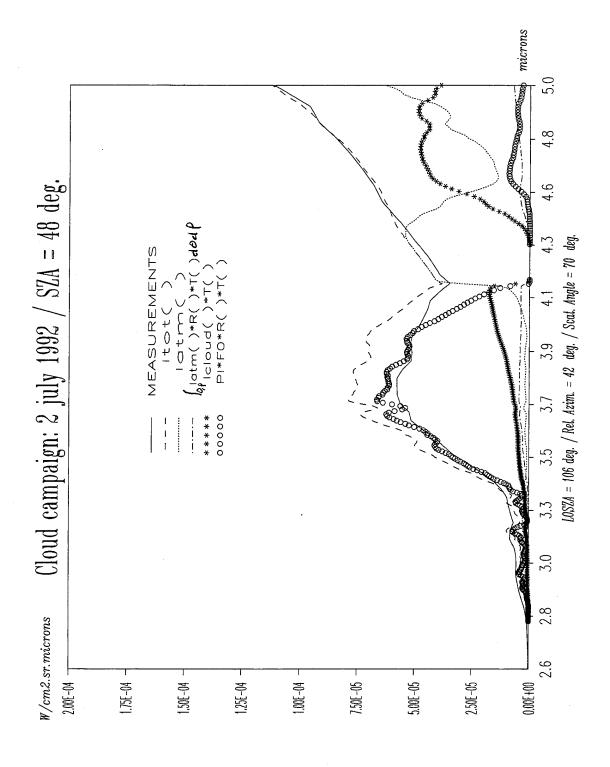
LOSZA = 106 deg. / Rel. Azim. = 42 deg. / Scat. Angle = 70 deg.

25

CONCLUSION

Fair agreement between measurements and models (LOWTRAN7, and NUALUM)

Improvement of the multiple scattering model by DOM

PERSPECTIVES

Constitution of a data bank from DISORT for different types of clouds

OSIC -- AN ULTRAVIOLET TRANSMISSION AND MULTIPLE SCATTER MODEL

Dr. Michael E. Neer
Dr. Katherine M. Crow

SciTec, Inc.
100 Wall Street
Princeton, NJ 08540
(609) 921-3892

OVERVIEW OF OSIC MODEL

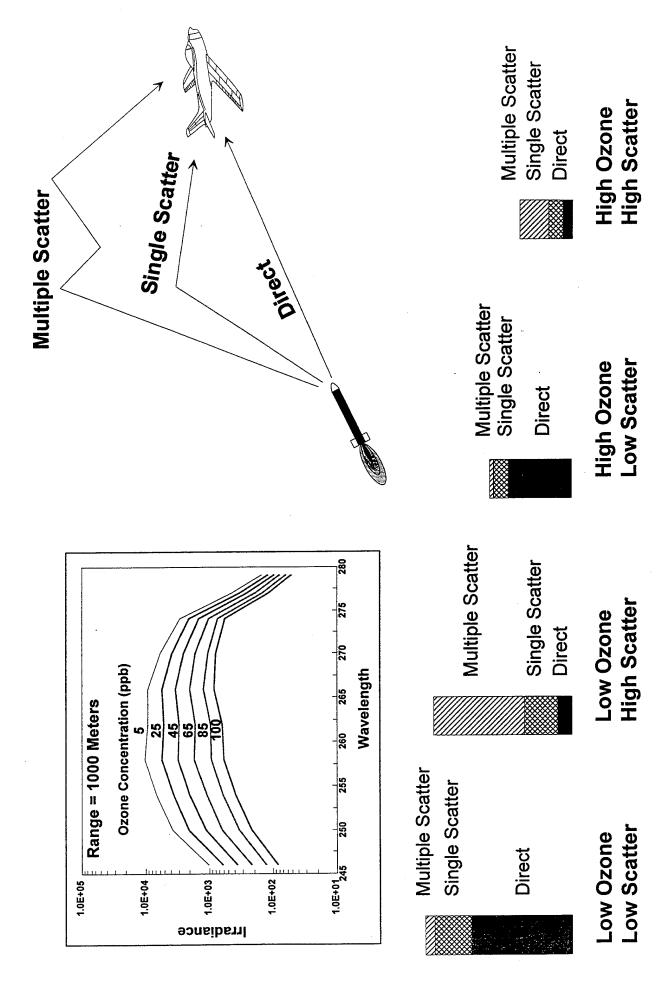**DESCRIPTION:** AN ULTRAVIOLET TRANSMISSION AND MULTIPLE SCATTER MODEL

ORIGINAL AUTHORS: M. NEER, J. SCHLUPF, B. MORGAN

DEVELOPMENT PERIOD: 1975-1982

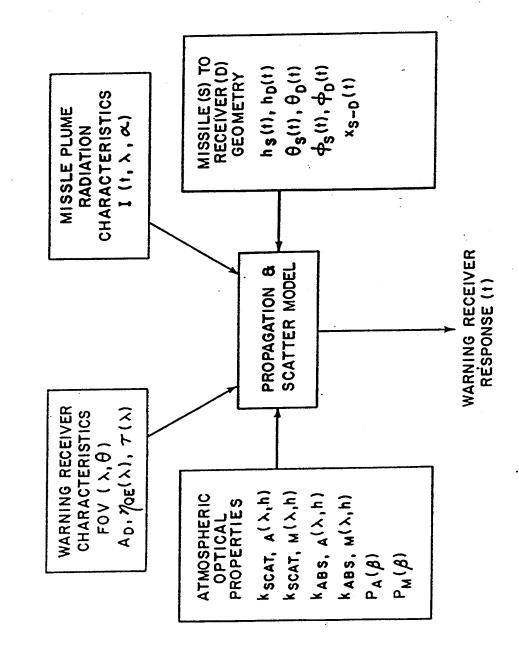**SPONSORED BY:** ARPA, PMTC, NOSC, AIR FORCE AVIONICS LAB, ARMY EWL, NAVELEX

PURPOSE: TO SUPPORT MISSILE WARNING AND NON-LINE-OF-SIGHT VOICE COMMUNICATION

UV PROPAGATION PHENOMENOLOGY

MWR MODEL

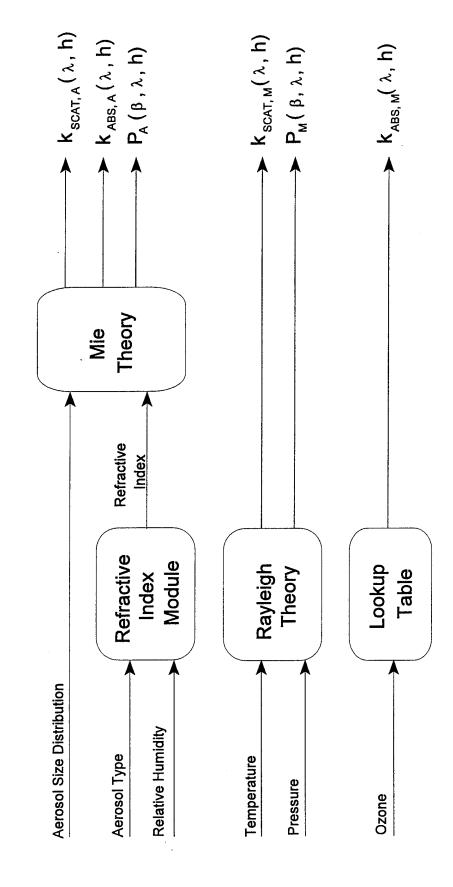MISSLE PLUME RADIATION CHARACTERISTICS $I(t, \lambda, \alpha)$

MISSILE (S) TO RECEIVER (D) GEOMETRY

$h_S(t), h_D(t)$
$\theta_S(t), \theta_D(t)$
$\phi_S(t), \phi_D(t)$
$x_{S-D}(t)$

WARNING RECEIVER CHARACTERISTICS
FOV (λ, θ)
$A_D, \eta_{QE}(\lambda), \tau(\lambda)$

ATMOSPHERIC OPTICAL PROPERTIES

$k_{SCAT, A}(\lambda, h)$
$k_{SCAT, M}(\lambda, h)$
$k_{ABS, A}(\lambda, h)$
$k_{ABS, M}(\lambda, h)$
$P_A(\beta)$
$P_M(\beta)$

PROPAGATION & SCATTER MODEL

WARNING RECEIVER RESPONSE (t)

SciTec ®

MODEL INPUTS:

GEOMETRY:

- SOURCE (e.g. MISSILE)
  - LOCATION (X_M, Y_M, Z_M)
  - ORIENTATION (φ_M, θ_M)

- SENSOR (e.g. WARNING RECEIVER)
  - LOCATION (X_S, Y_S, Z_S)
  - ORIENTATION (φ_S, θ_S)

SOURCE CHARACTERISTICS:

- RADIANT INTENSITY $I(\alpha, \lambda)$

RECEIVER CHARCTERISTICS:

- RESPONSIVITY $S(\lambda, FOV)$

192

IRRADIANCE MODELLING:

DIRECTLY TRANSMITTED -- COMPUTED EXACTLY INCORPORATES:

- AEROSOL ABSORPTION AND SCATTER
- MOLECULAR ABSORPTION AND SCATTER

FIRST SCATTER -- COMPUTED EXACTLY INCORPORATES:

- AEROSOL SCATTER
- MOLECULAR SCATTER

MULTIPLE SCATTER -- COMPUTED USING SEMI-EMPIRICAL MODEL

VERIFICATION OF SEMI-EMPIRICAL MODEL:

MODEL DEVELOPED FROM EXTENSIVE MEASUREMENT PROGRAM

- LOCATIONS: CHINA LAKE (DESERT), SAN NICOLAS ISLAND (MARITIME), SANDIA (DESERT), FT MONMOUTH (RURAL), ROUTE 1 CORRIDOR (URBAN)

- SEASONS: SUMMER, WINTER, FALL, SPRING

- OZONE: 0 TO 100 PPB
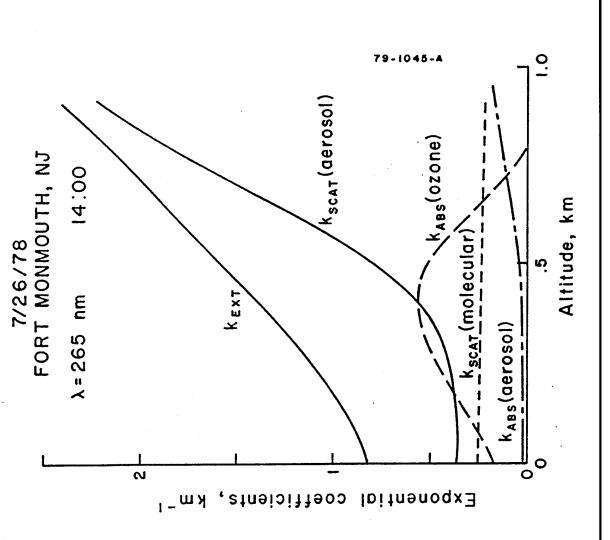
- VISIBILITIES: FOGS TO 100KM

- MODES: GROUND TO GROUND, GROUND TO AIR, AND NON-LINE-OF-SIGHT (OVER HORIZON)
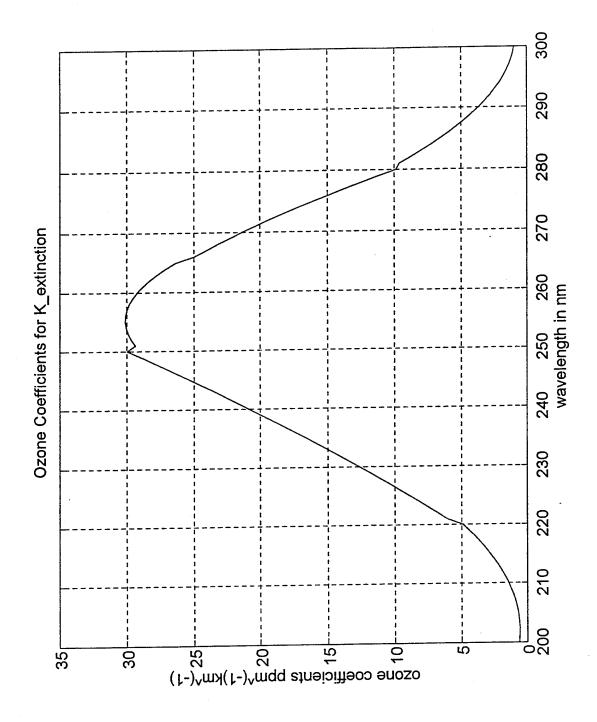
COMPARED TO MULTIPLE SCATTER CODES

- TPART MONTE CARLO (RADIATION RESEARCH ASSOCIATES)
- ZACHOR RECURSION FORMULA
- RIEWE & GREEN MONTE CARLO

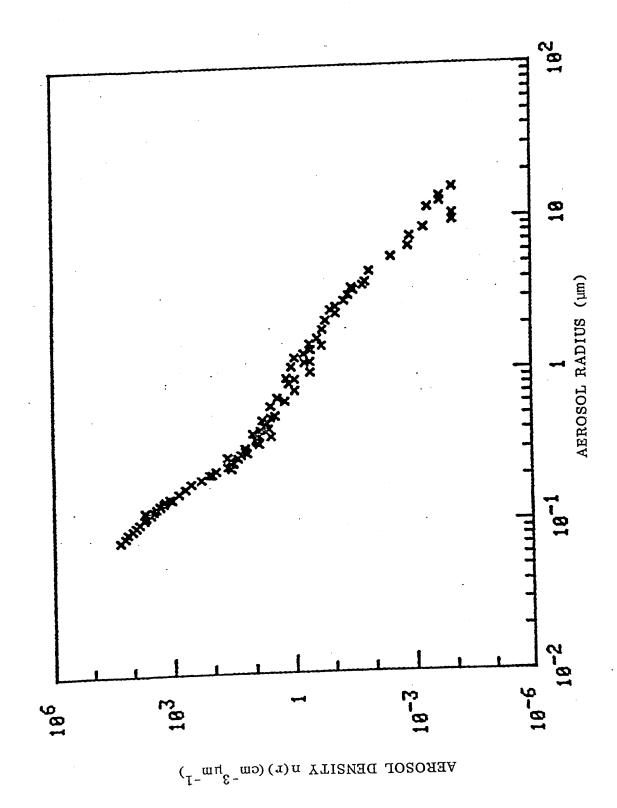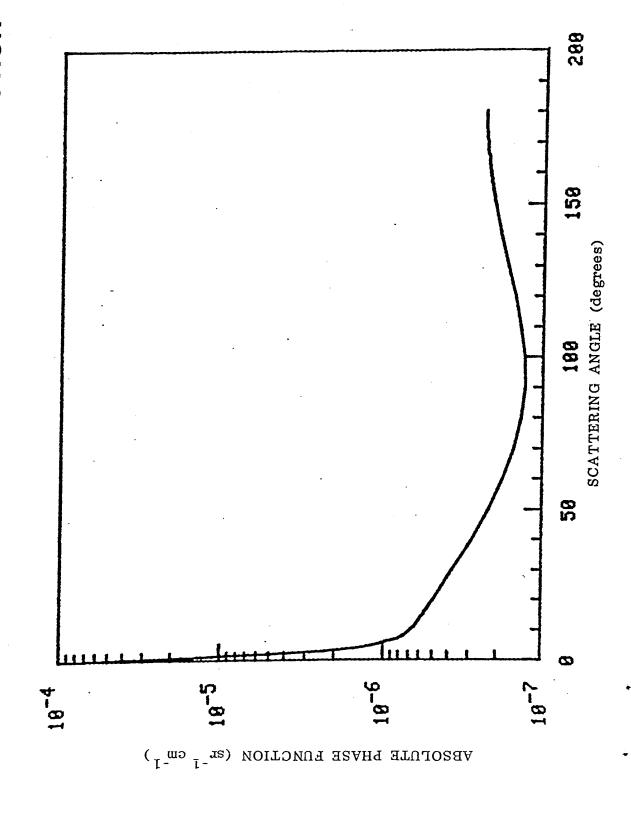## ALTITUDE VARIATION OF ATMOSPHERIC OPTICAL PROPERTIES ON JULY 26, 1978

7/26/78
FORT MONMOUTH, NJ
$\lambda = 265$ nm   14:00

79-1045-A

Ozone Coefficients for K_extinction

TYPICAL AEROSOL SIZE DISTRIBUTION

AEROSOL RADIUS (μm)

AEROSOL DENSITY n(r) $(cm^{-3}\mu m^{-1})$

TYPICAL ABSOLUTE SINGLE SCATTER PHASE FUNCTION
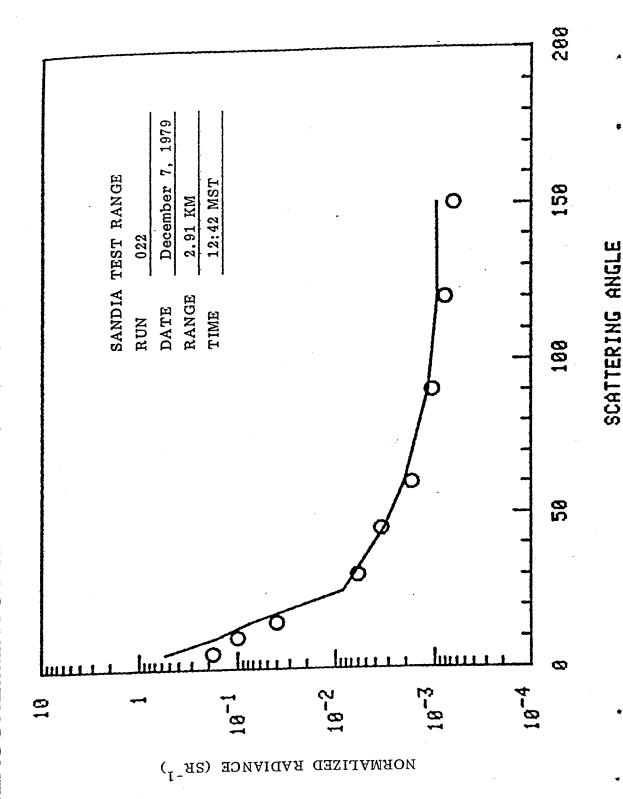
WAVELENGTH DEPENDENCE OF SCATTERING & ABSORPTION COEFFICIENTS:

λ (nm)	$k_{scat,aer}$	$k_{scat,mol}$	$k_{abs,aer}$	$k_{abs,mol}$
246	0.238	0.329	0.0863	2.62
250	0.232	0.306	0.0859	3
254	0.218	0.285	0.0835	3.01
258	0.208	0.266	0.0824	2.98
262	0.216	0.249	0.0844	2.83
266	0.227	0.233	0.0855	2.5
270	0.216	0.218	0.0847	2.14
274	0.198	0.204	0.0822	1.72
277	0.206	0.195	0.0825	1.37
279	0.207	0.189	0.0829	1.12

SciTec, Inc.
a wholly owned subsidiary of TRW

TRW
Defense Systems Division

COMPARISONS OF NORMALIZED SCATTERED RADIANCE
MEASUREMENTS AND PREDICTIONS FOR EXPERIMENT #022

SANDIA TEST RANGE

RUN   022
DATE   December 7, 1979
RANGE   2.91 KM
TIME   12:42 MST

SciTec, Inc.
a wholly owned subsidiary of TRW

TRW
Defense Systems Division

CURRENT APPLICATIONS:

- JTAMS

- NAVY MAWS LIVE FIRE TEST

- REVISION UNDERWAY (PC VERSION)

Inclusion of Accurate Multiple Scattering in MODTRAN

K. Stamnes, N. Larsen, and S.-C. Tsay
Geophysical Institute
University of Alaska Fairbanks
Fairbanks, AK 99775-0800

M. Yeh
Caelum Research Corporation
11229 Lockwood Drive
Silver Spring, MD 20901

Motivation

* Multiple scattering in MODTRAN is based on a 2-stream code (BMFLUX) with an isothermal layer approximation from which upward and downward fluxes are obtained.

* These fluxes are then converted into hemispherical intensities by assuming that the intensity is uniform in each hemisphere so that the hemispherical intensity is obtained from the flux by dividing it by π.

* Single scattering is already computed accurately in MODTRAN including curvature and refraction effects.

* This approach is justifiable if the single scattering contribution dominates as may frequently be the case for clear sky conditions. However,

In the presence of clouds and aerosols the multiple scattering contribution to the radiance may dominate!

Therefore, a better multiple scattering scheme is expected to improve

* calculations of atmospheric transmission and prediction

* accuracy of retrievals of remotely-sensed atmospheric properties that rely on the interpretation of measured radiances (ground-based or from space)

HOW do we Improve Multiple Scattering (MS) Treatment?

Simple answer: Replace existing scheme (based on BMFLUX) with a more accurate one based on a multi-stream approach (DISORT) to compute multiple scattering.

DISORT computes complete radiance, but MODTRAN needs only Multiple Scattering component of the source function. Therefore

More complete answer: To minimize changes in MODTRAN we have extended DISORT to compute MS component of source function.

IMPORTANT: Both MODTRAN and DISORT are very complex codes. Therefore

*   interfacing of DISORT with MODTRAN must be done very carefully;

*   extensive testing is required and must be carefully executed. This is a time-consuming undertaking.

POSSIBLE AND DESIRABLE EXTENSIONS

A. Multiple Scattering in Plane Geometry

Present inclusion of multiple scattering (as the one based on BMFLUX) deals exclusively with the azimuthally-averaged component of the radiance.

This represents no limitation in the infrared where the source function is azimuth-independent.

In the solar, however, the existing azimuth-dependence of the MS source function is ignored, although the single scattering contribution is computed correctly including azimuth-dependence. Therefore, the following questions arise:

How large an error do we make by ignoring the azimuth-dependence of the multiple scattering term?

How can we correct the error made by this approach?

POSSIBLE APPROACHES

First approach: Incorporate full azimuth-dependence of the intensity, by using DISORT. But implementation in present version of MODTRAN is difficult and may require substantial restructuring of MODTRAN in order to accomodate the interface with DISORT.

Second approach: Use MODTRAN to compute optical properties and let DISORT handle the complete radiative transfer computation. In fact, the new version of DISORT (to be released soon) will have fast computation of multiple scattering and 'exact' computation of the single scattering component of the radiance.

Third (hybrid) approach: If scattering is isotropic, then only the azimuthally-averaged component contributes and present approach is sufficient. Therefore, an approximate hybrid approach may consist of

(i) scaling the anisotropic scattering so that the problem is reduced to one with isotropic scattering (similarity transformation);

(ii) solving for the multiple scattering component based on the 'scaled' (isotropically scattering) problem for which only the azimuthally-averaged component contributes;

(iii) combining this approximate multiple scattering solution with the 'exact' single scattering solution based on the complete phase function.

The third approach is attractive because it is expected to be very efficient. Therefore it would be of great interest to find out under what conditions it is valid.

B. Multiple Scattering in Spherical Geometry

Possible Approach:

(i) Use plane geometry to approximate derivative term, but compute Chapman function correctly using spherical geometry.

(ii) Compute 'exact' single scattering solution as follows: Use iteration to incorporate the missing derivative terms due to plane geometry in the single scattering approximation. Thus, start by solving problem (i) above (ignoring multiple scattering) and use this solution to compute the missing terms. Add these contributions to the source term and solve problem (i) again with the additional source. Repeat this procedure, which should converge if the additional derivative terms due to spherical geometry are small enough. This should yield an 'exact' solution in the single scattering approximation.

(iii) Solve for the multiple scattering component based on the 'scaled' (isotropically scattering) problem for which only the azimuthally-averaged component contributes.

(iv) Combine this approximate multiple scattering solution with the 'exact' single scattering solution based on the complete phase function obtained as outlined in (ii) above.

This approach is expected to be quite efficient and may be accurate enough for many purposes.

Note:
A. For nadir and zenith directions there is no azimuth-dependence. Therefore this procedure will give the complete solution.

B. For isotropic scattering there is nothing 'driving' azimuth-dependence. So the solution will be azimuth-independent in this case.

C. Multiple Viewing Directions

MODTRAN presently computes the intensity for a single viewing direction and starts form 'scratch' when a new direction is desired. In contrast

DISORT can return an *arbitrary number of desired output directions* at insignificant additional computational cost.

Thus, if multiple viewing directions are desired it would be most efficient to:

(i) use MODTRAN to compute optical properties,

(ii) use MODTRAN's geometry package including curvature and refraction effects to compute the single scattering source term, and finally

(iii) use the new version of DISORT to do the complete radiance computation.

UV-Visible Radiation Field Model: Monte Carlo, DISORT and Integral Equation Methods

Donald E. Anderson and Robert DeMajistre

The Johns Hopkins University

Applied Physics Laboratory

Laurel, MD 20723

phone: 301-953-6174

email: donald_anderson@jhuapl.edu

230

Equations , Parameters et al.

Earth Albedo = 0.3   Overhead sun

Aerosol $\tau = 0.15$ g = 0.7

Aerosol + Cloud $\tau = 1.2$ g=0.8

$\lambda = 310\ 315\ 320\ 350\ 800$ nm [1 2 3 4 5]

Plane parallel atmosphere for scattering

Spherical atmosphere for solar energy deposition
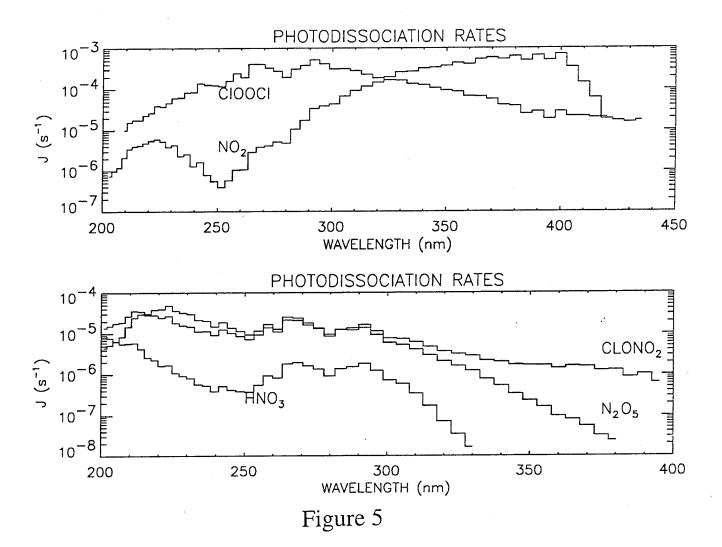
Spherical shell for radiance calculation

$Fo(\lambda,\mu,z) = \exp(-\tau/\mu)$ + single scatter albedo term

$F(\lambda,z) = \varepsilon(\lambda, z)/[\sigma(\lambda)* n(z)*Fs(\lambda)]$

Fs=solar flux incident at top of atmosphere

$\varepsilon \equiv$ volume scattering rate (photons/cm3/sec/A)

PHOTODISSOCIATION RATES

Figure 5

Figure 1

Figure 2a

Figure 2b

Figure 2c

Figure 3

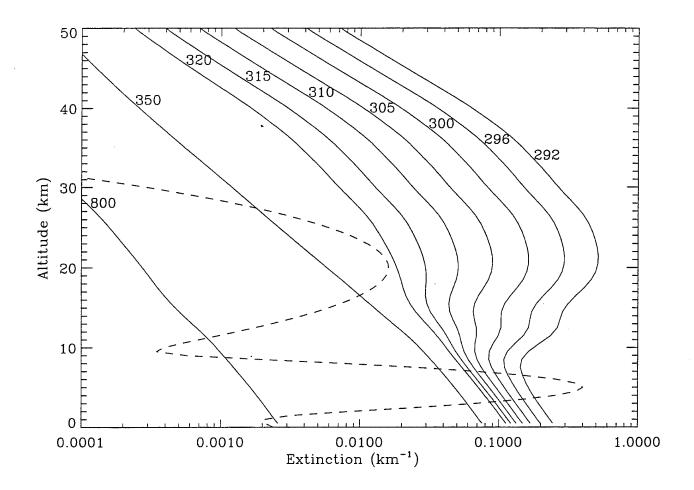Figure 4a

Figure 4b

Figure 5

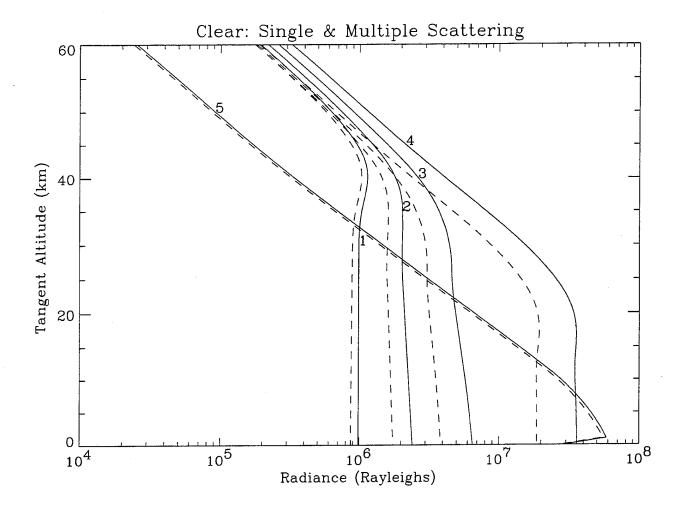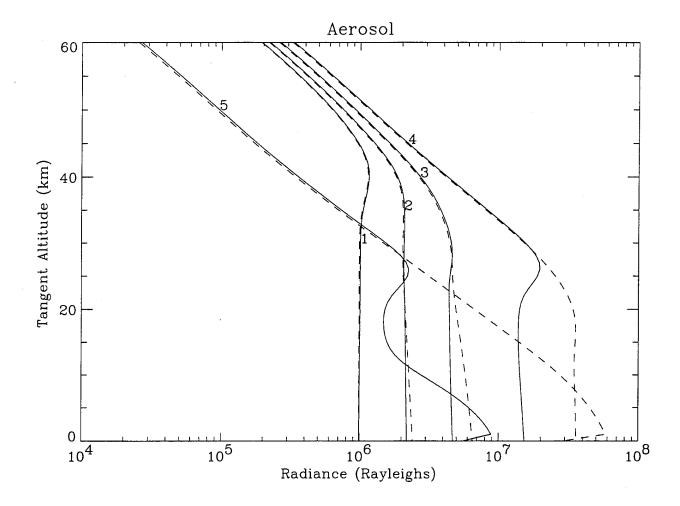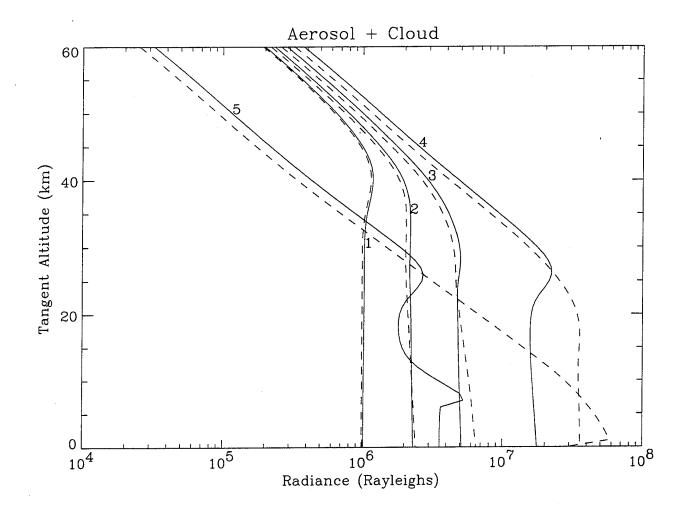Clear: Single & Multiple Scattering

Aerosol

Aerosol + Cloud
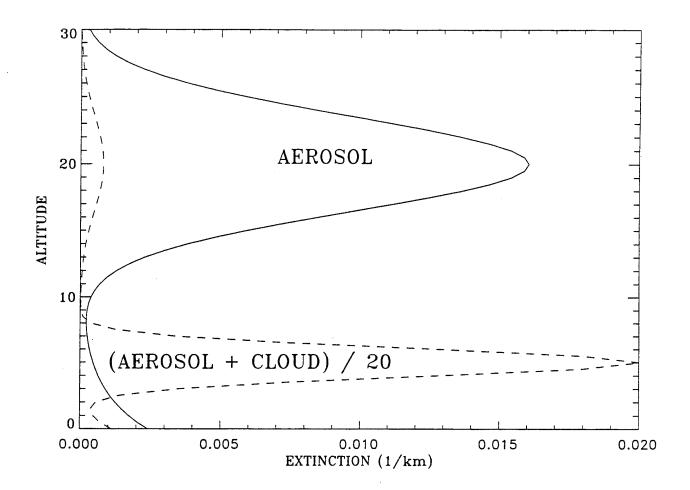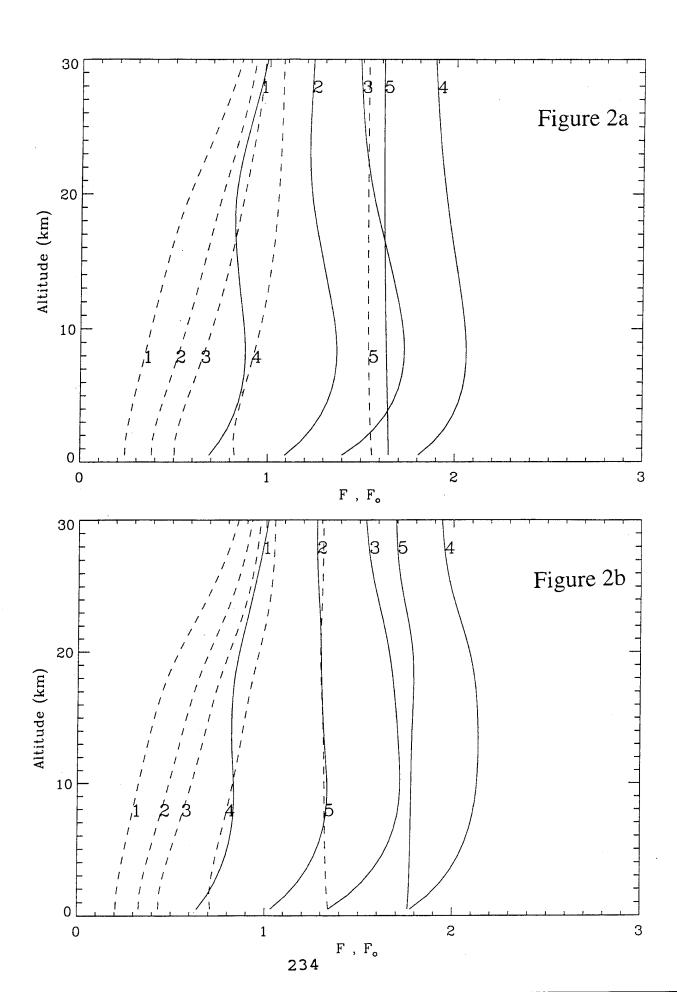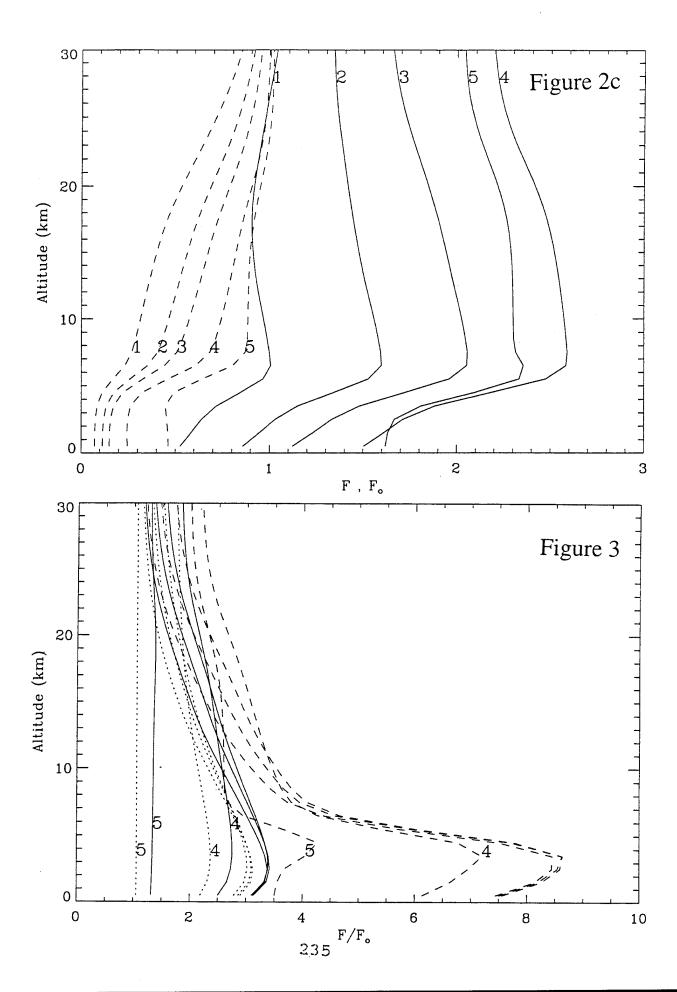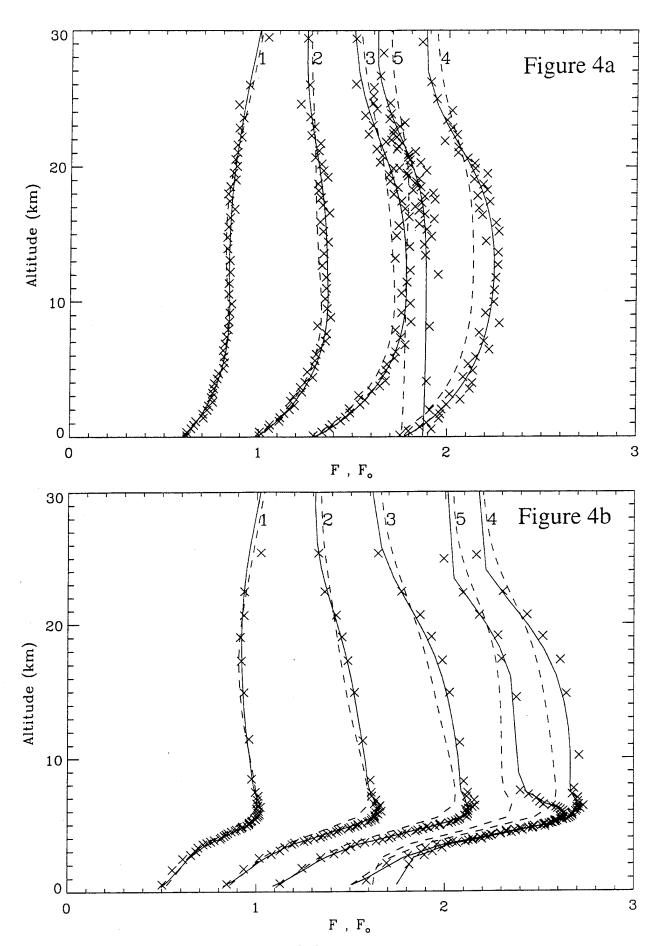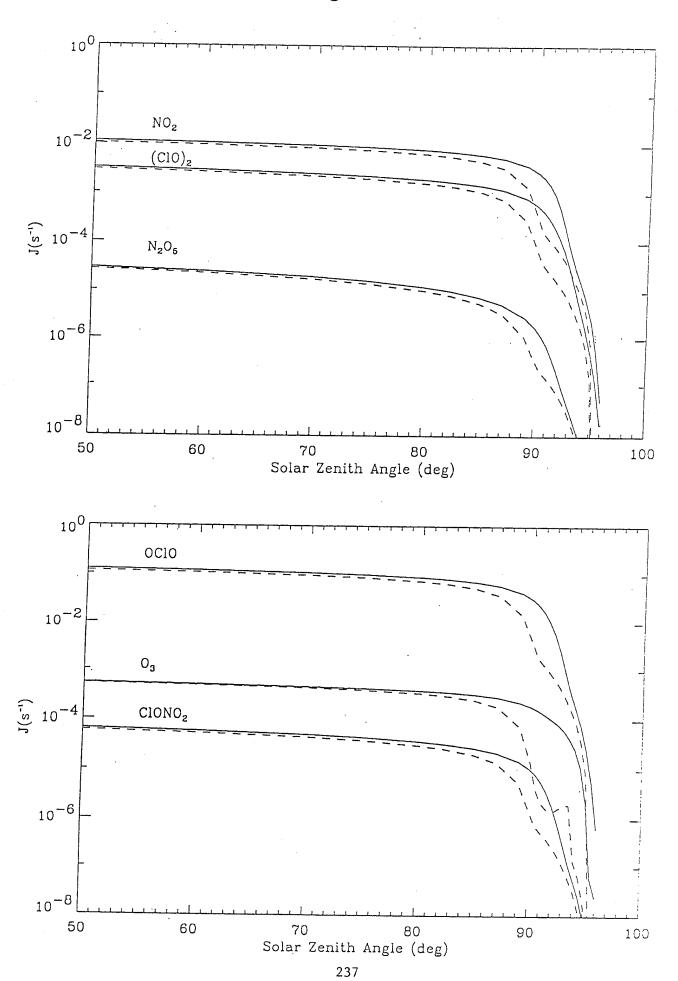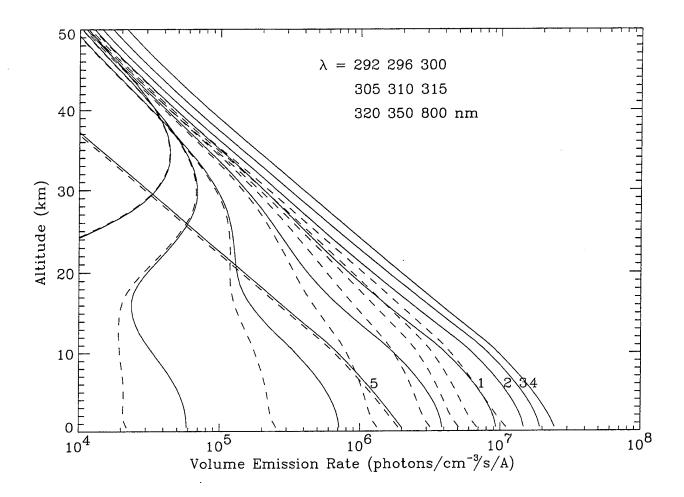
Summary

- Monte Carlo, DISORT, Integral Eq. agree to within ~5%

- Monte Carlo <=> DISORT essentially identical for range of parameters investigated

- When coupled with MODTRAN optical parameter data base, Integral Equation method provides a fast, accurate method for the determination of the UV-Visible radiation field volume scattering rate

- Integral Equation method offers a rapid means of determining UV-Visible limb radiance

An Application of Radiative Transfer Theory to Understanding Aerosol MTF

David Tofsted, Alan Wetmore, and Richard Shirkey
U.S. Army Research Laboratory

Brian Davis
Physical Sciences Laboratory

Andrew Zardecki
Los Alamos National Laboratory

ARMY *RESEARCH LABORATORY*

— 1994 Annual Review Conference on Atmospheric Transmission Models —

OVERVIEW

- Linear Filter Interpretation of Incoherent Imaging

- Forward Scattering Approximation

- Aerosol Phase Function Gaussian Decomposition

- Radiative Transfer Derivation of Aerosol MTF

- Sample Scenarios

- Conclusions

LINEAR FILTER INTERPRETATION OF INCOHERENT IMAGING

- Assumptions:

  - Vignetting and aberration effects can be ignored.

  - Optical system assumed diffraction limited.

  - Optics can be replaced by a cascaded set of linear operators.

— 1994 Annual Review Conference on Atmospheric Transmission Models —

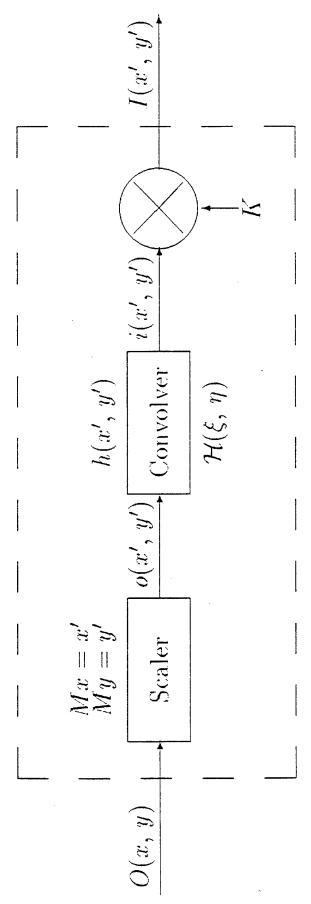# LINEAR FILTER INTERPRETATION OF INCOHERENT IMAGING

- Elements of the Linear Filter System consist of:

  - A 'Scaler' that magnifies the size of the object being viewed.

  - An LSI system that convolves the system point spread function over the image.

  - A Multiplier that scales the brightness of the resulting image due to system losses.

250

LINEAR FILTER INTERPRETATION OF INCOHERENT IMAGING

- Schematic:

FORWARD SCATTERING APPROXIMATION

- For snow and rain scattering species the probability of scatter within 10 degrees of the original propagation direction is greater than 90%.

- Under this condition the propagation direction variable $\vec{\Omega} = (\Omega_x, \Omega_y, \Omega_z)$ has $\Omega_z \approx 1$ and the phase function (differential scattering probability function) may be replaced by $P(\vec{\Omega}, \vec{\Omega}') \rightarrow P(\vec{\omega} - \vec{\omega}')$.

- In this approximation, $\vec{\Omega} = (\omega_x, \omega_y, 1) = (\vec{\omega}, 1)$.

7 JUN 94

252

RADIATIVE TRANSFER CALCULATION

- The general equation for radiative transfer is

$$\vec{\Omega} \cdot \nabla I + \sigma_e I = \sigma_s \int_{4\pi} P(\vec{\Omega}, \vec{\Omega'}) \, I(\vec{x}, \vec{\Omega'}) \, d\vec{\Omega'}.$$
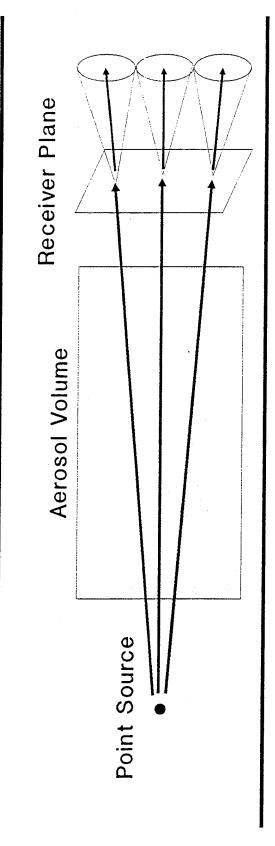
- Under the small angle approximation this becomes

$$\vec{\omega} \cdot \frac{\partial I}{\partial \vec{r}} + \frac{\partial I}{\partial z} + \sigma_e I - \sigma_s \cdot \int \int_{-\infty}^{\infty} P(\vec{\omega} - \vec{\omega'}) \, I(\vec{r}, z, \vec{\omega'}) \, d\vec{\omega'} = 0.$$
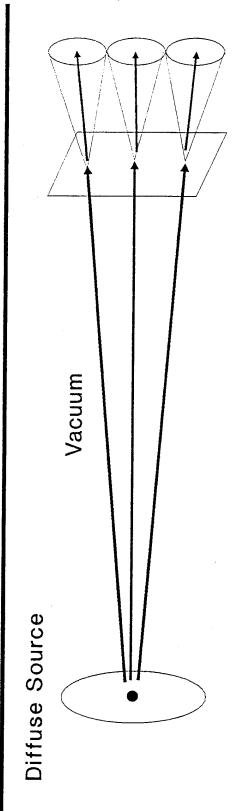
- Fourier transforming this equation ($\vec{\omega} \to \vec{\nu}; \vec{r} \to \vec{\kappa}$) converts the convolution to a product:

$$\left[-\vec{\kappa} \cdot \frac{\partial}{\partial \vec{\nu}} + \frac{\partial}{\partial z} + \sigma_e - \sigma_s \hat{P} \right] \hat{I} = 0.$$

7 JUN 94

253

AEROSOL POINT SPREAD FUNCTION

Receiver Plane

Aerosol Volume

Point Source

Propagation through aerosol volume is equivalent to a convolution over source plane using aerosol spread function.

Vacuum

Diffuse Source

GAUSSIAN PHASE FUNCTION APPROXIMATION

- Using $\vec{\omega}$, several researchers have utilized the Gaussian phase function approximation.

$$P(\omega) = \alpha^2 \exp(-\pi \, \alpha^2 \, \omega^2), \quad \omega = |\vec{\omega}|.$$

- We have extended this approach by modeling the phase function as a sum of Gaussian components:

$$P(\omega) = \sum_{i=0}^{N} C_i \, \alpha_i^2 \exp(-\pi \, \alpha_i^2 \, \omega^2).$$

7 JUN 94

255

GAUSSIAN PHASE FUNCTION UNDER FOURIER TRANSFORMATION

- Using the symmetric form for the Fourier transform,

$$\mathcal{F}\{\alpha^2 \exp(-\pi \alpha^2 \omega^2)\} = \exp(-\pi \nu^2/\alpha^2).$$

- Integrating this form over all angles

$$2\pi \int_0^\pi P(\theta) \sin(\theta) \, d\theta \approx 2\pi \int_0^\infty \alpha^2 \exp(-\pi \alpha^2 \omega^2) \, \omega \, d\omega = 1.$$

- The normalization condition for the composite Gaussian phase function is then $\sum_{i=0}^N C_i = 1.$
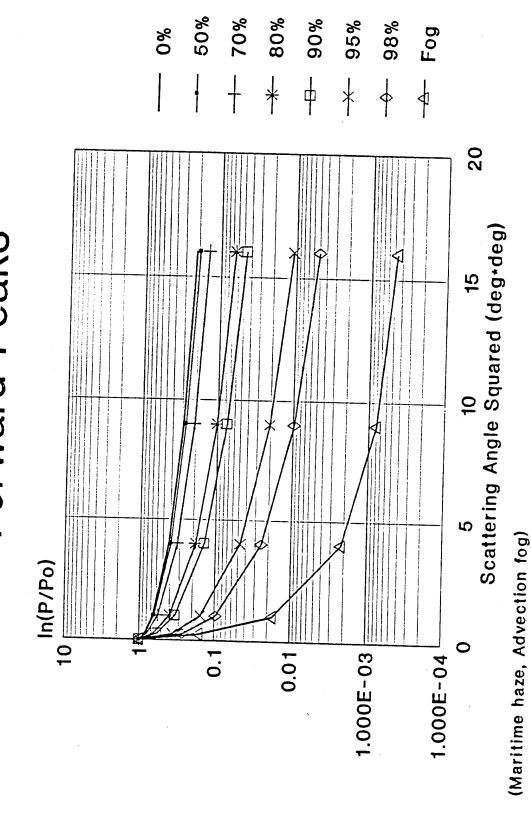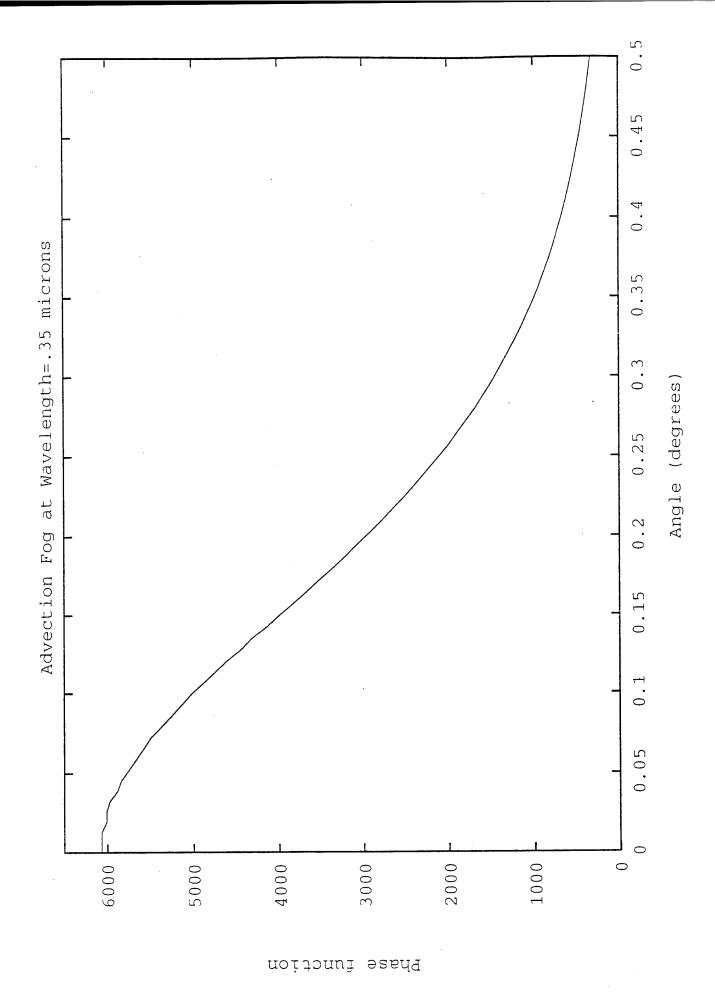
PHASE FUNCTION BEHAVIOR

- Let P_0 be the phase function peak value at a scattering angle of zero.

- Let σ be the angular value at which the phase function has dropped to $\exp(-0.5)$ of its value at the zero peak.

- Let λ be the radiation wavelength.

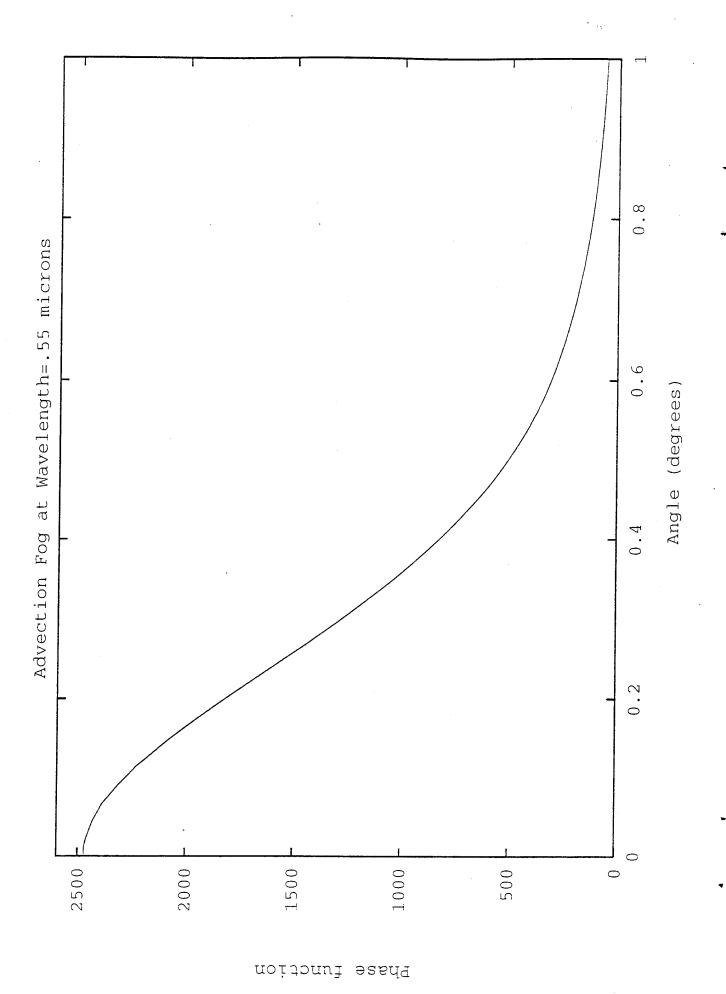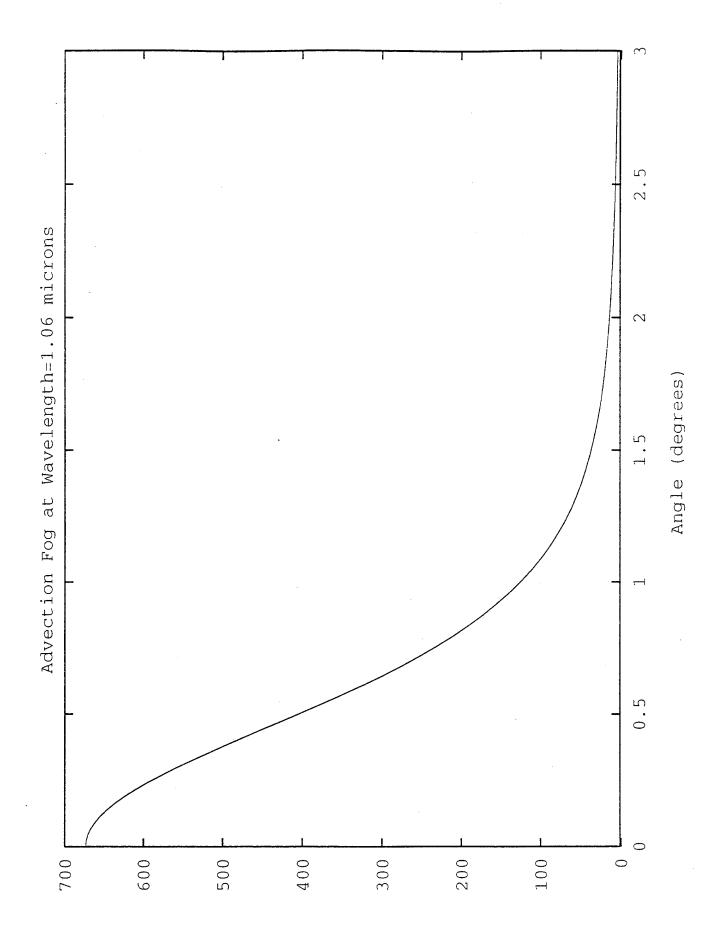- We observe that $P_0 \approx K_1/\lambda^2$, and $\sigma \approx K_2\lambda$, where K_1 and K_2 are constants.

Normalized Phase Function
Forward Peaks

ln(P/Po)

0%
50%
70%
80%
90%
95%
98%
Fog

Scattering Angle Squared (deg*deg)

(Maritime haze, Advection fog)

258

Advection Fog at Wavelength=.35 microns

Phase function

Angle (degrees)

Advection Fog at Wavelength=.55 microns

Phase function

Angle (degrees)

Advection Fog at Wavelength=1.06 microns

Phase function

Angle (degrees)

Advection Fog at Wavelength=.35 microns

Phase function

Angle (degrees)

Advection Fog at Wavelength=.35 microns

Phase function

Angle (degrees)

Advection Fog at Wavelength=.35 microns

Phase function

Angle (degrees)

264

Advection Fog at Wavelength=.35 microns

Phase function

Angle (degrees)

Advection Fog at Wavelength=.35 microns

Phase function

Angle (degrees)

SOLUTION TO EQUATION (I)

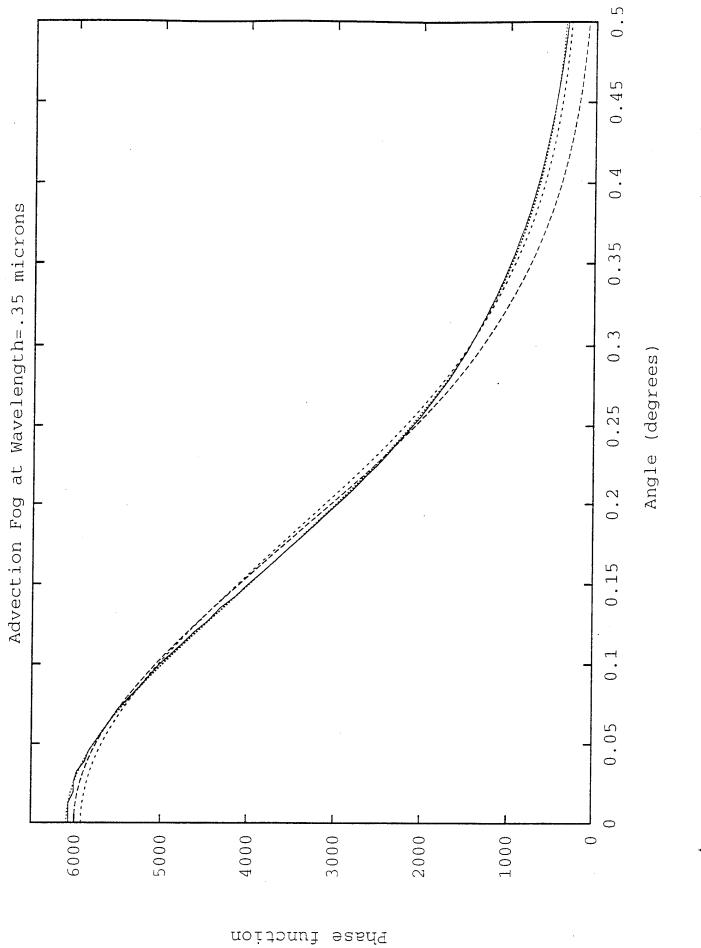- The transformed equation can be solved for $\hat{I}$ using an implicit solution technique (e.g., Smirnov, 1964).

- This technique results in a set of characteristic equations:

$$\frac{d\nu_x}{\kappa_x} = \frac{d\nu_y}{\kappa_y} = dz = \frac{d\hat{\hat{I}}}{\left[\left(\sigma_s \hat{P} - \sigma_e\right)\hat{\hat{I}}\right]}.$$

- Solving the first set reveals $\vec{\nu}$ and $\vec{\kappa}$ are dependent:

$$\vec{\nu} + \vec{\kappa}z = \vec{K}.$$

SOLUTION TO EQUATION (II)

- Solving for the relationship between z and $\hat{\hat{I}}$,

$$\hat{\hat{I}} = \hat{\hat{I}}_0 \, T \exp\left\{\int_0^Z \sigma_s \hat{P}\, dz\right\}, \text{ where } T = \exp\left\{-\int_0^Z \sigma_e \, dz\right\}.$$

- $\hat{\hat{I}}_0$ is a constant of integration.

- Since the non-scattering solution is known through other means, we transform this solution to determine $\hat{\hat{I}}_0$:

$$\hat{\hat{I}}_0 = I_0 \, \delta(\vec{\nu} + \vec{\kappa}\, z) = I_0 \, \delta(\vec{K}).$$

- From this solution and the delta sifting property

$$\vec{K} = 0 \longrightarrow \vec{\nu} = -\vec{\kappa}\, z.$$

AEROSOL MTF (I)

- Because $\exp\{\int_0^Z \sigma_s \hat{P}\, dz\}$ appears as a multiplier of the non-scattering solution, it must be the aerosol MTF.

- Since $\hat{P}$ is a function of $\vec{\nu}$, it can be integrated WRT z as

$$MTF(\vec{\kappa}) = \exp\left\{ \int_0^Z \sigma_s \sum_{i=0}^{N} C_i \exp(-\pi \kappa^2 z'^2 / \alpha_i^2)\, dz' \right\}.$$

- The scattering coefficient σ_s, the number N, the coefficient values C_i and α_i depend on path position. Assuming the path consists of sections with uniform properties the integral may be expressed as the exponential of a double sum.

AEROSOL MTF (II)

- Changing variables, $\kappa = \Psi/Z$, where Ψ is an angular frequency variable based in the sensor aperture viewing the object and Z is the optical path length.

- The aerosol MTF can then be written as

$$
MTF(\Psi) = \exp\left\{ \sum_{j=1}^{M} \sigma_{s,j} Z \sum_{i=0}^{N} \frac{\alpha_{ji}\, C_{ji}}{2\,\Psi} \right.
\left[\mathrm{erf}\left(\sqrt{\pi}\frac{Z_j}{Z}\frac{\Psi}{\alpha_{ji}} \right) - \mathrm{erf}\left(\sqrt{\pi}\frac{Z_{j-1}}{Z}\frac{\Psi}{\alpha_{ji}} \right) \right] \left. \right\}.
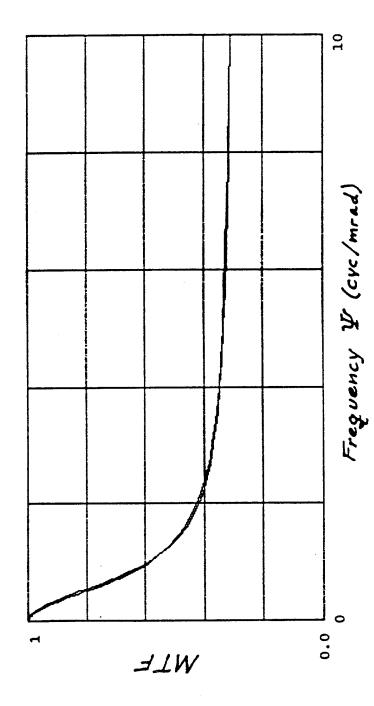$$

USING APPROXIMATE MTF

- Comparison of exponentially decreasing fog density case against appropriately scaled simplified MTF.

Frequency ψ (cyc/mrad)

MTF

1 DEC 93

271
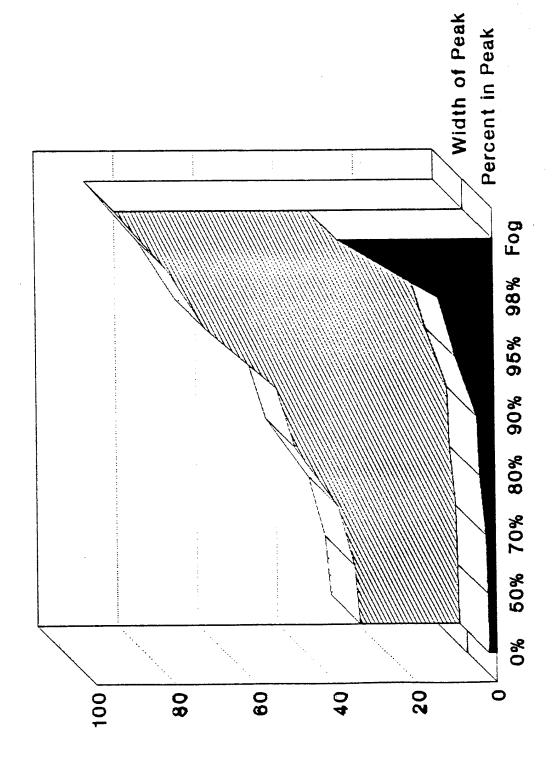
SAMPLE SCENARIO

- Advection fog model for 3 optical depth path w/ scatterers concentrated in only the first 10% of the path.

- Results obtained using 5 component gaussian phase function approximation show limited frequency effects.

- Effects predicted match intuitive understanding of fog case. That is, source energy appearing over several degrees off-axis from source origin.

- Majority of untruncated energy appears at frequencies below 1 cyc/mrad.

Haze Aerosol Forward Peaks

Width of Peak

Percent in Peak

0%   50% 70% 80% 90% 95% 98% Fog

100

80

60

40

20

0
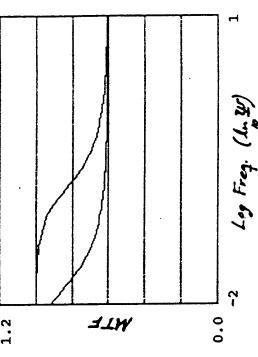
COMPARISON WITH BISSONNETTE MODEL

- Comparison of 100 μm and 1 mm aerosol MTF cases of Bissonnette against appropriately scaled results of gaussian phase function MTF.

CONCLUSIONS

- Angular frequency dependent aerosol MTF derived.

- Radiative transfer theory used directly in the derivation.

- Derivation confirms previous developments using mutual coherence approach.

- Derivation disputes recent findings of Sadot and Kopeika.

- Derivation extends single gaussian approximation for more accurate phase function representation.

— 1994 Annual Review Conference on Atmospheric Transmission Models —

7 JUN 94

Molecular and Aerosol Effects on Airborne Laser Propagation

Atmospheric Transmission Workshop
Air Force Phillips Lab
7-8 June 1993

Larrene Harada
Daniel Leslie
Doug Youmans
Matthew Savacool

WJSA

W.J. Schafer Associates, Inc.
1901 N. Fort Myer Dr.
Arlington, VA 22209
(703)558-7900

Introduction

- **Airborne Lasers and Laser Radar for Theatre Missile Defense**

- **Propagation Geometry for ABL**

- **Transmittance calculations using standard LOWTRAN models**

- **Volcanic Aerosols using standard models**

- **NASA SAGE and Lidar data**

- **Mount Pinatubo**

- **Wavelength scaling**

- **Cirrus**

06/10/94-001-2

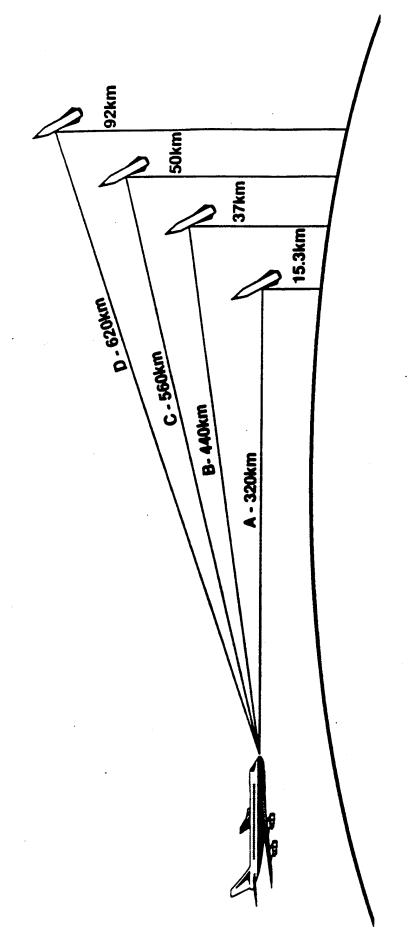# Airborne Lasers for Theater Missile Defense

- ABL is a boost-phase intercept system which can negate missiles at the speed of light at ranges of hundreds of kilometers

  - Solves submunitions problem

  - Allows for fewer assets to defend a larger area

  - More likely debris will fall on attacker's territory or short of its intended target

WJSA

06/10/94-001-3

Airborne Laser Radar for Theater Missile Defense

- Motivation for use of aircraft-based, high accuracy, passive and active threat track sensors

  - track of post-boost targets provides early cuing of interceptors, and increased defended area
  - accurate track provides launch point and impact point prediction
  - boost-phase track provides handover to boost-phase interceptor

- Atmospheric Transmission Issues (free of clouds & turbulence)

  - absorption and scattering calculations indicate acceptable transmittance for several candidate eye-safe laser wavelengths
  - acceptable transmission over ranges > 500 km is available to targets at < 10 km altitude

- Clouds & Turbulence

  - PCFLOS statistics for this geometry needed for theaters of interest
  - significant turbulence impact at lowest target altitudes (<20km)
    - beam spreading
    - complex intensity modulation in ranging signal - scintillation

279

ABL Cases A, B, C, D

92km

50km

37km

15.3km

D - 620km

C - 560km

B - 440km

A - 320km

At maximum ranges, elevation angles vary from
-0.8° (Case - A) to +4° (Case - D).

0001 - DL - 08/07/93

Candidate High Energy Lasers & Eye-Safe Laser Radars

	Wavelength (μ)	Frequency (cm^{-1})	Atmospheric Transmission			
			A	B	C	D
High Energy Lasers						
Nd:YAG	1.064	9397.26	.74	.82	.82	.91
COIL	1.315	7603.135	.82	.88	.88	.94
HF-OT $P_2(3)$	1.32	7618.467	.82	.88	.88	.94
HF-OT $P_2(4)$	1.32	7568.577	.83	.88	.89	.95
HF $P_1(10)$	2.92	3489.559	.53	.83	.84	.93
HF $P_2(9)$	2.92	3385.230	.81	.95	.95	.98
Laser Radars						
Nd:YAG / KTP	1.571	6365.4	.88	.93	.93	.97
Nd:YAG / CH$_4$	1.542	6483.3	.89	.93	.93	.97
Ho:YAG	2.096	4770.241	.96	.97	.97	.99
CO$^{18}_2$ R(18)	9.124	1095.965	.88	.90	.91	.95
CO$_2$ P(20)	10.591	944.194	.06	.02	.01	.03
C^{13}O$_2$ P(20)	11.149	896.909	.92	.92	.91	.95

Eye-Safe Laser Ranger Options
Available For Airborne Sensor Program

Diode-Pumped Solid-State Laser Ranger Systems
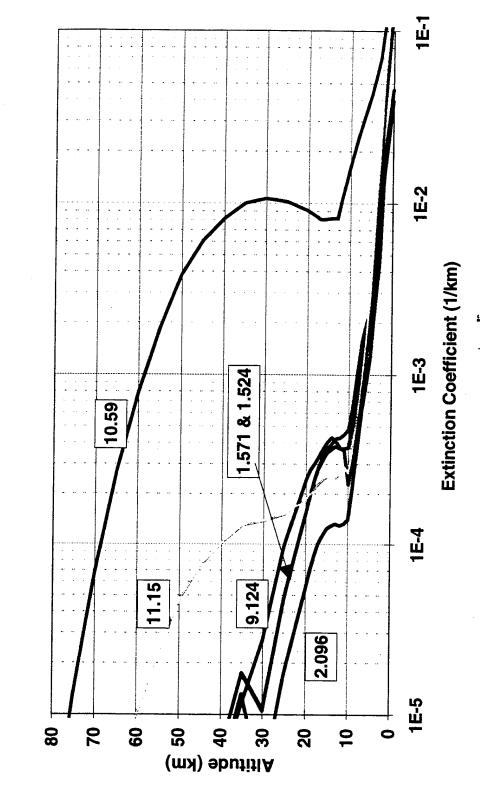
$\lambda(\mu)$	Laser	Detector	Comment
1.54	Nd:YAG Raman shifted in CH_4	InGaAs APD	thermal blooming in cell
1.55	Nd:YLF shifted OPO in KTP	InGaAs APD	1.053μ pump λ
1.56	Nd:YAG Raman shifted in D_2	InGaAs APD	thermal blooming in cell
1.57	Nd:YAG shifted OPO in KTP	InGaAs APD	demonstrated 0.45J/10Hz
1.61	Nd:YAG shifted OPO in KTA	InGaAs APD	new crystal for OPO
2.06	Tm,Ho:YAG	InGaAs PD	1J/5Hz demonstrated
2.09	Ho:YAG	InGaAs PD	2μ direct detection noisy

CO_2 Laser Ranger Systems

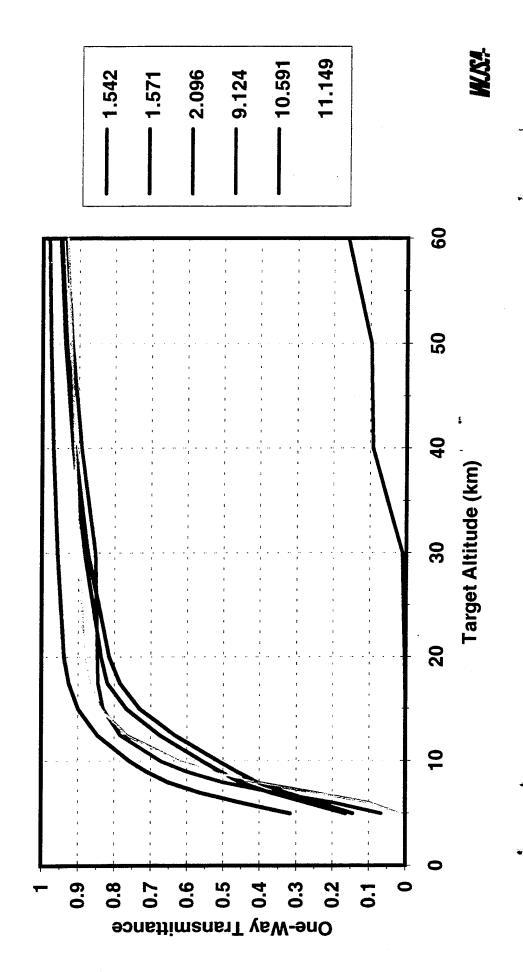|			
9.124	O^{18} Waveguide CW-FM	HgCdTe (Het)	100W demo; prop. Sig Proc
11.15	C^{13} LOWKATER pulse-tone	HgCdTe (Het)	3J/20Hz demo at 10.6μ

Assessment

- Several options are available now for an eye-safe >500km-range TMD system
- Numerous laser rangers are flying in US inventory (mostly short range 1.06μ)
- Biggest risk area is integration with IRST system & optics

Laser Atmospheric Extinction vs Altitude
FASCOD3P/HITRAN92; MLS, Bkg Strat/Mod Volc, Rural-23km Atmospheric Model

10.59

11.15

1.571 & 1.524

9.124

2.096

Altitude (km)

Extinction Coefficient (1/km)

WJSA

283

One-Way Laser Atmospheric Transmission

500 km range to target from 35 kft Aircraft
MLS, Bkg Strat/Mod Volc, Rural-23km Atmospheric Model

Legend:
- 1.542
- 1.571
- 2.096
- 9.124
- 10.591
- 11.149

MLS4

Transmittance Using Standard LOWTRAN Stratospheric Aerosol Models

AFGL Stratospheric Aerosol Model	Nd:YAG 1.06 μm	COIL 1.315 μm	Nd:YAG/KTP 1.571 μm	HF* 2.92 μm	$C^{13}O_2$ 11.149 μm
Stratospheric Background	.95	.96	.98	.99	.99
Background Type /Moderate Profil	.78	.85	.91	.96	.97
Background Type /High Profile	.76	.83	.90	.95	.96
Aged Volcanic Type/Moderate Profile	.65	.72	.80	.95	.98
Aged Volcanic Type/High Profile	.61	.69	.78	.94	.98
Fresh Volcanic Type/Moderate Profile	.42	.42	.44	.57	.77
Fresh Volcanic Type/High Profile	.38	.39	.40	.53	.75

* The HF transmission was calculated using 30% of $P_1(10)$ and 70% of $P_2(9)$.

06/10/94-001-8

Why SAGE II
(Stratospheric Aerosol and Gas Experiment)

SAGE II (October 1984 to present)

- global information

- large statistical set

- seasonal information

- has horizontal optical paths similar to the ABL

- detects cloud tops

- detects thin to subvisual cirrus down to extinction levels of 8×10^{-4} km^{-1}

- provides extinction coefficients for easier analysis

- multi-year availability

- Pre- and Post- Pinatubo behavior

WJSA

06/10/94-001-9

286

Hampton (LaRC) Lidar Parameters

General

Location:	37°N, 76°S
Technique:	Incoherent Backscatter
Range:	0 - 32 km
Vertical resolution:	150 m
Frequency (typical):	1 per week since 1974
Platform:	Laboratory setting with roof opening

Laser

Wavelength:	694 nm
Pulsed frequency:	1 pulse every 8 sec
Energy:	1 Joule
Beam divergence:	1 mrad

Receiver

Type:	Cassegrainian configured telescope
Size:	48 inch
FOV:	1 - 4 mrad

Detectors

3 photomultipliers, gated to increase dynamic range

Data Acquisition System

12 bit CAMAC

ref. M. Osborn, private communications 1993

WJSA

06/10/94-001-12

Mount Pinatubo 6/12/91

- Range performance estimates use SAGE data from 1984 to pre-Pinatubo.

- SAGE and LIDAR data are being used in the Post-Pinatubo recovery analysis.

- SAGE data: 11/84 to 5/93
  Most Post-Pinatubo profiles are incomplete. Sensitivity limit of instrument reached at high altitudes.

- LaRC Lidar data: 1974 to 11/93
  Lidar data used to look at periods where SAGE data is unavailable.
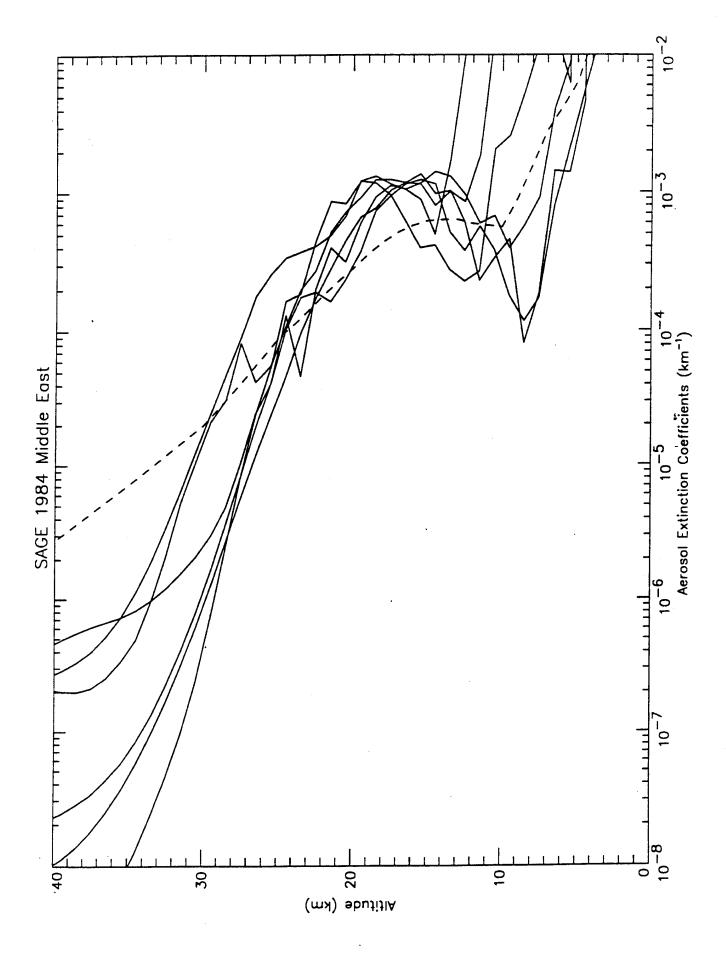
- Lidar scattering ratios translated to extinction coefficients using Fernald inversion algorithms and Deschler particle size distributions taken with dustsondes.
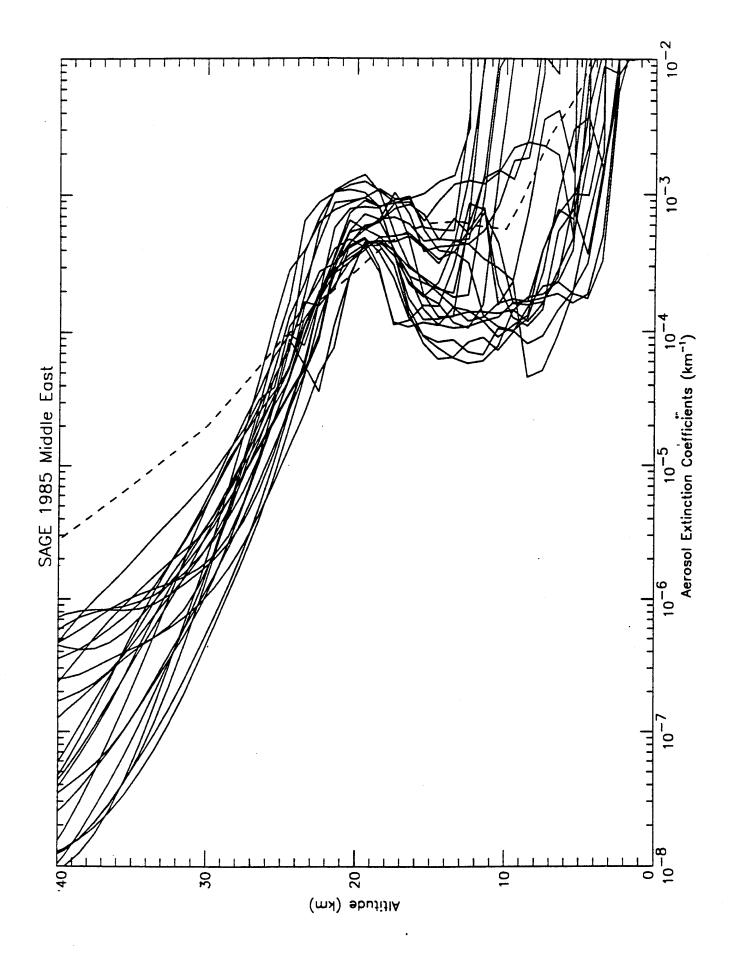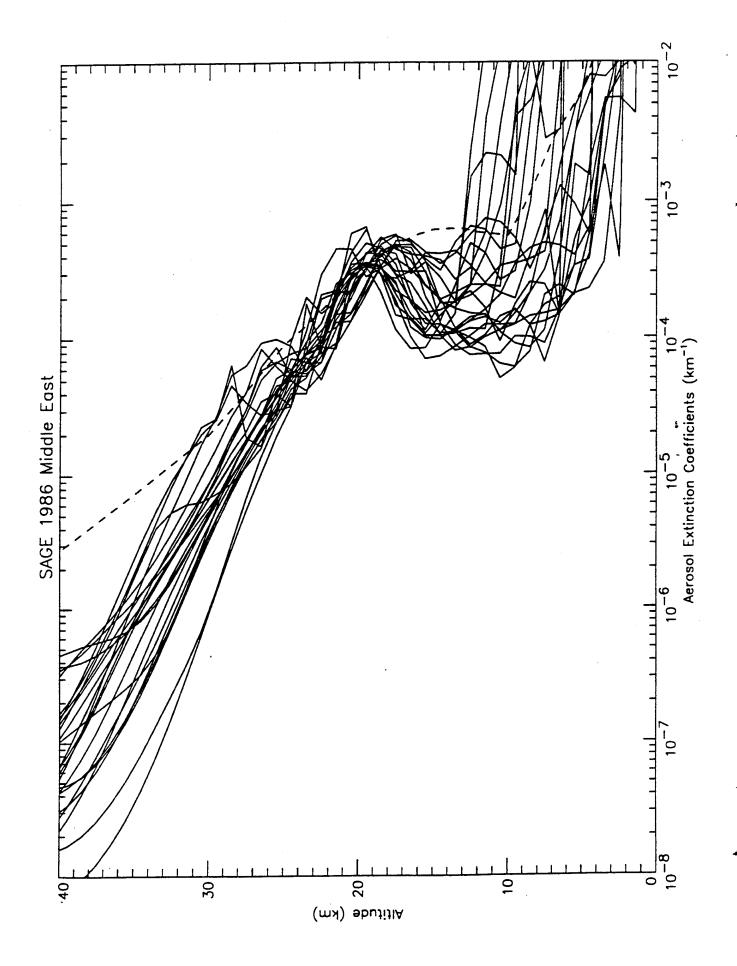
WJSA

06/10/94-001-13

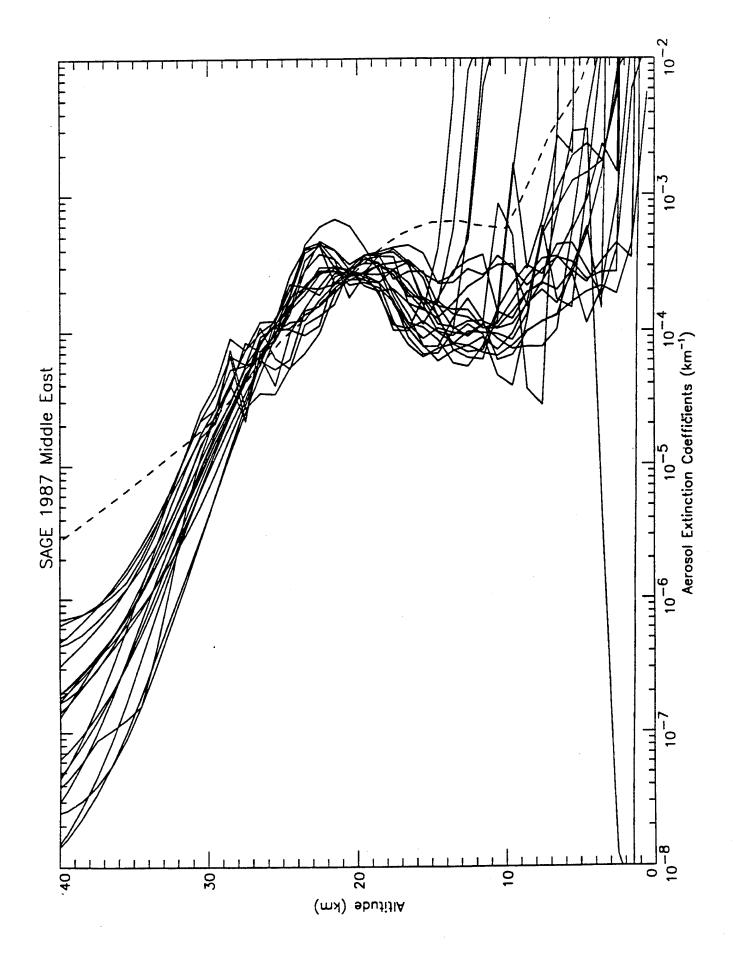# Middle East SAGE profiles 1984 to 1992

- Dashed line is COIL default using LOWTRAN Background Stratospheric/ Moderate Profile

- 1984-5 stratosphere still suffered from contamination by the El Chichon eruption in April 1982.

- Yearly progression shows gradual decrease in extinction with time.

- 1988 up to Pinatubo shows a clean background stratospheric atmosphere.

- Following Pinatubo there was a precipitous increase in extinction, first at lower altitudes and then into the stratosphere.

- The integrated extinction continued to increase until its peak in Feb 92.
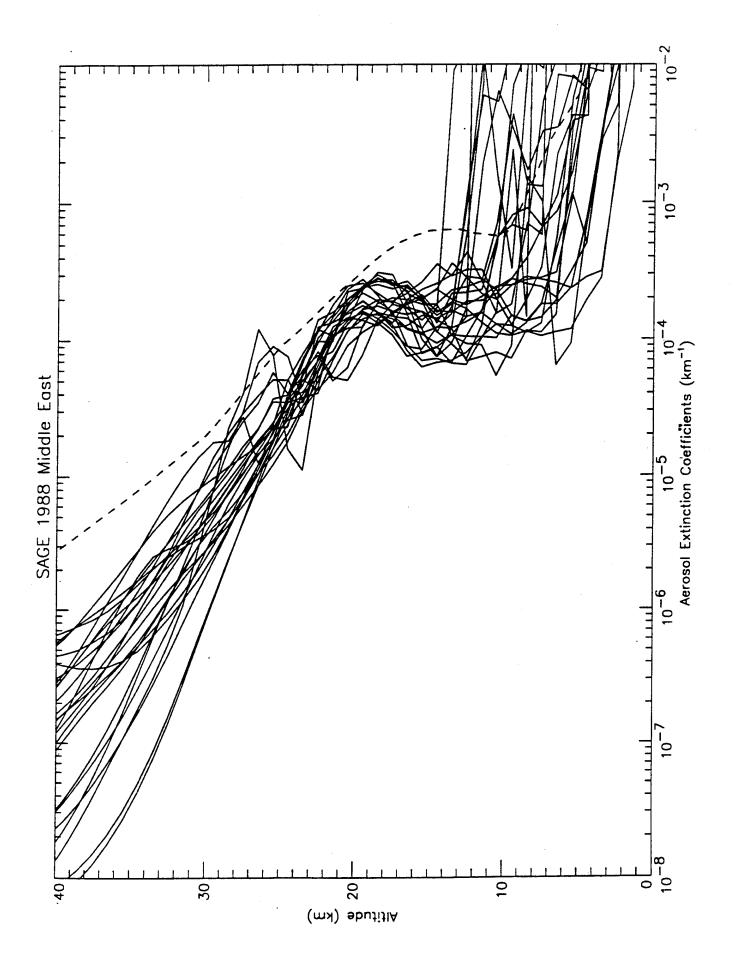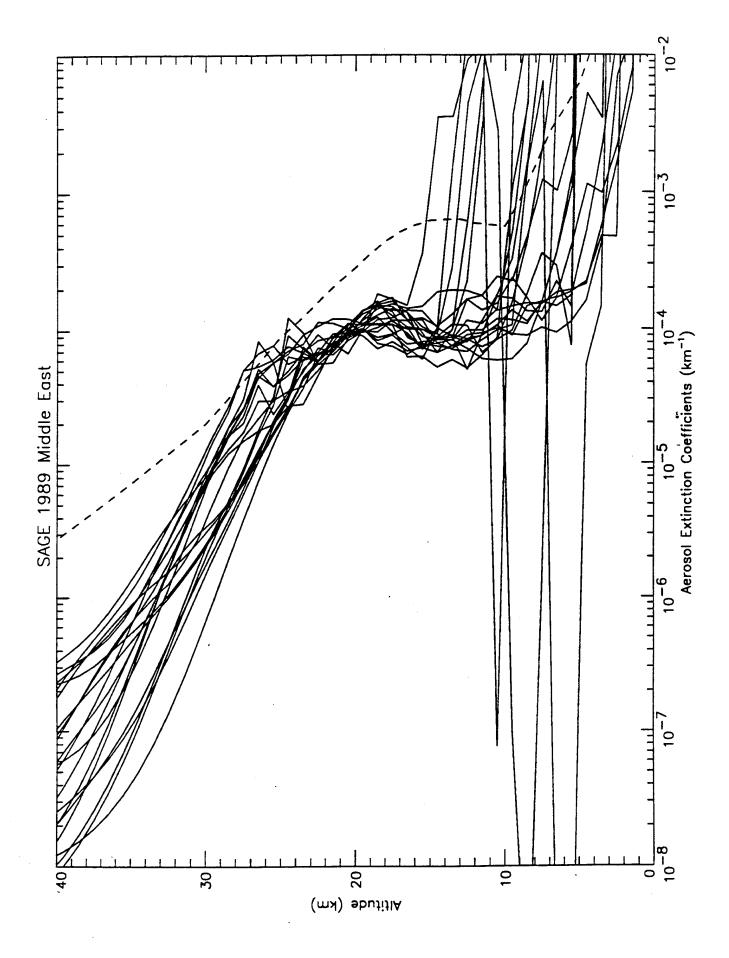
WJSA

SAGE 1984 Middle East

Altitude (km)

Aerosol Extinction Coefficients (km^{-1})

SAGE 1985 Middle East

Aerosol Extinction Coefficients (km⁻¹)

Altitude (km)

SAGE 1986 Middle East

Aerosol Extinction Coefficients (km^{-1})

Altitude (km)

292

SAGE 1987 Middle East

Altitude (km)

Aerosol Extinction Coefficients (km^{-1})

SAGE 1988 Middle East

Altitude (km)

Aerosol Extinction Coefficients (km^{-1})

SAGE 1989 Middle East

Altitude (km)

Aerosol Extinction Coefficients (km^{-1})

SAGE 1990 Middle East

Altitude (km)

Aerosol Extinction Coefficients (km^{-1})

SAGE 1991 Middle East

Aerosol Extinction Coefficients (km^{-1})

Altitude (km)

SAGE 1992 Middle East
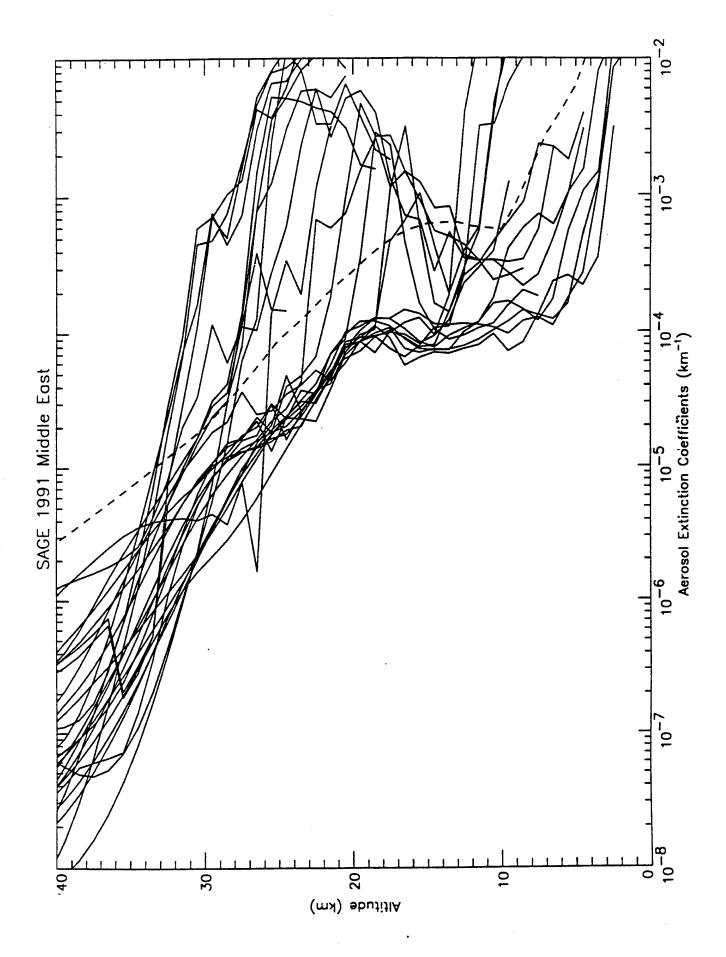
Altitude (km)

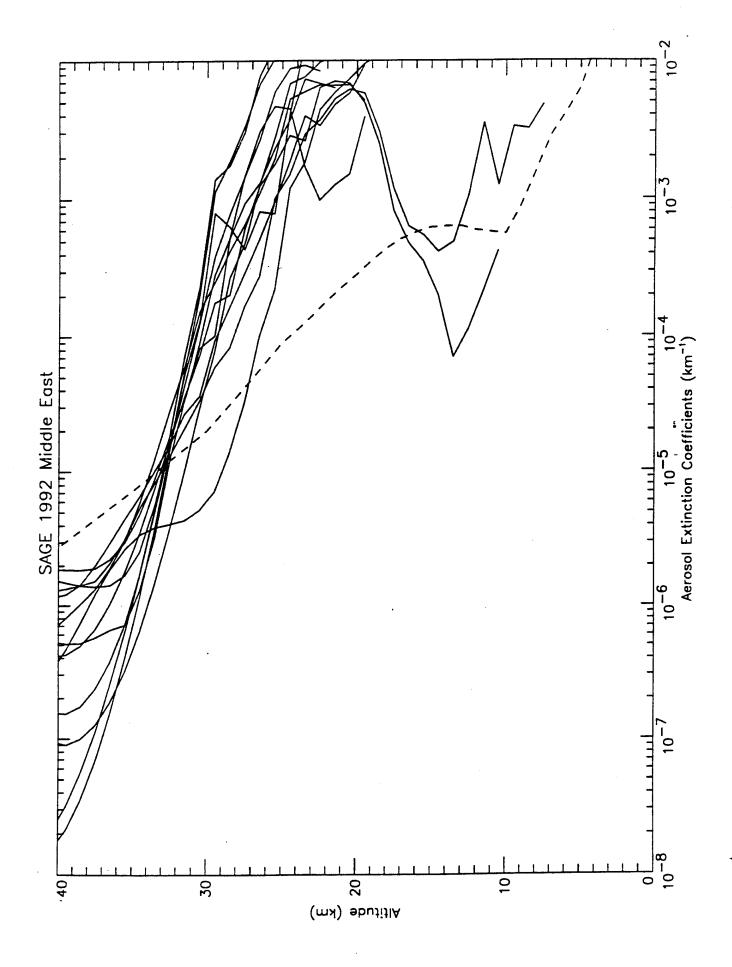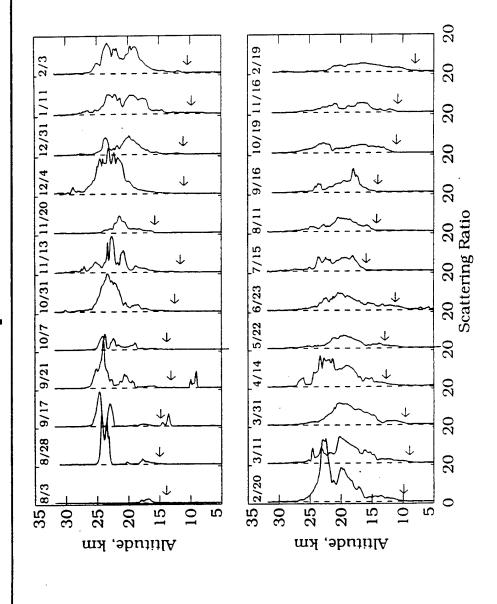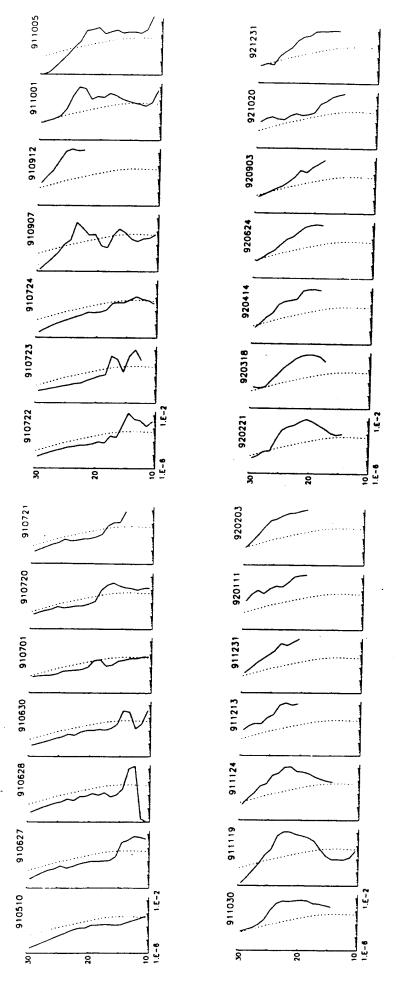Aerosol Extinction Coefficients (km^{-1})

**LaRC Lidar Scattering Ratios
8/3/91 to 2/19/93
Pinatubo Erupted in June 91**

ref. M. Osborn, private communications 1993

4/7/94 LKH

SAGE Extinction Profiles over Hampton from 5/10/91 to 12/31/92

The number above each figure gives the date. The first two numbers specify the year, the second two the month, and the last two the day.
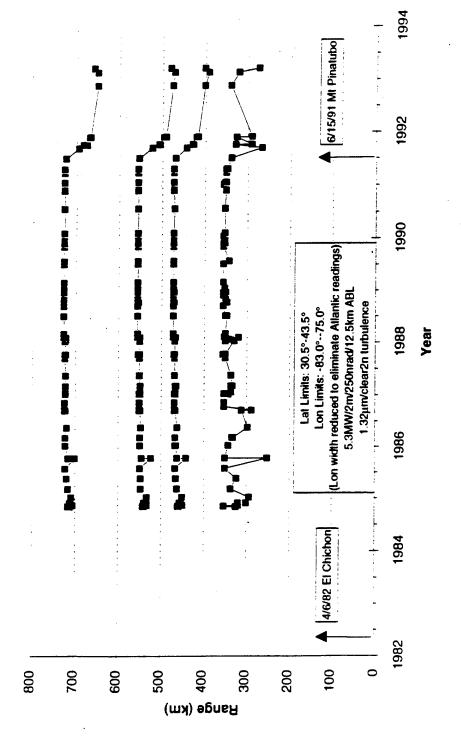
4/7/94 LKH

300

SAGE Volcanic Aerosol
Analysis Methodology

- SAGE database is scanned for all sunrise/sunset observations in the geographic region of interest.

- Measured extinction profiles at 1.02 μm are converted to 1.315 μm using LOWTRAN aerosol scaling factors.

- Profiles with interfering clouds are thrown out.

- Extinction profiles are used in WJSA - ABLE code to calculate range performance for a fixed power, or power required for fixed geometry.
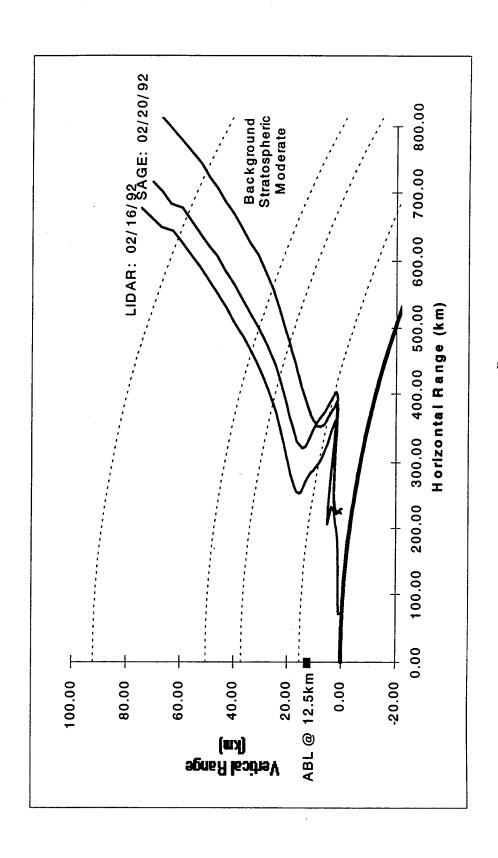
WJSA

Hampton SAGE
ABL Range Performance

Range (km) — Year

4/6/82 El Chichon

6/15/91 Mt Pinatubo

Lat Limits: 30.5°-43.5°
Lon Limits: -83.0°--75.0°
(Lon width reduced to eliminate Atlantic readings)
5.3MW/2m/250nrad/12.5km ABL
1.32µm/clear2n turbulence

Hampton SAGE range performance is similar to that of the Middle East. This implies we can use the LaRC Lidar data to fill in the gaps in the SAGE data for both locations.

WJSA

4/7/94 LKH

302

Lidar - SAGE Comparison

LIDAR: 02/16/92
SAGE: 02/20/92

Background
Stratospheric
Moderate

Horizontal Range (km)

Vertical Range (km)

ABL @ 12.5km

100.00 80.00 60.00 40.00 20.00 0.00 -20.00

0.00 100.00 200.00 300.00 400.00 500.00 600.00 700.00 800.00

WEATHER AND ATMOSPHERIC VISUALIZATION EFFECTS FOR SIMULATION (WAVES)

RICHARD SHIRKEY

DAVID TOFSTED

ALAN WETMORE

LOREN ESPADA

ARMY RESEARCH LABORATORY
BATTLEFIELD ENVIRONMENT DIRECTORATE
WHITE SANDS, NM

AND

ANDREW ZARDECKI
LOS ALAMOS CONSULTING
LOS ALAMOS, NM
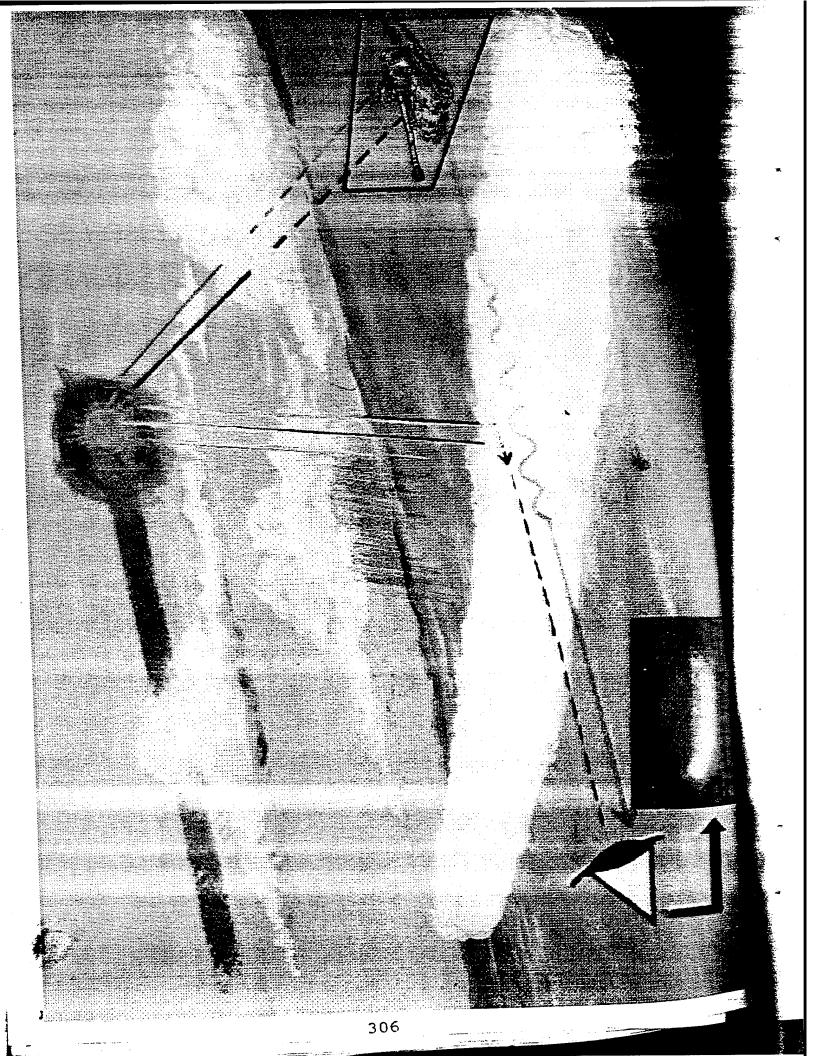
Visual & Thermal
Atmospheric Effects Modeling

The Big Picture

Predict the Effects of the Atmosphere on Target Acquisition for Constructive and Virtual Simulation using Visible and Infrared Sensors.

APPROACH

BATTLEFIELD ENVIRONMENT DIRECTORATE

Develop Accurate, Time-Dependent, Fast-Running Computer Models for Interactive Simulation and Visualization of Realistic Battlefield Environments Under all Seasons, Weather, Times of Day, and Locales

Waves

Wether & Atmospheric Visualization Effects for Simulation

- WAVES Components

  - BLIRB – Boundary Layer Illumination and Radiation Balance

  - ATMOS – Atmospheric Turbulence Structure

  - VIEW – Viewpoint Geometry and Transforms

  - PIXELMOD – Modification of Images, pixel-by-pixel

APPLICATION

Provide Models that Predict Atmospheric and Battlefield Induced Degradation for Insertion into Scene Creation Models, Target Acquisition Models, War games, and Interactive Simulations; Develop Innovative Techniques/Measurements for Model Verification and Validation
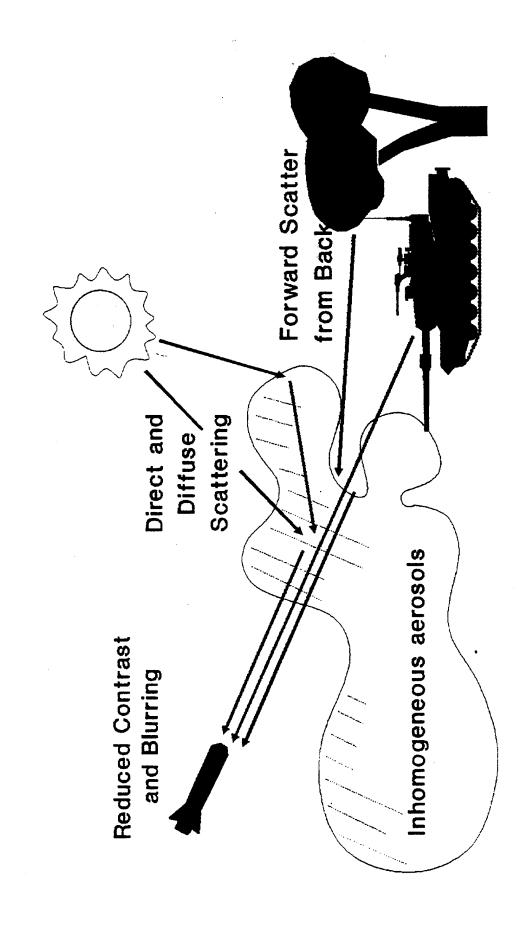
Atmospheric Effects Model (BLIRB)
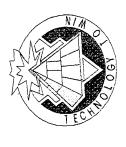
The Boundary layer Illumination and Radiation Balance (BLIRB) model calculates the directional fluxes of visible and infrared radiation throughout a part of the near earth environment using a 8-stream multiple scattering approach

- Varying Illumination

- Horizontal Radiative Transport

- 3-D Inhomogeneous Cloud Structure

VIEWING MODEL USING BLIRB DATABASE

Direct and Diffuse Scattering

Reduced Contrast and Blurring

Forward Scatter from Back

Inhomogeneous aerosols

VIEW

- Use BLIRB database to produce a set of range-dependent tabulated transmittance, path radiance, and edge smoothing effect parameters for desired line of sights

- Transmittance determined by tracing a path through a series of BLIRB space cells, integrating the additional losses of energy in each cell.
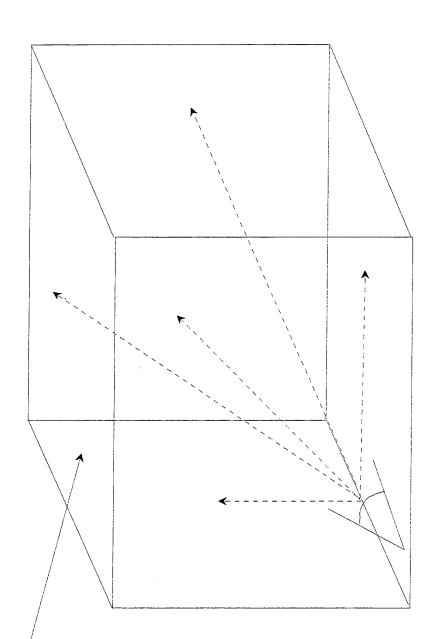
VIEW
(continued)

- Path radiance determined by integrating effects of diffuse and direct radiation scattering into optical path in each cell.

- Forward scattering computed using integration of phase function effects over optical path.

View
Geometry Routine

BLIRB
SPACE

Region of Structure

PIXELMOD PROGRAM

BATTLEFIELD ENVIRONMENT DIRECTORATE

- Image Modification Code to Simulate the Appearance of an Image Under Different Atmospheric Conditions. Utilize Previously Run BLIRB Atmospheric Radiance Field Data Sets.

- Compute Statistics for Multiple Lines of Sight Within BLIRB Space Using the VIEW Code.

  Produces:

  Transmittance, Path Radiance, Turbulent and Aerosol Forward Scatter Blurring Parameters.
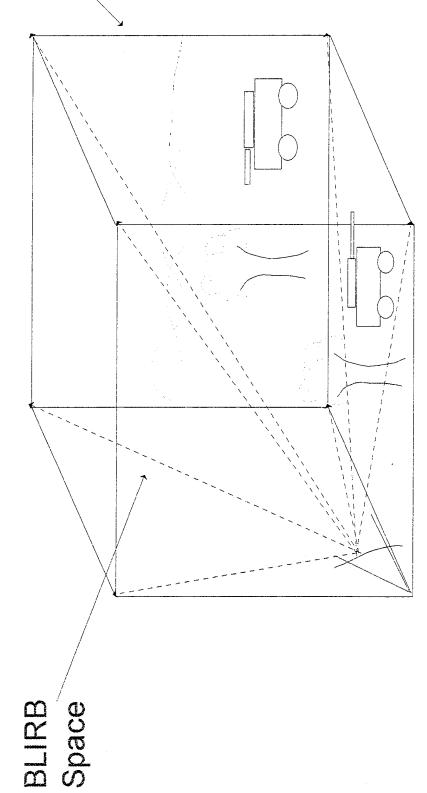
PIXELMOD PROGRAM
(continued)

- Spectral Estimation Technique Converts RGB Pixels into Spectral Radiances that can be Propagated.

- User Interface to Control Observer Perspective Characteristics and Allow User Selection of Weather Scenario.
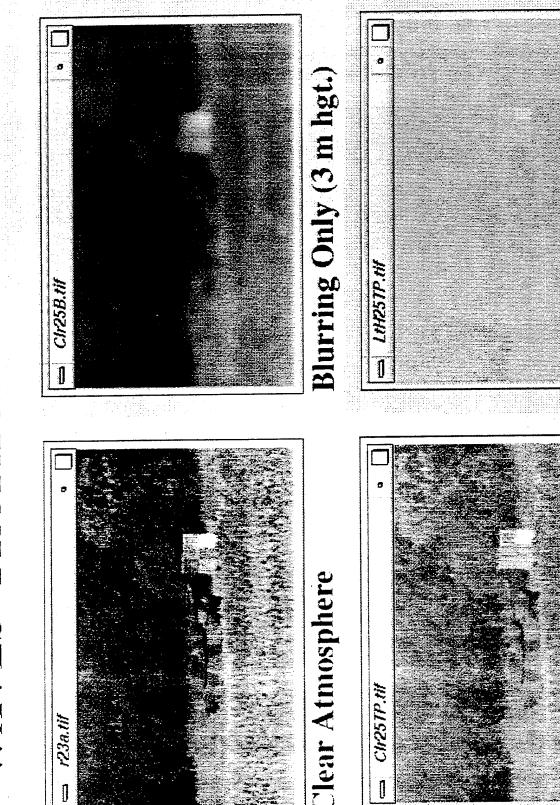
PIXELMOD
Scene Modification

BATTLEFIELD ENVIRONMENT DIRECTORATE

Inserted
Scene

BLIRB
Space

WAVES PROPAGATION MODEL

Clr25B.tif

Blurring Only (3 m hgt.)

LtH25TP.tif

10 km Vis (no blurring)

r23a.tif

Clear Atmosphere

Clr25TP.tif

23 km Vis (no blurring)

318

SUMMARY

Physically realistic Atmospheric Models are being applied to Distributed Interactive Simulation (E2DIS), and to the Army's Target Acquisition modeling Improvement Plan (TAMIP), and Parametric Representation for Constructive Simulation (War Games).

SPARTA'S LIDAR SIMULATION CODE, BACKSCAT VERSION 4.0

by

D.R. Longtin, M.G. Cheifetz, J.R. Jones, and
J.R. Hummel

Annual Review Conference on
Atmospheric Transmission Models
Phillips Laboratory/Geophysics Directorate
Hanscom AFB, MA

7-8 June 1994

SPARTA, Inc.
24 Hartwell Avenue
Lexington, MA 02173

WHAT IS BACKSCAT?

- Simulates Lidar Backscatter for Atmospheric Applications (UV, Visible, IR) on a PC
  - Extensive Database of Aerosols/Clouds
  - Molecular Scattering from Database or Radiosonde
- Models Aerosol Backscatter, Raman, and Coherent Doppler Lidar Systems
  - Signal-to-Noise Performance and Estimates of Range and Velocity Accuracy
  - Built-In or User-Defined Detectors
- User-Friendly Menu Interface System
  - Accepts Simulation Inputs
  - Saves and Recalls Previous Simulation Conditions
  - Displays Results Graphically

BACKSCAT APPLICATIONS

- Remote Sensing Analysis

- System Design and Trade Offs

- Lidar Performance Predictions with Different Laser Systems and Atmospheric Conditions

- Predictions of Lidar Field Tests

GROWTH OF BACKSCAT

1990 Version 1.0

FORTRAN Based System With

AFGL Aerosol Models as

Built-in Defaults

1991 Version 2.0

- New C-Based Menu System
- Cirrus Clouds and Desert

  Aerosols Added

1992 Version 3.0

- Surface Reflections Added
- User-Defined Aerosols
- System Efficiency Considered
- Raman Lidars Simulated

1994 Version 4.0

- Signal-to-Noise Added
- Library of Detectors Included
- Coherent Doppler Lidar Simulated
- Water Clouds Included
- Estimates of Molecular Absorption Available

323

NEW FEATURES IN BACKSCAT 4.0

- Signal-to-Noise Performance Models
  - Relations for Aerosol Backscatter (*i.e.*, Direct Detection) and Coherent Doppler Lidar Systems
  - Estimates of Range and Wind Speed Accuracy
  - Built-In or User-Defined Detectors

- Water Cloud Option as Built-In Cloud Type
  - Wavelength Scaling Factors from LOWTRAN
  - Input Cloud Type, Base, Thickness, and β_{ext} at 0.55 μm (or Accept Defaults)

NEW FEATURES IN
BACKSCAT 4.0 (cont.)

- MABS, An Auxiliary Package That Estimates Molecular Absorption Profiles
  - LOWTRAN Resolution (20 cm^{-1})
  - Input Lidar Wavelength and Model Atmosphere (or User-Defined Data)
  - Automatically Creates Input File For Use in BACKSCAT

- Automated Utility for Installing BACKSCAT on User's PC

- Upgrade Radiosonde Edit/Create Program
  - Includes Wind Speed and Direction for Coherent Doppler Analysis

SNR PERFORMANCE MODEL

PERFORMANCE MODEL INCLUDES EFFECTS FROM:

SIGNAL

- Hardware Optical Efficiencies
- Atmospheric Attenuation
- Aerosol Backscatter
- Detector Quantum Efficiency
- Aperture Size/Obscuration
- Laser Output Power
- Laser Beam Quality

NOISE

- Signal Photon Shot Noise
- Background Photon Shot Noise
- Thermal (Johnson) Noise
- Detector Dark Current
- Preamplifier Noise
- Spatial/Spectral/Temporal Noise Suppression
- Hardware Optical Efficiencies
- Detector Quantum Efficiency
- Detector NEP & Excess Noise

Figure

SNR MODEL ASSUMPTIONS

- Signal-to-Noise Relatively Large
  - $SNR_V > 1$
  - Not in Photon Counting Regime

- Matched Filter in Detection System

- Turbulence Effects Not Included

- Pulsed Laser System
  - No CW Scanning Systems

- Matched Receiver and Transmitter Field-Of-View

- Flicker Noise Not Considered

- Local Oscillator Power Is Large Enough to Provide Shot-Noise-Limited Operation of the Receiver*

- Unity Mixing Efficiency of Local Oscillator with Return*

  (* Coherent Doppler Systems Only)

ESTIMATES OF RANGE AND VELOCITY ACCURACY

- Accuracy Estimates Confined to a System's Inherent Measurement Capability

  - For Coherent Doppler Systems, They Refer to the Ability of the Doppler Processor to Estimate the Center Frequency of the Received Signal Having a Finite Signal-to-Noise Ratio and Finite Observation Time

- Assumptions

  - No Short-Term or Long-Term Pointing Errors

  - Rectangular Pulse of Length τ

  - Stationary Lidar

  - Estimates of Wind Speed Accuracy Independent of Wind Field Structure*

  - No Frequency Jitter in Local Oscillator*

  (* Coherent Doppler Lidar Systems Only)

BACKSCAT MAIN MENU

- Lidar System Parameters
  - Pulse Wavelength, Energy, Duration
  - System Optical Size and Efficiencies
  - Detector Type

- Viewing Conditions
  - Lidar Height
  - Viewing Elevation and Azimuth Angles
  - Output Grid for Results

- Atmospheric Parameters
  - Aerosol, Molecular, Wind Profiles
  - Cloud Properties
  - Raman Molecule

- Change Lidar System
  - Aerosol Backscatter
  - Raman Scattering
  - Coherent Doppler
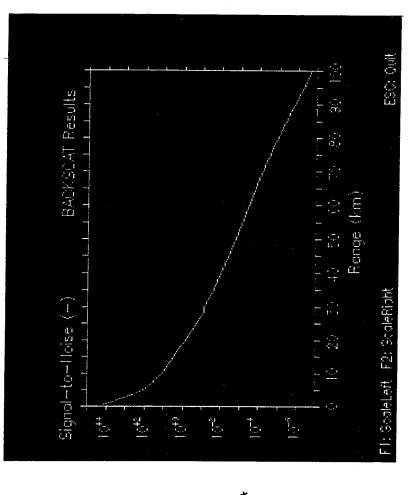
BACKSCAT OUTPUT AND PLOTS

- Output Products
  - Attenuation Coefficients Along Line-of-Sight (LOS)
  - Optical Depth
  - Backscattered Power
  - Signal-to-Noise Performance
  - Range Accuracy
  - Wind Speed Accuracy*
  - Observed Wind Profile*
  - Radial Wind Speed Along LOS*
    (* Coherent Doppler Only)
- Available Plots
  - Backscatter vs. Range
  - Backscatter vs. Altitude
  - Signal-to-Noise vs. Range
  - Signal-to-Noise vs. Altitude

FUTURE UPGRADES

- DIAL System
- Scanning Systems
- MS Windows Interface and On-Line Help
- Inclusion of Turbulence

331

POINTS OF CONTACT

- Technical Questions

  David Longtin

  SPARTA, Inc.

  24 Hartwell Avenue

  Lexington, MA 02173

  (617)-863-1060

- Obtaining BACKSCAT

  Capt. Mark Cloutier/GPOA

  Phillips Laboratory

  Hanscom AFB, MA 01731-5000

  (617)-377-3018

THE SOLAR IRRADIANCE BY COMPUTATION

Robert L. Kurucz

Harvard-Smithsonian Center for Astrophysics
60 Garden St, Cambridge, MA 02138

I am now able to compute a purely theoretical model photo-sphere (Kurucz 1992a;b;c) that reproduces the irradiance measure-ments of Neckel and Labs (1984) in the visible for bandpasses of approximately 2 nm. That model, and Avrett's empirical quiet sun model (Fontenla, Avrett, and Loeser 1993) that includes the chromosphere, are used to predict the irradiance out to 200 microns at low resolution.

To get a feel for the scope of the monochromatic irradiance problem I have computed the spectrum from 150 nm to 200 microns at a resolution of 500000 using 58 million lines, both predicted and observed. If this spectrum is degraded to the resolution of the model it looks like the model. At any given wavelength the spectrum is not reliable. But at a resolution of 10000, say, it approaches measurement accuracy. In regions of low transmission it is more reliable than existing measurements. I will publish tables of these irradiance spectra.

I am producing atlases of the solar flux, central intensity, and limb spectra taken by James Brault at Kitt Peak. One atlas "Solar Flux Atlas from 294 to 1300 nm" by Kurucz, Furenlid, Brault and Testerman (1984), has been published thus far. I have have the Photometric Atlas of the Solar Spectrum from 1,850 to 10,100 cm-1" by Delbouille, Roland, Brault, and Testerman (1981) also taken at Kitt peak. In addition I have the ATMOS central intensity atlas from 650 to 4800 cm-1 taken by Farmer and Norton (1989) from Spacelab 3. The replacement for the flux atlas will be printed on demand in 4 parts of about 500 pages each. Each page will show the observed spectrum normalized to a continuum, the state-of-the art computed transmitted spectrum on the day the atlas is printed, and line identifications. Each part will cost $100, plus shipping if sent overseas. If I can obtain a color laser printer, I will make a $200 version with color coded solar spectrum, transmission spectrum, transmitted spectrum, and the line indentifications. I will produce CD-ROMS with the spectrum and line data. I have spectra that will continue the atlas out to 5 microns. I am reducing SMM spectra at shorter wavelengths. Similar atlases will be made for the solar center and limb in collaboration with my colleague Barbara Bell.

Parts of the flux atlases directly give the residual irradiance spectrum but much is confused or obscured by terrestrial lines. I can compute them away except where the transmission is too low. Then I will fill in with the purely theoretical solar spectrum. In this way I will finally produce an atlas showing the solar spectrum above the atmosphere.

I use these atlases to test the pure calculations of solar spectra and transmission spectra. I identify problems with the line data and I try to make generic corrections that improve hundreds or thousands of lines at a time. If the spectrum calculations look good in the regions of high transmission, I can have some confidence that the regions of low transmission are computed accurately. The main problem has been continuum placement. Ozone and O2 "dimer" features are difficult to determine because the atlases are each made up of a number of sharply peaked FTS scans. The continuum placement affects the appearance of line wings and the apparent depth of weak features.

REFERENCES

Delbouille, L., Roland, G., Brault, J., and Testerman, L. 1981. Photometric Atlas of the Solar Spectrum from 1850 to 10000 cm-1. (Tucson: Kitt Peak National Observatory), 189 pp.

Farmer, C.B. and Norton, R.H. 1989. A High-Resolution Atlas of the Infrared Spectrum of the Sun and Earth Atmosphere from Space. NASA Reference Pub. 1224, in two volumes, 1216 pp.

Fontenla, J.M., Avrett, E.H., and Loeser, R. 1993. Energy balance in the solar transition region. III. Helium emission in hydrostatic, constant-abundance models with diffusion. Astrophysical Journal 406, 319-345.

Kurucz, R.L. 1992a,b,c
Atomic and molecular data for opacity calculations. pp.45-48
"Finding" the "missing" solar ultraviolet opacity. pp.181-186
Remaining line opacity problems for the solar spectrum.187-194.
All presented at the Workshop on Astrophysical Opacities, Caracas, 15-19 July 1991. Revista Mexicana de Astronomia y Astrofisica, vol. 23.

Kurucz, R.L., Furenlid, I., Brault, J., and Testerman, L. 1984. Solar Flux Atlas from 296 to 1300nm. (Sunspot, New Mexico: National Solar Observatory), 240 pp.

Neckel, H. and Labs, D. 1984. The solar radiation between 3300 and 12500 A. Solar Physics 90, 205-258.

Annual Review Conference on Atmospheric Transmission Models

Phillips Laboratory, Hanscom AFB, MA, 7-8 June 1994

New Visible and Near IR Ozone Absorption Cross-Sections for MODTRAN

Eric P. Shettle, NRL, Washington, DC 20375

and

Stuart M. Anderson, Augsburg College, Minneapolis, MN 55454

Ozone cross-sections for the Chappuis and Wulf absorption bands

* Knowledge of the ozone absorption cross-sections is important for:

  - Modeling the propagation of radiation through the atmosphere
  - Deriving the atmospheric ozone concentration from measurements of the spectral character of transmitted or scattered radiation.

* Visible cross-sections are unchanged since the original LOWTRAN and are not given at all for $\lambda > 769$ nm.

* Have combined several recent studies of the ozone Chappuis and Wulf absorption bands

* Provide the ozone cross-section from 407 to 1089 nm.
  Temperature dependence is also given for 407 to 762 nm.

Spectral Measurements of Ozone Absorption

Reference	Wavelengths [nm]	Resolution [nm]	Data Interval [nm]
Burkholder, J.B. and R.K. Talukdar, *Geophys. Res. Lett.*, **21**, 581, 1994. [BT]	407 to 762	3 to 4	1
Anderson, S.M., J. Maeder, and K. Mauersberger, *J. Chem. Phys.*, **94**, 6351-6357, 1991. [AMM91]	450 to 850	2.3	0.28
Anderson, S.M., P. Hupalo, and K. Mauersberger, *Geophys. Res. Lett.*, **20**, 1579-582, 1993. [AHM-GRL]	784 to 1098	3.1	0.31
Anderson, S.M., P. Hupalo, and K. Mauersberger, *J. Chem. Phys.*, **99**, 737-739, 1993a. [AHM-JCP]	929 to 1090	1.6	0.16

Compilation of the Data

* ## Normalize Spectral Measurements to the Absolute Cross-Sections of:

   Anderson and Mauersberger, *GRL*, (1992) and Anderson et al., *GRL*, (1993)

* ## Interpolate Normalized Measurements onto Uniform Wavelength Intervals

   Intervals choosen such that 4 point interpolation would reproduce the original values to better than 1%

   (BT 1 nm, AMM91 0.5 nm, AMM90 0.5 nm, & AHM-JCP 0.25 nm)

* ## Combine the Data Sets

   Merging overlapping regions with smoothly weighted average

Improved Visible and Infrared Ozone Cross-Sections

Wavelengths [nm]	Source
407 to 450	Burkholder, J.B. and R.K. Talukdar, *Geophys. Res. Lett.*, **21**, 581, 1994. [BT]
450 to 500	w(λ)*[BT] + {1 - w(λ) }*[AMM91]
500 to 785	Anderson, S.M., J. Maeder, and K. Mauersberger, *J. Chem. Phys.*, **94**, 6351-6357, 1991. [AMM91]
785 to 820	w(λ)*[AMM91] + {1 - w(λ) }*[AHM-GRL]
820 to 929	Anderson, S.M., P. Hupalo, and K. Mauersberger, *Geophys. Res. Lett.*, **20**, 1579-582, 1993. [AHM-GRL]
929 to 1089	Anderson, S.M., P. Hupalo, and K. Mauersberger, *J. Chem. Phys.*, **99**, 737-739, 1993a. [AHM-JCP]

Highlights of Laboratory Measurements

Ozone-friendly single-pass aluminum absorption cell, 0.46m optical path

Fractional absorption detection limits below 0.05% (1 sec), optical depths of 0-10%

Visible region

Precision capacitance manometer calibrated against primary pressure standard on-site

Impurity gas pressures measured and corrected for in real-time
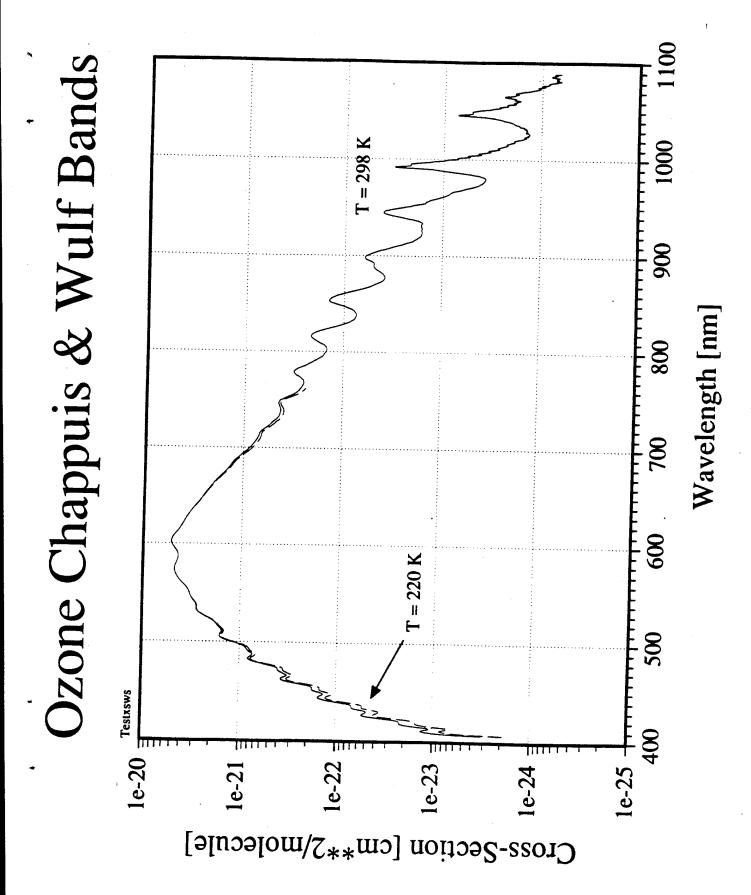
Five HeNe laser transitions span Chappuis band, eliminate wavelength uncertainty
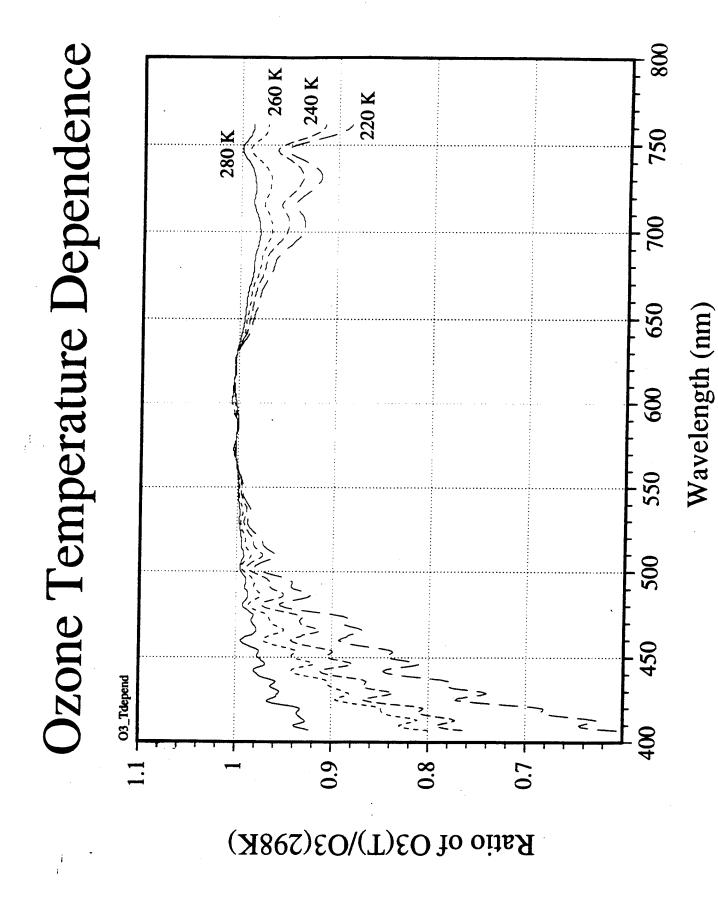
Ozone concentrations cover nearly a factor of 20 (1.8 to 35 x 10^{16} cm^{-3} as well as zero)

Near-IR region
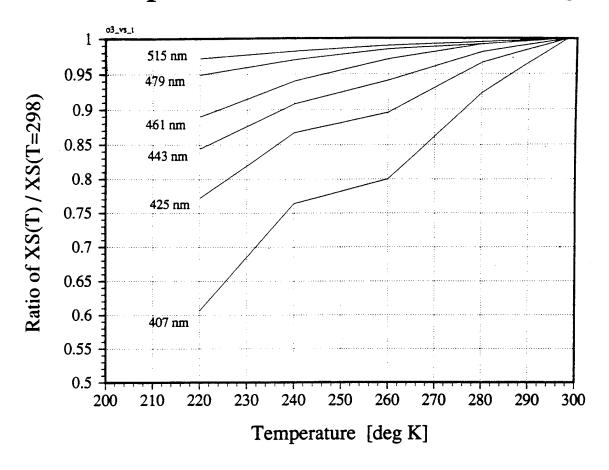
Ozone densities determined in real-time by absorption at 632.8nm HeNe laser transition
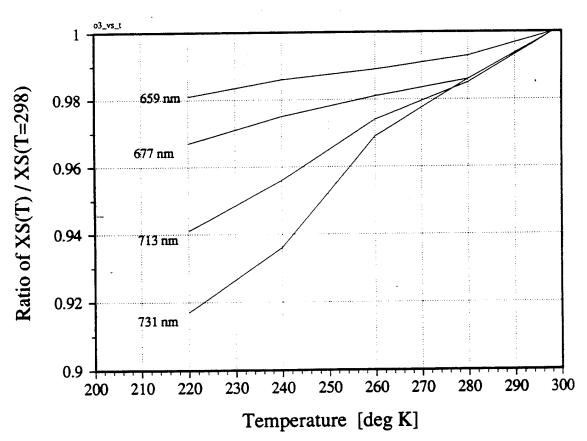
Ozone concentrations cover nearly a factor of 10 (0.8 to 7 x 10^{18} cm^{-3} as well as zero)

Ozone Chappuis & Wulf Bands

Ozone cross-section spectrum showing Chappuis and Wulf bands. Axes: Wavelength [nm] (400–1100) vs Cross-Section [cm**2/molecule] (1e-25 to 1e-20). Curves labeled T = 220 K and T = 298 K. Label: Tesixsws

Ozone Temperature Dependence

O3_Tdepend

280 K
260 K
240 K
220 K

Ratio of O3(T)/O3(298K)

Wavelength (nm)

342
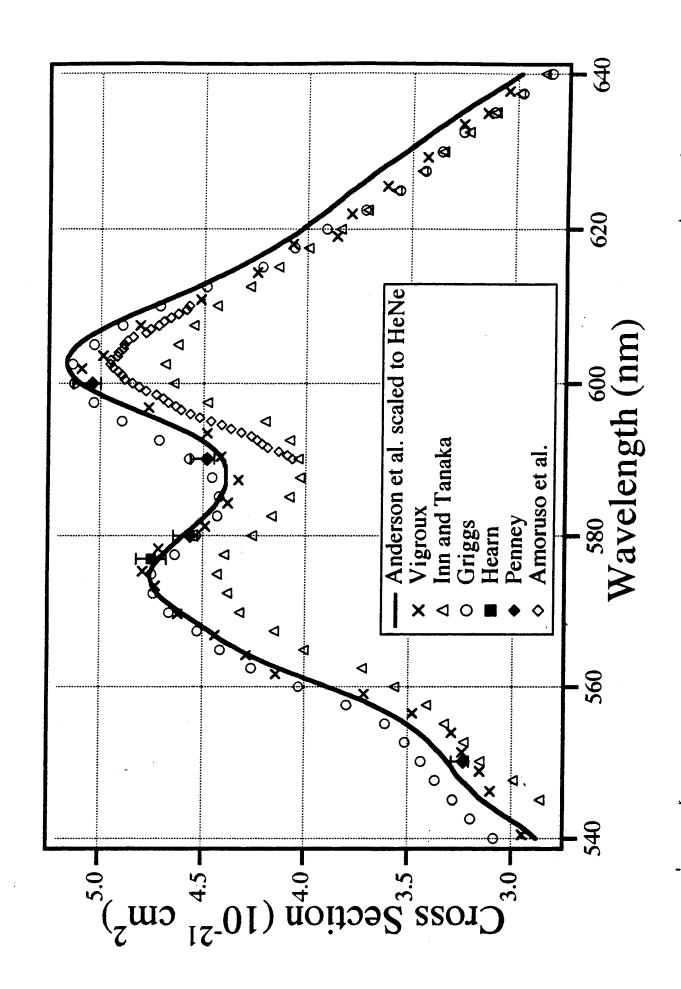
T dependence of O3 vs wavelength

Ozone Chappuis & Wulf Band References

Anderson, S.M., P. Hupalo, and K. Mauersberger, "Rotational structure in the near-infrared absorption spectrum of ozone", *J. Chem. Phys.*, **99**, 737-739, 1993a. [AHM-JCP]

Anderson, S.M., P. Hupalo, and K. Mauersberger, "Ozone absorption cross section measurements in the Wulf bands", *Geophys. Res. Lett.*, **20**, 1579-582, 1993. [AHM-GRL]

Anderson, S.M., J. Maeder, and K. Mauersberger, "Effect of isotopic substitution on the visible absorption spectrum of ozone", *J. Chem. Phys.*, **94**, 6351-6357, 1991. [AMM91]

Anderson, S.M. and K. Mauersberger, "Laser measurements of ozone absorption cross sections in the Chappuis band", *Geophys. Res. Lett.*, **19**, 933-936, 1992. [AM92]

Anderson, S.M., J. Morton, and K.Mauersberger, "Near-infrared absorption spectra of $^{16}O_3$ and $^{18}O_3$: Adiabatic energy of the $^1A_2$ state?", *J. Chem. Phys.*, **93**, 3826-3832, 1990. [AMM90]

Burkholder, J.B. and R.K. Talukdar, "Temperature dependence of the ozone absorption spectrum over the wavelength range 410 to 760 nm", *Geophys. Res. Lett.*, **21**, 581, 1994. [BT]

Shettle, E.P., and S.M.Anderson (1994) to be submitted to *J. Geophys. Letters.*

Absorption Cross Section Measurements of Carbon Dioxide in the Wavelength Region 118.7 nm - 175.5 nm and the Temperature Dependence
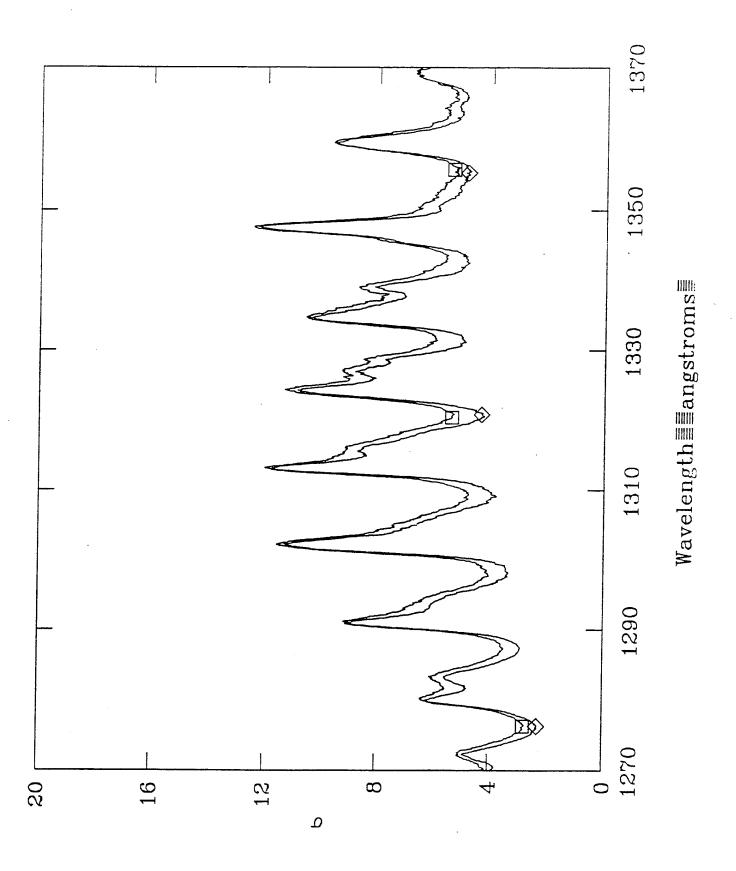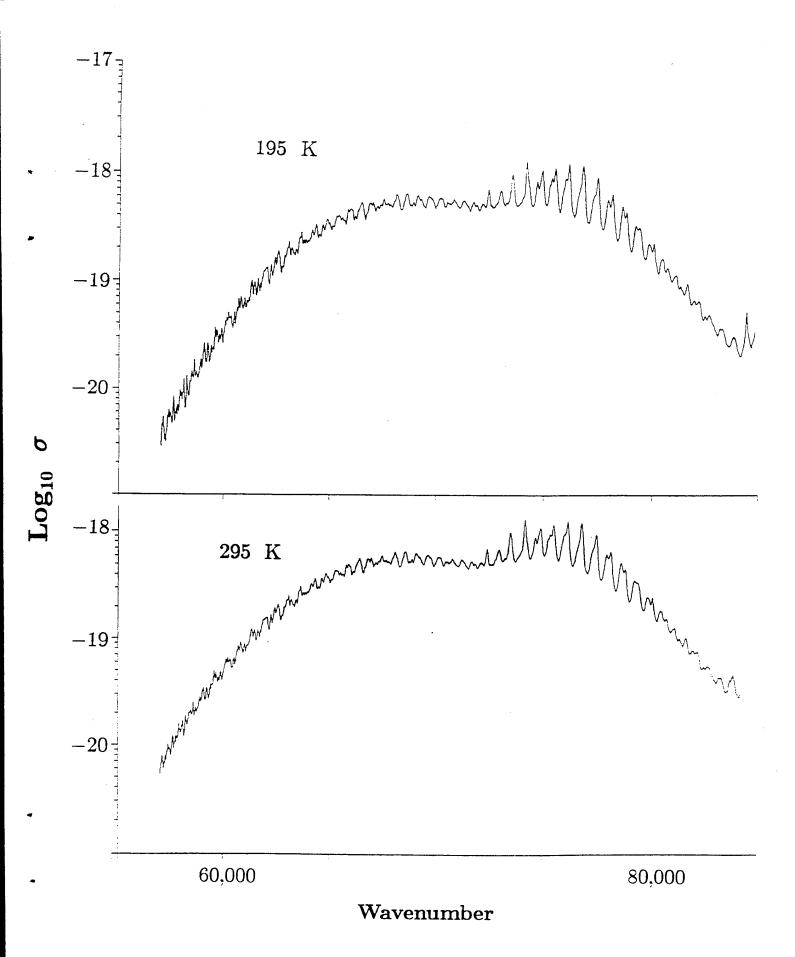
K. Yoshino,[1] J.R. Esmond,[1] K. Ito,[2] T. Matsui[2] and W.H. Parkinson[1]

[1]Harvard-Smithsonian Center for Astrophysics, Cambridge, MA 02138
[2]Photon Factory, KEK, Tsukuba, Ibaraki 305, Japan

TABLE 1. Absolute Absorption Cross Sections of Carbon Dioxide
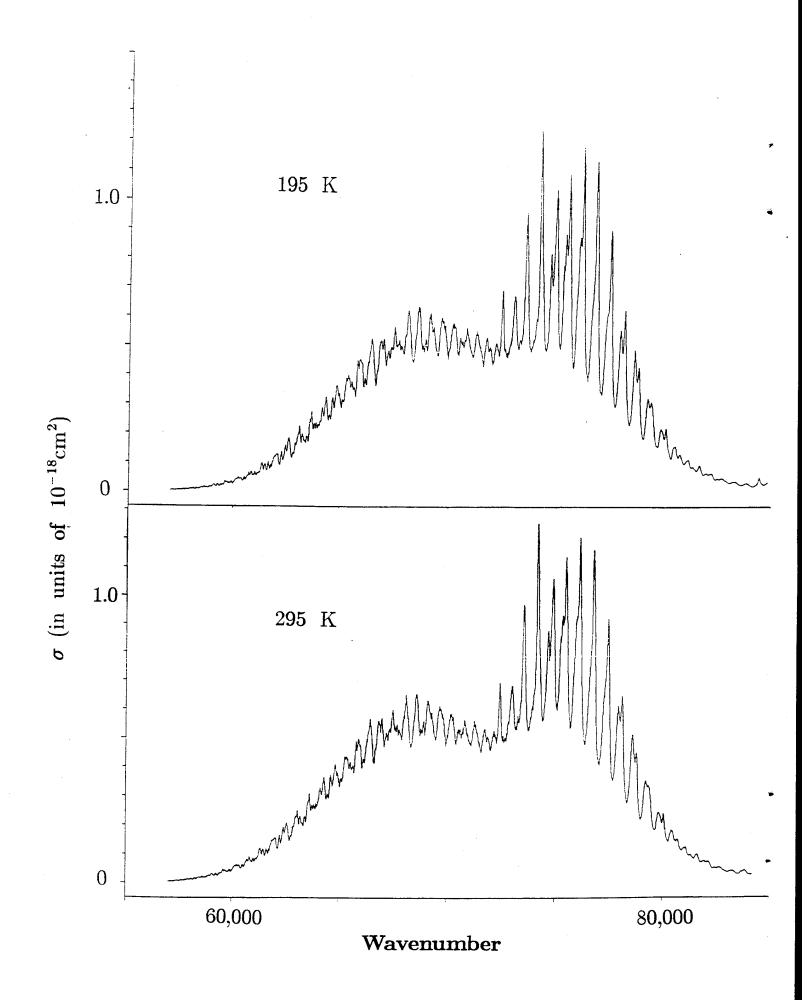
Wavelength nm	Wavenumber cm^{-1}	Cross Section[a]		$\sigma_{195}/\sigma_{295}$
		295 K	195 K	
121.36	82399.	5.08 ± 0.09	4.37 ± 0.06	0.86
125.58	79630.	18.29 ± 0.24	15.98 ± 0.22	0.87
127.63	78351.	27.7 ± 0.4	22.9 ± 0.2	0.83
132.05	75729.	53.7 ± 1.0	43.1 ± 0.5	0.80
135.56	73768.	53.6 ± 0.5	48.5 ± 0.3	0.90
140.60	71124.	47.8 ± 1.2	46.0 ± 0.4	0.96
143.87	69507.	49.3 ± 0.6	46.6 ± 0.5	0.95
150.02	66658.	41.2 ± 0.4	36.5 ± 0.6	0.89
153.72	65053.	33.3 ± 0.4	29.7 ± 0.3	0.89
160.79	62193.	11.91 ± 0.19	9.27 ± 0.03	0.78
168.98	59179.	2.68 ± 0.04	1.84 ± 0.05	0.69
171.91	58170.	1.209 ± 0.084	0.659 ± 0.007	0.55

[a]Cross sections are given in units of $10^{-20} cm^2$.

FAScode for for the Environment: *FASE*

J. L. Moncet and William Gallery

AER, Inc.

Gail Anderson

Phillips Lab/Optical Physics Division

Goals

- On-going Development of FASCODE

- State-of-the-Art Line-by-line Atmospheric Radiation Model

- Satisfy Needs of:

  - Current users--defense community

  - Emerging environmental applications

- Incorporate Best Physics and Software Engineering

Physics:

- Include Latest Advances from ARM

- Continuua: Latest Available or User Supplied

- Simultaneous Radiance and Derivatives for Inversions

- Improved Cross-Section Models

- Voigt Shape Used Throughout

- Spectral Scanning Using FFT's

New Applications

- Training Fast Parameterizations
- Cooling Rates
- Inversion
- Multiple Scattering Through Interface with External Code

Software:
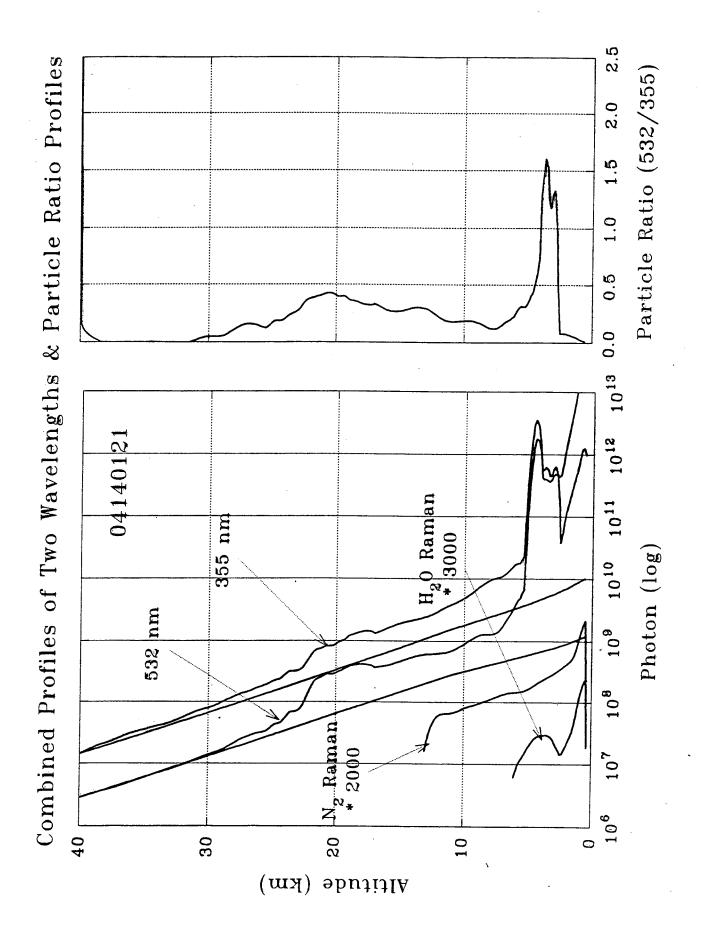
- Improved User Interface

- Modern Coding Techniques: e.g. Include Files for Common Blocks

- Improved Numeric Accuracy

- Vectorization for Parallel Processing

- Improved Documentation, Including Interfaces
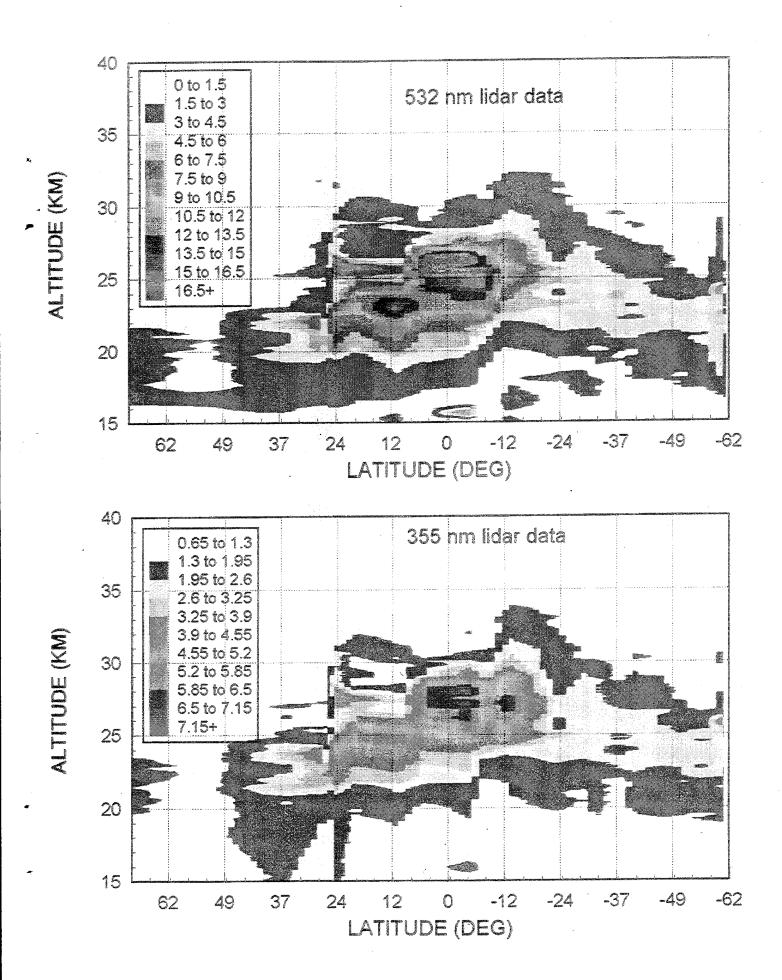
Packaging
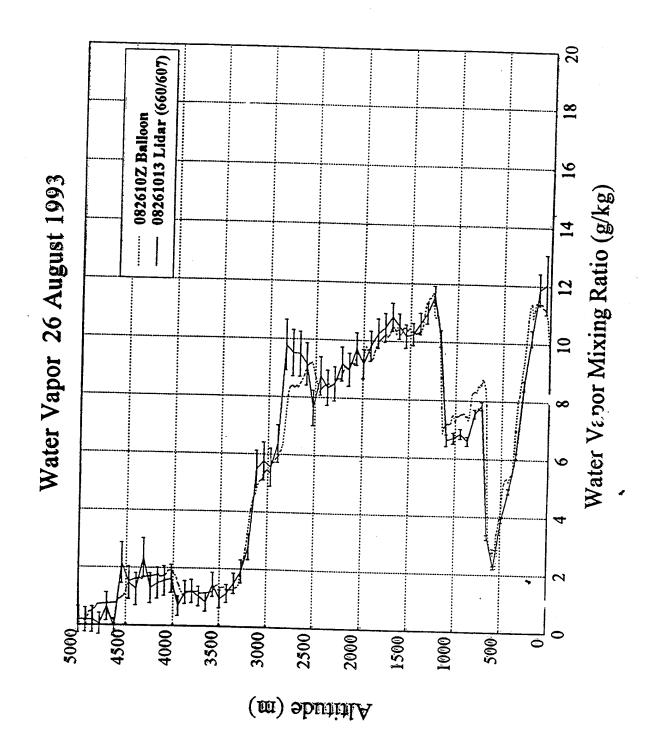
- **All Independent Modules**

  - **Atmosphere, Optical Depth, Radiative Transfer, Filtering, Scanning, Plotting**

  - **Run Together Through Scripts (Batch Files) or Drivers**

- **Makefiles: Unix, VMS, MS-DOS**

- **Distribution by tar or zip File**

- **Under Configuration Control: SCCS**

356

Lidar Measurements of Atmospheric Optical Properties
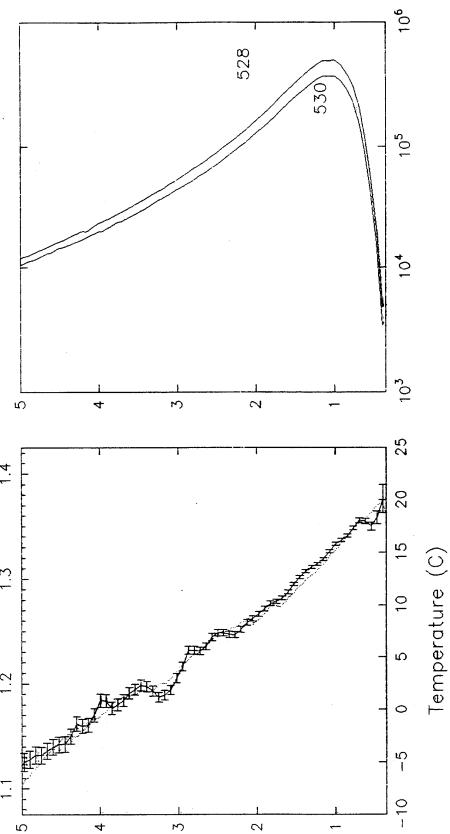
C. R. Philbrick, S. Maruvada and T. D. Stevens

Department of Electrical Engineering and

Applied Research Laboratory

Penn State University

University Park PA 16802

Combined Profiles of Two Wavelengths & Particle Ratio Profiles

04140121

532 nm

355 nm

N_2 Raman *2000

H_2O Raman *3000

Altitude (km)

Photon (log)

Particle Ratio (532/355)

Water Vapor 26 August 1993

Legend:
- 082610Z Balloon
- 08261013 Lidar (660/607)

Altitude (m)

Water Vapor Mixing Ratio (g/kg)

Lidar vs. Balloon Temperature
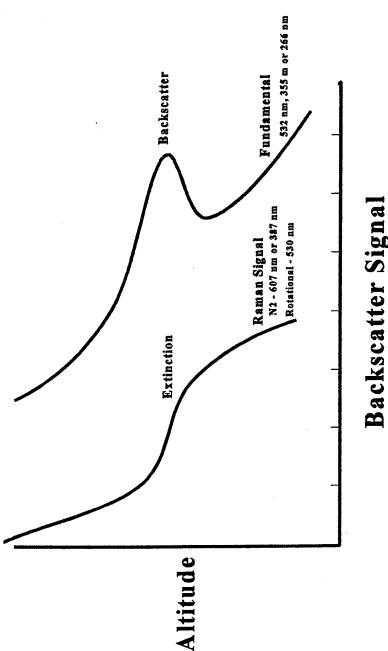
30 minute run begun on 06-13-93 @ 02:09 UT

Balloon launched on 06-13-93 @ 0230UT

528/530

528

530

Temperature (C)
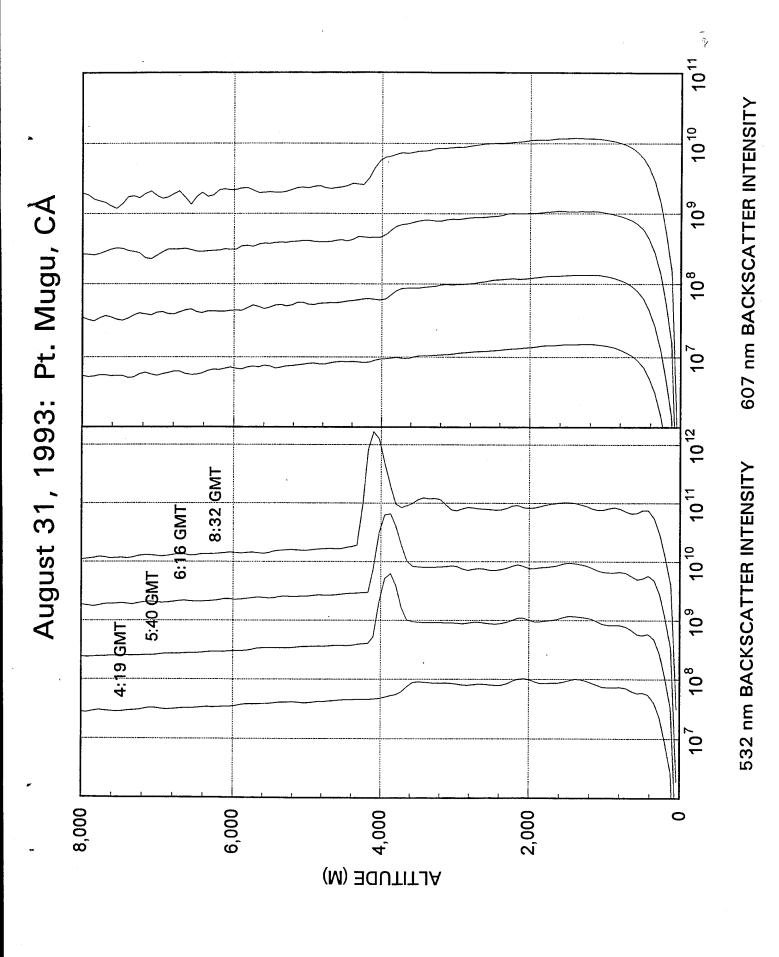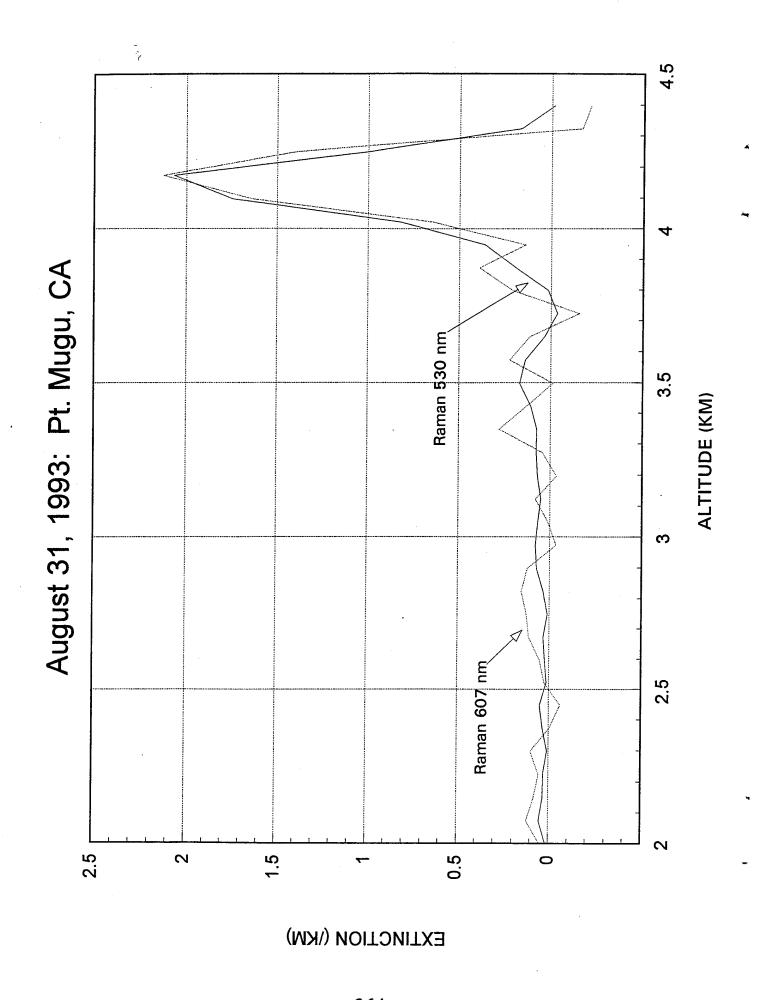
Raman Lidar Optical Properties
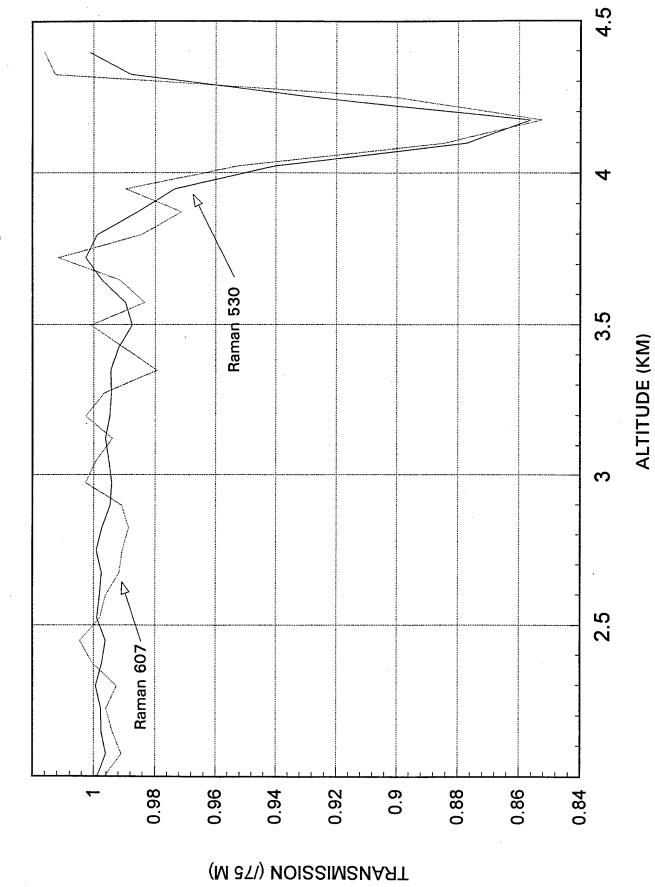
Backscatter signals from lidar at the transmitted wavelength have been shown to be of very limited use (ceiling height) except for limited cases of stratospheric aerosols, fog, and other examples of mono-dispersed particles. The Raman signal provide molecular profiles from which the extinction can be directly determined. By combining extinction and backscatter at several wavelengths, the particle group can be defined.

Altitude

Extinction

Backscatter

Raman Signal
N2 - 607 nm or 387 nm
Rotational - 530 nm

Fundamental
532 nm, 355 m or 266 nm

Backscatter Signal

August 31, 1993: Pt. Mugu, CÀ

4:19 GMT

5:40 GMT

6:16 GMT

8:32 GMT

ALTITUDE (M)

8,000   6,000   4,000   2,000   0

532 nm BACKSCATTER INTENSITY

607 nm BACKSCATTER INTENSITY

10^7 10^8 10^9 10^{10} 10^{11} 10^{12}

10^7 10^8 10^9 10^{10} 10^{11}

August 31, 1993: Pt. Mugu, CA

Raman 530 nm

Raman 607 nm

EXTINCTION (/KM)

ALTITUDE (KM)

August 31, 1993: Pt. Mugu, CA

April 5, 1993: State College, PA

6:44 GMT
7:28 GMT
8:19 GMT

ALTITUDE (KM)

15
12.5
10
7.5
5
2.5
0

532 nm BACKSCATTER INTENSITY

10^6 10^7 10^8 10^9 10^{10} 10^{11} 10^{12}

607 nm BACKSCATTER INTENSITY

10^5 10^6 10^7 10^8

April 5, 1993: State College, PA

EXTINCTION (/KM)

ALTITUDE (KM)

April 5, 1993: State College, PA

TRANSMISSION (775M)

ALTITUDE (KM)
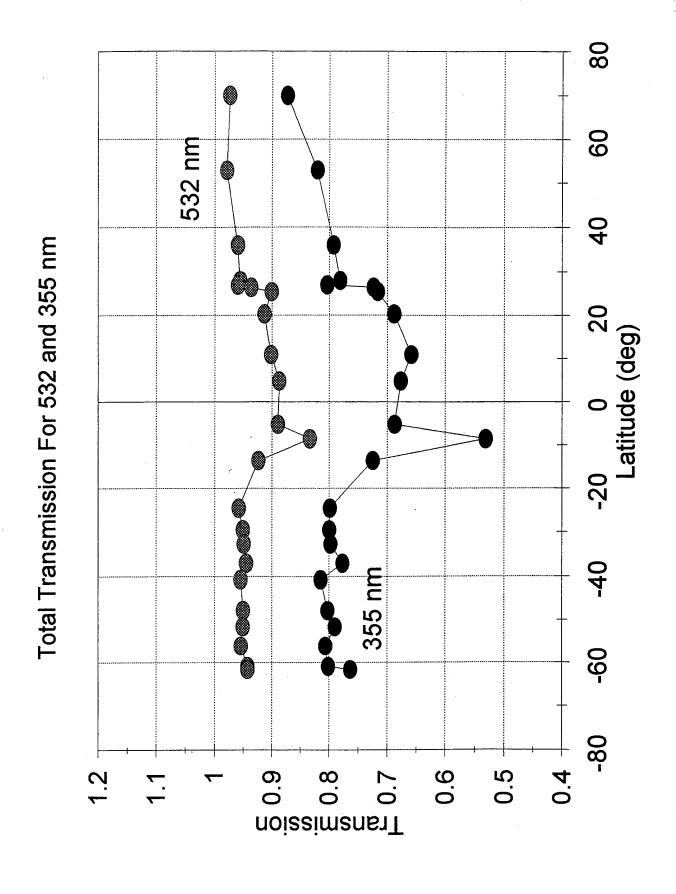
Pinatubo Extinction Profile for 11/27/91

4.8 degrees north
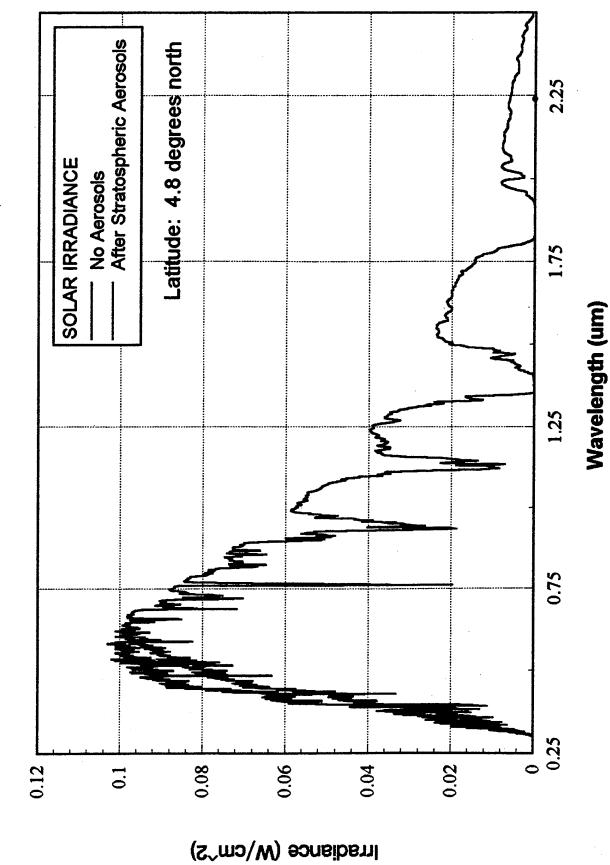
Total Transmission For 532 and 355 nm

Total Extinction Coefficients
For 355 and 532 nm

Solar Irradiance from LOWTRAN 7

SOLAR IRRADIANCE
— No Aerosols
— After Stratospheric Aerosols

Latitude: 4.8 degrees north

Irradiance (W/cm^2)

Wavelength (um)

Ground-Based Measurements of HF and HCl

Hilary E. Snell* and Paul B. Hays

Space Physics Research Laboratory
Department of Atmospheric, Oceanic, and Space Sciences
The University of Michigan
2455 Hayward
Ann Arbor, MI 48109-2143

*Currently with AER, Inc., Cambridge, MA

Abstract

This poster describes remote sensing observations of HF and HCl column densities over Ann Arbor, Michigan. Spectra were collected between October 1992 and July 1993 using a ground-based Michelson interferometer and the technique of solar absorption spectroscopy. While the column densities computed from these spectra agree with other groups' measurements of these species, we have noticed that the HCl spectral line at $2925.897 \, cm^{-1}$ appears strongly asymmetric. It is our belief that this is due to spectral contamination by another chemical species and not instrumental phase errors as previously reported by other groups.

Introduction

Hydrogen chloride (HCl) and hydrogen fluoride (HF) are important gases in stratospheric chemistry. Hydrogen chloride is both a reservoir and a sink for chlorine atoms, which play an integral role in the chemistry of ozone. Hydrogen fluoride is chemically inert in the stratosphere and serves as a sink for fluorine atoms through diffusion to the tropopause and subsequent rainout. The concentration of HF is determined by the destruction of anthropogenically-emitted fluorine-containing compounds while the HCl concentration has both anthropogenic and natural components. The relative abundance of HF and HCl provides an indication of the relative importance of CFC's to other sources of chlorine in the total amount of chlorine present in the stratosphere.

Remote sensing of HCl and HF has been routinely accomplished by analysis of the near-infrared spectrum of each species' fundamental (1-0) rotation-vibration band. Numerous lines from these bands have been used for atmospheric density measurements and the FASCODE atmospheric model was used to determine the suitability of each of the lines for ground-based measurements. Only some of the HF and HCl lines can be used in ground-based measurements due to absorption by methane and water vapor. It is for this reason that much of the remote sensing of HCl and HF has been done from balloons. For both HF and HCl the R_1 transition was selected as the most suitable line for this study, 2925.897 cm^{-1} for HCl and 4038.962 cm^{-1} for HF.

Instrumentation

The measurements described in this poster were accomplished using a Bomem DA-8 Michelson interferometer with a calcium fluoride (CaF$_2$) beamsplitter and indium-antimonide (InSb) detector. A potassium-bromide (KBr) window at the instrument entrance aperture enabled instrument evacuation during data collection. An optical filter was placed at the limiting aperture to reduce the spectral region incident on the detector and allow for an increase in the amplifier gain settings. Solar tracking was accomplished with a roof-mounted heliostat system and the light was collimated before entering the instrument.

The interferograms were acquired through a maximum optical path difference of 200 cm to yield an unapodized spectral resolution of 0.0025 cm^{-1}. This optical path difference is much larger than the interferogram-halfwidth of the HF and HCl features and the spectral lines are completely resolved. Each set of data consists of two co-added interferograms and required a total of about 10 minutes of data collection. Due to the Bomem software and computer memory limitations only data from a 10 cm^{-1} wide spectral region was saved.

Spectra representative of measurements from Ann Arbor are shown in Figure 1. The spectrum in Figure 1a was measured on 1 October 1992 at a solar zenith angle of 67.04° while the spectrum in Figure 1b was collected on 20 January 1993 at a solar zenith angle of 78.26°. As indicated the HF and HCl absorption features lie on the edge of very strong absorption due to methane.
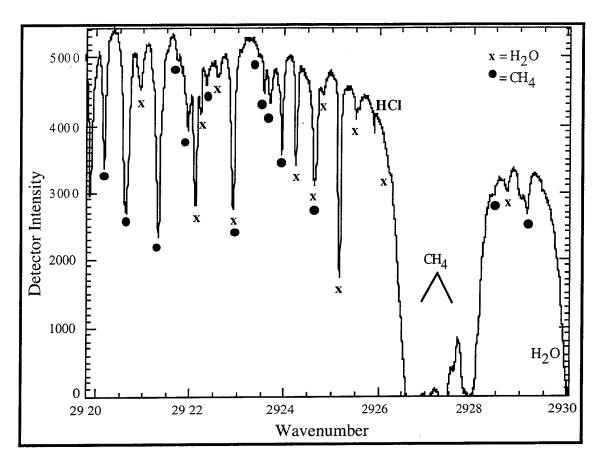
Figure 1a Spectrum computed from the interferogram collected at 8:44 est on 1 October 1992. This is the result of two scans with a maximum optical path difference of 200 cm, which yields an unapodized spectral resolution of 0.0025 cm^{-1}.
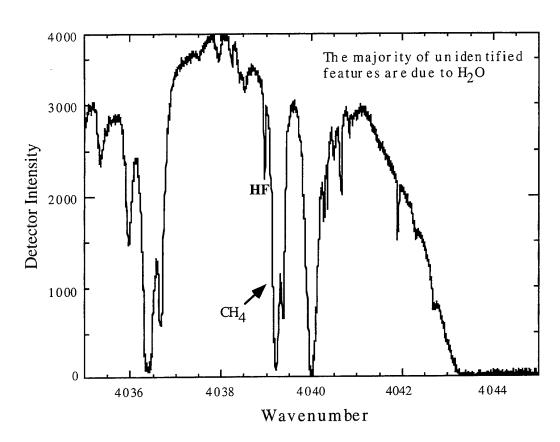
Figure 1b Spectrum computed from the interferogram collected at 9:17 est on 20 January 1993. This is the result of two scans with a maximum optical path difference of 200 cm, which yields an unapodized spectral resolution of 0.0025 cm^{-1}.

Determination of Column Density

The column density was retrieved from the spectra by removing the background absorption and fitting the spectral line of interest. Removing the background simplifies data analysis because it is difficult to quantify parameters such as the exact field of view of the instrument, detector gain and spectral response, and optical losses to the signal from light-collecting optics and within the instrument itself.

The spectral lines were fit by assuming a Voigt lineshape and U.S. Standard Atmosphere temperature and pressure profiles. The Air Force extension to the U.S. Standard Atmosphere provides the HF and HCl mixing ratios to be used as a starting point for the fit to the spectral data. These profiles represent a mean value for the desired constituents. The fit was accomplished by allowing variation in mixing ratio magnitude and altitude. Thus

$$\xi_{measured}[z] = M\xi_{af}[z*(1+\delta)] \qquad [1]$$

where $\xi_{af}(z)$ is the Air Force standard profile, M accounts for a magnitude shift in this profile, and the quantity $(1+\delta)$ allows for vertical transport of the species of interest. Depending on the value of δ the mixing ratio profile will expand or contract in altitude; a positive value of δ indicates subsidence and the mixing ratio profile will be compressed. This method of varying the mixing ratio profile is more realistic than simply shifting the profile in altitude. Once a mixing ratio profile has been determined it is used to compute the column density.
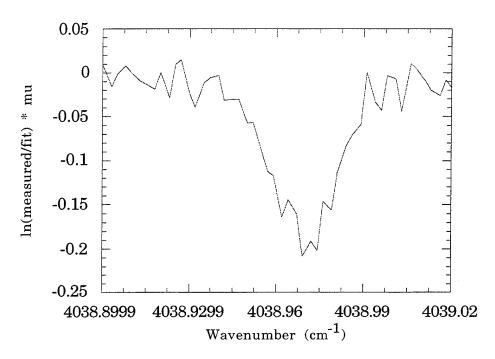
Figure 3 The measured HF absorption after the removal of the background absorption and airmass correction factor μ.

Method of Removing the Background Absorption

The measured spectrum may be written as the product of background transmission and the transmission of the species of interest. For the case of the spectral regions chosen for HF and HCl, the background spectrum consists of absorption due to methane and water vapor. Because the expression for the Voigt lineshape must be evaluated numerically, it is computationally more convenient to implement a fitting routine using the analytic solutions for the Lorentz and Doppler shapes. In these spectral regions the water and methane lines are strongly absorbing and, for the purpose of fitting the background, we have treated them only as Lorentzian lines. The wings of these features will still have a Doppler component due to stratospheric absorption but exclusion of this term introduces little error to the final fit. The initial values for computation of the Lorentz shape of these lines are tabulated in the HITRAN database. In order to eliminate the HF or HCl line from the criteria for a good fit to the background, only the spectrum greater than three halfwidths away from the HCl or HF absorption was included in the background fit.

While we attempted to use realistic parameters to fit the background we soon found that doing so is extremely difficult. In particular, we found that (1) the methane linewidth information in the HITRAN database is not always reliable; (2) line mixing strongly affects the wings of methane lines, particularly in the region around the HCl line we have chosen; and (3) line mixing is most severe in the low-wavenumber wings of the methane P-branch which, again, is where the HCl line is located. To overcome these problems we decided to allow the half-widths, magnitudes, and center wavenumbers to vary while computing the background fit. This does not produce a geophysically-meaningful result but it did allow us to remove the shape of the background.

Asymmetric HCl Line

The first thing one notices when examining Figure 5 is that the HCl line is not symmetric. This shape has been noticed by other groups and has been attributed to instrumental effects, such as a problem with the phase correction. We argue that if the problem were instrumental one would expect the other lines in this spectral region to be distorted as well. Unfortunately this spectral region does not contain isolated lines with the same magnitude of absorption as the HCl feature. Close examination of isolated, but stronger, spectral lines indicates that the other features in this spectrum are not asymmetric. Examination of the region used to measure HF also does not show any obvious asymmetries. Furthermore, this shape is observed in all of our measurements taken over several months, changes magnitude with solar zenith angle in the manner expected for a spectral feature, and appears to be similar to spectra measured by other groups at Mauna Loa, Hawaii, and Antarctica (Rinsland *et al.*, 1988; Liu *et al.*, 1992).

As a means of eliminating instrumentation errors as a source of the asymmetry, data was collected using different mirror scan velocities (0.5 cm s^{-1} and 1 cm s^{-1}), different beamsplitters (CaF$_2$ and KBr), different widths of the saved spectral region (2920-2930 cm^{-1}, 2922-2932 cm^{-1}, and 2923-2929 cm^{-1}), and different spectral resolutions (0.0025 cm-1 and 0.005 cm^{-1}). In all cases the line shape is asymmetric. Figure 6 illustrates spectra measured with the KBr and CaF$_2$ beamsplitters at the two different spectral resolutions. The change in the slope of the lines connecting points clearly indicates that the spectral line is asymmetric. If the line shape was symmetric these connecting lines would be parallel; the lines would be parallel with zero slope if one of the resolution elements fell exactly on the peak of the feature. If the asymmetric shape was caused by a problem in mirror alignment through the scan one might expect the asymmetry to be reduced if the measurement is made at a lower spectral

resolution. As can be seen in Figure 6 this is not the case. Thus we believe that the asymmetric shape of the line is real and is not an artifact of the instrument.

In order to support the hypothesis of the presence of another species, the absorption by HCl was computed and removed from the spectrum shown in Figure 6. The residual, shown in Figure 7, reveals what appears to be another spectral line. Though there is a solar CO line in the vicinity of the HCl absorption, its line intensity is several orders of magnitude weaker than that of HCl. The width of the residual feature is approximately 0.047 cm^{-1} indicating a pressure width corresponding to about 500 mb. This in turn indicates that the gas causing the absorption is uniformly distributed with altitude. Furthermore, because it is present in spectra obtained at Antarctica and Mauna Loa it is not a chemical species endemic to Ann Arbor. Unfortunately we have been unable to determine exactly what species accounts for this absorption feature.
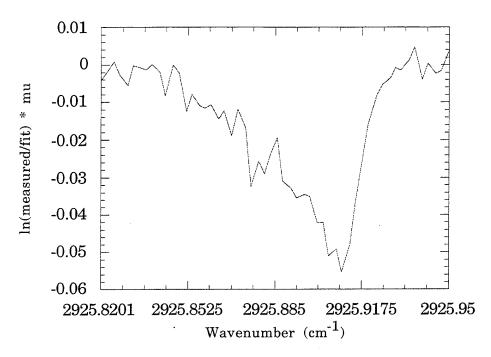
Figure 5 The measured HCl absorption after removal of the background absorption and airmass correction factor.
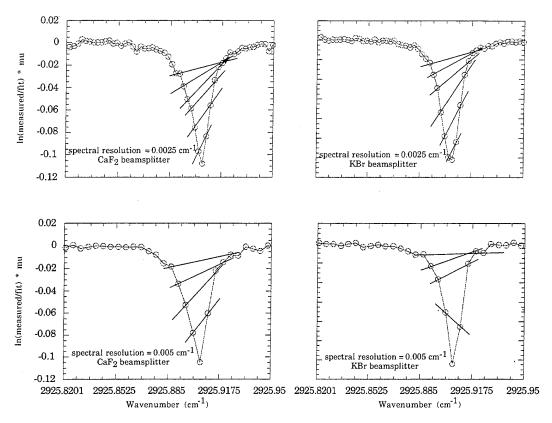
Figure 6 Comparison of data collected using the KBr and CaF$_2$ beamsplitters at unapodized resolutions of 0.0025 and 0.005 cm^{-1}. Background absorption and the airmass correction factor μ have been removed from the spectra.
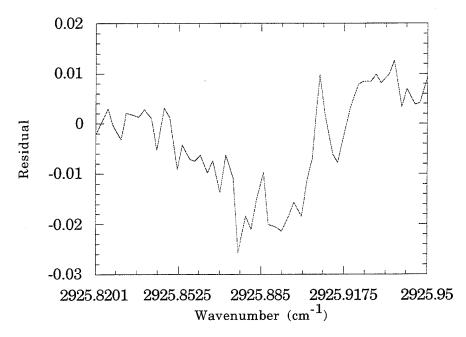
Figure 7 Difference between the absorption shown in Figure 5 and the computed HCl absorption. This residual illustrates the presence of another spectral feature.

Retrieved Densities

Utilizing the above analysis techniques we have measured the column content for HF and HCl. The column density computed from each of the spectra collected on a given day was averaged and the (1σ) standard deviation computed. Information about the measurements is summarized in Table 1, while Table 2 summarizes the results for HCl and Table 3 summarizes the HF data.

A potential source of error in determining the column density is related to the calculation of the solar zenith angle. A single spectrum is derived from two interferograms which were added to increase the SNR and requires about 10 minutes to record. As such there is some ambiguity as to the time which should be used to compute the SZA. To estimate the magnitude of this error the column density computed using the time attached to the data file was compared to the density computed with a time ±5 minutes from the recorded time. Examination of this error shows that for most cases it is insignificant compared to the overall scatter in the data.

The number of spectra collected was limited by several factors. As one might expect, thick clouds make it difficult to collect solar-absorption spectra, though even near-sub-visual cirrus clouds caused problems in the instrument phase correction routine. Consequently most of the spectra were obtained before local noon. Data collection was further limited because the instrument is shared by several research groups. Furthermore, measurement of HF and HCl required the use of different optical filters. Changing filters requires time to re-evacuate the instrument (a sure sign that it would soon become cloudy!). Thus on any given day data was usually obtained only for a single spectral region.

Measurements of atmospheric HCl for this study were conducted between October 1992 and July 1993. The derived column densities are shown in Figure 10 as a function of the airmass correction factor. Averaging all of the data yields a column density of $4.14 \pm 1.08 \times 10^{15}$ molecules cm^{-2}. The large standard deviation can be

attributed to errors in the fit due to the asymmetric shape of the HCl feature. Errors in tracking due to the variation in the solar zenith angle over the course of the measurement were found to be negligible compared to other sources of error.

Because the HF line is symmetric and yields a much better fit than HCl, measurements of the HF column density were made to a higher precision than the HCl measurements. The data from Table 3 is shown in Figure 11 as a function of the airmass correction factor. Averaging all of the data yields a column density of $1.62 \pm 0.24 \times 10^{15}$ molecules cm^{-2}. The standard deviation for the HF data is much less than for the HCl measurements because the HF line is symmetric and a much better fit is obtained. As with the HCl measurements the errors due to the calculation of the solar zenith angle are insignificant.

Date	Day Number	HCl Spectra	HF Spectra
1-OCT-1992	92-275	43	-
27-DEC-1992	92-362	4	7
18-JAN-1993	93-018	-	4
19-JAN-1993	93-019	9	20
20-JAN-1993	93-020	-	6
1-MAR-1993	93-060	22	-
7-MAR-1993	93-066	-	30
18-MAR-1993	93-077	15	-
10-JUL-1993	93-191	26	-
13-JUL-1993	93-194	17	-

Table 1 Summary of HF and HCl spectra.

Day Number	Column Density (molecules cm^{-2})	Estimated Accuracy	Error due to SZA Calculation
92-275	3.4412 x 10^{15}	19.42%	1.75%
92-362	3.7538 x 10^{15}	25.58%	0.38%
93-019	3.9644 x 10^{15}	15.81%	3.55%
93-060	3.8136 x 10^{15}	11.94%	3.65%
93-077	5.1441 x 10^{15}	9.05%	3.52%
93-191	4.5841 x 10^{15}	36.23%	2.51%
93-194	5.9122 x 10^{15}	1.90%	2.81%
Average of all data	4.1395 x 10^{15}	26.06%	2.74%

Table 2 Summary of HCl column density measurements.

Day Number	Column Density (molecules cm^{-2})	Estimated Accuracy	Error due to SZA Calculation
92-362	1.2715 x 10^{15}	7.45%	1.26%
93-018	1.3741 x 10^{15}	4.69%	5.87%
93-019	1.5748 x 10^{15}	13.12%	0.78%
93-020	1.6597 x 10^{15}	11.56%	5.26%
93-066	1.7651 x 10^{15}	9.90%	1.59%
Average of all data	1.6212 x 10^{15}	15.10%	1.84%
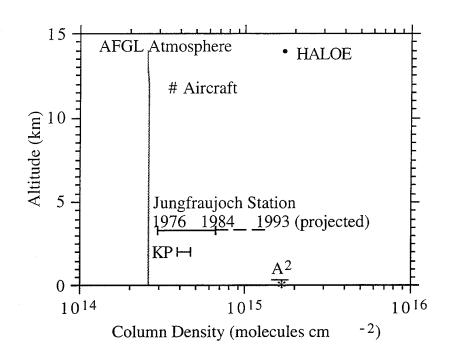
Table 3 Summary of HF column density measurements.

Comparison with Other Measurements
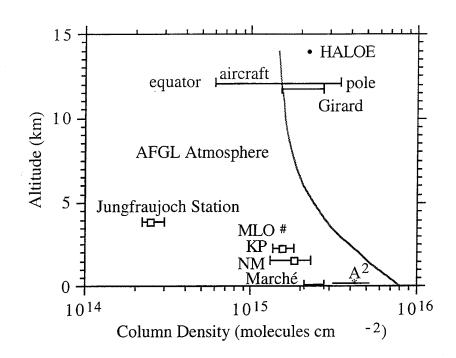
As a means of validating the ground-based HF and HCl measurements made from Ann Arbor, Michigan we have examined other column density measurements of HF and HCl. These comparisons are shown in Figure 12 for HF and Figure 13 for HCl.

One source of recent data for comparison is the Halogen Occultation Experiment (HALOE). One of several instruments aboard the Upper Atmosphere Research Satellite (UARS), HALOE uses solar occultation techniques to measure the atmospheric mixing ratio profiles of several gas species, including HF and HCl. The instrumental requirements, experimental objectives, and geographical coverage are described by Russell *et al.* (1993). We have examined HALOE mixing ratio profiles measured close to the location of Ann Arbor (42.28° N, 83.71° W). The lower altitude limit for the HALOE data is about 14 km and the mixing ratio profile can be integrated to yield a column density from this point to the top of the atmosphere. From this data the column density for HF is 1.76×10^{15} cm^{-2} while the HCl column density is 2.23×10^{15} cm^{-2}. These values are accurate to 10-15% (Russell *et al.*, 1993). Hydrogen fluoride does not have a significant tropospheric source and the HALOE value falls well within the error bars of our measurement ($1.62 \pm 0.24 \times 10^{15}$ cm^{-2}). Hydrogen chloride does have a tropospheric component. If the density decreases at the rate projected by the AFGL atmospheric profile the HCl column density we have measured ($4.14 \pm 1.08 \times 10^{15}$ cm^{-2}) is actually too low when compared to HALOE data (see the Air Force column density profile shape in Figure 13).

The other comparisons shown in Figures 12 and 13 illustrate that the column densities we have measured are comparable to previous measurements. However, due to differences in latitude, season, and year we would not expect these values to be in exact agreement.

Because the HF line is symmetric and yields a much better fit than HCl, measurements of the HF column density were made to a higher precision than the HCl measurements. The data is shown as a function of the airmass correction factor. Averaging all of the data yields a column density of $1.62\pm0.24 \times 10^{15}$ molecules cm^{-2}. The standard deviation for the HF data is much less than for the HCl measurements because the HF line is symmetric and a much better fit is obtained. As with the HCl measurements the errors due to the calculation of the solar zenith angle are insignificant.

Measurements of atmospheric HCl for this study were conducted between October 1992 and July 1993. The derived column densities are shown as a function of the airmass correction factor. Averaging all of the data yields a column density of 4.14±1.08 x 10^{15} molecules cm^{-2}. The large standard deviation can be attributed to errors in the fit due to the asymmetric shape of the HCl feature. Errors in tracking due to the variation in the solar zenith angle over the course of the measurement were found to be negligible compared to other sources of error.

Summary

Using the technique of solar absorption spectroscopy we have measured the atmospheric absorption due to HF and HCl. From this information we are able to calculate the column density. Comparison of our data with that of other groups indicates that the values are in good agreement with other measurements at this latitude.

Examination of the HCl absorption feature at 2925.897 cm^{-1} under various experimental conditions indicates that the observed asymmetry in the shape of the line is not introduced by the interferometer. Determination of the species causing this absorption is necessary if this spectral line is to be used to measure the density of HCl.

Acknowledgments

AN ATMOSPHERIC MODEL FOR GRAVITY WAVE INDUCED TURBULENT LAYERS (BLINI) BASED ON THE SATURATED CASCADE MODEL

E. DEWAN   PL/GPOS
N. GROSSBARD   BOSTON COLLEGE
T. VANZANDT   NOAA

<u>OUTLINE</u>

- PROBLEM TO BE SOLVED

- SOLUTION TO PROBLEM

- GRAVITY WAVE SIMULATIONS

- RESULTS

- CONCLUSIONS

EDE6194GPO

PROBLEM TO BE SOLVED

- AF SYSTEMS USING HIGH POWERED LASER BEAMS ARE LIMITED BY ATMOSPHERIC TURBULENCE

- TURBULENCE OCCURS IN THIN LAYERS CALLED "BLINI" (RUSSIAN FOR "PANCAKES") DIMENSIONS: 100 M VERTICAL
  100 KM HORIZONTAL

- CAUSE OF TURBULENCE LAYERS = GRAVITY WAVES [BY HYPOTHESIS]

- PROBLEM: HOW TO SIMULATE "BLINI" BEHAVIOR?

EDE6194GPO

3

<u>SOLUTION TO PROBLEM</u>

- LINEAR INSTABILITY DUE TO WAVE SHEARS

$$Ri \equiv \frac{N^2}{S^2} \leq 0.5$$

- USE SATURATED CASCADE THEORY TO SIMULATE WAVE FIELD

- REALIZATIONS MUST BE BASED ON THE THEORETICAL SPECTRA

- THE SHEAR REGION WHERE $S^2 \geq 2N^2$ WILL DEFINE THE BLINI LOCATION IN X-Z (DISTANCE-ALTITUDE) SPACE [N = CONST.]

EDE6194GPO

SATURATED CASCADE SPECTRA AND RELATIONS

THEORETICAL SPECTRUM

$$\Psi_{V_x}(k_z) = \alpha \, N^2 \, k_z^{-3} \cdot 2\pi = \left(5 \times 10^{-4}\right) k_z^{-3}$$

$V_x \equiv$ HORIZONTAL VEL. FLUCT.

$$k_x = k_z^3 \left(\frac{2\pi\varepsilon a_2}{a_1 N^3}\right) = 250 \, k_z^3$$

$\varepsilon = 2 \times 10^{-5} \, m^2 s^{-3}$ (STRATOSPHERE), $\quad \dfrac{a_2}{a_1} = 15.9$

$N = 2 \times 10^{-2} \, s^{-1}$ (STRATOSPHERE),

EDE6194GPO

REALIZATIONS OF v_x FROM $\Psi_{v_x}(k_z)$

$$v_x^r = \sum_{l=1}^{M} v_x(k_z(l))$$

$$v_x(k_z) = A(k_z) \cdot \sin(k_x X + k_z Z)$$

$$\boxed{A^2(k_z(l)) \equiv \int_{\left(\frac{1}{2}\right)[k_z(l) + k_z(l-1)]}^{\frac{1}{2}[k_z(l) + k_z(l+1)]} \left[\Psi_{v_x}(k_z)\,dk_z\right]} = \frac{\Psi_{v_x}(k_z)}{L} \quad \text{(ALT.)}$$

(NOT FOR ENDPOINTS)

$$L \equiv \text{TOTAL LENGTH} \equiv N'\Delta Z \quad (\Delta Z = \text{SPACING})$$

EDE6194GPO

6

BLINI OCCUR IF:

$$\frac{dv_x^r}{dz} \equiv S\,(x,z) \geq 2.8 \times 10^{-2}\ s^{-1}$$

ALTERNATIVE APPROACH

$$S\,(X,Z) = \sum_{l=1}^{M} B(k_z\,(l))\ \sin\,(k_z X + k_z Z)$$
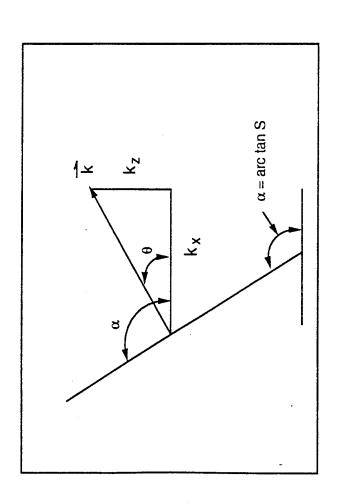
$$B^2\,(k_z\,(l)) = \int_{\left(\frac{1}{2}\right)[k_z\,(l) + k_z\,(l-1)]}^{\frac{1}{2}[k_z\,(l) + k_z\,(l+1)]} k_z^2\ \Psi_{v_x}\,(k_z)\ dk_z$$

TO PROVIDE RANDOM PHASES AND AMPLITUDES, MULTIPLICATION OF A (k_z) OR B (k_z) BY FOURIER TRANSFORMED WHITE GAUSSIAN NOISE IS USED.
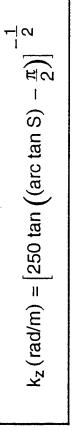
SLOPE(S) OF BLINI (WAVE PHASE-PLANE)

$$\alpha = \theta + (\pi/2)$$

$$\theta = \text{arc tan} \ (k_z/k_x)$$

$$k_z \ (\text{rad/m}) = \left[250 \ \tan \left((\text{arc tan } S) - \frac{\pi}{2}\right)\right]^{-\frac{1}{2}}$$
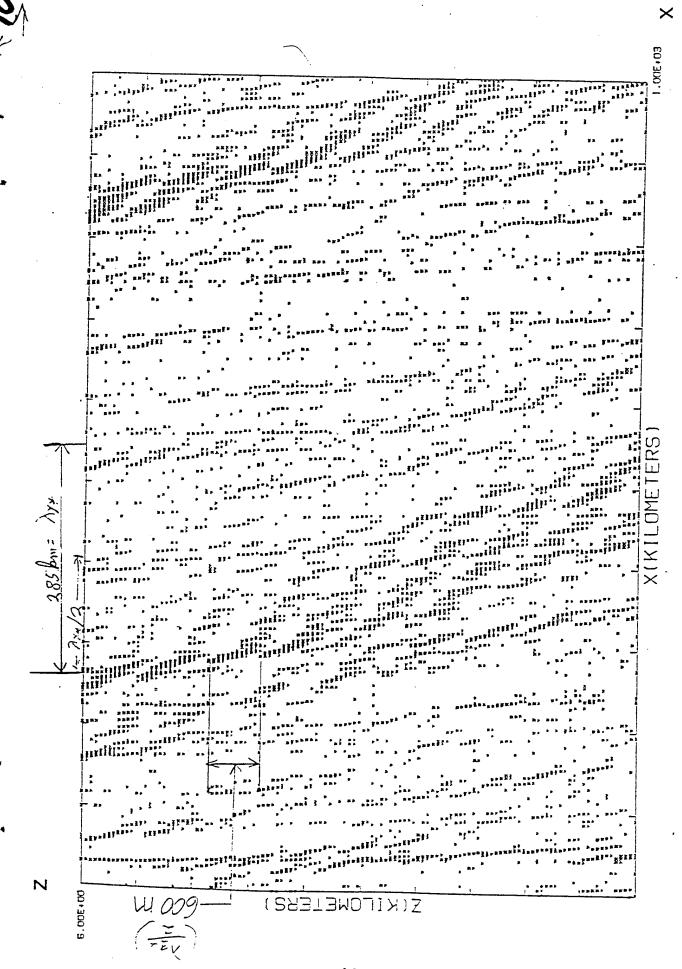
THE FOLLOWING SIMULATIONS USE THE SATURATED-CASCADE SPECTRAL MODEL

a – X-Y PICTURE OF BLINI
b – SHEAR SPECTRUM
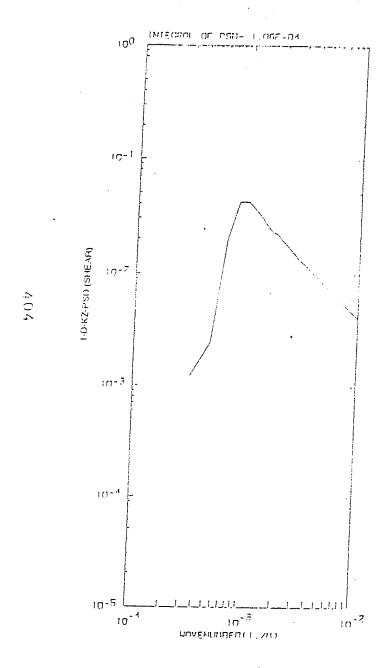
VERTICAL SPACING $\quad = \dfrac{\lambda_{z.}}{2} = 600 \text{ m} \quad, \quad \lambda_{z_{min}} = 100 \text{ m}$
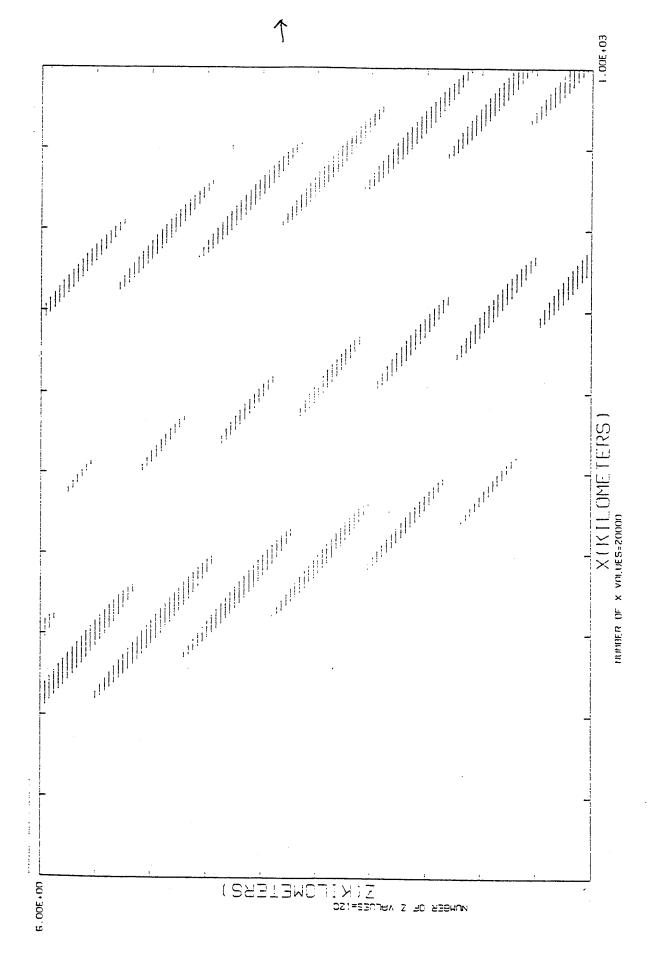
HORIZONTAL SPACING $\quad = \dfrac{\lambda_{x.}}{2} = 285 \text{ km} \quad, \quad \lambda_{x_{min}} = 100 \text{ m}$

X

1.00E+03

$3.85 \, km = \lambda_{xz}$

$\leftarrow \lambda_{xx}/3 \rightarrow$

X(KILOMETERS)

130 k's   RANDOM PHASES ONLY

Z

6.00E+00

6.00E+00

$600 \, m$

$\left(\dfrac{\lambda_{zz}}{\lambda_{zx}}\right)$

Z(KILOMETERS)

INTEGROL OF PSD= 1.06E-04

I-O-KZ-PSD (SHEAR)

10^0

10^{-1}

10^{-2}

10^{-3}

10^{-4}

10^{-5}

10^{-4}

10^{-3}

10^{-2}

WAVENUMBER (1./N)

$4.5 \times 10^{-3} < k_z < 6 \times 10^{-3}$ rad/m, PH = 0

12

X(KILOMETERS)

NUMBER OF X VALUES=20000

Z(KILOMETERS)

NUMBER OF Z VALUES=120

6.00E+00

1.00E+03

6.00E+00

405

RANDOM PHASES AND AMPLITUDES.

130 k's

X(KILOMETERS)

NUMBER OF X VALUES=20000

Z(KILOMETERS)

NUMBER OF Z VALUES=120

1.00E+03

6.00E+00

13

406

INTEGRAL OF PSD= 1.17E-04

WAVENUMBER(1./M)

200 k's RANDOM PHASE AND AMPLITUDE
(VELOCITY)

x (KILOMETERS)

INTEGRAL OF PSD= 1.13E-04

WAVENUMBER(1./M)

PAD WITH ZEROS TO 1024   VALUES FOR PSD

AVERAGE OF 101 PERIODOGRAMS

RANDOM PHASE AND AMPLITUDE
(VELOCITY)

12 k's

x (KILOMETERS)

Z (KILLOMETERS)

19

410

INTEGRAL OF PSC= 1.24E-04

1-O-KZ-PSD(SH)

10^1
10^0
10^{-1}
10^{-2}
10^{-3}
10^{-4}
10^{-5}
10^{-6}
10^{-7}

2

1

WAVENUMBER(1./M)

10^{-5} 10^{-4} 10^{-3} 10^{-2} 10^{-1}

PAD WITH ZEROS TO 1024   VALUES FOR PSD

AVERAGE OF 101 PERIODOGRAMS

CONCLUSIONS

- WE HAVE EXPLORED THE BEHAVIOR OF TURBULENT BLINI THAT ARE DUE TO GRAVITY WAVES.

- THE SATURATED CASCADE THEORY WAS USED TO PRODUCE SIMULATIONS.

- BLINI APPEAR TO BE PERIODIC AND BLINK ON AND OFF WITH RESPECT TO X (OR t) AS WELL AS WITH ALTITUDE: SPACING IS AT $\lambda_x/2$ AND $\lambda_z/2$ DISTANCES RESPECTIVELY.

- THEY SLOPED FROM UPPER LEFT TO LOWER RIGHT WITH OUR MODEL.

- THESE SLOPES WERE CONSISTENT WITH THE MOST DOMINANT FREQUENCIES IN THE SHEAR SPECTRA.

- IT WAS FOUND THAT BLINI OCCURRED WITH AND WITHOUT THE USE OF RANDOM AMPLITUDES IN THE PSD'S USED TO PRODUCE THE REALIZATIONS. THIS WAS NOT EXPECTED. IT DID NOT OCCUR IN THIS MANNER WITH A LESS SOPHISTICATED MODEL USED EARLIER (THE "SEPARABLE MODEL").

- MULTIPLE PERIODS WERE FOUND IN BLINI WITH LOW NUMBER OF WAVE NUMBER SIMULATIONS AND THEY WERE CONSISTENT WITH DOMINANT FREQUENCIES IN THE SHEAR SPECTRA.

- EVIDENCE FOR THE SATURATED-CASCADE THEORY.

EDE6194GPO

ARECIBO 430 MHz RADAR
22 JAN 1980

Figure 1. Radar echo-power of backscatter signals from turbulent fluctuations of clear air in the stratosphere and upper troposphere. Shade levels are every 4 dB. A piecewise linear trend has been subtracted with 0, 2, 5, and 12 dB of attenuation at 9, 14, 19, and 24 km, respectively. Results obtained with the 430 MHz Arecibo radar at 150 meter resolution. Unpublished material courtesy of Woodman, Rastogi and Sato.

PAGES 414-430 NOT USED

Structure in Radiative Excitation as a Source of High Altitude Radiance Structure: CO(v=1) Radiance

Jeremy R. Winick
R.H. Picard
Phillips Laboratory, Optical Environment Division, Hanscom AFB, MA 01731

P.P. Wintersteiner
Arcon Corporation, Waltham, MA

J.A. Dodd
Stewart Radiance Laboratory, Bedford, MA.

Outline

- CO(v=1) is highly non-LTE and dominated by radiative processes

- Nighttime radiance above 60km excited by "earthshine" from below

- Lower boundary can provide significant contribution

  - Ground or cloud blackbody contribution determined by down-looking opacity

  - Enhancement of minor isotopic components ($^{13}C^{16}O$ (36) and $^{12}C^{18}O$ (28)) observed in CIRRIS 1A and ARC model calculations demonstrate importance of lower boundary radiative pumping.

- Use ARC model to examine extreme case of lower boundary effect

  - Tropical clear atmosphere

  - Tropical atmosphere with optically thick high altitude cloud (15km, T=198K)

  - Large change in $^{13}C^{16}O$ emission, smaller but significant change in $^{12}C^{16}O$ emission.

- ARC is 1-D model, estimate effects for various realistic cases (scale sizes of cloud/clear regions

- Applicability to other emitters
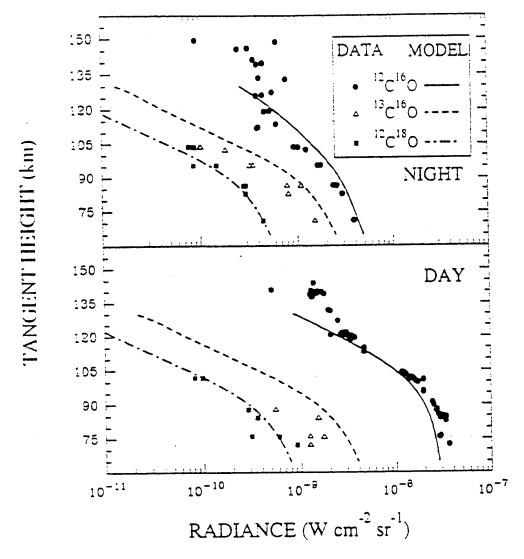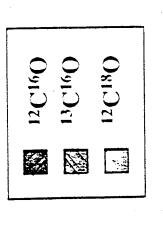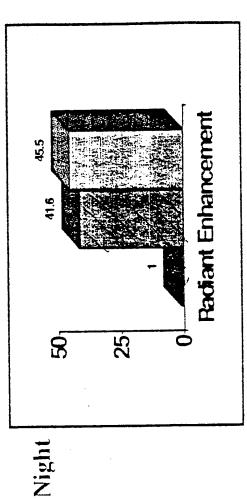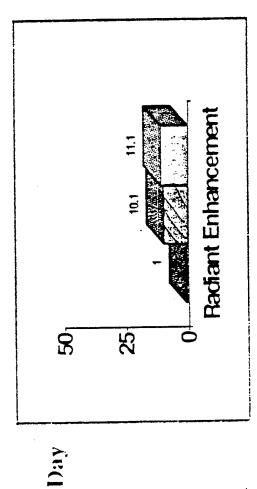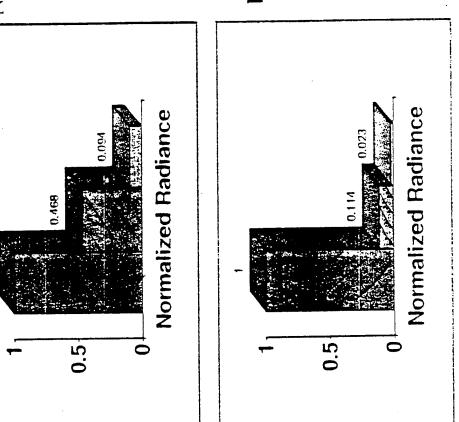
Fig. 3. Integrated radiance from the 1-0 fundamental bands of $^{12}C^{16}O$, $^{13}C^{16}O$, and $^{12}C^{18}O$, as determined from spectral fits to numerous scans from the CIRRIS 1A database, under nighttime (top) and daytime (bottom) conditions. The lines superimposed on the data points are predictions made by the Atmospheric Radiance Code (ARC) model [*Wintersteiner et al.*, 1992].

Limb Line-of-Sight Radiance
75 km Tangent Height

Model description:

CO - 4.7 μm non-LTE Radiance

- Processes - Production and Loss

  Collisions $CO(v=0) + M \leftrightarrow CO(v=1) + M$

  $M=N_2(v)$ is most efficient

  Radiation $CO(v=0) + hcv \leftrightarrow CO(v=1)$

- Above ~45 km, $^{12}C^{16}O$ radiation is **non-LTE**, as low as15 for 36 and 28 isotopes

- Above ~65 km, $^{12}C^{16}O(v=1)$ is in **Radiative Equilibrium** (~30 for minor isotopes

  Day: Efficiently pumped by <u>solar</u> radiation

  Night: Pumped by <u>earthshine</u>, originating most importantly from the stratopause for 26 isotope, lower boundary for 36, 28 isotopes

- The ARC line-by-line non-LTE code is used to calculate the CO vibrational temperatures and the resulting band limb radiance.

  - CO mixing ratio profiles must be supplied to model

  - All CO profiles exhibit unusual behavior, with large increase in mixing ratio in stratosphere and mesosphere

  - Large uncertainty in CO mixing ratio profiles

Validity of climatology database is uncertain (limited data)

Large seasonal and latitudinal variation predicted

AFGL Lowtran atmosphere (A1-A6) 0-120km (all have the same tropospheric profile - dominates opacity to ground level)

Day/night transition occurs around SZA=90

Vibrational temperature in daytime greatly exceeds nighttime consistent with data.

• Model band limb radiance is obtained from line-by-line non-LTE code integrating over the same 0.01 radian FOV as CIRRIS 1A detector #2.
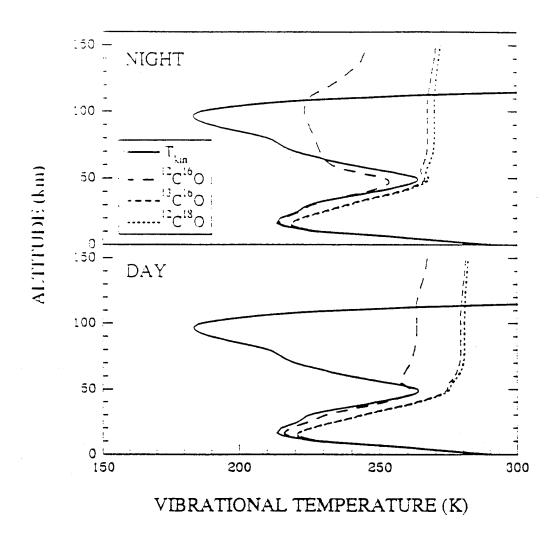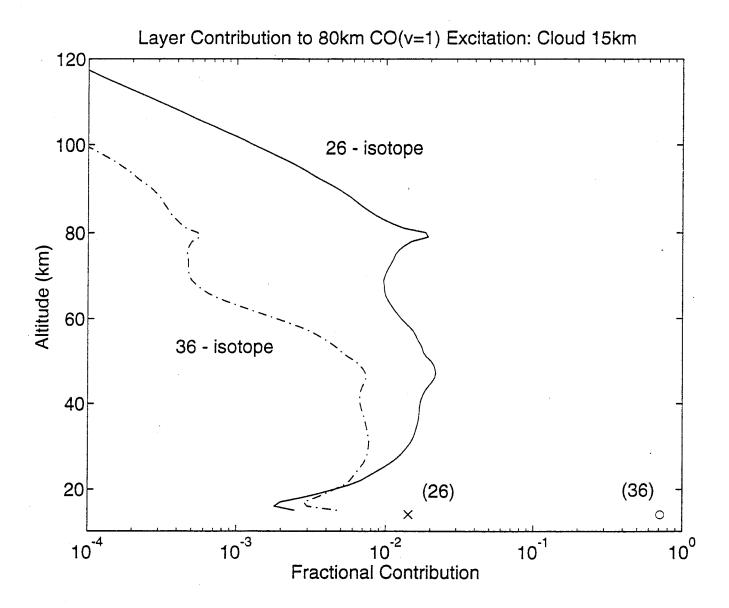
Fig. 4. Nighttime (top) and daytime (bottom) vibrational temperature profiles for $^{12}C^{16}O$, $^{13}C^{16}O$, and $^{12}C^{18}O$, as predicted by the ARC model. Also shown for reference is the kinetic temperature input to the ARC calculation.

437

Layer Contribution to 80km CO(v=1) Excitation: Cloud 15km
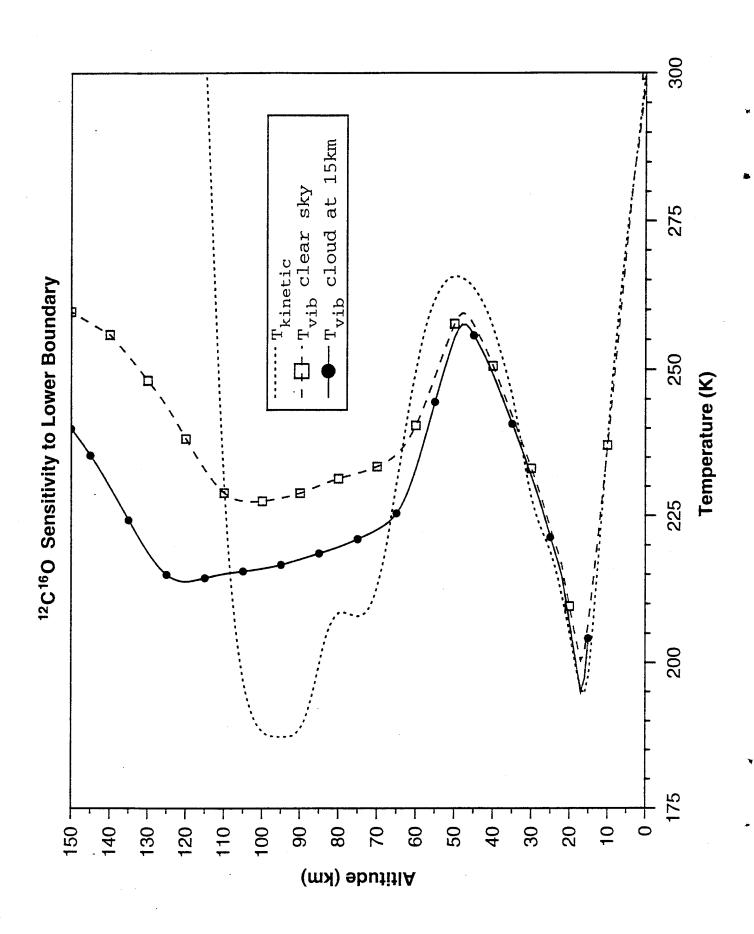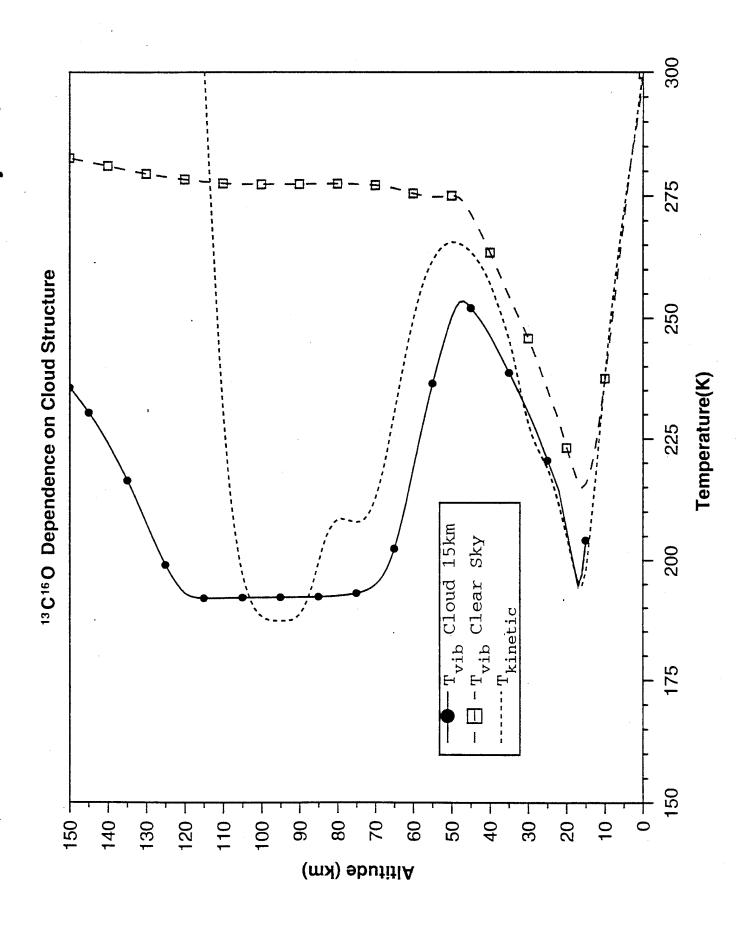
Lower Boundary Effects
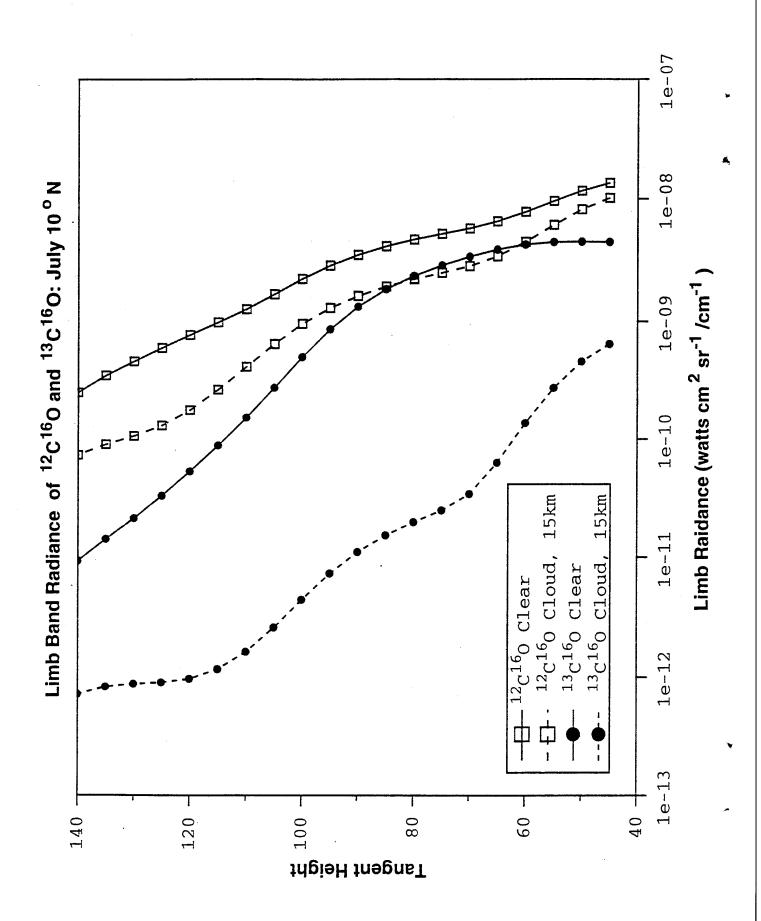
- Most important for nighttime where earthshine dominates
  - cloud, albedo effects on solar pumping will be investigated later

- Test cases for 26 and 36 isotopes

Radiator	Clear	Clear	Cloud 15km	Cloud 15km
	T_{vib} 80km	Pumping from lower boundary	T_{vib} 80km	Pumping from lower boundary
$^{12}C^{16}O$	233	0.14	220	0.01
$^{13}C^{16}O$	277	0.95	193	0.71

- Boundary effect dominates 36 isotope, significant for 26

- 26 isotope opacity depends upon [CO] profile, thin 36 less sensitive

- Limb Radiance for 1-D case:
  - $^{12}C^{16}O$ ratio clear/cloud = 1.6-3.0
  - $^{13}C^{16}O$ ratio clear/cloud >10

$^{13}C^{16}O$ Dependence on Cloud Structure

Legend:
- T_{vib} Cloud 15km (● solid line)
- T_{vib} Clear Sky (□ dashed line)
- $T_{kinetic}$ (dotted line)

Axes:
- Altitude (km)
- Temperature(K)

Limb Band Radiance of $^{12}C^{16}O$ and $^{13}C^{16}O$: July 10° N

Legend:
- $^{12}C^{16}O$ Clear
- $^{12}C^{16}O$ Cloud, 15km
- $^{13}C^{16}O$ Clear
- $^{13}C^{16}O$ Cloud, 15km

X-axis: **Limb Raidance (watts cm^2 sr^{-1} /cm^{-1})**

Y-axis: **Tangent Height**
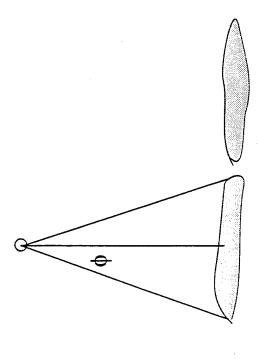
Structure in Optical Atmospheric Radiance

- SOAR - AFOSR 6.1 research program to characterize and understand structured optical radiance

- Modeling has concentrated on acoustic gravity wave effects on radiance, primarily airglow emissions in the mesopause region (OH(v))

- CO(v=1) vibrational temperature dependence upon lower boundary conditions provides a source of structured emission independent of local changes in temperature, pressure, or species density (which can be caused by waves and turbulence).

- ARC predicts that CO(v=1) will produce structured emission in response to structure in the upwelling radiance from lower boundary, most significantly for the most optically thin minor isotopes.

Structure in 3-D atmosphere

- Clear/Cloud areas are not of infinite extent

- Scale size of clear/cloud areas depends upon altitude (solid angle subtended of upwelling radiation)

  - For optically thin 36 or 28 isotope directly proportional to projected volume

  - For optically thick species must consider that larger angles have more opacity also.

ϕ
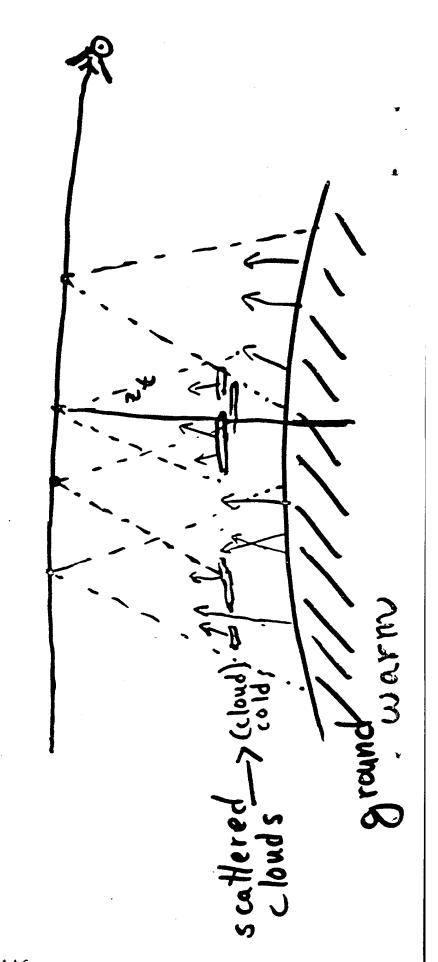
- Angles $\phi>75$ probably don't contribute for optically thin case, smaller angle for optically thick can define effective cloud width.

- For cloud scale size $<< z_h$ fraction of cloud cover important parameter.

- LOS limb radiance involves another dimension to integrate over, this horizontal scale is in most cases larger than effective cloud width defined above.

- Statistical methods should be considered as opposed to examining in detail numerous (multi-dimensional) cases

Structure along LOS
Cloud Structure

scattered clouds

→ (cloud): colds

ground

warm

446

Conclusions

- CO(v=1) non-LTE radiance above about 70km, sensitive to lower boundary condition.

  - Effect is most important for:

    nighttime

    weak 36 and 28 isotopes

    Atmosphere with warm surface, cold cloud tops (tropical)

- For tropical case studied, Limb Radiance for 1-D case:

  - $^{12}C^{16}O$ ratio clear/cloud = 1.6-3.0

  - $^{13}C^{16}O$ ratio clear/cloud >10

- More realistic 2- or 3-D scenes will produce radiance intermediate between clear and cloud case

  - Structure from clouds below will be somewhat smoothed, especially edge effects

  - Structured radiance from lower boundary clouds likely to be at least as important (nighttime) as in situ variability (gravity waves -> T, [M])

INFRARED RADIANCE FLUCTUATIONS IN THE UPPER ATMOSPHERE
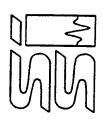
JOHN GRUNINGER, ROBERT SUNDBERG
AND PIALI DE

SPECTRAL SCIENCES, INC.
BURLINGTON, MA

JAMES BROWN

PHILLIPS LABORATORY/GPOS
HANSCOM AFB, MA

JUNE 8, 1994

PRESENTATION OUTLINE

- GOALS

- OVERVIEW OF APPROACH
  - NLTE CHEMISTRY
  - RADIANCE FLUCTUATIONS AND STATISTICS

- SAMPLE CALCULATIONS (CIRRIS BAND PASSES)
  - PREDICTIONS OF WEIGHTING MODEL
  -- COMPARISONS WITH NSS MODEL AND DATA
  -- SAMPLE BAND PASS IMAGES

- SUMMARY

SHARC GOALS

- DEVELOP THE CAPABILITY TO PREDICT THE STATISTICS OF ATMOSPHERIC RADIANCE FLUCTUATIONS AND TO GENERATE IR IMAGES FOR USE IN SYSTEM STUDIES

  INPUT GAS TEMPERATURE/TOTAL DENSITY FLUCTUATIONS

  PREDICT RO-VIBRATIONAL STATE POPULATION FLUCTUATIONS

  PREDICT RADIANCE COVARIANCE AND PSD

  -LOS NOT RESTRICTED TO LIMB

  STRUCTURE TIME SCALE

  -TIME SCALE > TIME TO REACH STEADY STATE

  -TIME SCALE > MEASUREMENT TIME

  CONSTRUCT IMAGE REALIZATIONS OF STRUCTURE

  -ARBITRARY BAND PASS AND LOS

SHARC APPROACHES
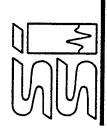
- BRUTE FORCE STATISTICAL SAMPLING

  GENERATE 3-D ARRAY OF ATMOSPHERIC FLUCTUATIONS

  STATISTICAL SAMPLING OF LOS THROUGH THE ARRAY

  NO ASSUMPTION OF LINEARITY

- LOS WEIGHTING APPROACH

  USE SHARC ΔT_{vib} AND RADIATION TRANSPORT MODULES

  PREDICT EFFECTS OF LOCAL FLUCTUATIONS ON RADIANCE

  CALCULATE LOS WEIGHTING FUNCTION

  MAP LOCAL STATISTICAL QUANTITIES

  INTO SENSOR RADIANCE STATISTICS
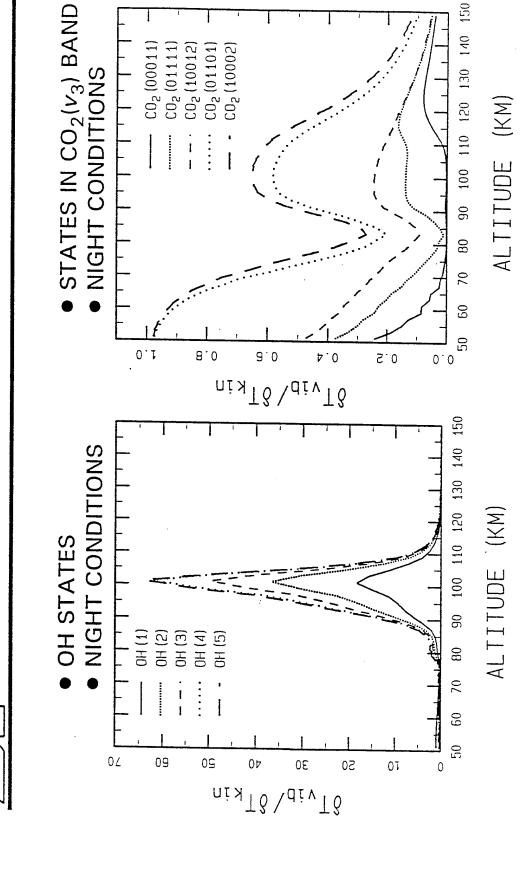
- TODAY'S TOPIC IS LOS WEIGHTING
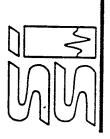
OVERVIEW OF APPROACH

- REQUIRES GAS TEMPERATURE STATISTICS
  - LOCKHEED MODEL (STRUGALA ET AL., 1993 SPIE)

- VIBRATIONAL STATE TEMPERATURE FLUCTUATIONS
  - EXPANSION IN KINETIC TEMPERATURE FLUCTUATIONS

- RADIANCE STATISTICS
  - DERIVE COVARIANCE AND PSD
  - INCORPORATE EFFECTS OF BAND PASS, FOV, AND LOS
  - GENERATE RADIANCE IMAGES

VIBRATIONAL TEMPERATURE DERIVATIVES

- STATES IN $CO_2(v_3)$ BAND
- NIGHT CONDITIONS

- OH STATES
- NIGHT CONDITIONS

OVERVIEW LOS RADIANCE STATISTICS

- RADIANCE PSD:

  WEIGHTED SUM OF VOLUME EMISSION PSDs ALONG LOS

- RADIANCE CORRELATION LENGTHS:

  WEIGHTED VOLUME EMISSION CORRELATION LENGTHS

  THE RADIANCE PSDs HAVE DIFFERENT FUNCTIONAL FORMS

  RADIATION TRANSPORT FILTERS HIGH FREQUENCY STRUCTURES

  RADIANCE PSDs HAVE HIGHER SPECTRAL SLOPE
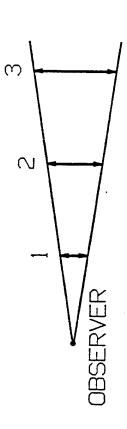
- IMAGES OF RADIANCE STRUCTURE

  BAND PASS, FOV, LOS AND DAY/NIGHT DEPENDENCE
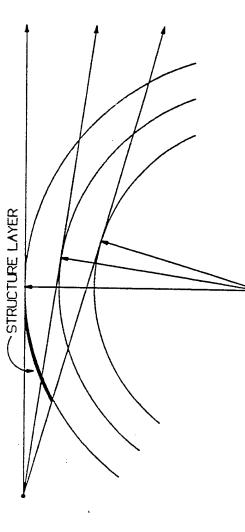
  SCALING OF "OVERLAYS" IS INADEQUATE
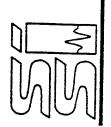
FIELD OF VIEW EFFECTS ON
CORRELATION LENGTHS

OBSERVER

STRUCTURE LAYER

- ALL THREE OBJECTS APPEAR THE SAME SIZE TO OBSERVER
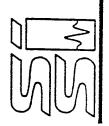
- SAME CORRELATION LENGTH LOOKS LARGER IN LOS'S
  LOOKING BELOW STRUCTURE LAYER

INITIAL MODEL APPLICATIONS

- CIRRIS 1A RADIANCE STATISTICS
  - DETERMINED BY T. CONLEY AND R. SEARS

- ASPECTS OF MODEL FOR 4.3 μm BAND
  - HORIZONTAL CORRELATION LENGTH COMPARISONS:
    - NSS MODEL AND DATA
    - FOV EFFECTS
  - MODEL PREDICTS STRONG DIURNAL EFFECTS

- SAMPLE RADIANCE IMAGES
  - DAY/NIGHT COMPARISON FOR 4.3 μm

- QUICK LOOK AT OTHER BANDS
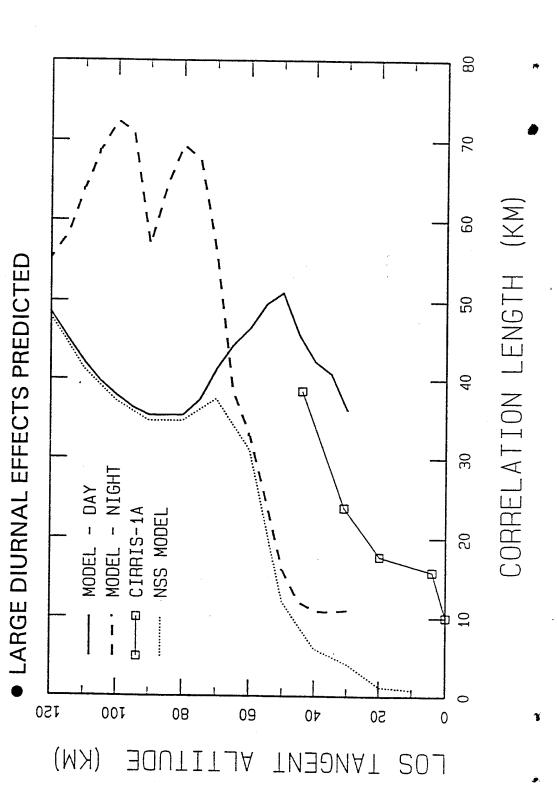
CIRRIS-1A RADIOMETER BANDPASSES
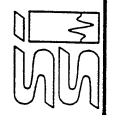
Filter	Bandpass $(\mu m)^a$	Major Radiators
*0	8.5 - 18	$CO_2(\nu_2)$, $O_3(\nu_3)$
*1	4.1 - 4.5	$CO_2(\nu_3)$, $CO(\Delta v=1)$, $NO^+(\Delta v=1)$
2	4.9 - 7.0	$NO(\Delta v=1)$, $H_2O(\nu_2)$
3	6.0 - 8.8	$H_2O(\nu_2)$, $O_3(\nu_1)$, $CH_4(\nu_4)$
*FP 2	2.6 - 3.3	$OH(\Delta v=1)$, CO_2, aerosols
5	11.1 - 12.8	CO_2, $O_3(\nu_3)$, HNO_3
6	17.9 - 23	H_2O(Rot)
*7	8.0 - 11.8	$O_3(\nu_3)$, CO_2

[a] 25% spectral response limits
* USED IN CURRENT SIMULATIONS

457

HORIZONTAL RADIANCE CORRELATION LENGTHS

CIRRIS-1A (4.1 - 4.5 μm)

● LARGE DIURNAL EFFECTS PREDICTED
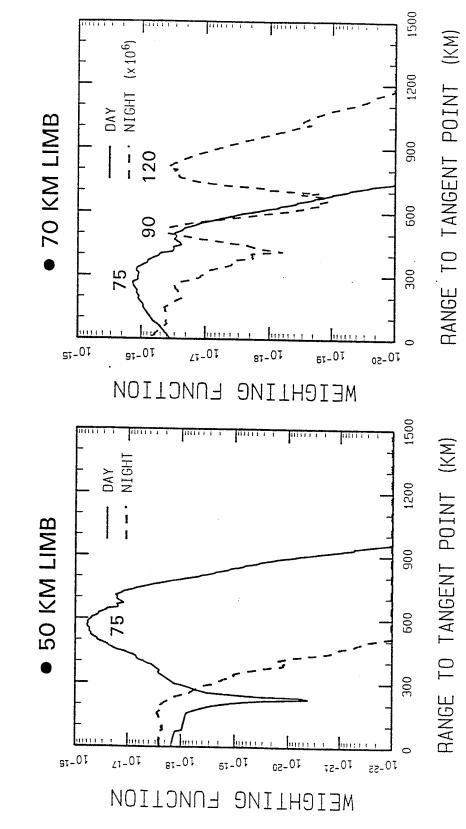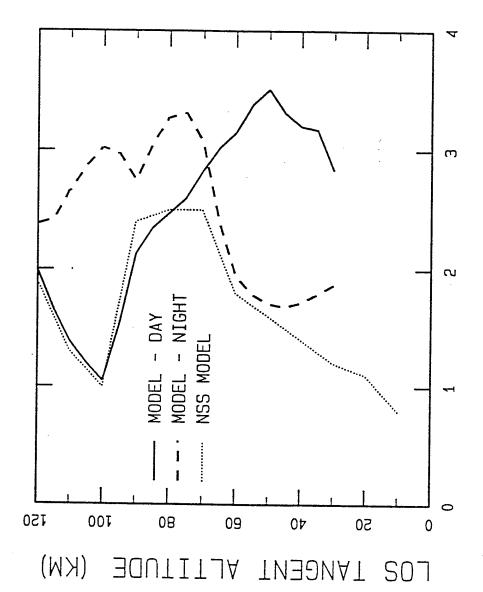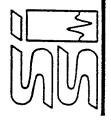
LOS WEIGHTING FUNCTION
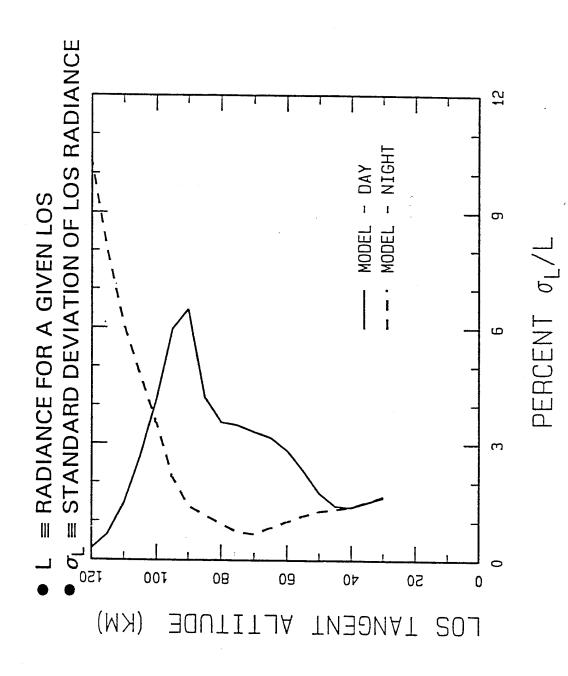## CIRRIS-1A (4.1 - 4.5 μm)

● 70 KM LIMB

● 50 KM LIMB

VERTICAL RADIANCE CORRELATION LENGTHS

CIRRIS-1A (4.1 - 4.5 μm)
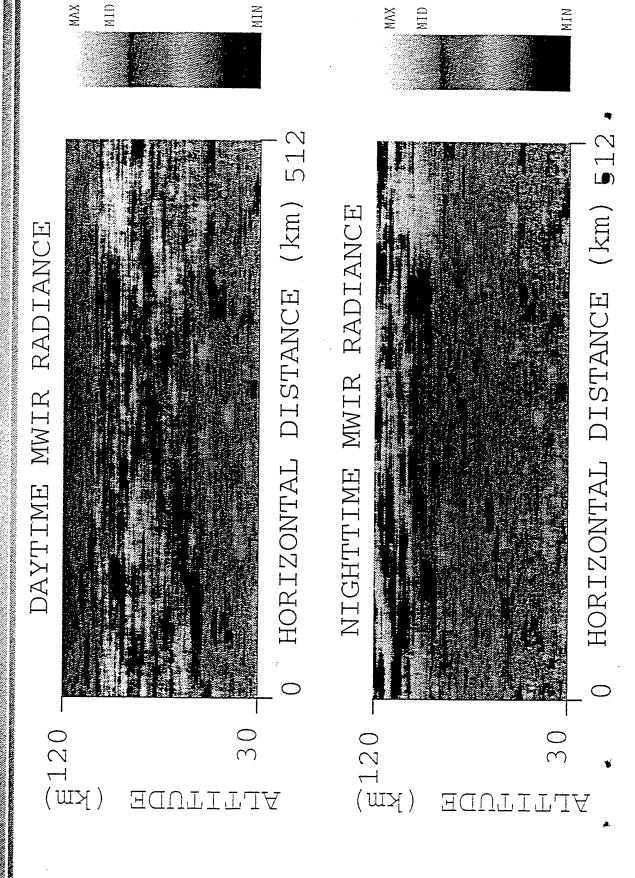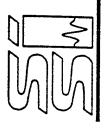
RADIANCE STANDARD DEVIATION

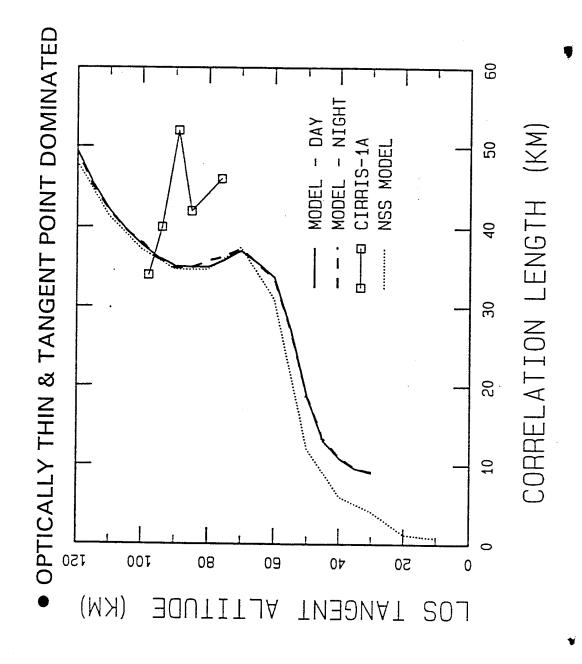## CIRRIS-1A (4.1 – 4.5 μm)

● L ≡ RADIANCE FOR A GIVEN LOS

● σ_L ≡ STANDARD DEVIATION OF LOS RADIANCE

MODEL – DAY
MODEL – NIGHT

PERCENT σ_L/L

LOS TANGENT ALTITUDE (KM)

CO_2 RADIANCE IMAGE

DAYTIME MWIR RADIANCE

NIGHTTIME MWIR RADIANCE

462
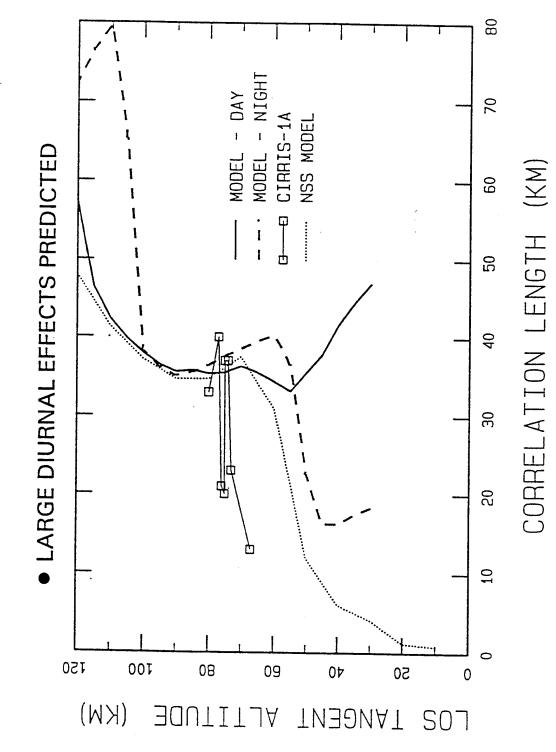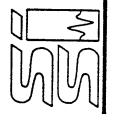
HORIZONTAL RADIANCE CORRELATION LENGTHS
CIRRIS-1A (2.6 - 3.3 μm)

● LARGE DIURNAL EFFECTS PREDICTED

463
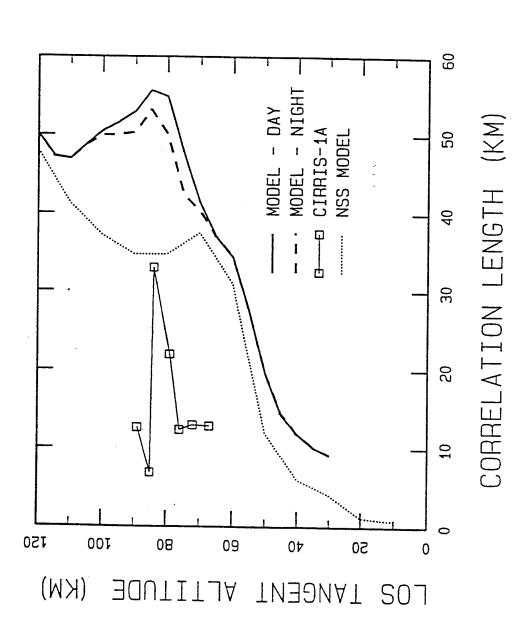
HORIZONTAL RADIANCE CORRELATION LENGTHS

CIRRIS-1A (8.0 - 11.8 μm)

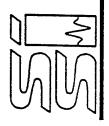● OPTICALLY THIN & TANGENT POINT DOMINATED

464

HORIZONTAL RADIANCE CORRELATION LENGTHS
CIRRIS-1A (8.5 - 18 μm)

PRELIMINARY RESULTS

- RADIANCE STRUCTURE DETERMINED BY FULL LOS
  - NSS MODEL AND NEW MODEL AGREE WHEN
    - OPTICALLY THIN AND TANGENT POINT DOMINATED
- PRELIMINARY MODEL PREDICTIONS ARE:
  - CONSISTENT WITH AVAILABLE CIRRIS DATA IN
    - THE 4.3 ,8 -12, and the 2.7 bands
  - INCONSISTENT WITH AVAILABLE CIRRIS DATA IN
    - THE 8.5-18 $CO_2(v_2)$ band
  - STRONG DIURNAL EFFECTS IN SYSTEMS BANDS
- MORE ANALYSIS AND/OR MEASUREMENTS NEEDED
  - MANY PREDICTIONS WITH NO COMPARISONS
  - MUCH DATA WITH NO PREDICTIONS

CONCLUSION

- MODEL DETERMINES RADIANCE STATISTICS
  - REQUIRES TEMPERATURE STATISTICS AS INPUT
  - PROVIDES NEEDED OUTPUT FOR IR SCENES
  - SCENARIO, FOV AND BANDPASS DEPENDENT

- RADIANCE FLUCTUATIONS DETERMINED BY FULL LOS
  - TANGENT POINT REGION MAY NOT BE DOMINANT
  - DOMINANT ALTITUDES VARY WITH SCENARIO
    -- HIGHLY DEPENDENT ON EMISSION SPECIES
    -- SENSITIVE TO BANDPASS OPTICAL DEPTH EFFECTS

- APPLICATIONS
  - ANALYSIS AND PREDICTION OF RADIANCE STRUCTURE
  - INVERSION TO TEMPERATURE STATISTICS